e-ISSN 2586-9396

Current Applied Science and Technology

Vol. 21 No.1
January - March 2021

KING MONGKUT'S INSTITUTE OF TECHNOLOGY LADKRABANG

Advisory Board

Current Applied Science and Technology or CAST, formerly KMITL Science and Technology Journal published by King Mongkut's Institute of Technology Ladkrabang (KMITL), has been established since its inception as KMITL Science Journal in 2001. The journal has been dedicated to publishing advanced and applied knowledge in the form of high-quality research and review articles covering the main areas of Biotechnology, Environmental Science, Agricultural Technology, Food Science and other fields related to Applied Science and Technology. Special issues devoted to important topics in advanced science and technology will occasionally be published.

The journal is an open access peer-reviewed and double blinded journal using Online Journal System (OJS) publishing online academic research and review articles. Previously, articles were published in print on a regular basis (two issues per year) since 2001 and since 2010 onward the articles have been published both in print and electronic forms starting from volume 10. In 2017, the journal title has been changed from *KMITL Science and Technology Journal* to *Current Applied Science and Technology* (CAST) (e-ISSN 2586-9396) to be more identifiable to the international scientific community according to the suggestion of Thai-Journal Citation Index Centre. The journal has been published online only since volume 17(2) (July-December, 2017). In addition, the journal has attracted researchers from other countries more than 22% according to the data. Because of more demands on publication in CAST, the editorial board has decided to publish online original academic research and review articles four issues per year (January-March, April-June, July-September and October-December) from 2021 onward.

Furthermore, the advisory board and editorial board comprises honorable and well-known members from around the world in which 50% of editorial board members are from various countries like U.K., Norway, Japan, India, China, Canada, Estonia and Egypt. Only 25% of Thai editorial board members are from the publisher organization and 25% from other publisher organizations. Most of advisory and editorial board members have high H-index according to SCOPUS.

The journal is also committed to maintaining the high level of integrity in the content published and has a Conflict of Interest policy in place. The journal uses plagiarism detection software to screen the submissions. The journal has been working closely with Thai-Journal Citation Index Centre to ensure that the journal complies with international standard of SCOPUS.

Current Applied Science and Technology (CAST)

(formerly KMITL Science and Technology Journal)

Editor

Dusanee Thanaboripat
King Mongkut's Institute of Technology Ladkrabang, Thailand

Editorial Board

CONTENTS

Current Applied Science and Technology Vol. 21 No. 1 (January-March 2021)

Heavy Metal Content and Spatial Distribution to Determine the Water Pollution Index in Depapre Waters, Papua, Indonesia

Baigo Hamuna[1, 3]* and Rosye Hefmi Rechnelty Tanjung[2, 3]

[1]Department of Marine Science and Fisheries, Cenderawasih University, Jayapura City, Papua Province, Indonesia
[2]Department of Biology, Cenderawasih University, Jayapura City, Papua Province, Indonesia
[3]Center for Environmental Studies, Cenderawasih University, Jayapura City, Papua Province, Indonesia

Received: 27 March 2020, Revised 8 June 2020, Accepted: 2 July 2020

Abstract

A determination of water quality should be conducted as a reference to determine the status of pollution in waters. This study aims to determine the content and distribution of several heavy metals and to determine the pollution index of those heavy metals in Depapre waters, Jayapura Regency, Papua. The sampling of seawater was conducted in October 2017 at five observation stations. The results were then compared to the quality standards of seawater for marine biota based on the Decree of the Minister of Environment No. 51 year 2004. Heavy metal concentrations in the seawater samples were analysed using Atomic Absorption Spectrophotometer (AAS). The results showed that concentrations of Cd, Pb, Cu, and Zn ranged between 0.00-0.003 mg/l, 0.001-0.005 mg/l, 0.464-0.600 mg/l, and 0.003-0.008 mg/l, respectively. Mercury was not detected because its concentration was lower than the detection limit of the tool used. The Hg, Pb, and Zn concentrations fell within the concentration limits specified in the quality standards of seawater for marine biota, whereas the Cd concentrations at stations 1, 2, and 4, and Cu concentrations at all observation stations exceeded the limits specified in the quality standards of seawater for marine biota. Based on the water pollution index, all observation stations fell into the moderately polluted category with a pollution index range of 6.94-7.34. The Cu concentration was the biggest contributor to a high pollution index in the Depapre waters, Jayapura Regency.

Keywords: Depapre waters; heavy metals; water pollution index; water quality standard
DOI 10.14456/cast.2021.4

*Corresponding author: Tel.: +62 821 9980 1101
E-mail: bhamuna@yahoo.com.sg

1. Introduction

The main problem faced in the marine areas investigated was the condition of the water, which had often been contaminated, and was thus of impaired quality. Ideally, seawater quality for marine biota should meet the standards specified for physical, chemical, and biological parameters [1-4]. A significant decrease in water quality due to high concentrations of poisonous inorganic and or organic materials is not only bad for the marine environment; it can also cause disruption and loss in the economy and society. One of the pollutants that needs to be paid attention to is heavy metals [5]. Although a certain concentration of heavy metals was found in seawaters, the concentration was still under threshold value that could danger marine organisms [6]. However, even in such cases, bad things can happen when the heavy metals that pollute seawaters accumulate in sediments and marine organisms [7].

A range of research work has shown that several bodies of seawater in Indonesia were atrociously contaminated by heavy metals. Heavy metals contamination was found to be a serious problem in Jakarta Bay waters, but the concentrations of heavy metals such as copper (Cu), cadmium (Cd), and lead (Pb) found there were shown to have not been on decreasing or increasing trends [8]. Likewise, pollution that occurred in Central Java waters was caused by the heavy metal concentrations of mercury (Hg), Pb, and Cd that came from domestic wastes, farming activities, and marine transportation that surpassed the quality standards of seawater [9-11]. The Pb and Cd concentrations in Ambon waters also surpassed the standards of quality for marine biota [12]. Moreover, the sediments in the coastal waters of Tangerang were polluted by Hg and surpassed the threshold with higher concentrations [13]. Lead and cadmium were found to have contaminated fishes and marine biota, like *Strombus Canarium* and *Anadara* sp, in the Kalabat Bay waters of Bangka Island [14] and *Euthynnus* sp in North Java coastal waters [15].

Pollutants that enter a body of water can cause the waters to become polluted. To assess the status of pollution in waters, the Government of Indonesia, through Decree of the Minister of Environment No. 115 year 2003, has established several methods to determine the status of pollution in waters, one of which is the water pollution index [16]. The water pollution index is used to determine the level of pollution relative to permitted water quality parameters [17]. The water pollution index has been widely used to determine the status of water pollution in Indonesia in seawaters [3, 11, 18], rivers [19-22], and lakes [23]. The results of water quality assessment based on water pollution index can be used as input to improve water quality if there is a decrease in quality due to the presence of pollutants.

The area of Depapre waters is one of the coastal areas in Papua that underwent significant development in the areas of port construction, marine tourism, settlement housing, marine transportation, and aquaculture and fisheries. All of these activities were suspected of contributing to water pollution. Hamuna *et al.* [24] showed that the Depapre waters were lightly to moderately polluted, with several physical and chemical parameters exceeding the specified quality standards. However, the water chemical parameters studied in the study did not include heavy metals, and there has been little or no information regarding the concentration of heavy metals in Depapre waters to date.

The purpose of this study was to determine the concentration and spatial distribution of various heavy metals in Depapre waters, Jayapura Regency, Papua Province. The analyzed heavy metals in this study were Mercury (Hg), Cadmium (Cd), Lead (Pb), Copper (Cu), and Zinc (Zn). These heavy metals are very dangerous if their concentrations exceed the threshold determined by the Government of Indonesia in the Minister of Environment Decree No. 51 year 2004, which deals with Seawater Quality Standards [25]. The obtained heavy metal concentrations were analyzed further to determine the pollution index of heavy metals in Depapre waters.

2. Materials and Methods

2.1 Study area

The area of this study was the Depapre waters, Papua Province, Indonesia. It was conducted in October 2017. The locations for measurement and sampling of seawater included 5 stations, namely (1) Harlem tourism beach waters, (2) coastal waters of Tablasupa Village (settlement houses in around the waters), (3) Dua Island waters, (4) waters in the construction area of Depapre harbor, and (5) Depapre Village waters (settlement houses in surrounding land). The sampling location in this study is presented in Figure 1.

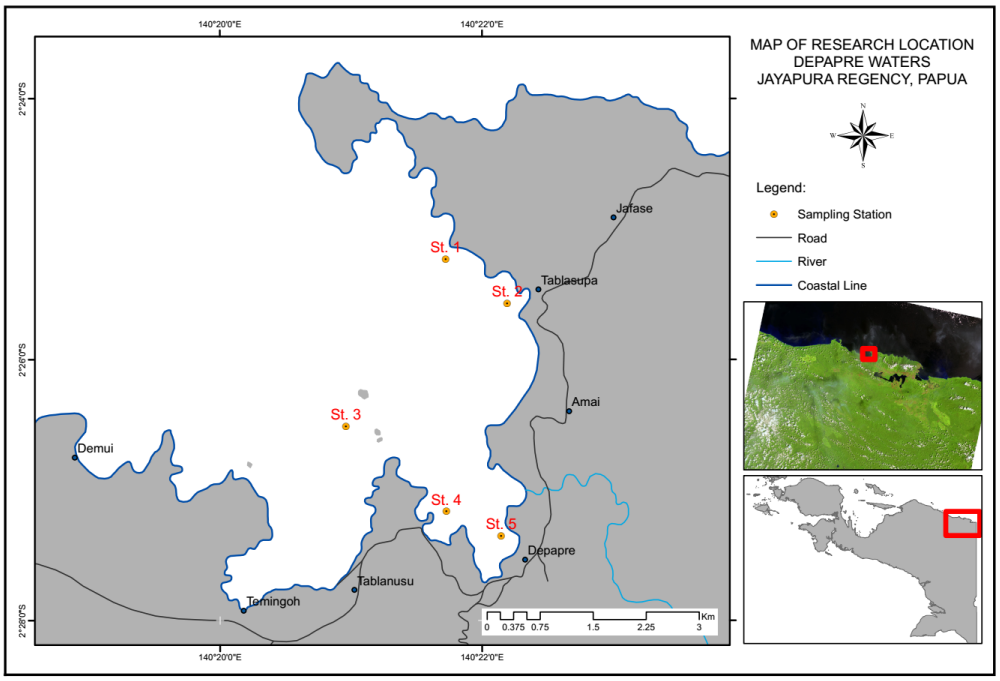

Figure 1. Locations of the sampling stations in Depapre waters, Papua Province, Indonesia

2.2 Seawater sampling and analysis

The seawater sampling was done based on the Indonesian National Standard (Standar Nasional Indonesia - SNI) method No. 6964.8.2015. In this study, seawater samples were taken once from each research station. Each sample was taken at a depth of 50 cm from the sea surface using a water sampler (Vandorn bottle). The sample was then filtered with cellulose nitrate filter paper (0.45 µm). A total of 250 ml of the sample was put into a Niskin bottle that had been filled with concentrated nitric acid (HNO_3) for the sample preservation process. Furthermore, each sample was stored in a cool box until being analyzed in the laboratory.

In the laboratory, the seawater samples were analyzed using Atomic Absorption Spectrophotometer (AAS) in the Jayapura Health Laboratory of Papua Province. The types of heavy metals and standard analysis are presented in Table 1. The data analysis was done by comparing the results of laboratory analysis with the seawater quality standards based on Minister of Environment

Decree No. 51 year 2004, which is concerned with Seawater Quality Standards that relate to lives of marine biota [25].

Table 1. Standard and analytical methods of heavy metals for seawater quality

Heavy metals	Quality standards (mg/l) *	Analytical methods
Hg	0.001	SNI 19-6964.2-2003
Cd	0.001	Standard Method 2005, Section 3111-Cd.B
Pb	0.008	Standard Method 2005, Section 3111-Pb.C
Cu	0.008	IKM/5.4.38/BLK-Papua (Spectrophotometer)
Zn	0.05	Standard Method 2005, Section 3500-Zn.C

* Minister of Environment Decree No. 51 year 2004 about Seawater Quality Standards for Marine Biota

2.3 Spatial distribution of heavy metals

The heavy metals data and coordinates were then analyzed using the Geographic Information System approach. The analysis of the spatial distribution of heavy metals involved interpolation. Interpolation is a method used to predict values on grids that are not represented by sample points [26]. The interpolation method applied in this study was the Inverse Distance Weight (IDW). IDW is a method that shows interpolation results that are similar to the maximum and minimum values of the sample data and will change linearly according to the distance from the sample data [26, 27]. The IDW method can be used on a small number of data samples whose distribution is representative [28].

2.4 Analysis of water pollution index

One of the most important indices in water quality assessment is the water pollution index [29]. The water pollution index is a useful tool to provide information about water quality. It was determined based on the Decree of the Minister of Environment No. 115 year 2003, using the following formula [17]:

$$PI_j = \sqrt{\frac{(C_i/L_{ij})_M^2 + (C_i/L_{ij})_R^2}{2}} \quad (1)$$

where:

L_{ij} : standard water quality parameter for each parameter at specified water quality purpose (j)
C_i : measured water quality parameters i
PI_j : the pollution index for a specified j water quality purpose (j)
$(C_i/L_{ij})_M$: maximum value of C_i/L_{ij}
$(C_i/L_{ij})_R$: average value of C_i/L_{ij}

The relation between the level of water pollution and the pollution index criteria based on the Decree of the Minister of Environment No. 115 year 2003 about Determination of Water Quality Status is as follows [16]:

$0 \leq PI_j \leq 1$: good quality
$1 < PI_j \leq 5$: lightly polluted
$5 < PI_j \leq 10$: moderately polluted
$PI_j > 10$: heavily polluted

3. Results and Discussion

3.1 Concentration and spatial distribution of heavy metals

This study was concerned with analysis of the quality of seawater in the Depapre waters and in particular examined whether those waters were safe or harmful to marine biota. Ideally, marine waters should meet the specified physical, chemical, and biological quality standards and waters that fail to do so are considered to be contaminated. The laboratory analysis showed that the concentrations of Cd, Pb, Cu, and Zn ranged between 0.001-0.003 mg/l, 0.001-0.005 mg/l, 0.464-0.600 mg/l, and 0.003-0.008 mg/l, respectively. Meanwhile, the concentration of Hg could not be detected because the value was smaller than the limit of detection of the tool used. The results of the analysis of heavy metals concentration in Depapre waters are presented in Table 2.

Table 2. The heavy metals concentration in Depapre waters, Jayapura Regency, Papua, Indonesia

Stations	Heavy metals concentration (mg/l)				
	Hg*	**Cd**	**Pb**	**Cu**	**Zn**
1	<0.0008	0.003	0.001	0.600	0.004
2	<0.0008	0.002	0.005	0.554	0.003
3	<0.0008	0.001	0.002	0.464	0.005
4	<0.0008	0.002	0.003	0.502	0.003
5	<0.0008	0.001	0.005	0.592	0.008

* <0.0008 mg/l are below the detection limit.

According to the quality standards for heavy metals concentration for marine biota, the concentrations of Hg, Pb, and Zn met the quality standards of seawater. On the contrary, the concentration of Cd at stations 1, 2, and 4, and also the Cu concentration at all observation stations was higher than the quality standards for marine biota. Even low concentrations of heavy metals in seawater do not mean that these pollutants will not have a negative impact, and this is especially the case with non-essential heavy metals. Heavy metals can be dangerous for marine biota, especially if the concentration inside the seawater is higher than the quality standard [30, 31]. Heavy metals that accumulate in sediments and marine organisms may be of increased concentration depending on the condition of the waters [32]. Hg, Pb, Cd, and Cu can be very dangerous because of biomagnification, which means that they accumulate in an organism's body over time and reach toxic levels [33].

The spatial distribution of heavy metals (except Hg) in Depapre waters are presented in Figure 2. Generally, heavy metals concentrations (except Zn) in research locations tended to be higher nearer to the beach and lower towards the open water. Heavy metals distributions in seawaters can be influenced by several inputs and water dynamics [13], topography, patterns of wind movement, and circulation of surface currents [34, 35]. The availability of heavy metals in the waters is influenced by dynamic system influences (tidal flow), hydraulic systems, organic materials, and salinity [36].

The sources of heavy metals varied in each body of seawater. Heavy metals in Depapre waters were thought to be the results of human activities and natural sources. Because there is no waste in the area due to industrial activity, which is one of the biggest sources of heavy metal pollution in waters, the heavy metals in Depapre waters are suspected to have come from activities such as household waste disposal, small-scale agricultural, fisheries, and marine transportation. Research has shown that in general, the higher the level of human activities in coastal and seawaters

areas, the bigger the possibility of an increase of heavy metals concentrations in seawaters. Naturally, heavy metals concentrations in seawater are very low (around 10^{-5}-10^{-2} ppm); however, they can accumulate in seawaters by various means [6]. Mercury can get into waters from volcanic activities and groundwater seepages that have passed through areas of mercury deposits. Lead enters the sea through crystallization in the air and then with the assistance of rain, as well as from mineral stones that erode due to waves and wind. Copper also finds its way into bodies of water due to erosion of minerals. Furthermore, Cu compounds present on the atmosphere can be brought down by the rain. Cadmium naturally enters waters in smaller amounts [37].

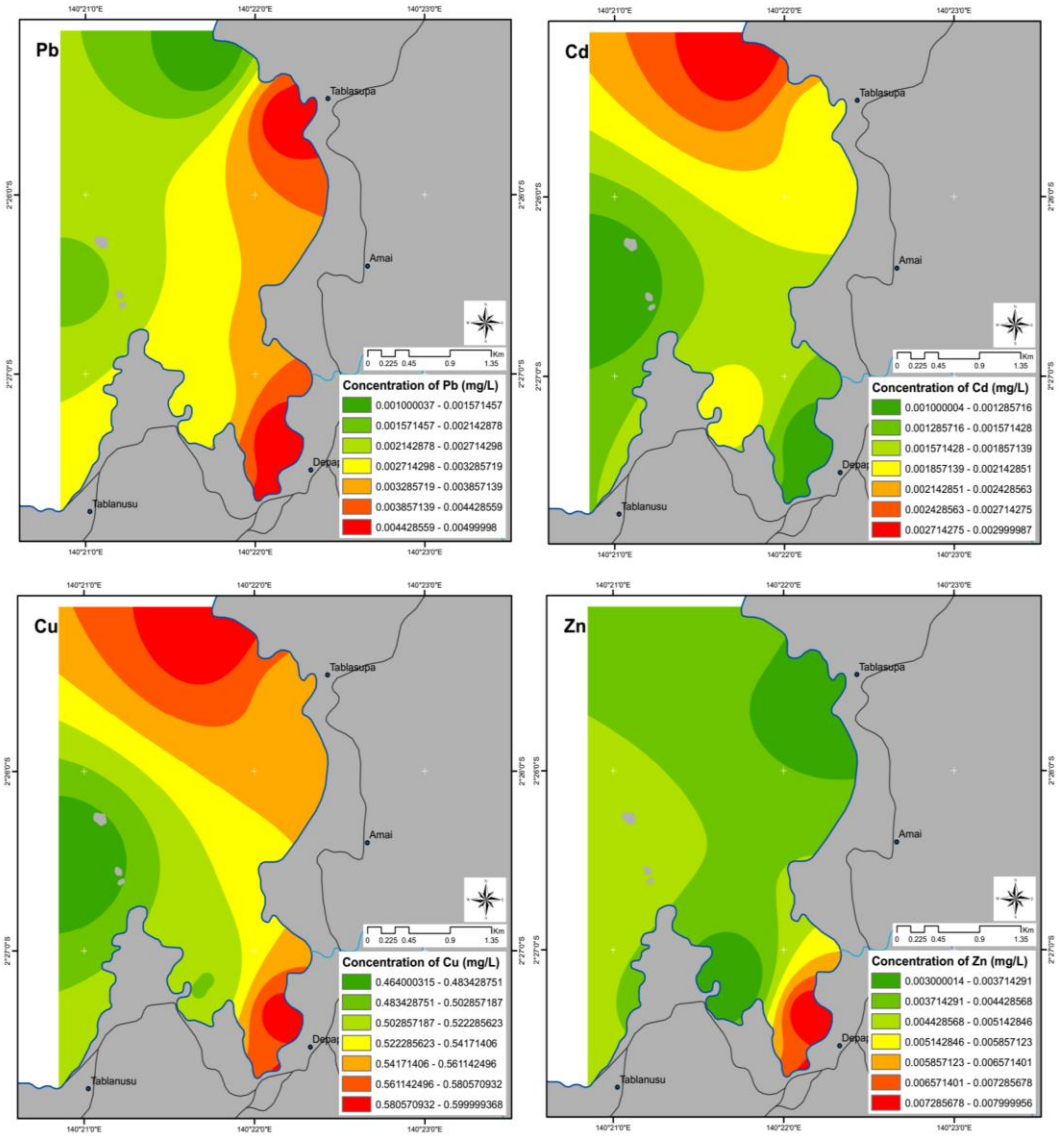

Figure 2. The spatial distribution of heavy metals concentrations (Pb, Cd Cu, and Zn) in Depapre waters, Papua Province, Indonesia

Spatially, the interpolation results of the distribution of Cu and Cd in Depapre waters exceed the quality standards. Although Cu is classified as an essential heavy metal that is needed by aquatic organisms, it can be highly toxic to aquatic organisms at higher concentrations. This is in contrast to Cd, which is classified as a non-essential heavy metal that is very dangerous for aquatic organisms. It needs special attention because Cd is toxic even though its concentration in seawaters is low and because it is persistent. In aquatic ecosystems, Cd contamination has great effects on ecosystem function, structure, and biogeochemical nutrition of water [38, 39]. Heavy metal pollution in seawaters can act as an important intermediary for subsequent pollution in aquatic ecosystems or public health [40]. Various human activities are suspected to be sources of Cd in Depapre waters, and included are household waste disposal, agricultural waste disposal, and marine transportation activities.

3.2 Water pollution index based on heavy metal concentrations

The water pollution index functions as a tool to discover and express pollution levels in waters. The water pollution index provides a single assessment score of various environmental parameters, and it is analyzed to interpret the water quality [41]. The results from the analysis of the pollution index values at each station are fully presented in Figure 3. According to the results of the pollution index evaluation of heavy metals, all the research stations can be classified in the moderately polluted category with water pollution index values in the range of 6.94-7.34.

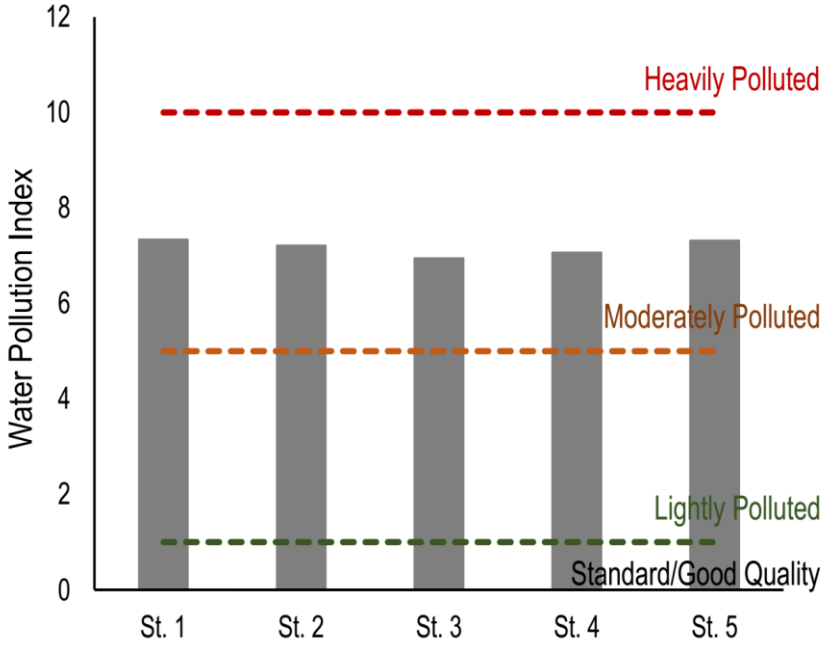

Figure 3. Water pollution index based on heavy metals concentration in Depapre waters, Papua Province, Indonesia

Based on the analysis of heavy metal concentrations, the high concentration of Cu was the largest input contributing to the high index of heavy metal pollution in Depapre waters. This high Cu concentration needs to be monitored because if the Cu concentration keeps increasing, it will surely have a negative impact on marine biota and the local society. The Cd concentration also influenced the determination of the water pollution index, although it was not as significant as the Cu concentration. The evaluation of the results of water pollution index-based study of heavy metals concentrations may provide solutions for decision-makers who must value the quality of waters for allocations, and fix up the quality of waters if there is quality decrease caused by the presence of contaminated materials.

Although the water pollution index only shows the level of relative pollution, it can be used as a reference for the regional government to mitigate pollution in local seawaters. Therefore, the regional government must define strategies and actions for the prevention and control of seawater pollution and the recovery of seawater quality. The purpose of monitoring is not to detect minor fluctuations that are quickly disappearing but to detect significant changes in sea waters and aquatic ecosystems, so spatial and temporal monitoring of seawater quality is needed.

4. Conclusions

The heavy metals found in Depapre Waters came from household waste disposal, farming activities, minor-scaled fisheries, marine transportation, and also from natural processes. The copper concentration in all locations, and cadmium in three research stations, were higher than the limits indicated in the water quality standards, whereas the concentrations of mercury, lead and zinc in all locations were within standard range for water quality for marine biota. Heavy metals distributions (except Zn) tended to be higher near to the beach and lower towards open water. According to the results of the pollution index of heavy metals, the Depapre waters have been classified into the moderately polluted category, and show water pollution indexes in the range of 6.94-7.34. The concentrations of Cu and Cd as inputs caused the high value of the heavy metal pollution index in Depapre waters. There is a need for policies and regulations from the regional government to regulate the disposal of waste in an effort to control pollution in the area's seawaters, and the disposal of both anthropogenic and industrial waste need to be monitored. The research also suggests that authorities need to keep a close eye on the disposal of fuel and ballast water of ships. If the concentration of heavy metals in seawaters can be controlled, the quality of sea waters will also be good. This assessment of the concentration and distribution of pollutants provides more than just a way of determining the water pollution index; it also provides information on water quality that gives a picture of the overall level of water pollution. The concentrations of heavy metals in seawaters that come out of this study can be used as baseline data for future activities.

References

[1] Chen, C.-W., Kao, C.-M., Chen, C.-F. and Dong, C.D., 2007., Distribution and accumulation of heavy metals in the sediments of Kaohsiung harbor, Taiwan. *Chemosphere*, 66(8), 1431-1440.

[2] Drira, Z., Sahnoun, H. and Ayadi, H., 2017. Spatial distribution and source identification of heavy metals in surface waters of three coastal areas of Tunisia. *Polish Journal of Environmental Studies*, 26(3), 1057-1069.

[3] Hamuna, B., Tanjung, R.H.R. and Alianto, 2019. Assessment of water quality and pollution index in coastal waters of Mimika, Indonesia. *Journal of Ecological Engineering*, 20(2), 87-

94.

[4] Tanjung, R.H.R., Hamuna, B. and Yonas, M.N., 2019. Assessing heavy metal contamination in marine sediments around the coastal waters of Mimika Regency, Indonesia. *Journal of Ecological Engineering*, 20(11), 35-42.

[5] Suryono, C.A. and Rochaddi, B., 2013. Connectivity heavy metals in shallow groundwater, sediment and seawater in coastal area. *Ilmu Kelautan: Indonesian Journal of Marine Science*, 18(2), 91-96. [in Indonesian]

[6] Hutagalung, H.P., Setiapermana, D. and Khozanah., 1997. Organochlorine, oil and heavy metals in Siak estuary, Riau, Indonesia. *Proceedings of the ASEAN Canada Technical Conference on Marine Science*, Penang, Malaysia, June 24-29, 1996, 817 pp.

[7] Ismarti, I., Ramses, R., Amelia, F. and Suheryanto, S., 2017. Concentration of copper (Cu) and lead (Pb) in seagrass *Enhalus accoroides* harvested from Batam waters, Riau Islands, Indonesia. *Depik*, 6(1), 23-30. [in Indonesian]

[8] Koropitan, A.F. and Cordova, M.R., 2017. Study of heavy metal distribution and hydrodynamic simulation in green mussel culture net, Cilincing water - Jakarta Bay. *Makara Journal of Science*, 21(2), 91-99.

[9] Riza, F., Bambang, A.N. and Kismartini., 2016. Water environment pollution of heavy metals Pb, Cd and Hg in Jepara Kartini beach Central Java, Indonesia. *Research Journal of Marine Sciences*, 4(1), 1-4.

[10] Tjahjono, A., Bambang, A.N. and Anggoro, S., 2017. Analysis of heavy metal content of Pb in ballast water tank of commercial vessels in port of Tanjung Emas Semarang, Central Java Province. *Journal of Ecological Engineering*, 18(2), 7-11.

[11] Tjahjono, A. and Suwarno, D., 2018. The spatial distribution of heavy metal lead and cadmium pollution and coliform abundance of waters and surface sediment in Demak. *Journal of Ecological Engineering*, 19(4), 43-54.

[12] Tupan, C.I. and Uneputty, P.A., 2017. Concentration of heavy metals lead (Pb) and cadmium (Cd) in water, sediment and seagrass *Thalassia hemprichii* in Ambon Island waters. *AACL Bioflux*, 10(6), 1610-1617.

[13] Hariyadi, S., Muflih, A., Mashar, A., Widigdo, B. and Wardiatno, Y., 2017. Spatial distribution of some heavy metals in the sediments of Tangerang Coastal waters, Banten Province, Indonesia. *AES Bioflux*, 9(2), 120-134.

[14] Arifin, Z., 2011. Heavy metals concentrations in water, sediment and biota in Kelabat bay, Bangka Island. *Jurnal Ilmu dan Teknologi Kelautan Tropis*, 3(1), 104-114. [in Indonesian]

[15] Hananingtyas, I., 2017. Studi pencemaran kandungan logam berat timbal (Pb) dan kadmium (Cd) pada ikan tongkol (*Euthynnus sp*.) di Pantai Utara Jawa. *BIOTROPIC: The Journal of Tropical Biology*, 1(2), 41-50. [in Indonesian]

[16] Kementerian Negara Lingkungan Hidup., 2003. *Keputusan Menteri Lingkungan Hidup Nomor 115 Tahun 2003 Tentang Penetapan Status Mutu Air*. Jakarta: Kementerian Negara Lingkungan Hidup. [in Indonesian]

[17] Nemerow, N.L. and Sumitomo, H., 1970. *Benefits of Water Quality Enhancement*. Report No. 16110 DAJ, prepared for the U.S. Environmental Protection Agency.

[18] Zulfa, N., Effendi, H. and Riani, E., 2016. Preliminary rapid fishing port water quality assessment with pollution index. *AES Bioflux*, 8(1), 96-106.

[19] Effendi, H. 2016., River water quality preliminary rapid assessment using pollution index. *Procedia Environmental Sciences*, 33(2016), 562-567.

[20] Sutadian, A.D., Muttil, N., Yilmaz, A.G. and Perera, B.J.C., 2018. Development of a water quality index for rivers in West Java Province, Indonesia. *Ecological Indicators*, 85, 966-982.

[21] Saraswati, S.P., Ardion, M.V., Widodo, Y.H. and Hadisusanto, S., 2019. Water quality index performance for river pollution control based on better ecological point of view (a case study in Code, Winongo, Gadjah Wong streams). *Journal of the Civil Engineering Forum*, 5(1), 47-

55.
[22] Widodo, T., Budiastuti, M.T.S. and Komariah., 2019. Water quality and pollution index in the Grenjeng River, Boyolali Regency, Indonesia. *Caraka Tani: Journal of Sustainable Agriculture*, 34(2), 150-161.
[23] Yani, A., Amin, M., Rohman, F., Suarsini, E. and Haerunnisa., 2019. Water quality and pollution index of Lake Tempe in South Sulawesi, Indonesia. *Pollution Research*, 38(3), 568-574.
[24] Hamuna, B., Tanjung, R.H.R., Suwito, Maury, H.K. and Alianto, 2018. Kajian kualitas air laut dan indeks pencemaran berdasarkan parameter fisika-kimia di perairan Distrik Depapre, Jayapura. *Jurnal Ilmu Lingkungan*, 16(1), 35-43. [in Indonesian]
[25] Kementerian Negara Lingkungan Hidup., 2004. *Keputusan Menteri Negara Lingkungan Hidup Nomor 51 Tahun 2004 Tentang Baku Mutu Air Laut*. Jakarta: Kementerian Negara Lingkungan Hidup. [in Indonesian]
[26] Childs, C., 2004. *Interpolating Surfaces in ArcGIS Spatial Analyst, Esri Education Series*. [online] Available at: https://www.esri.com/news/arcuser/0704/files/interpolating.pdf
[27] Yang, C., Kao, S., Lee, F. and Hung, P., 2004. Twelve different interpolation methods: A case study of Surfer 8.0. *20th International Congress for Photogrammetry and Remote Sensing; ISPRS XXth Congress*, 35(B2), 778-785.
[28] Yasrebi, J., Saffari, M., Fathi, H., Karimian, N., Moazallahi, M. and Gazni, R., 2009. Evaluation and comparison of ordinary kriging and inverse distance weighting method for prediction of spatial variability of some soil chemical parameters. *Research Journal of Biological Science*, 4(1), 93-102.
[29] Dunca, A.M., 2018. Water pollution and water quality assessment of major transboundary rivers from Banat (Romania). *Journal of Chemistry*, 2018, 1-8.
[30] Pinet, P.R., 2009. *Invitation to Oceanography*. 5th ed. Ontario: Jones and Bartlett Publishers.
[31] Arifin, Z. and Fadhlina, D., 2009. Fraksinasi logam berat Pb, Cd, Cu dan Zn dalam sedimen dan bioavailabilitasnya bagi biota di perairan Teluk Jakarta. *Ilmu Kelautan: Indonesian Journal of Marine Science*, 14(1), 27-32. [in Indonesian]
[32] Edward, 2015. Evaluation on heavy metals pollution in sediment in Morotai Island waters, North of Maluku. *Depik*, 4(2), 95-106. [in Indonesian]
[33] Siregar, T.H. and Murtini, J.T., 2008. Kandungan logam berat pada beberapa lokasi perairan Indonesia pada tahun 2001 sampai dengan 2005. *Squalen*, 3(1), 7-15. [in Indonesian]
[34] Sagala, S.L., Bramawanto, R., Kuswardani A.R.T.D. and Pranowo, W.S., 2014. Distribution of heavy metals in Natuna coastal waters. *Jurnal Ilmu dan Teknologi Kelautan Tropis*, 6(2), 297-310. [in Indonesian]
[35] Sagala, S.L., Kusumaningtyas, M.A., Adi, R.A., Kuswardani, A.R.T.D. and Pranowo, W.S., 2013. Distribution of polycyclic aromatic hydrocarbons (PAH) in Natuna coastal waters. *Asian Journal of Water, Environment and Pollution*, 10(4), 25-31.
[36] Laing, G.D., Vanthuyne, D., Tack, F.M.G. and Verloo, M.G., 2007. Factors affecting metal mobility and bioavailability in the superficial intertidal sediment layer of the Scheldt estuary. *Aquatic Ecosystem Health and Management*, 10(1), 33-40.
[37] Palar, H., 2008. *Pencemaran dan Etoksiologi Logam Berat*. Jakarta: PT Rineka Cipta. [in Indonesian]
[38] Hayes, F., Spurgeon, D.J., Lofts, S. and Jones, L., 2018. Evidence-based logic chains demonstrate multiple impacts of trace metals on ecosystem services. *Journal of Environmental Management*, 223, 150-164.
[39] Zhao, D., Li, J., Lv, L., Zhang, M., Liu, Z. and An, S., 2019. Effect of cadmium contamination on the eutrophic secondary pollution of aquatic macrophytes by litter decomposition. *Journal of Environmental Management*, 231, 1100-1105.

[40] Aly-Salem, D.M.S., Khaled, A., El-Nemr, A. and El-Sikaily, A., 2014. Comprehensive risk assessment of heavy metals in surface sediments along the Egyptian Red Sea coast. *Egyptian Journal of Aquatic Research*, 40, 349-362.

[41] Popović, N.Z., Đuknić, J.A., Atlagić, J.Z.C., Raković, M.J., Marinković, N.S., Marinković, B.P. and Paunović, M.M., 2016. Application of the water pollution index in the assessment of the ecological status of rivers: a case study of the Sava river, Serbia. *Acta Zoologica Bulgarica*, 68(1), 97-102.

Productivity Improvement of Motorcycle Headlight Assembly through Line Balancing Using Simulation Modeling: A Case Study

Woraya Neungmatcha and Atiwat Boonmee*

Industrial Engineering Department, Faculty of Engineering at Kamphaeng Saen, Kasetsart University, Nakon Pathom, Thailand

Received: 13 April 2020, Revised: 15 June 2020, Accepted: 13 July 2020

Abstract

The purpose of this paper is to increase the efficiency of the production of motorcycle headlights by balancing the assembly line in order to achieve maximum utilization of manpower. Since the motorcycle headlight assembly in question is a new production line, this research can be seen as providing a supportive approach to achieving work full efficiency. It was observed that improvements can be made to the arrangements of the various elements that form the production line. Therefore, the reseachers proposed a solution that incorporates production line balancing and improvements of work techniques. Simulation with the Arena program is used to analyze the results of the current working conditions and these are compared to the various alternative strategies proposed. The results show that the proposed improvements can help to increase the productivity of motorcycle headlight production line (production cycle time reduced by 25.51 % and production capacity increased by 28.36 % compared to the current situation) and involve more efficient use of manpower (the utilization of manpower increased by 13.33 % compared to the exisitng situation). Moreover, this research and the proposed improvements point to further research aimed at better meeting the monthly demands for product of customer.

Keywords: Motorcycle headlight; line balancing; work improvement; simulation
DOI 10.14456/cast.2021.5

1. Introduction

The Thai automotive industry is likely to expand further as the domestic economy and the global economy improve. Motor vehicle production has been continuously increasing, and this has stimulated the automotive parts industry to develop and grow in accordance with the directions of the automobile and motorcycle production industries. The parts that continue to be in demand are mechanical parts such as car frames and bodies, suspensions, car accessories and lighting systems, all of which are expected to continue to increase in demand. The company involved in this case study is one of the companies that produce automotive lighting equipment for a large automotive distribution company. At present, the company studied in this research, which produces automotive lighting devices, has problems that relate to insufficient labor resources when demand for product is high. This case study of the motorcycle headlight assembly line found that as the motorcycle

*Corresponding author: Tel.: (+66)-893956932 Fax: (+66) 343511404
E-mail: fengawbo@ku.ac.th

headlight parts were new models, there was no development plan for the assembly line. Furthermore, the research showed that even when the current line setup operates at maximum capacity, the level of production is still less than the maximum demand of customers. It was also found that the main problem of this assembly process is an improper balancing of the production line. Notably, the company had a policy to reduce the use of employees in this production process from 6 people to 5 people. Therefore, the aim of this research, which is concerned with the flow process and working charts of the motorcycle headlight assembly line, is to improve the production efficiency of the line.

Line balancing is about equalizing the workload or assigning working operations to workstations across all operations along the production line in order to remove bottlenecks and excess capacity [1]. Assembly line balancing was first proposed in Helgeson and Birnie [2]. The various techniques of line balancing, which vary according to specific aspects of the manufacturing process, have been widely used and applied for many years [3, 4]. Manufacturing throughput is dependent on the length of time each task requires on the line. With so many different and potentially conflicting requirements on the system, the outcomes of line balancing processes can be difficult to predict. Factors such as the rapid rate of and uncertainty that occur in each process, interactions among employees, and the different transfer times between workstations make it difficult to optimize. Although analytical methods can be used, there are limitations due to the dynamic nature of the system [5, 6]. Therefore, a simulation model is an easier way to create a model that can identify problems and bottlenecks in the real system, and thus facilitate better production efficiency, resource usage, and time usage [7, 8]. In this work, simulation was used to analyze the current system and propose and study an optimized alternative before implementation in the real system, thus minimizing risk, error, and uncertainty [7]. Simulation techniques have been widely used for development and decision-making support in many fields, such as manufacturing, transportation, production distribution, banking and health care [9]. The advantages of simulation were found to be reasonableness, provability and output comparison. It gives a re-configurable assembly line the flexibility needed to improve the throughput of the assembly line and working cells while reducing the need for manpower. These outcomes can all help the enterprise to meet growing customer demand. In addition, more effective techniques of work can reduce wasted time, increase production efficiency and facilitate smooth production levels [1]. Therefore, the important criteria to do with motorcycle headlight production in this paper are whether or not assembly line output meets the demands of the customers, and how employees are being utilized. To realize this approach, various combinations of work improvement, line balancing and simulation technique are applied to the assembly line to increase the efficiency of the motorcycle headlight assembly line. The proposed model 1 is a line balancing technique (LB model) and the proposed model 2 involves eliminating unnecessary work and work technique improvements (LB+Work Improvement model). Moreover, the results of the research can not only improve the system studied; they can also be implemented on a bigger scale in larger industrial situations.

2. Materials and Methods

2.1 Analysis of production process flow

A study of work and data collection using an operations chart shows that there are work sequences and division of 22 sub-tasks, and the details of each step is shown in Figure 1.

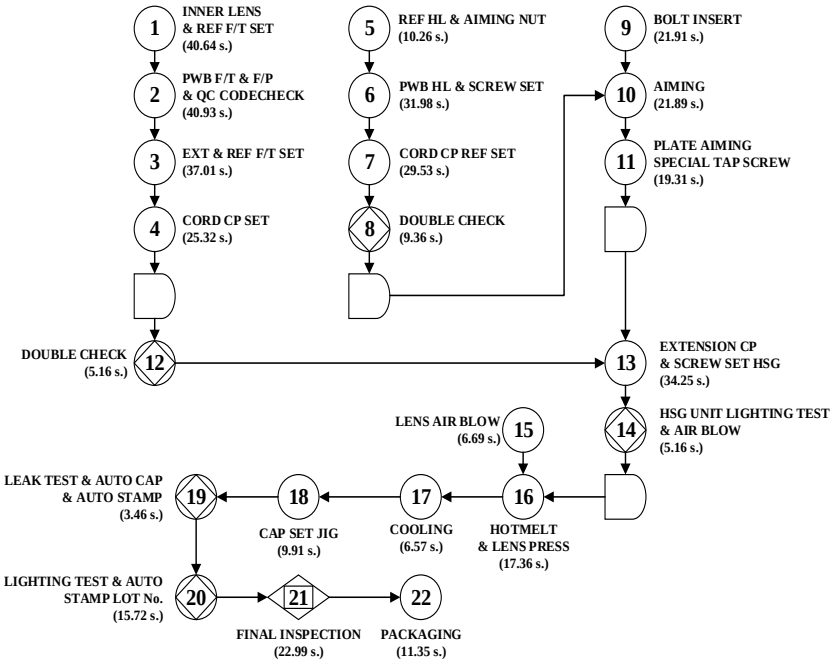

Figure 1. The flow process of the motorcycle headlight assembly line

Under present working conditions, it is found that there are production plans in the case of using 6 employees and 5 employees (the latter being part of a plan to reduce resources). The working diagram of the production process in both cases is shown in Figures 2 and 3, respectively.

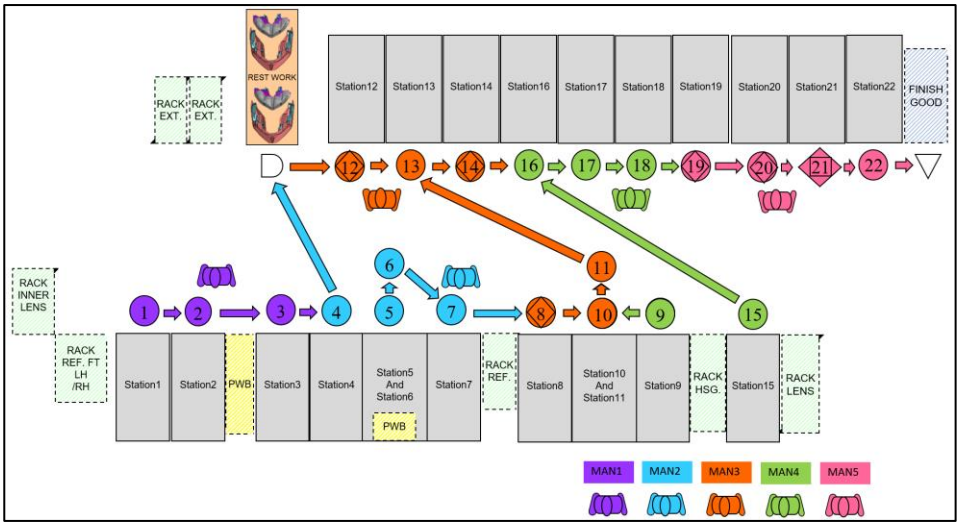

Figure 2. The operation of the motorcycle headlight assembly while operating with 5 people

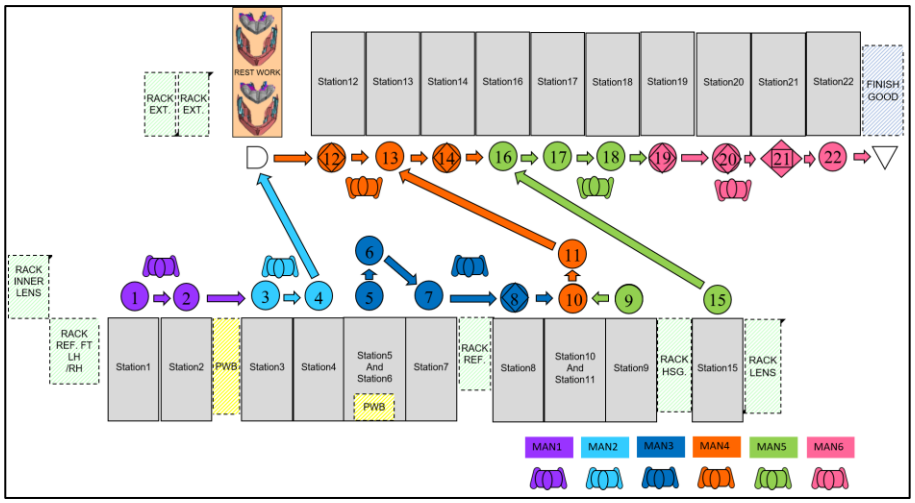

Figure 3. The operation of the motorcycle headlight assembly while operating with 6 people

2.2 Analysis of causes of problems and solutions

The analysis of the causes of the problems and the solutions to the problems is based on the why-why analysis principles. These can summarize the causes of the problems and the solutions, and are shown in Table 1. The root cause of the problem consists in the skill of the staff because it is a new production line. The solution is to train employees to be fluent in their positions. In addition, the utilization and the working order are not consistent with the alignment of the machines. The solution is to line balance and adjust the workstation positions along the production line.

Table 1. The why-why analysis

Problem/Why?	Why?	Answer	Solution
1) Skill of the staff	Why do employees not have expertise in their work?	This is a new production line.	Training of employees
2) Some staff are not working at full utilization	Why are employees not working at full utility?	Work assignments are not balanced.	Line Balancing
	Can the workload be balanced?	Yes, but it must comply with the work order conditions	
3) The work order does not correspond to the alignment of the machine.	Why is it not consistent?	The formatting of the layout in the production line and the work order are unbalanced.	Re-position the production line
	Can the workload be balanced?	Yes, but it must comply with the work order conditions	Line Balancing

2.2.1 Product demand quantity and takt time

Table 2 shows a list of quantity of orders in units per month. The quantity of product demand is used to calculate the takt time (takt time = net working time /number of work pieces needed) according to the customer's requirements. The company has 21 working hours per month and 20 h per day (net working time = (20x3600)x21 = 1,512,000 s).

Table 2. Product demand quantity (pieces/month) and takt time (second per piece)

Month	Demand quantity	Takt time	Month	Demand quantity	Takt time
1	12,876	117.43	7	16,086	93.99
2	20,839	72.56	8	14,790	102.23
3	17,653	85.65	9	17,102	88.41
4	15,944	94.83	10	15,928	94.93
5	14,534	104.03	11	15,062	100.39
6	14,420	104.85			

2.2.2 Cycle time

From the analysis of data on current production work, a summary has been prepared that shows the workload of each person assigned and the cycle time of work of each person in the production of one workpiece in the case of 5 employees per line (Figure 4), and for 6 people employees per line (Figure 5). The figures also show the workload utilization of the production line.

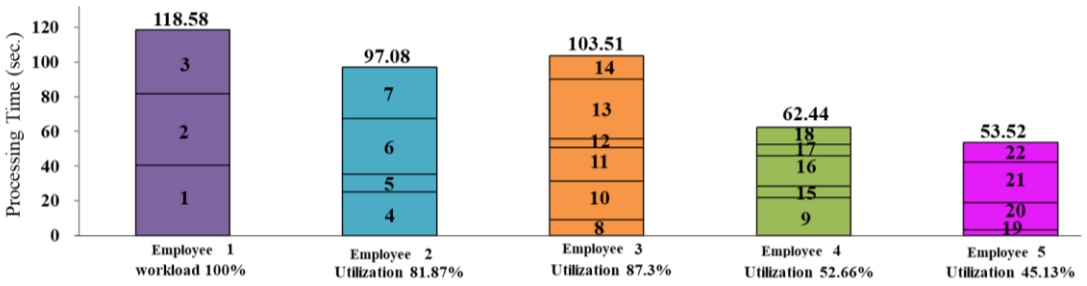

Figure 4. Workload in the case of having 5 production line staff

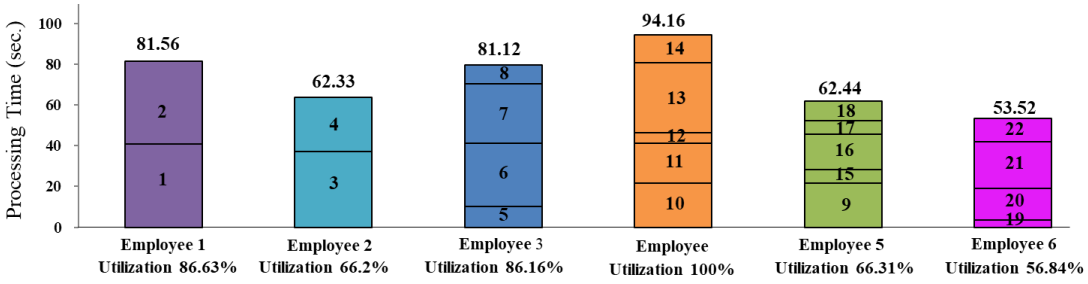

Figure 5. Workload in the case of having 6 production line staff

2.3 Production improvement

2.3.1 Line balancing technique (LB model)

In this research, we balance the production line with the rank positional weight method [10], which includes a network of all 22 sub-tasks, as shown in Figure 6.

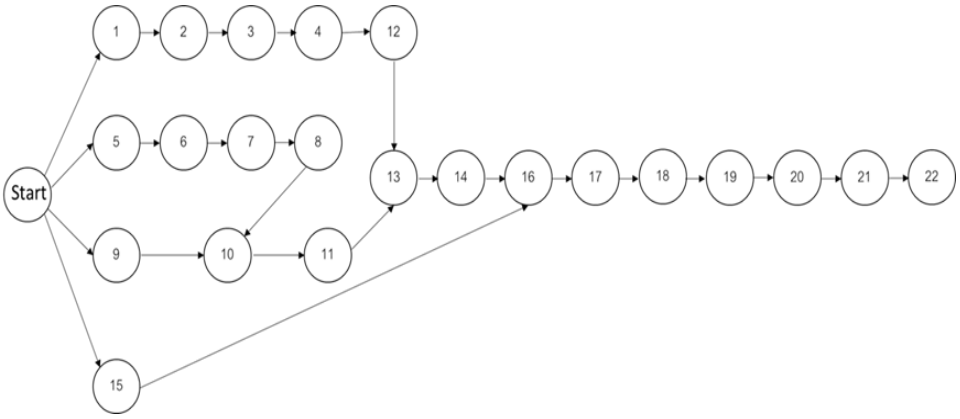

Figure 6. The network of all 22 sub-tasks

The conditions of production are sub-tasks between pairs 3 and 4, pairs 5 and 6, pairs 13 and 14, and pairs 18 and 19, which are tasks that need to be done on the same machine. In addition, the inspection tasks in steps 8 and 12 cannot use the same workers that work in steps 7 and 4, respectively. A summary of the assigned workload utilization of the production line after line balancing is detailed in Figures 7 and 8.

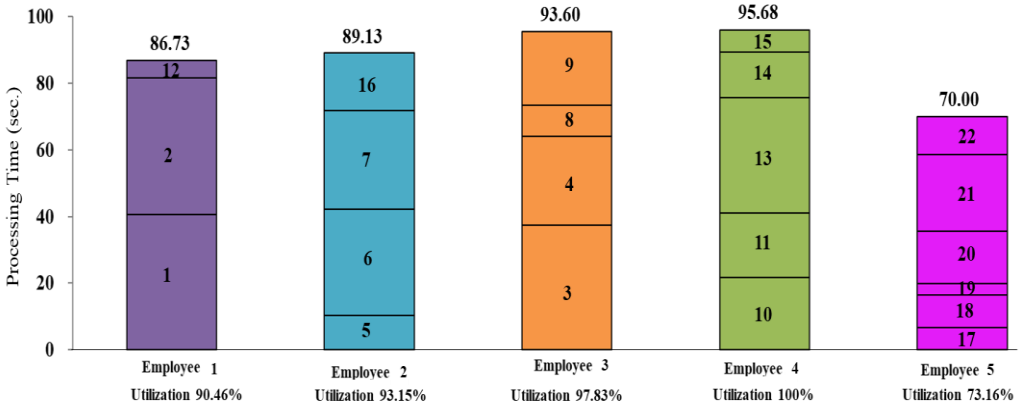

Figure 7. Workload in the case of having 5 employees after balancing the production line

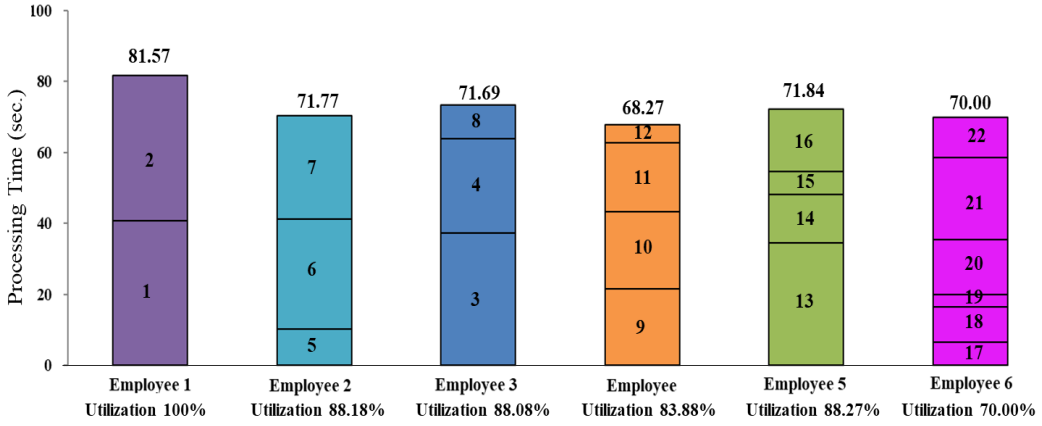

Figure 8. Workload in the case of having 6 employees after balancing the production line

After balancing the production line, the position of the workload has changed. The layout and placement of machines in the new production process are critical and must be in line with the new work order. Furthermore, the layout and placement of machines must be adjusted under the constraints of the production line space and the possibilities of relocating each machine. A updated flowchart that reflects the balancing is shown in Figures 9 and 10, respectively.

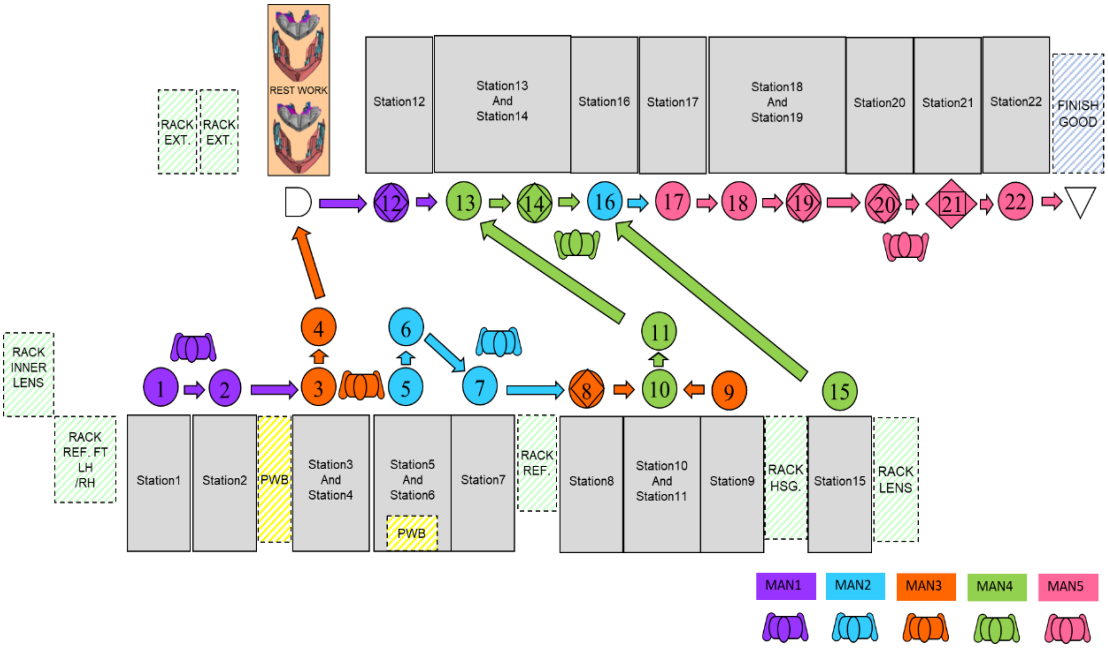

Figure 9. Workflow after balancing the production line with 5 people working

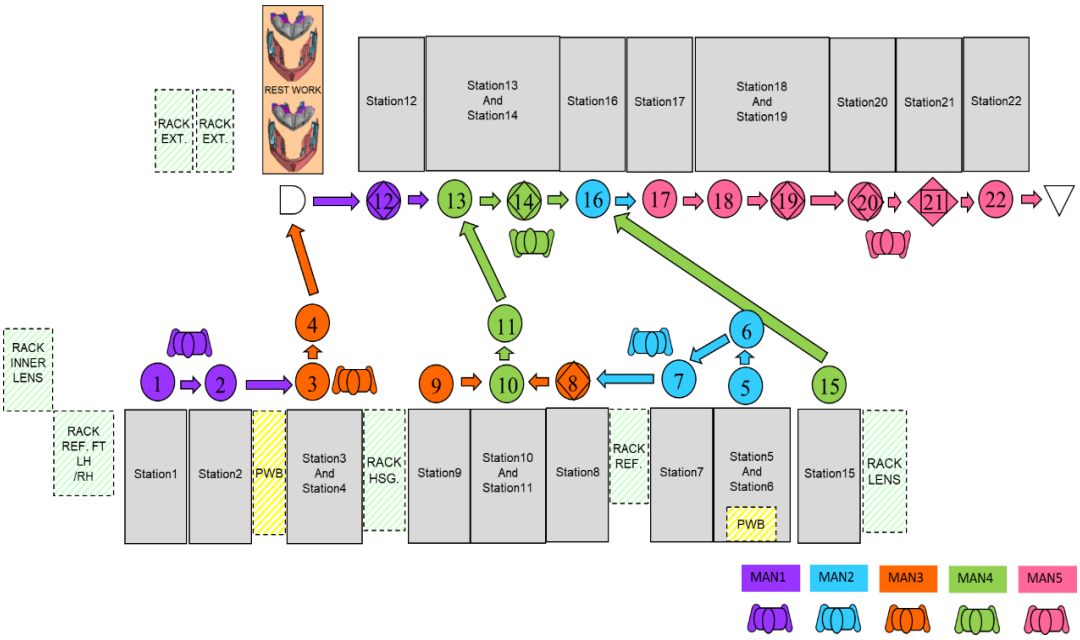

Figure 10. Workflow after balancing the production line with 6 people working

2.3.2 Eliminating unnecessary work with work improvement techniques (LB+work improvement model)

The analysis of the current process reveals that the 1st sub-task is a task that prepares parts from the previous production line. The application of ECRS technique (Eliminate, Combine, Rearrange, Simplify) eliminates this sub-task from the process, reducing the total time to 40.64 s. After cutting the 1st sub-task from the process, the effects of rebalancing the production line for both 5 and 6 employees on the assigned workload utilization of the production line is detailed in Figures 11 and 12, respectively.

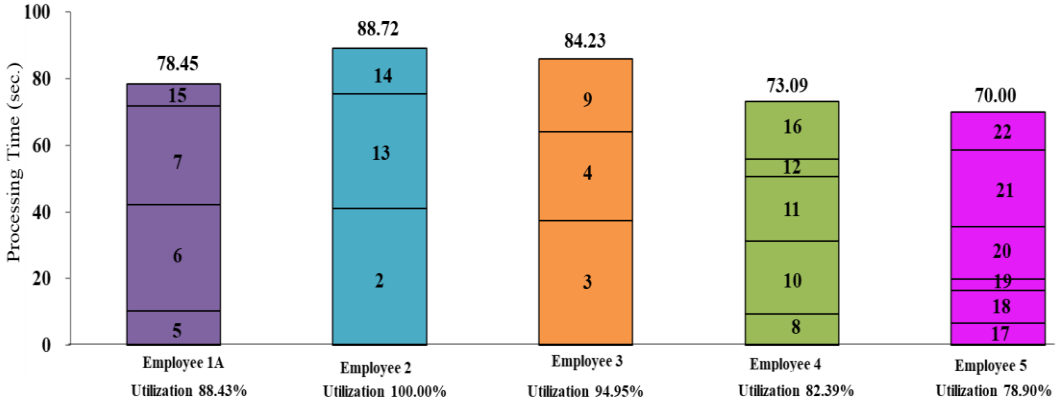

Figure 11. Workload in case of having 5 staff members after line balancing and work improvement

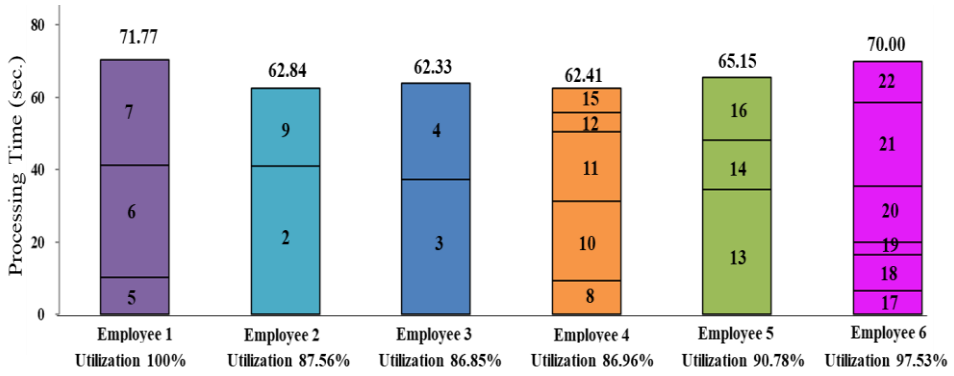

Figure 12. Workload in case of having 6 staff members after line balancing and work improvement

2.4 Simulation model

The study of the process flow of the system and the collection of the necessary information enables the development of the current workflow model using the Arena program. The systematic diagram (Figure 13) that shows the entities that are fed into the system through each process is clear and most consistent with the actual situation. The model that was developed (represented in Figure 14) mimics the actual production process. Data obtained from the model's processing, when analyzed, supports the uncertainty of the real situation. The system of interest in this study consists in the important components as shown in Table 3. The working time data for each workstation is analyzed for distribution with the input analyzer in the Arena program. Hypothesis testing is performed using the chi-square test at the 95% confidence interval. The p-value is greater than 0.05, causing all data used in the test to have probability distributions that can be used to represent the data in the simulation. The distribution of time in the motorcycle front lamp assembly line of each workstation is shown in Table 4.

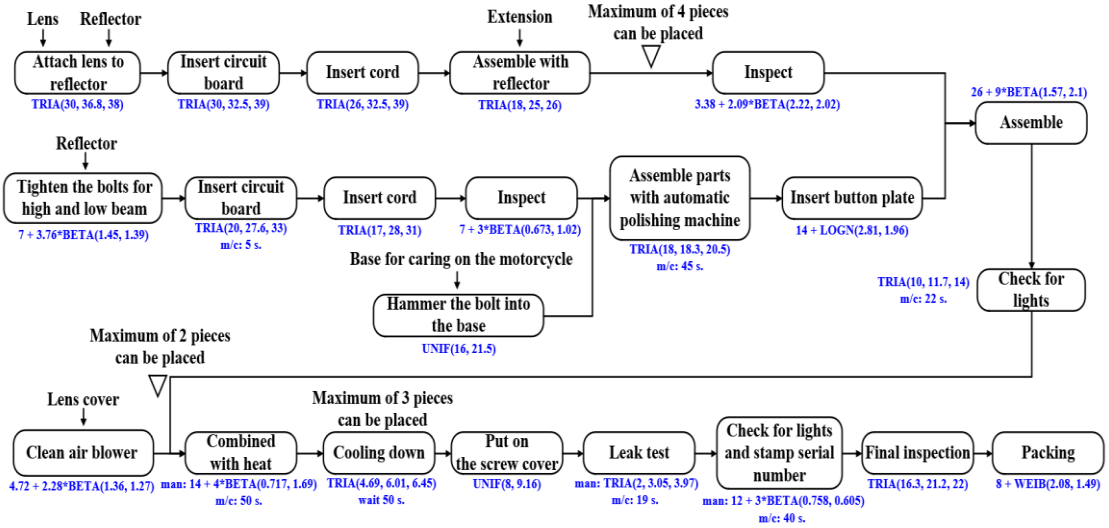

Figure 13. Systematic diagram

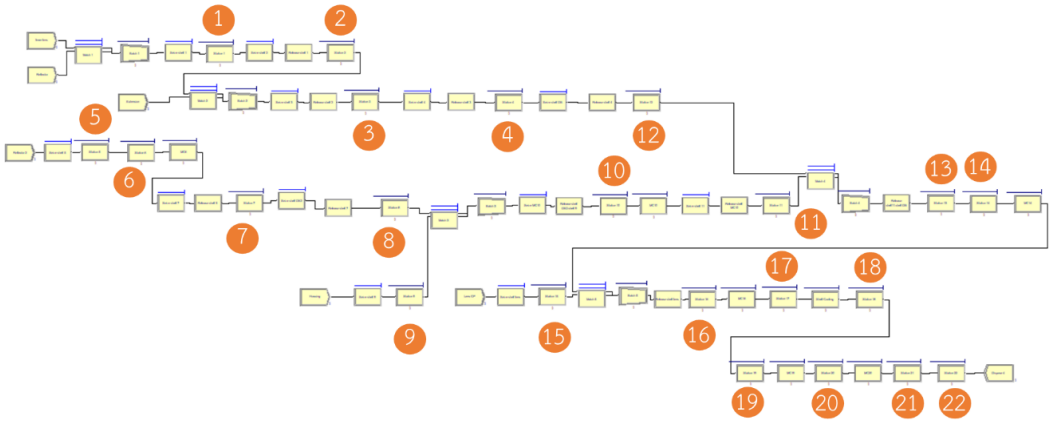

Figure 14. Simulation model

Table 3. Details of system components of the simulation model

Components	Details
Entity	The object of interest that flows into the system is the motorcycle headlight component.
Resource	Resources used in activities such as employees, machinery, etc.
Activity	Operations that occur at a certain time, such as assembly, etc.
Variable	System status indicators such as assembly time, etc.
Event	Activities that result in and change the status of variables such as entering the assembly line or ending the assembly, etc.

Table 4. Distribution of time (s) of each workstation

St.	Expression	St.	Expression	St.	Expression
1	TRIA(30,36.8,38)	9	UNIF(16,21.5)	17	TRIA(4.69,6.01,6.45)
2	TRIA(30,35.8,41)	10	TRIA(18,18.3,20.5)	18	UNIF(8,9.16)
3	TRIA(26,32.5,39)	11	14+LOGN(2.81,1.96)	19	TRIA(2,3.05,3.97)
4	TRIA(18,25,26)	12	3.38+2.09*BETA(2.22,2.02)	20	12+3*BETA(0.758, 0.605)
5	7+3.76*BETA(1.45,1.39)	13	26+9*BETA(1.57,2.1)	21	TRIA(16.3,21.2,22)
6	TRIA(20,29.2,33)	14	TRIA(10,11.7,14)	22	8+WEIB(2.08,1.49)
7	TRIA(17,28,31)	15	4.72+2.28*BETA(1.36,1.27)		
8	7+3*BETA(0.673,1.02)	16	14+4*BETA(0.717,1.69)		

Note: St. = Station

2.4.1 Model verification

In this step, the standard time of work is examined for the accuracy of the simulation model by comparing the workload utilization in the real system with the workload utilization from the simulation model in the cases of 5 and 6 employees as shown in Table 5. The results show that

average workload utilization in both cases (5 and 6 persons) for real system and simulation model were not significantly different (between 0-0.37%).

Table 5. Comparison of workload utilization

Number of workers	Workload utilization in real system (%)		Workload utilization of model (%)		Percentage difference (%)	
	5 persons	6 persons	5 persons	6 persons	5 persons	6 persons
1	100.00	86.63	100	87	0.00	0.37
2	81.87	66.20	82	66	0.13	0.20
3	87.30	86.16	87	86	0.30	0.16
4	52.66	100.00	53	100	0.34	0.00
5	45.13	66.31	45	66	0.13	0.31
6	-	56.84	-	57	-	0.16

2.4.2 Model validation

This section examines the suitability of the model to check whether the computer model can replace the real system. The values obtained from the computer model, such as the number of products produced daily, must be close to the actual values and have a half width not more than 5% of the current actual data. Therefore, it can be concluded that the computer model can represent the current system. The first step in verifying the suitability of the model is to specify the information used to configure the run setup. The values from the current work system data are determined by using the average time in the system of 5 employees in a day with 20 working hours per day. According to the operating period considered, the average quantity of work produced is 606 pieces per day. The model is considered to be appropriate by requiring a half width deviation of not more than 5% (confidence interval value 95) of the current actual data. Therefore, the number of workpieces resulting from the model must be in the range of 606±30.3 pieces. The model examination has been performed in 20 replications in order to find the average amount of work produced each day. The result shows that the average number of workpieces produced each day is equal to 606.15, which is only +0.15 pieces different from the actual system which is less than the specified half width (±30.3 pieces). Moreover, the model was validated against the real system by comparing the average number of products produced by using t-test for statistic validation, and it was found that the p-value is 0.83, greater than 0.05. Therefore, in this paper, it is found that the simulation model can represent the current system by specifying number of replications to be 20 cycles.

3. Results and Discussion

The improvement of a motorcycle headlight production line using the production line balancing method following analysis of the current working methods via Arena simulation program was studied. The generated model was run for 20 replications, in the cases of 5 and 6 employees, and the results are summarized in Figures 15 and 16. It can be seen that the application of production line balancing and task improvement (by the elimination of the first sub-task), followed by re-balancing of the line, results in a higher average utility cost of employee. Each employee is given a more balanced workload, resulting in a balanced production line and reduced production cycle time. Similarly, the modifications help to increase productivity in production. The analysis of the ability to respond to customer product demand using demand data from the past 11 months of the company was compared with the results of the capacity analysis obtained from the model, both in the case of

improvements by balancing production lines and improving work by eliminating unnecessary sub-tasks. As noted, the model was run through 20 replications, and importantly each cycle was of the actual operating time of the company. The case study covers 21 days per working month. The production capacity per month for various cases is shown in Table 6.

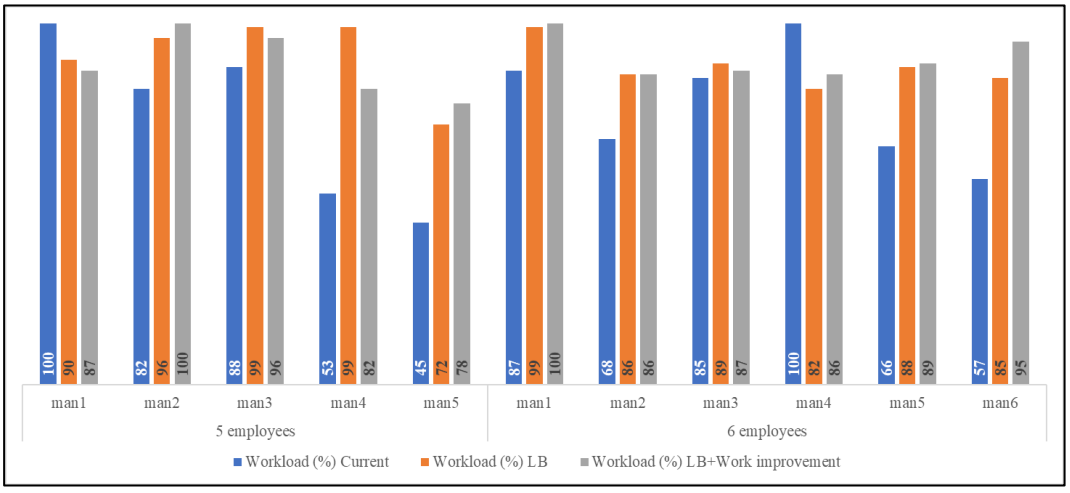

Figure 15. Comparison of workload utilization

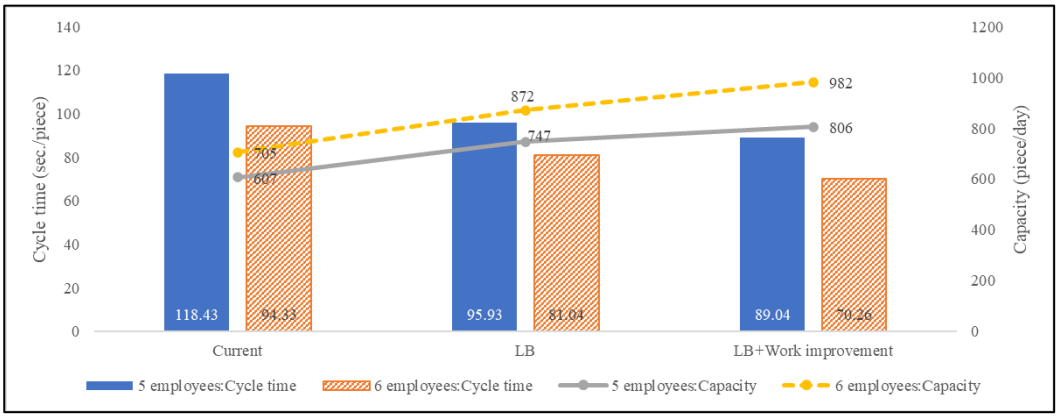

Figure 16. Comparison of production cycle time and capacity

Table 6. Production capacity per month

Instance	**Current system**		**LB**		**B + Work improvement**	
#Employees	5	6	5	6	5	6
Capacity (pieces/month)	12,755	16,059	15,709	18,325	16,985	20,630

The production capacity data (pieces / month) for each case is compared with the demand for the products in each month, in the cases of both 5 and 6 employees. Figure 17 shows that the proposed improvement results in a positive trend of production that better corresponds to the customers' product requirements than does current, which is not covered by the 11-month case of using 5 employees and covering 8 months from 11 months in the case of using 6 employees. In the latter part of the improvement, by balancing the production line in the case of using 5 employees, it was found that the demand can be covered for up to 5 months from 11 months, and in the case of using 6 employees covering 10 months from 11 months. The improvement of work by eliminating unnecessary work in conjunction with production line balancing shows that in the case of using 5 employees, the demand will be covered for up to 7 months from 11 months and in the case of using 6 employees, it is covered for 10 months from 11 months. Both types of improvement guidelines in the case of using 6 employees can meet almost all needs. There is only the 2nd month that may not yet be able to respond to the demand. Additional information from the company suggested that the 2nd month is the beginning of the production line. This new product therefore has more demand than usual, which, after that month, will return to normal at an average of 15,931 pieces / month. Therefore, it can be demonstrated that the proposed improvement approach can lead to a comprehensive case study to meet the needs of each month.

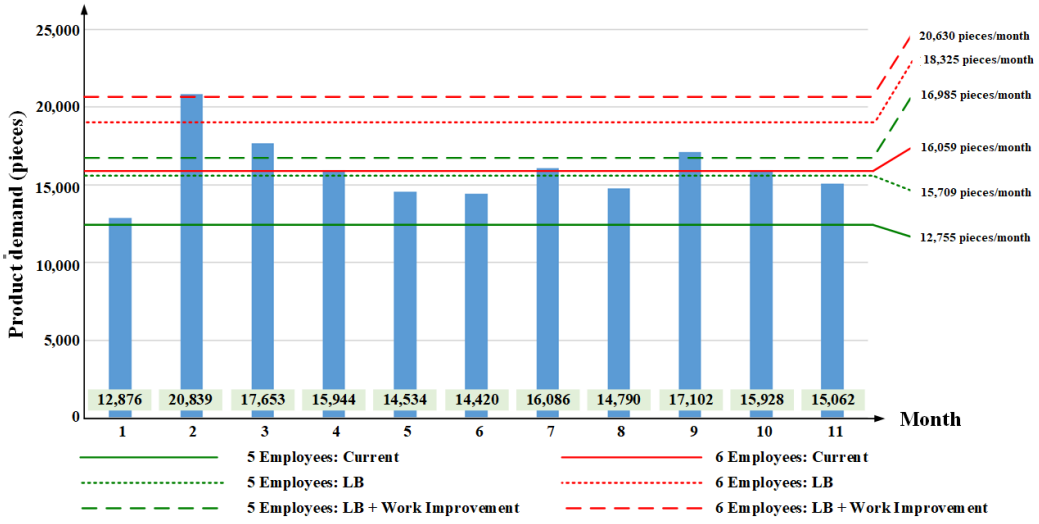

Figure 17. Comparison of production capacity and product demand after improvement

4. Conclusions

The results show that the current operation in the case of using 5 production line employees is still unable to respond to demand and can only respond to demand for 8 months from 11 months in the case of using 6 production line employees. Therefore, in order to increase the efficiency of the motorcycle headlight production line and to allocate the most efficient use of manpower, two solutions are proposed as follows: The application of line balancing found that when using 5 workers in a production line, there was a production cycle of 95.93 seconds per piece which is a reduction of 18.99% compared to the current situation. Production capacity increased to 747 pieces per day, which is an increase of 23.06% compared to the current situation. The utilization of the production

line is 91.2%, which is 17.6% increase on the current situation and in the case of using 6 production line employees, the production cycle time is 81.04 seconds per piece, which represents a reduction of 14.08% on the current situation. Production capacity increased to 872 pieces per day, which is an increase of 13.99 % compared to the current situation. The utilization of the production line is 88.17%, which represents an 11% increase compared to the current situation. Addition, in the case of improving production line efficiency by using work improvement, it was found that when 5 workers were used in the production line, there was a production cycle of 89.04 seconds per piece, which is a reduction of 24.81% from the current situation. Production capacity increased to 806 pieces per day, an increase of 32.78% compared to current. The utilization of the production line is 88.6%, which is a 15% increase over current. Furthermore, in the case of 6 production line employees, the production cycle time is 70.26 seconds per piece, a reduction of 25.51 % from the current situation. Production capacity increased to 982 pieces per day, which is an increase of 28.36 % over current. The utilization of the production line is 90.5 %, a 13.33 % increase compared to the current situation. Furthermore, further studies may consider ways to further improve the efficiency of the work, and included here could be improved tools or the supply of support equipment to ease the work and shorten the production cycle time. Finally, as the demand for each period is unstable, further studies may be conducted in order to better understand instabilities and variations in product demand and thus better match workload and customer demand.

References

[1] Zupan, H. and Herakovic, N., 2015. Production line balancing with discrete event simulation: A case study. *IFAC-PapersOnLine*, 48(3), 2305-2311.

[2] Helgeson, W.B. and Birnie, D.P., 1961. Assembly line balancing using the ranked positional weighting technique. *Journal of Industrial Engineering*, 12, 394-398.

[3] Becker, C. and Scholl, A., 2006. A survey on problems and methods in generalized assembly line balancing. *European Journal of Operational Research*, 168, 694-715.

[4] Battaïa, O. and Dolgui, A., 2013. A taxonomy of line balancing problems and their solution approaches. *International Journal of Production Economics*, 142(2), 259-277.

[5] Suwiwattana, S., Kasemset, C. and Khwanngern, K., 2020. Healthcare service network analysis: Northern region's healthcare service network of cleft lip and cleft palate. *Current Applied Science and Technology*, 20(2), 198-207.

[6] Aungkulanon, P., Phruksaphanrat, B. and Luangpaiboon, P., 2020. Dynamic maintenance scheduling with Fuzzy data via biogeography-based optimization algorithm and its hybridizations. *Current Applied Science and Technology*, 20(2), 226-237.

[7] Güner, M.G. and Ünal, C., 2008. Line Balancing in the Apparel Industry Using Simulation Techniques, *Fibres & Textiles in Eastern Europe*, 16(2), 75-78.

[8] Kusoncum, C., Sethanan, K., Erni, P.P., Neungmacha, W., 2018. Simulation-based approaches for processes improvement of a sugar mill yard management system: A case study of the sugar industry in the central region of Thailand. *Engineering and Applied Science Research*, 45(4), 320-331.

[9] Carson J.S., 2005. Introduction to modeling and simulation. *Proceedings of the 2005 Winter Simulation Conference*, Orlando, USA, December 4, 2005, 9-16.

[10] Krantikumar, B.C. and Abid M.M., 2015. Application of Ranked Position Weighted (RPW) Method for Assembly Line Balancing, *International Journal for Research in Applied Science & Engineering Technology*, 3(6), 254-262.

Current Applied Science and Technology Vol. 21 No. 1 (January-March 2021)

Drying of Fluid Saturated Porous Materials by Electroosmosis

Luong Duy Thanh[1]*, Rudolf Sprik[2], Phan Van Do[1], Nguyen Van Nghia[1] and Pham Thi Thanh Nga[1]

[1]Thuyloi University, Hanoi, Vietnam
[2]Van der Waals-Zeeman Institute, University of Amsterdam, Amsterdam, The Netherlands

Received: 3 June 2020, Revised: 29 June 2020, Accepted: 14 July 2020

Abstract

Electroosmosis is generated by the relative displacement of an electrolytic fluid with respect to solid surfaces under application of an electric field. The induced flow can assist in drying wet porous materials such as masonry used in buildings. In this work, the effectiveness of electroosmotic water transport induced by the application of a constant voltage across a wet porous sample is studied. A quantitative evaluation of water content is then performed at three different positions of the sample using a capacitive sensor. From the measured capacitance, the change of the dielectric constant of the wet sample over time is deduced. A model is then used to estimate the water content from the dielectric constant of the sample. It is seen that under application of constant voltages, the water content of the wet porous sample at the position close to the positive electrode decreases drastically. However, the water content remains almost constant in the middle of the sample and at a position close to the negative electrode. The reason is that water is pushed from the positive electrode to the negative electrode under application of electric field. Therefore, the water content becomes almost saturated right after applying a voltage across the sample. The results suggest that the electroosmotic technique can be applied to the drying of wet walls of buildings, and to stone and earth masonry structures, especially in cases where traditional techniques have not been able to solve the problems. Additionally, it is shown that our use of capacitive sensors is a technique that could be used to monitor the water content in wet porous materials.

Keywords: rising damp; capillary; masonry; electroosmosis
DOI 10.14456/cast.2021.6

1. Introduction

The existence of water in buildings and masonry structures is generally one of the most common issues influencing architectural heritage. The water may be present for various reasons including accident, wind driven rain, flooding, and rising damp from the ground [1-3]. The existence of rising damp creates a bad ambiance in buildings. It also enhances damaging processes such as the degradation of building materials, the loss of thermal resistance of building walls, and the decrease in the mechanical performance of the masonry [4-6].

*Corresponding author: E-mail:thanh_lud@tlu.edu.vn

Several methods have been presented to limit rising damp. One method, a mechanical one, consists in the insertion of an impermeable layer in building walls. Another method, a chemical one, consists in drilling holes at the horizontal base of walls and filling those holes with chemical products. Additionally, another method is based on electroosmosis in porous materials. The application of an electric field on porous media can generate a motion of water in pores and that effect is called electroosmosis. Electroosmosis is related to the electrical double layer at interfaces between solid surfaces and water.

The effectiveness of the electroosmotic technique is still controversial in the literature. For example, Bertolini *et al*. [7] concluded that the chances of applying the electroosmotic technique effectively in drying damp masonry are extremely low. However, some authors state positive results on potential applications of this technique [8, 9]. Especially, Stanley and McFeat-Smith [10] have applied the electroosmotic technique using multi-pulse sequencing in the field for removing water from building walls. The results show that electroosmosis is a good method of driving moisture out of concrete and other masonry structures. In the literature, quantitative results on the variation of humidity over time under electroosmosis are scarce and sometimes unsatisfactory [7]. For example, Nevertheless, Ottosen and Rorig-Dalgaard [8] evaluated the change of water content in a brick under an electric field by cutting the brick into several pieces with a hammer. The water content was then measured as weight loss in each piece. However, the cutting itself may have changed the water content of each piece of the brick due to friction. Besides that, the porosity in each piece may not have been the same. Consequently, the assessment of water content in that work may have been less than accurate. Similarly, Ivliev [9] evaluated the variation of the water content by weight loss measurement after a given period of time.

In this work, electroosmotic water transport is obtained by applying an electric field to a sandstone sample. A quantitative evaluation of water content is then performed at three different positions of the sample using a capacitive sensor. We use the Texas Instruments FDC1004 integrated capacitance sensor. From the variation of the measured capacitance, the change of the dielectric constant of the wet sample over time is deduced. A model is then used to estimate the water content from the dielectric constant. The change of water content with position along the sample at a given applied voltage is used to evaluate the effectiveness of electroosmotic technique in drying wet porous materials.

2. Materials and Methods

2.1 Electroosmosis in porous media

Porous materials are created by solid grains. When solid grain surfaces contact with water, the surfaces become electrically charged [11]. This leads to the charge distribution termed the electrical double layer (EDL) at the water-solid interface (Figure 1). The EDL consists of the Stern layer where ions are immobile, and the diffuse layer where ions are free to move [11]. The zeta potential (ζ) is the potential at the shear plane in the diffuse layer separating the mobile liquid from the liquid that is attached to solid surfaces (Figure 1). The zeta potential depends on mineral compositions of porous materials, properties of fluid, pH, temperature, etc. [12, 13].

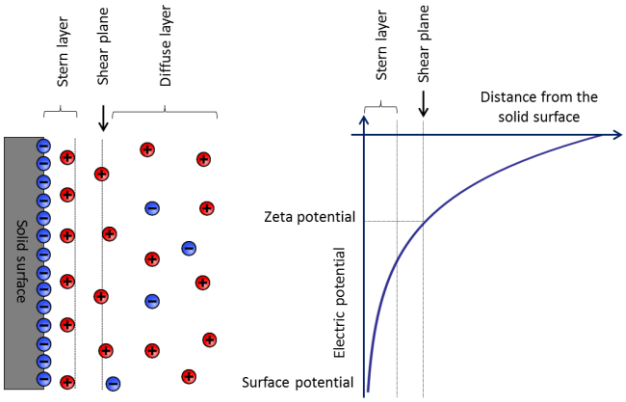

Figure 1. Stern model for the charge and electric potential distribution in the EDL [14, 15]

Electroosmosis was first performed by Reuss for a clay-sand-water mixture [16]. When an electric field is setup parallel to walls of capillary tubes, ions in the EDL suffer an electrical force and move, which creates a fluid movement in the capillary. That effect is called electroosmosis (Figure 2). A porous material can be conceptualized as a bundle of parallel capillaries of the radius a with zeta potential ζ. The volume flow rate in a capillary under application of an electric field E is given by Gad-el-Hak [17]:

$$q = \frac{\varepsilon\varepsilon_o|\zeta|.E.\pi.a^2}{\eta} = \frac{\varepsilon\varepsilon_o|\zeta|.V.\pi.a^2}{L.\eta} \quad (1)$$

where ε is the relative fluid permittivity, ε_o is the dielectric permittivity in vacuum, ζ is the zeta potential, η is the dynamic fluid viscosity, V is applied voltage across the porous material and L is the length of the capillary.

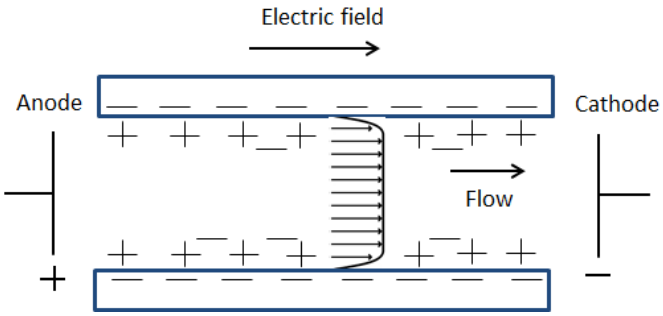

Figure 2. Electroosmotic flow in a capillary tube

Equation (1) indicates that the fluid flow through a capillary is proportional to the zeta potential, the applied electric field, and the capillary size. It should be noted that besides the main electroosmotic mechanism during the drying process, there may also be other mechanisms contributing to water movement in porous media such as diffusion, gravity, external pressure difference, capillary action and convection. Different models are available in the literature for the drying process of porous media [18].

2.2 Dielectric constant in water saturated porous media

A porous material consists of three components: water, air and solid grains. Its dielectric constant (ε_r) is dependent on the dielectric constant and relative volume of each component. The dielectric constants of air and solid grains are normally considered unchanging. Namely, ε_r of air is taken as 1 and ε_r of solid grains is taken between 2 to 10. Those values are much smaller than that of pure water ε_w= 80.2 at 20ºC [19]. Therefore, any change of the amount of water in porous materials will cause change of the ε_r. The ε_r of water-filled porous media is very sensitive to the water content and weakly sensitive to solid particle-specific parameters such as grain radius, mineral composition of solid grain, solid density, and temperature [20]. Consequently, the dielectric constant deduced from capacitance measurements is a good indicator of water content. There have been several empirical equations proposed that relate the ε_r of a porous material to the water content θ_l. For example, one is provided for a Caen stone in the range $0 < \theta_l < 39$ % [21]:

$$\varepsilon_r = 2.1 + 24.1\theta_l \tag{2}$$

Due to the similarity in mineral composition, type of porous media (consolidated rock) and type of liquid (water) of the Caen stone sample and the rock sample used in this work, equation (2) will later be used to quantitatively estimate the water content from the ε_r of the porous sample in this work.

2.3 Experiments

To assess the variation of water content in fluid saturated porous media, we use an experimental setup as shown in Figure 3. A porous sample is a slab of Berea sandstone (10 cm×5 cm×3 cm). The porosity of the sample is measured as 25% by a simple method described in Thanh *et al*. [22]. The fluid used to saturate the porous sample is tap water. The electrical conductivity and pH of the water as measured are 0.73 mS/cm and 7.3, respectively. The sample is first dried in an oven at 105ºC for 24 h, cooled down to room temperature, and filled with water using the setup shown in Figure 4.

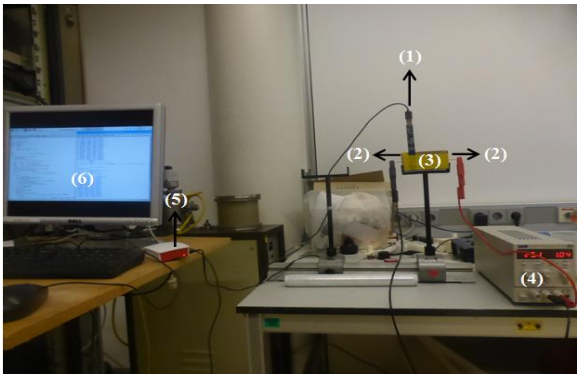

Figure 3. Experimental setup for electroosmotic measurements
(1) Capacitance sensor, (2) Copper electrodes, (3) Porous sample, (4) DC power supply,

(5) Raspberry Pi used for data collection, (6) Monitor

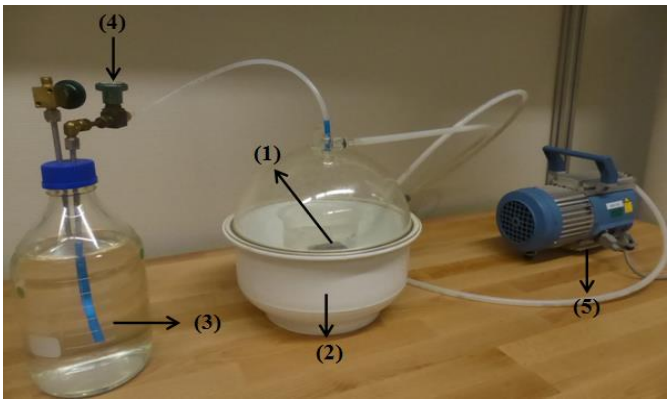

Figure 4. Experimental setup used to saturate porous samples
(1) Porous sample, (2) Desiccator, (3) Tap water container, (4) Valve, (5) Vacuum pump

The sample is taken out of the water bath and scrubbed with wet tissue paper. The water content of the wet sample is then measured as 20 % (by weighing the wet and dry samples). The sample is put in place as shown in the experimental setup (Figure 3). Copper electrodes are placed against the ends of the porous sample and fixed. The electrodes have a surface area of 5 cm x 3 cm and they are connected to a power supply (Aim-TTi PLH250-P). Constant voltages of 25 V and 12.5 V are selected in this work because those values are enough to observe the effect in porous bricks as stated in Ottosen and Rorig-Dalgaard [8] (50 V/23 cm) and to disregard air bubbles generated at two copper electrodes and electrode processes. To decrease the resistance between the brick and the electrodes, steel wool is used. The sample, steel wool and electrodes are wrapped carefully with plastic film during measurement in order to minimize evaporation. The electrical current (I) through the sample is measured by an Ampere meter in the power supply. The result shows that electrical current decreases over time and becomes stable after a certain amount of time. For example, at the beginning of the application of 25 V across the sample, the current is measured to beI_{i} = 1.3 mA and the stable value is measured to be I_{f} = 0.1 mA after 30 hours. This observation is the same as that inferred from the work of Ivliev [9], in which it was shown that the specific resistivity of porous medium increases over time under application of an electric field. The reason for the increase of specific resistivity of the sample may be that there is electrolysis at the anode and the cathode under applied voltage. These electrode reactions produce ions and gas at both electrodes. These reactions induce a low pH at the anode, a high pH at the cathode, and a decrease in electrical conductivity of fluid. Additionally, water redistribution along the sample under an applied voltage may lead to an increase of the specific resistivity.

To quantitatively evaluate the variation of water content over time at a given position on the sample, capacitance measurements are performed with the capacitive sensor (FDC1004) obtained from Texas Instruments. The sensor is pressed against the plastic-wrapped sample at three different positions as shown in Figure 3 (the sensor is not directly in contact with the wet sample).

Before carrying out the capacitance measurements under applied voltages across the sample, reference experiments are also performed. The first reference used for capacitance measurement is with the sensor in air without contact with the sample. The second one used for the capacitance measurement is with the sensor in contact with the dry sample. The third one is with the sensor in contact with the wet sample but without applied electric field.

The experiment is run on a Raspberry Pi (Figure 3), which uses Python as the programming language. Based on the code of the Python program that is not shown in this work, we are able to set the number of data points and the time between two consecutive data points in a way we want to. The measured data are recorded and saved into .csv files on the Raspberry Pi. The .csv files are then transferred to a computer to be analyzed by Matlab.

3. Results and Discussion

The variation of capacitance with time in the reference experiments is shown in Figure 5. The results show that the capacitance in the cases of the sensor in air and the sensor in contact with the dry sample do not vary over time. It means the lab conditions (humidity, temperature, etc.) that may affect the capacitance are stable. In the case of the sensor being in contact with the wet sample without an applied electric field, the capacitance slightly decreases at the beginning (for around an hour) and then becomes nearly constant over time. Hence, the water content does not change over time under gravity when the wet sample is placed in the setup. The reason is that water is held onto rock particles by adhesion or by capillary force for the fine rock samples, as mentioned in Harter and Rollins [23].

Figure 6 shows the variation of the capacitance with time under application of a constant voltage of 25 V across the wet sample for 35 h when the sensor is placed next to the positive electrode. As expected, the capacitance of the sensor and therefore the water content decreases

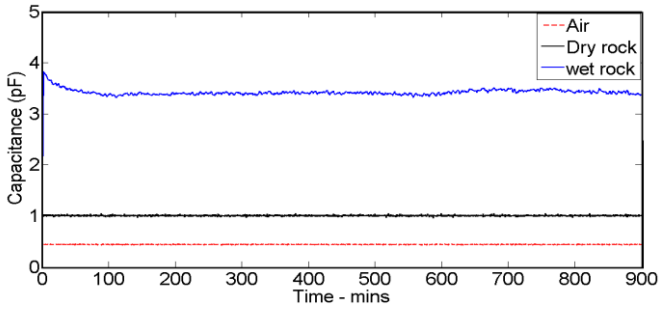

Figure 5. Variation of the capacitance with time (15 h) for the reference experiments

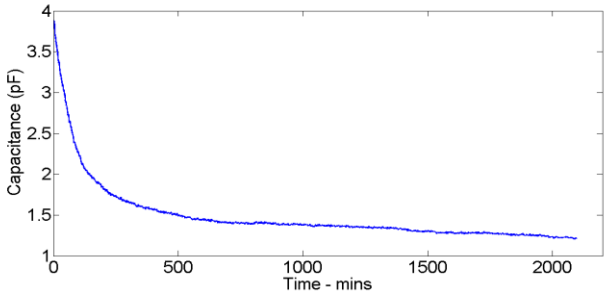

Figure 6. Variation of the capacitance with time in 35 h under an applied voltage of 25 V when the sensor is placed next to the positive electrode

over time. The rate of decrease of the capacitance for around the first four hours is much higher than that for the next 30 h. This can be inferred from the time constants obtained by exponential fitting and is shown in Figure 6. On average, the relative change of the capacitance in 35 h $\Delta C/C$ and therefore the relative change of the dielectric constant of the wet sample $\Delta\varepsilon_r/\varepsilon_r$is approximately 69% (the area *A* and distance *d* between two plates of the capacitor do not vary). From Eq. (2), it is deduced that the water content of the sample decreases by around 69%.

To estimate the time to push water out of a capillary (the capillary is assumed to be fully occupied by water) under application of a voltage of 25 V, equation (3) is used:

$$t = \frac{Volume_{capillary}}{q} = \frac{\pi a^2 L}{q} = \frac{\eta L^2}{\varepsilon\varepsilon_o|\zeta|\pi V} \tag{3}$$

Where *L* is the length of the sample of 0.1 m, *V* is taken as 25 V, $|\zeta|$ is approximately taken as 0.04 V for the tap water-rock system [24]. Therefore, the time to get a stable water content is calculated to be 50 hours and this number is in agreement with that observed in this work (35 h).

Figure 7 shows the variation of the capacitance with time under application of a constant voltage of 25 V when the sensor is placed at the middle of the sample and next to the negative electrode, respectively. It is seen that the capacitance of the sensor slightly decreases with time for the middle position. In particular, the capacitance barely changes over time at the negative electrode position. That observation can be explained by the fact that under application of anelectric field, water is pushed from the positive electrode to negative electrode. Therefore, water content becomes almost saturated right after applying an electric field at the position close to the negative electrode. The total loss of water in the sample wrapped by the plastic film after 40 hexperiments is measured as around 2 %.

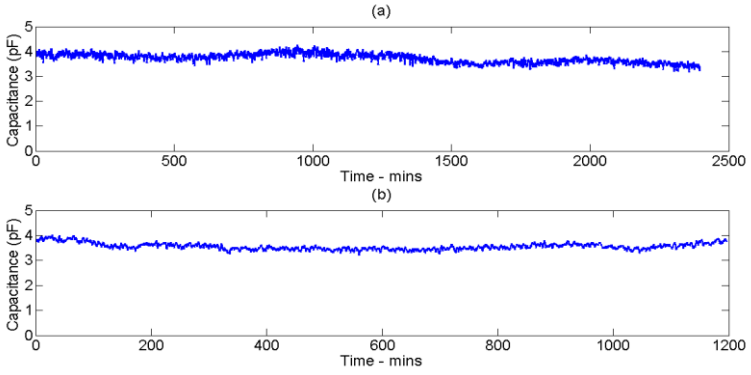

Figure 7. Variation of the capacitance with time under a constant voltage of 25 V when the sensor is placed at the middle of the sample (a) and next to the negative electrode (b)

Figure 8 shows the variation of capacitance with time under application of a constant voltage of 12.5 V when the sensor is placed next to the positive electrode. For the same argument mentioned above, it is seen that the water content of the sample decreases by around 28% in this case. This value is significantly smaller than that of the 25 V voltage application.

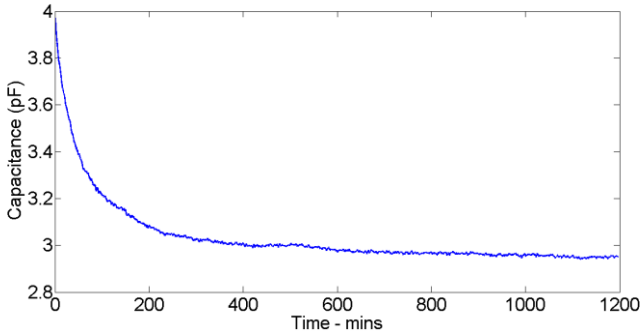

Figure 8. Variation of capacitance with time for 20 h under a constant voltage of 12.5 V when the sensor is placed next to the positive electrode.

Similarly, the time to get stable water content is calculated to be 25 h and this value is in the same range as that observed in Figure 8 (around 20 h).

The results show that techniques based on electroosmosis might be effective in drying wet buildings, and stone and earth masonry structures. Thus, the concept of water movement in porous material by applying a voltage is effective and is consistent with the observations of others [8-10]. Based on the findings of this work, it can be inferred that the effectiveness of the electroosmotic technique in the drying of wet porous materials is proportional to the applied voltage. However, if the applied voltage exceeds a certain value, there will be electrolysis and therefore air bubbles at the electrodes. Generated air bubbles may block the water movement in rock capillaries and affect the electroosmotic technique. Hence, further studies to determine the optimal voltages as well as the distance between electrodes for wet porous media need to be carried out.

4. Conclusions

In this work, electroosmotic water transport is obtained by applying a voltage across aporous sample. A quantitative evaluation of water content is then performed at three different positions of the sample using a capacitive sensor. We use the Texas Instruments FDC1004 integrated capacitance sensor. It is a low cost, digital high precision sensor that operates at low power and is easily interfaced toa data collecting microcomputer. From the variation of the measured capacitance, the change of the ε_r of the water filled sample over time is deduced. A model is then used to estimate the water content from the ε_r of the sample. The results show that under application of constant voltages of 25 V and 12.5 V, the water content of the wet porous sample at the position close to the positive electrode decreases drastically by around 69 % and 28 %, respectively. However, the water content remains almost constant in the middle of the sample and at a position close to the negative electrode. The reason is that water is pushed from the positive electrode to the negative electrode under application of an electric field. Therefore, water content becomes almost saturated right after applying the electric field in the middle of the sample and atthe position close to the negative electrode. The results suggest that the electroosmotic technique can be applied in the drying of moisture in buildings, and in stone and earth masonry structures. Additionally, it is shown that our use of capacitive sensors is a promising technique for monitoring the water content in wet porous materials.

References

[1] Blocken, B. and Carmeliet, J., 2010. Overview of three state-of-the-art wind-driven rain assessment models and comparison based on model theory. *Building and Environment*, 45, 691-703.

[2] Socoloski, R.F. and Masuero, A.B., 2019. Evaluation of the efficiency of the treatment for rising damp on walls through the insertion of chemical barriers by gravity. *Construction and Building Materials*, 210, 660-672.

[3] Franzoni, E., 2014. Rising damp removal from historical masonries: A still open challenge. *Construction and Building Materials*, 54, 123-136.

[4] Franzoni, E., 2018. State-of-the-art on methods for reducing rising damp in masonry. *Journal of Cultural Heritage*, 31(Supplement), S3-S9.

[5] Salmon, D., Williams, R. and Tye, R., 2002.Thermal conductivity and moisture measurements on masonry materials. In: A. Desjarlais and R. Zarr, eds. *Insulation Materials: Testing and Applications*. *Vol. 4.* West Conshohocken: ASTM International, pp. 8-75.

[6] Gentilini, C., Franzoni,E., Bandini,S. and Nobile, L., 2012. Effect of salt crystallisation on the shear behavior of masonry walls: an experimental study. *Construction and Building Materials*, 37, 181-189.

[7] Bertolini, L., Coppola, L., Gastaldi, M. and Redaelli, E., 2009.Electroosmotic transport in porous construction materials and dehumidification of masonry. *Construction and Building Materials*, 23, 254-263.

[8] Ottosen, L.M., and Rorig-Dalgaard, I., 2006. Drying brick masonry by electro-osmosis.*Proceedings of the Seventh International Masonry Conference*.British Masonry Society, London, U.K., 30 October-1 November, 2006. (CD-rom).

[9] Ivliev, E.A., 2007. Electroosmotic drying of building walls and basements.*Surface Engineering and Applied Electrochemistry*, 43, 291-296.

[10] Stanley, C., and Mcfeat-Smith, I., 2008. Electro-osmosis using multi pulse sequencing for removing and repelling water out of buildings and other structures.*33rd Conference on Our World in Concrete and Structures*,Singapore, 25-27 August, 2008.

[11] Masliyah, J.H. and Bhattacharjee, S., 2006. *Electrokinetic and Colloid Transport Phenomena*.New Jersey: Wiley-Interscience.

[12] Hunter, R.J., 1981.*Zeta Potential in Colloid Science*. New York: Academic Press.

[13] Davis, J.A., James, R.O. and Leckie, J.O., 1978. Surface ionization and complexation at the oxide/water interface. I. computation of electrical double layer properties in simple electrolytes. *Journal of Colloid and Interface Science*, 63(3), 480-499.

[14] Stern, O., 1924. Zur theorie der electrolytischen doppelschist. *Z. Elektrochem*, 30, 508-516.

[15] Ishido, T. and Mizutani, H., 1981. Experimental and theoretical basis of electrokinetic phenomena in rock-water systems and its applications to geophysics. *Journal of Geophysical Research*, 86, 1763-1775.

[16] Reuss, F., 1809. Sur un nouvel effet de l'electricit galvanique. *Mmoires de la SocietImperiale de Naturalistes de Moscou*, 2, 327-336.

[17] Gad-el-Hak, M., 2006. *MEMS: Introduction and Fundamentals*. 2nd ed. Boca Raton: Taylor and Francis.

[18] Vu, H.T. and Tsotsas, E., 2018. Mass and heat transport models for analysis of the drying process in porous media: A review and numerical implementation. *International Journal of Chemical Engineering*, 2018, https://doi.org/10.1155/2018/9456418

[19] Kaatze, U., 1997. The dielectric properties of water in its different states of interaction. *Journal of Solution Chemistry*, 26, 1049-1112.

[20] Topp, G.C., Davis, J.L. and Annan, A.P., 1980. Electromagnetic determination of soil water content: Measurements in coaxial transmission lines. *Water Resources Research*, 16, 574-582.
[21] Fen-Chong, T., Fabbri,A.,Guilbaud, J.P. and Coussy, O., 2004. Determination of liquid water content and dielectric constant in porous media by the capacitive method. *Comptes Rendus Mecanique*, 332, 639-645.
[22] Thanh, L.D., Sprik, R. and Nguyen, X.C., 2019. Zeta potential of porous rocks in contact with mixtures of monovalent and divalent electrolytes. *Geophysical Prospecting*, 67, 1354-1368.
[23] Harter, T., and Rollins, L., 2008.*Watersheds, Groundwater and Drinking Water: A Practical Guide.* California: University of California. Agriculture and Natural Resources Publications.
[24] Vinogradov, J., Jaafar, M.Z. and Jackson, M.D., 2010. Measurement of streaming potential coupling coefficient in sandstones saturated with natural and artificial brines at high salinity. *Journal of Geophysical Research*, 115, https://doi.org/10.1029/2010JB007593

Phytochemical Screening and Fruit Quality of Commercial Eggplants

Hathairat Chokthaweepanich[1]*, Suwalak Sriwicha[1], Anyamanee Auvuchanon[2] and Suriyan Supapvanich[3]

[1]Department of Agriculture and Resources, Faculty of Natural Resources and Agro-Industry, Kasetsart University, Chalermphrakiat Sakon Nakhon Province Campus, Sakon Nakhon, Thailand
[2]Department of Horticulture, Faculty of Agriculture at Kamphaeng Saen, Kasetsart University, Kamphaeng Saen Campus, Nakhon Pathom, Thailand
[3]Department of Agricultural Education, Faculty of Industrial Education and Technology, King Mongkut's Institute of Technology Ladkrabang, Ladkrabang, Bangkok, Thailand

Received: 10 March 2020, Revised: 8 July 2020, Accepted: 29 July 2020

Abstract

Ten commercial eggplant cultivars and two allies were collected from Northeastern region of Thailand in order to examine fruit quality and screen for selected phytochemicals. Eggplants were classified into three species including *Solanum torvum*, *S. violaceum* and *S. melongena*. There were 10 cultivars in *S. melongena* (commercial eggplants) containing cv. 'Makhuea kai tao khaw', 'Makhuea khuen', 'Makhuea pro chao phraya', 'Makhuea pro look lai', 'Makhuea pro muang', 'Makhuea tor lae kaew', 'Makhuea tor lae khaw', 'Makhuea yao kaew', 'Makhuea yao khaw', and 'Makhuea yao muang'. The analysis indicated that there were significant differences ($p \leq 0.05$) in fruit quality traits including color, thickness, hardness, TSS and moisture. All samples could be divided into three groups based on fruit color including white, purple, and green groups. The commercial eggplants had more thickness than *S. torvum* and *S. violaceum*, but these two species had more TSS contents than commercial eggplants. The results of phytochemical screening showed that *S. torvum* tended to have higher alkaloid, tannin, saponin and steroid contents from the staining technique. Furthermore, 'Makhuea yao muang' showed the highest DPPH radical scavenging capacity (49.33%) compared to all others. The principal component and cluster analysis based on correlation of fruit traits and phytochemicals showed that all commercial eggplants were clustered in the same group. The correlation analysis indicated that TSS contents positively correlated with saponin and steroid, while TSS contents negatively correlated with thickness and moisture contents. As this study, commercial eggplants showed higher fruit quality and antioxidant activity than related species.

Keywords: eggplant; *Solanum* spp.; fruit quality; phytochemicals; antioxidant activity
DOI 10.14456/cast.2021.7

*Corresponding author: Tel.: (+66)939159615
E-mail: hathairat.ch@ku.th

1. Introduction

Solanum L., one of the largest genera of Solanaceae, consists of 1,400 species and is cosmopolitan [1, 2]. The geographic distribution of these species is in all continents, especially in Central and South America [3-5]. Twenty-two species of *Solanum* are found in Thailand and about half of them are found in other countries [6]. Although *Solanum* are reported as poisonous and non-edible plants, some species play an important role in food and agriculture including spice, herb, food ingredient, insecticide, and fungicide. Moreover, they have been also used in medicinal ingredients to treat asthma, bruise, cough, diarrhea, fever, headache, and rheumatic fever [4, 7-9].

Eggplants (*Solanum melongena* L.) are a domestic vegetable of the genus *Solanum* that has the worldwide gross production value in 2016 of about 38,373.83 million US$ and of about 6.39 million US$ in Thailand [10]. Within Asia, they are cultivated over areas that extend from northeast India and Burma to Southwest China, Vietnam, Laos, and Northern Thailand [11]. Increasingly, eggplants are grown worldwide about 2,644,517 hectares and widely cultivated in China (59.41%), India (27.72%), Egypt (1.82%), Indonesia (1.66%), and Turkey (0.97%) [12] because they are annual plants, well adapt to various environments, and diverse in color, shape and size based on varieties [11, 13]. Besides being good sources of nutrients, eggplants also contain several bioactive compounds including alkaloids, phenolic compounds, anthocyanin, antioxidants, and flavonoids [14-21]. These secondary compounds can attribute to the traditional medicinal efficacy in analgesic activity [22], antimicrobial [23, 24], and antioxidant [25, 26].

Eggplants and wild species are the important sources of basic ingredients in Thai food and components in herbal medicine [7, 27-29]. There are many eggplant cultivars for domestic production in Thailand, but little information regarding the comparison between fruit quality and phytochemical screening among commercial eggplants in Thailand has been reported. Thus, the objectives of this study were to evaluate the fruit quality and phytochemical profiles of commercial eggplants.

2. Materials and Methods

2.1 Materials

The samples of commercial eggplants and allies were collected in Sakon Nakhon province, Northeastern region of Thailand. All fruits were harvested at commercial maturity stages after flowering at 7-10 days. The fruits were kept in polyethylene bag and transferred to laboratory at Kasetsart University, Chalermphrakiat Sakon Nakhon Province Campus within 2 h after harvest. All fruits were cleaned with tap water and then air-dried at room temperature for 30 min. Five replications (3 fruits per replicate) of each cultivar were taken to determine quality attributes. The fruits were then sliced and dried in hot air oven at 70^{o}C. The dried samples were kept in hermetically sealed plastic bags to determine phytochemicals screening and antioxidant activity.

2.2 Fruit quality evaluation of eggplant samples

The peel colors of eggplants were measured using a HunterLab Miniscan EZ 4500L colorimeter (Hunter Associates Laboratory Inc.; Reston, VA, USA). The *L**, *a**, *b** and hue values of the fruits were recorded from colorimeter. The peel colors were measured at three different positions of fruit such as top, middle and bottom. The texture of eggplants was measured using a Hardness Tester No.510-1 Model FHR-1 (Nippon Optical Works Co., Ltd., Japan). The maximum force of measurement was recorded as the fruit hardness and the data were expressed as newton unit. The thickness of fruit flesh (from exocarp to outer layer of endocarp) was

determined using a vernier calipers. The total soluble solids (TSS) content of fruit was measured using a Milwaukee instrument MR series hand refractometer (Milwaukee, USA) and expressed as ^{o}Brix.

2.3 Moisture content determination

Moisture content analysis was examined using the modified method of Kasikawattana *et al*. [30]. The eggplants were sliced into thin pieces and 20 g of sample was taken to determined moisture content. The samples were dried in hot air oven at 70^{o}C for 48 h or until sample weight was stable. The percentage of moisture content was calculated using the equation shown below.

Moisture content (%) = [(flesh weight (g) – dry weight (g))/flesh weight] x 100 (1)

2.4 Phytochemical screening of commercial eggplants

2.4.1 Crude extracts preparation

The samples were dried in a hot air oven at 40^{o}C and ground in a blender. Powder samples (6 g) were soaked in 50 ml of absolute ethanol for 7 days in the dark at ambient temperature. The samples were then filtered with a Whatman filter paper no. 42 and the filtrate was evaporated using a rotary vapor BUCHI R-200 (BÜCHI Labortechnik AG, Switzerland) at 40^{o}C and 100 atm for 30-45 min. The crude extracts were collected and kept in an amber bottle at 4^{o}C [31] for further analysis.

2.4.2 Phytochemical screening

The crude extract was examined qualitatively for their phytochemical components within 5 days after extraction to reveal the presence of some secondary metabolites. The results were presented as + (light color), ++ (moderate color), +++ (dark color), and – (non-color changes) based on the color intensity with standard methods [32].

(1) Alkaloid testing: The alkaloids were determined using the modified method of Djaafar and Ridha [32]. One ml of Dragendoff's reagent was mixed with 50 mg of crude extracts. The mixture was shaken and incubated at room temperature for 10 min. The appearance of orange precipitate showed the positive result.

(2) Tannin testing: Tannin testing was conducted according to Kumar *et al*. [31] with slight modification. A 50 mg of crude extract in each sample was mixed with 0.5 ml of 70% nitric acid. Tannin presence was observed when the color of mixture was formed from reddish to yellow.

(3) Saponin testing: Saponin was evaluated using a foam test adopted from Kumar *et al*. [31]. One ml of distilled water was mixed with 50 mg of crude extract and vigorously shaken for 30 s. Persistent froth forming indicated the presence of saponin.

(4) Steroid testing: Steroid was determined by Liebermann-Burchard's test [33]. Crude extract (50 mg) was mixed with 0.2 ml of glacial acetic and 0.2 ml of concentrated sulfuric acid. The formation of a green solution showed steroid presence.

2.5 Antioxidant activity determination

The antioxidant activity was determined using DPPH (2, 2-Diphenyl-1-picrylhydrazyl) radical scavenging activity assay described by Brand-Williams *et al*. [34]. Six grams of sample powder was extracted with 99.8% ethanol and then filtered with a Whatman filter paper no. 42. One µl of aqueous filtrate of extract was added into 3 ml of DPPH solution (200 µM dissolved in 80% ethanol). The mixture was incubated at room temperature and under dark condition for 30 min. The absorbance of the solution was measured at 515 nm by the T60 UV-VIS spectrophotometer (PG Instruments Limited, United Kingdom). The antioxidant activity was expressed as the percentage of DPPH free radical scavenging using the following formula.

DPPH free radical scavenging activity (%) = $[(A_0-A_1)/A_0] \times 100$ (2)
A_0 = the wavelength absorbance at 0 min
A_1 = the wavelength absorbance at 30 min

2.6 Data analysis

The variance and mean differences of data were statistically analyzed value using ANOVA and the means were compared using the Least Significant Difference (LSD) with Statistix 8.0 program (Analytical Software; Tallahassee, FL, USA) at the significant level $p \leq 0.05$. The correlation and cluster analysis based on fruit quality and phytochemical properties were examined by PAST ver. 3.25 [35]. The relative qualitative differences of phytochemicals were scored from the comparison of presence/absence based on color intensity. The phytochemical presences were given scores ranging from 0 to 3. A value of 3 represented an abundant presence, while values of 2 and 1 were assigned to apparently moderate and slightly presence, respectively. A value of 0 means that the phytochemical was not detected in this study.

3. Results and Discussion

3.1 Morphological traits of eggplant samples

All collected samples of *Solanum* were classified into 3 species based on Zhi-yun *et al*.'s classification [3] including *S. torvum* Swartz. (Makhuea Phuang), *S. violaceum* Ortega (Ma Waeng Ton), and *S. melongena* L. with 10 cultivars containing *S. melongena* cv. 'Makhuea kai tao khaw', 'Makhuea khuen', 'Makhuea pro chao phraya', 'Makhuea pro look lai', 'Makhuea pro muang', 'Makhuea tor lae kaew', 'Makhuea tor lae khaw', 'Makhuea yao kaew', 'Makhuea yao khaw', and 'Makhuea yao muang'. The members in species of *S. melongena* were commercial eggplants. Most of collected samples in this research were glabrous and non-prickly, except for *S. violaceum.* They could be divided into 3 groups based on their shape (Figure 1 and Table 1) composing of (1) elongated shape: *S. melongena* cv. 'Makhuea yao kaew', 'Makhuea yao khaw' and 'Makhuea yao muang' (2) oval shape: *S. melongena* cv. 'Makhuea kai tao khaw', 'Makhuea khuen', 'Makhuea pro chao phraya', 'Makhuea pro look lai' and 'Makhuea pro muang' and (3) round shape: *S. torvum, S. violaceum, S. melongena* cv. 'Makhuea tor lae kaew' and 'Makhuea tor lae khaw'.

From the color data (Figure 1 and Table 1), all samples could be classified into three groups depended on fruit color including (1) white group with brightness value (L^*) = 79.53-84.39 and hue angle between 44.77-47.87 such as *S. melongena* cv. 'Makhuea kai tao khaw', *S. melongena* cv. 'Makhuea tor lae khaw', *S. melongena* cv. 'Makhuea yao khaw', (2) purple group with a^* = 18.80-35.50 and hue angle between 316.23-320.64 such as *S. melongena* cv. 'Makhuea pro muang' and *S. melongena* cv. 'Makhuea yao muang', and (3) green group with a^* = -18.60 to -7.00 and hue angle 64.08-71.84 and this group could further be separated into 2 subgroups, i.e. (3.1) light green subgroup such as *S. torvum, S. melongena* cv. 'Makhuea tor lae kaew', and *S. melongena* cv. 'Makhuea yao kaew', and (3.2) green with white striped eggplant subgroup such as *S. violaceum, S. melongena* cv. 'Makhuea khuen', *S. melongena* cv. 'Makhuea pro chao phraya', and *S. melongena* cv. 'Makhuea pro look lai'.

The results confirmed that *Solanum* was a very diverse genus in terms of fruit size, shape and color [36, 37]. Color quality evaluation of eggplants and allies presented the color divergence in each sample based on CIE L^*, a^*, b^* and hue values [38]. The L^* indicated the lightness from black (0) to white (100). Therefore, white eggplants showed higher L^* value than did the eggplants of other colors. The value of a^* meant the green-red component with green in the negative value ($a^* < 0$) and red in the positive value ($a^* > 0$). This is a reason that the purple eggplants represented the positive a^*, whereas green and white groups showed the negative a^*.

Figure 1. Morphological traits of commercial eggplants and related species (a) *S. torvum*, (b) *S. violaceum*, (c) *S. melongena* cv. 'Makhuea kai tao khaw', (d) *S. melongena* cv. 'Makhuea khuen', (e) *S. melongena* cv. 'Makhuea pro chao phraya', (f) *S. melongena* cv. 'Makhuea pro look lai', (g) *S. melongena* cv. 'Makhuea pro muang', (h) *S. melongena* cv. 'Makhuea tor lae kaew', (i) *S. melongena* cv. 'Makhuea tor lae khaw', (j) *S. melongena* cv. 'Makhuea yao kaew', (k) *S. melongena* cv. 'Makhuea yao khaw', and (l) *S. melongena* cv. 'Makhuea yao muang'

Table 1. Fruit shape, fruit color and color parameters of commercial eggplants

	Fruit shape	Fruit color	Color parameters			
			*L**	*a**	*b**	h^o
S. torvum	R	G	43.38^{h}±2.93	-15.66^{f}±2.31	34.82^{b}±1.98	71.84^{b}±2.89
S. violaceum	R	G/W	24.99^{i}±3.15	-7.00^{d}±3.56	21.97^{de}±15.71	65.37^{b}±3.36
cv. 'Makhuea kai tao khaw'	O	W	79.53^{b}±0.64	-1.37^{c}±0.32	17.79^{ef}±0.53	44.77^{c}±0.90
cv. 'Makhuea khuen'	O	G/W	51.98^{ef}±2.31	-9.50^{de}±0.64	26.66^{cd}±1.31	64.08^{b}±1.70
cv. 'Makhuea pro chao phraya'	O	G/W	68.43^{c}±1.05	-11.18^{e}±0.35	26.78^{cd}±2.02	67.54^{b}±1.46
cv. 'Makhuea pro look lai'	O	G/W	45.73^{gh}±5.03	-14.96^{f}±0.79	34.35^{bc}±1.42	70.83^{b}±1.42
cv. 'Makhuea pro muang'	O	P	49.62^{fg}±2.86	18.80^{b}±2.45	-8.15^{g}±1.08	316.23^{a}±1.25
cv. 'Makhuea tor lae kaew'	R	G	60.48^{d}±1.69	-15.71^{f}±0.75	39.13^{b}±0.88	68.26^{b}±0.88
cv. 'Makhuea tor lae khaw'	R	W	79.55^{b}±1.08	-1.86^{c}±0.17	14.62^{ef}±0.27	46.88^{c}±0.51
cv. 'Makhuea yao kaew'	E	G	54.00^{e}±2.96	-18.60^{g}±1.38	48.87^{a}±1.11	68.22^{b}±1.55
cv. 'Makhuea yao khaw'	E	W	84.39^{a}±0.97	-2.00^{c}±0.07	13.30^{f}±1.14	47.87^{c}±0.62
cv. 'Makhuea yao muang'	E	P	14.86^{j}±2.30	35.50^{a}±2.26	-19.68^{h}±2.03	320.64^{a}±27.82
F-test			**	**	**	**
C.V. (%)			4.65	-45.61	22.62	7.86

Note: E = elongate, O = oval, R = round, G =green, G/W = green with white stripes, P = purple, W =white, Y = yellow

The *b** meant the blue-yellow component with blue in the negative value and yellow in the positive value [38]. Moreover, the hue value represented a color appearance parameter that was used to explain the quality of color. The results reported that hue angle was related to eggplant colors including purple group (h^o > 310), green group (h^o = 64.08-71.84), and white group (h^o = 44.77-47.87). Since blue-yellow color was not found in these samples, the *b** value was not considered for classification in this analysis.

3.2 Fruit quality evaluation of eggplants

There were significant differences ($p \leq 0.05$) in fruit quality traits as shown in Table 2, which was in agreement with Gajewski and Arasimowicz [39] who reported that the quality of eggplant fruits could be affected by cultivars and maturity stage. *S. violaceum* and *S. torvum* had less flesh thickness than commercial eggplants because of morphological diversity and genetic traits [36, 37]. Commercial eggplants were bred to obtain a larger fruit for economic value adding [40, 41]. The average of hardness value in this study was 8.29 N. The highest hardness was found in *S. melongena* cv. 'Makhuea tor lae khaw' (9.41 N), whereas *S. melongena* cv. 'Makhuea yao kaew' had the lowest value (6.26 N). These differences were due to fruit peel properties such as toughness and thickness [42]. Oval and round shaped eggplants were crispy, while *S. torvum, S. violaceum* and elongated eggplants were tough. The crispiness and toughness were factors that affected the hardness value of eggplants. The crispy eggplants had higher hardness value than tough eggplants. Moreover, hardness value also depended on the postharvest and storage conditions. The longer storage periods resulted in more fruit ripening, causing the hardness value to be lower [39].

Table 2. Hardness, thickness, TSS and moisture contents in eggplants and allies

	Thickness (cm)	Hardness (N)	TSS (°Brix)	Moisture (%)
S. torvum	$0.11^{d}\pm0.00$	$8.00^{b}\pm1.54$	$15.13^{a}\pm0.35$	$82.36^{e}\pm0.95$
S. violaceum	$0.10^{d}\pm0.31$	$7.91^{b}\pm2.77$	$10.93^{b}\pm1.62$	$79.99^{f}\pm0.84$
cv. 'Makhuea kai tao khaw'	$0.39^{c}\pm0.07$	$8.90^{a}\pm0.42$	$5.13^{ef}\pm0.41$	$92.41^{a}\pm0.42$
cv. 'Makhuea khuen'	$0.48^{bc}\pm0.52$	$8.83^{a}\pm2.95$	$5.93^{e}\pm0.26$	$84.35^{d}\pm0.43$
cv. 'Makhuea pro chao phraya'	$0.47^{bc}\pm0.07$	$8.91^{a}\pm0.52$	$5.07^{ef}\pm0.26$	$91.07^{a}\pm0.92$
cv. 'Makhuea pro look lai'	$0.57^{ab}\pm0.09$	$7.69^{b}\pm2.82$	$5.80^{e}\pm0.41$	$91.77^{a}\pm0.48$
cv. 'Makhuea pro muang'	$0.37^{c}\pm0.05$	$8.90^{a}\pm0.35$	$7.06^{d}\pm0.88$	$91.14^{a}\pm0.76$
cv. 'Makhuea tor lae kaew'	$0.35^{c}\pm0.08$	$9.35^{a}\pm3.06$	$5.20^{ef}\pm0.56$	$88.40^{c}\pm0.76$
cv. 'Makhuea tor lae khaw'	$0.36^{c}\pm0.06$	$9.41^{a}\pm0.31$	$7.93^{c}\pm1.10$	$89.07^{bc}\pm0.37$
cv. 'Makhuea yao kaew'	$0.66^{a}\pm0.12$	$6.26^{c}\pm0.36$	$4.60^{fg}\pm0.63$	$92.25^{a}\pm0.64$
cv. 'Makhuea yao khaw'	$0.58^{ab}\pm1.24$	$7.59^{b}\pm0.46$	$4.07^{g}\pm0.26$	$91.21^{a}\pm2.21$
cv. 'Makhuea yao muang'	$0.41^{c}\pm0.16$	$7.67^{b}\pm0.61$	$5.33^{ef}\pm0.62$	$90.64^{ab}\pm0.31$
F-test	**	**	**	**
C.V. (%)	31.25	7.52	11.20	1.76

Note: In each column, different superscripts represent significant differences ($p \leq 0.05$).

Total soluble solid (TSS) of eggplants and related species were in range of 4.07-15.13°Brix (Table 2). The highest TSS was found in *S. torvum* (15.13°Brix) and the lowest TSS was shown in *S. melongena* cv. 'Makhuea yao khaw' (4.07°Brix). The moisture contents of eggplants and allies were higher than 80%. The highest moisture content was recorded in *S. melongena* cv. 'Makhuea kai tao khaw' (92.41%) and the lowest moisture content was found in *S. violaceum* (79.99%). The results showed that all cultivars of *S. melongena* had lower TSS contents than other species. A cause of different TSS contents in each sample was the variety of species and cultivars [43]. Contrarily, all eggplant cultivars in this study had more moisture contents than *S. torvum* and *S. violaceum*. These results were coincident with Koundinya *et al*. [43], who reported that average of moisture content in eggplants ranged from 84.60-90.40%.

3.3 Phytochemical screening in commercial eggplants

The results of phytochemical screening of eggplants and related species are shown in Table 3. Abundant alkaloids were found in *S. torvum, S. violaceum, S. melongena* cv. 'Makhuea kai tao khaw', *S. melongena* cv. 'Makhuea khuen', *S. melongena* cv. 'Makhuea pro muang', and *S. melongena* cv. 'Makhuea yao khaw'. A large amount of saponin was also observed in *S. torvum*.

Table 3. Phytochemical screening of some samples

	Alkaloids	Tannins	Saponins	Steroids
S. torvum	+++	+++	+++	+++
S. violaceum	+++	-	++	++
cv. 'Makhuea kai tao khaw'	+++	++	+	-
cv. 'Makhuea khuen'	+++	-	+	++
cv. 'Makhuea pro chao phraya'	++	-	+	-
cv. 'Makhuea pro look lai'	++	-	++	-
cv. 'Makhuea pro muang'	+++	-	++	-
cv. 'Makhuea tor lae kaew'	++	-	+	+
cv. 'Makhuea tor lae khaw'	+	-	++	-
cv. 'Makhuea yao kaew'	++	-	++	++
cv. 'Makhuea yao khaw'	+++	++	+	-
cv. 'Makhuea yao muang'	++	-	++	-

Note: +++ = abundant presence, ++ = moderate presence, + = slightly presence, - = absence

Moreover, tannin existed in *S. torvum, S. melongena* cv. 'Makhuea kai tao khaw', and *S. melongena* cv. 'Makhuea yao khaw'. Steroids were found in *S. torvum, S. violaceum*, *S. melongena* cv. 'Makhuea khuen', *S. melongena* cv. 'Makhuea yao kaew', and *S. melongena* cv. 'Makhuea tor lae kaew', respectively.

The different existences of phytochemicals do not only affect on genetic diversity of eggplants, but also on different organs, age, cultivation, harvesting, and storage [44, 45]. Phytochemical variations in eggplant extracts were distinct from related eggplant extracts. The analysis showed that the presences of alkaloids, tannins, saponins, and steroids were more abundant in *S. torvum* than others. According to Koomson *et al*. [46], ethanolic extracts of *S. torvum* fruits were a source of alkaloids, tannins, and saponins. Most of *Solanum* are bitter because of the presences of alkaloid, especially glycoalkaloids. However, alkaloid compounds found in eggplants are edible. Otherwise, 14 % of glycoalkaloid levels of *S. melongena* were considered as toxic [47]. Although alkaloids are toxic and cause diarrhea, they are known to be analgesic property [23], inhibit microbial activity and prevent plants from microbial pathogens [48, 49]. Tannins are a kind of water-soluble polyphenol that are astringent and bitter. Tannins also have antimicrobial, anti-inflammatory and wound healing properties [50, 51]. From the results of the screening tests, the commercial eggplant tested expressed non or moderately tannin presence compared with *S. torvum*. This is because of the breeding and selection program to reduce astringent and bitter flavor in commercial eggplants. Saponins are glycosides that have soapy characteristic and have properties of coagulating red blood cells, antimicrobial and anti-cancer activity [52, 53]. These phytochemical screening of ethanolic extracts of eggplant give confidence for folkloric uses and further development in plant breeding.

3.4 DPPH radical scavenging activity

The DPPH radial-scavenging activity of different eggplants is shown in Figure 2. The coefficient of variation for this statistical analysis was 6.38 and percentages of scavenging activity in all samples were significant difference ($p \leq 0.05$). The analysis revealed that *S. melongena* cv. 'Makhuea yoa muang' had the highest antioxidant activity. This might be related to anthocyanin contents in eggplants. Anthocyanin has been reported to be an effective antioxidant [54, 55] and belongs to flavonoid group [56]. More anthocyanin has been commonly found in the purple pigment than other pigments [54]. Moreover, anthocyanin was not in the peel of green or white eggplants [57, 58]. In this study, we only used absolute ethanol extraction solvent, which unlikely affected the DPPH result. Do *et al*. [59] reported that 100% ethanol was the most effective extraction solvent for antioxidant activity, phenolic and flavonoid compounds. As observed in the present study, the different peel color of *Solanum* displayed the

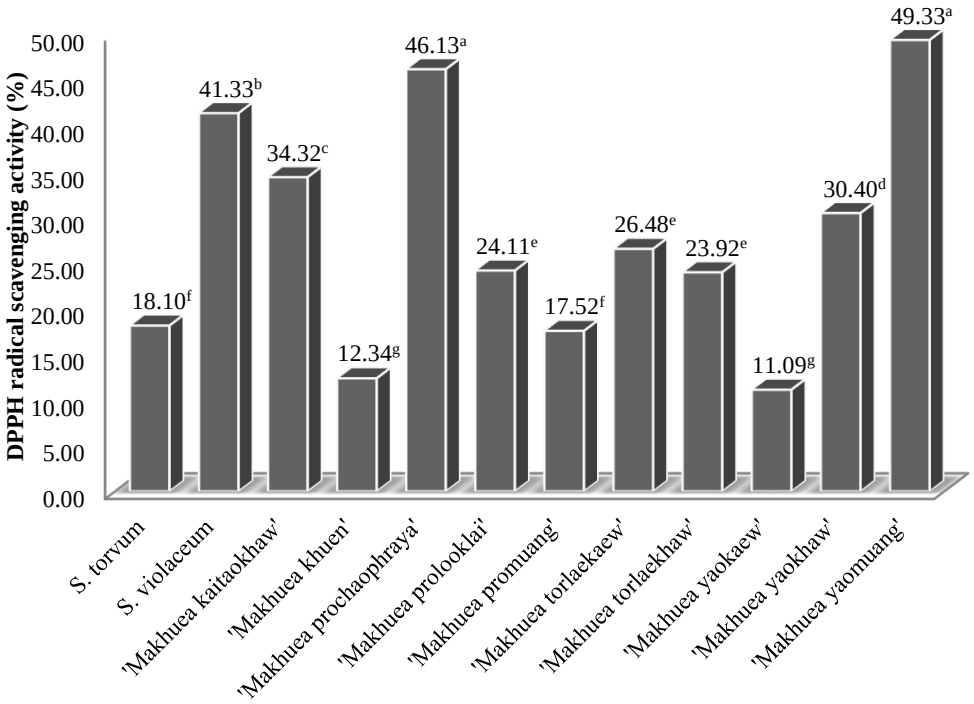

Figure 2. The DPPH radical scavenging activity of commercial eggplants

distinctions of antioxidant activity, which was in agreement with Somawathi *et al*. [60], who reported that purple eggplant exhibited the greatest DPPH radical scavenging activity.

3.5 Correlation analysis between fruit quality and phytochemical properties

The correlation analysis of some fruit quality and phytochemical properties using principal component analysis (PCA) showed that variations of cultivars in eggplants affected physical and chemical properties. The examination found that the first principal component (PC1) and the second principal component (PC2) presented the variance of variables as 54.974%. The variance of first principal component was 38.286% comprising TSS, alkaloid, tannin, saponin, and steroid. The variance of second principal component was 16.688% including h^o value, hardness, TSS, and DPPH radical scavenging activity (Table 4). The correlations between principal component and eggplant cultivars are shown in Figure 3 and the correlation coefficients between fruit quality components and phytochemical properties are presented in Table 5. The TSS parameter was found to positively correlate with saponin and steroid presences with correlation coefficients of 0.75 and 0.64, respectively. TSS is a parameter that determines certain solids dissolved within a substance, and TSS value is often used to indicate the sweetness in fruit as sugar content [61, 62]. As saponin and steroid are mostly presented in glycoside forms containing an aglycone unit linked to sugar molecules [63, 64], a high TSS content correlated to an abundance of saponin and steroid in fruit. From the results, species that had abundant steroids and saponin also had high TSS values. On the other hand, the TSS parameter was negatively correlated with thickness and moisture contents. These analyses are in agreement with Rashidi *et al*.'s report [65] that the correlation between TSS and water content followed a linear regression. Thus, the more water content is, the less TSS content in fruit will be. Notably, DPPH radical scavenging activity did not correlate with either fruit quality or phytochemical properties in this study.

Table 4. Total variation and eigenvalue of eggplants based on principal component analysis

Characters	PC1	PC2	PC	Eigenvalue	% variance	Cumulative % variance
h^o value	-0.075	0.256	1	3.829	38.286	38.286
Thickness	-0.410	-0.444	2	1.669	16.688	54.974
Hardness	-0.036	0.546	3	1.484	14.844	69.818
TSS	0.484	0.122	4	1.185	11.853	81.671
% Moisture	-0.441	-0.147	5	0.823	8.231	89.902
Alkaloid	0.231	-0.096	6	0.773	7.739	97.641
Tannin	0.240	-0.154	7	0.142	1.416	99.057
Saponin	0.321	-0.078	8	0.061	0.606	99.663
Steroid	0.412	-0.302	9	0.031	0.310	99.973
DPPH activity	-0.110	0.522	10	0.003	0.027	100.00

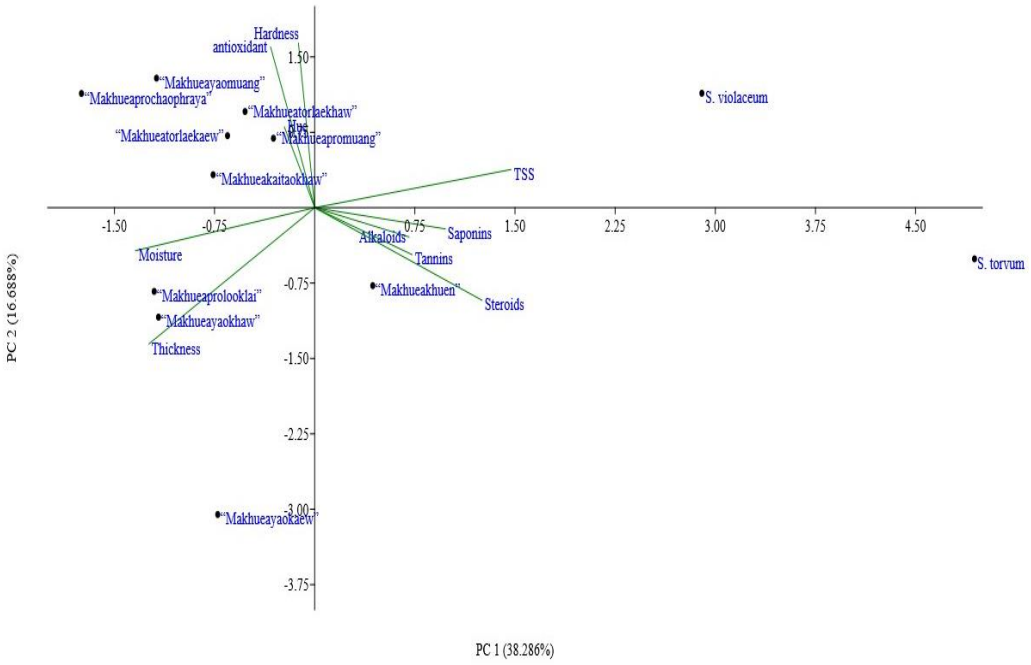

Figure 3. PCA projection for physical and chemical traits of eggplants and related species

Cluster analysis based on correlation data using UPGMA method presented the Cohen's correlation as 0.81. All samples could be classified into two major groups (Figure 4), the first group consisted of the non-eggplant group including *S. torvum* and *S. violaceum*, and the second group comprised all cultivars of *S. melongena* or the eggplant group. *Solanum torvum* and *S. violaceum* were clustered into the same group because both species exposed the small fruit with ample or moderate presences of alkaloids, saponins and steroids. The members within *S. melongena* group could be divided into three subgroups based on morphological and chemical traits, except for *S. melongena* cv. 'Makhuea yao kaew'. The first subgroup was classified by fruit color comprising *S. melongena* cv. 'Makhuea pro muang' and *S. melongena* cv. 'Makhuea yao muang' since these two eggplants were purple (h^o = 316.23-320.64). The second subgroup was isolated from other eggplants based on tannin presences. The members in second subgroup were *S. melongena* cv. 'Makhuea kai tao khaw' and *S. melongena* cv.

Table 5. Correlation coefficients between quality components and DPPH scavenging activity

	Thickness	Hardness	TSS	Moisture	Alkaloid	Tannin	Saponin	Steroid	DPPH
h^o	-0.05	-0.03	-0.07	0.21	0.06	-0.28	0.27	-0.30	0.19
Thickness		-0.35	-0.84**	0.77**	-0.28	-0.28	-0.45	-0.42	-0.21
Hardness			0.03	-0.09	-0.10	-0.09	-0.37	-0.31	0.11
TSS				-0.78**	0.26	0.42	0.75**	0.64*	-0.13
Moisture					-0.36	-0.13	-0.34	-0.75**	0.05
Alkaloid						0.51	-0.07	0.35	-0.10
Tannin							0.17	0.24	-0.08
Saponin								0.42	-0.22
Steroid									-0.44

Note: * = significantly different at $p \leq 0.05$ level, ** = significantly different at $p \leq 0.01$ level

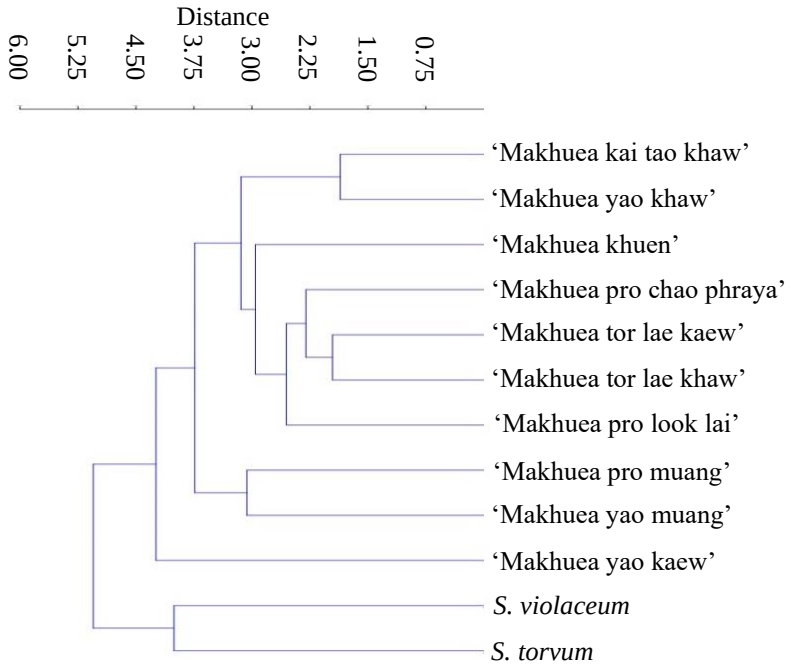

Figure 4. Dendrogram of commercial eggplants and related species using UPGMA clustering based on correlation matrix

'Makhuea yao khaw' The representatives in third subgroup involved *S. melongena* cv. 'Makhuea khuen', *S. melongena* cv. 'Makhuea pro chao phraya', *S. melongena* cv. 'Makhuea toe lae kaew', *S. melongena* cv. 'Makhuea tor lae khaw' and *S. melongena* cv. 'Makhuea pro look lai'. These eggplant cultivars were classified together because most of them were green fruit and lacked tannin. This analysis could interpret that fruit quality and phytochemical data could be used as a criterion to separate all cultivars of *S. melongena* from the two related species. Furthermore, fruit color and tannin presences were able to be a parameter for eggplant clustering.

4. Conclusions

The fruit quality of commercial eggplants and related species were significantly different. Peel color was distinct and it depended on main pigment content in eggplants. The maximum of *L** value was found in the white eggplant group. The highest *a** value was in *S. melongena* cv. 'Makhuea yao muang'. Moreover, commercial eggplants (*S. melongena*) presented more flesh thickness and moisture content than other species, whereas a high TSS was found in *S. torvum* and *S. violaceum*. The phytochemical screening showed that *S. torvum* was a good source of secondary metabolites including alkaloids, tannins, saponins, and steroids, while commercial eggplants presented moderate or slight phytochemical contents. All samples had the DPPH radical scavenging activity, while *S. melongena* cv. 'Makhuea yao muang' showed the highest activity. The correlation analysis between fruit quality and phytochemical data indicated a significant correlation between TSS content and saponin and steroid presence. Additionally, the examination could classify all cultivars of *S. molongena* from two related species using cluster analysis. In overall conclusion, commercial eggplants had higher fruit quality, phytochemical content, and antioxidant activity than *S. torvum* and *S. violaceum*. Future studies should be conducted to identify and quantify the phytochemical compounds in eggplants.

5. Acknowledgements

This research was supported by grants funded by Kasetsart University Research and Development Institute. The authors thank the Faculty of Natural Resource and Agro-Industry, Kasetsart University, Chalermphrakiat Sakon Nakhon province campus for providing instruments.

References

[1] Frodin, D.G., 2004. History and concepts of big plant genera. *Taxon*, 53(3), 753-776.
[2] Bohs, L., 2005. Major clades in *Solanum* based on *ndhF* sequence data. In: D.C. Keating, V.C. Hollowell and T.B. Croat, eds. *A Festschrift for William G. D'Arcy: The Legacy of a Taxonomist [Monographs in Systematic Botany from the Missouri Botanical Garden*, Vol. 104. St. Louis: Missouri Botanical Garden Press, pp. 27-49.
[3] Wu, Z.Y. and Raven, P.H. 1994. *Flora of China Vol.17*: *(Verbenaceae Through Solanaceae)*. Beijing: Science Press.
[4] de Padua, L.S., Bunyapraphatsara, N. and Lemmons, R.H.M.J., 1999. *Plant Resources of South-East Asia No.12: Medicinal and Poisonous Plants 1*. Leiden: Backhuys Publishers.
[5] Knapp, S., Vorontsova, M.S. and Särkinen, T., 2019. Dichotomous keys to the species of *Solanum* L. (Solanaceae) in continental Africa, Madagascar (incl. the Indian Ocean islands), Macaronesia and the Cape Verde Islands. *PhytoKeys*, 127, 39-76.
[6] Smitinand, T. 2014. *Thai Plant Names*. Bangkok: The Forest Herbarium, Royal Forest Department.
[7] Cannon, J.R., Dampawan, P., Lojanapiwatna, V., Phuriyakorn, B., Sinchai, W., Sitirugsa, P., Suvatabhandhu, K. and Wiriyachitra, P. 1980. A contribution to the Thai phytochemical survey. *Journal of the Science Society of Thailand*, 6, 46-53.
[8] Changbunjong, T., Wongwit, W., Leemingsawat, S., Tongtokit, Y. and Deesin, V., 2010. Effect of crude extract of *Solanum xanthocarpum* against snails and mosquito larvae. *Southeast Asian Journal of Tropical Medicine and Public Health*, 41(2), 320-325.
[9] Yousaf, Z., Wang, Y. and Baydoun, E., 2013. Phtochemistry and pharmacological studies *Solanum torvum* Swartz. *Journal of Applied Pharmaceutical Science*, 3(4), 152-160.
[10] FAOSTAT, 2017. *Value of Agricultural Production; Eggplants (aubergines)*. [online] Available at: http://www.fao.org/faostat/en/#data/QV
[11] Daunay, M.-C. and Janick, J., 2007. History and iconography of eggplant. *Chronica Horticulturae*, 47(3), 16-22.
[12] FAOSTAT, 2017. *Country Rank in the World, by Commodity; Eggplants (aubergines)*. [online] Available at: http://www.fao.org/faostat/en/#data/QC
[13] Taher, D., Solberg, S.Ø., Prohens, J., Chou, Y., Rakha, M. and Wu, T., 2017. World vegetable center eggplant collection: origin, composition, seed dissemination and utilization in breeding. *Frontiers in Plant Science*, https://doi.org/10.3389/fpls.2017.01484
[14] Azuma, K., Ohyama, A., Ippoushi, K., Ichiyanagi, T., Takeuchi, A., Saito, T. and Fukuoka, H., 2008. Structures and antioxidant activity of anthocyanins in many accessions of eggplant and its related species. *Journal of Agricultural and Food Chemistry*, 56(21), 10154-10159.
[15] Raigón, M.D., Prohens, J., Muñoz-Falcón, J.E. and Nuez, F. 2008. Comparison of eggplant landraces and commercial varieties for fruit content of phenolics, minerals, dry matter and protein. *Journal of Food Composition and Analysis*, 21(5), 370-376.
[16] Frary, A., Doganlar, S. and Daunay, M.C., 2007. Eggplant. In: C. Kole, ed. *Vegetables SE-9, Genome Mapping and Molecular Breeding in Plants*. Berlin: Springer, pp. 287-313.
[17] Frary, A. and Doganlar, S., 2013. Eggplants. In: B.C. Kang and C. Kole, eds. *Genetics, Genomics and Breeding of Peppers and Eggplants*. Boca Raton: CRC Press, pp. 116-143.

[18] U.S. Department of Agriculture, Agricultural Research Service, 2013. *USDA National Nutrient Database for Standard Reference* [online] Available at: http://www.ars.usda.gov/ba/bhnrc/ndl.
[19] Gürbüz, N., Uluişik, S., Frary, A., Frary, A. and Doğanlar, S., 2018. Health benefits and bioactive compounds of eggplant. *Food Chemistry*, 268(1), 602-610.
[20] Rodriguez-Jimenez, J.R., Amaya-Guerra, C.A., Baez-Gonzalez, J.G., Aguilera-Gonzalez, C., Urias-Orona, V. and Nino-Medina, G., 2018. Physicochemical, functional, and nutraceutical propertoes of eggplant flours obtained by different drying methods. *Molecules*, 23(12), 3210, https://doi.org/10.3390/molecules23123210
[21] Kaunda, J.S. and Zhang, Y.J., 2019. The genus *Solanum*: An ethnopharmacological, phytochemical and biological properties review. *Natural Products and Bioprospecting*, 9, 77-137.
[22] Plazas, M., Andújar, I., Vilanova, S., Hurtado, M., Gramazio, P., Herraiz, F.J. and Prohens, J., 2013. Breeding for chlorogenic acid content in eggplant: Interest and prospects. *Notulae Botanicae Horti Agrobotanici Cluj-Napoca*, 41(1), 26-35.
[23] AL-Janabi, A.A.H.S. and AL-Rubeey, S.A.H., 2010. Detection of antimicrobial activity of *Solanum melongena* L. (eggplant) against pathogenic microorganisms. *Pharmacognosy Journal*, 2(15), 35-39.
[24] Erturk, A.G., Erturk, O., Ayvaz, M.Ç. and Erturk, E.Y., 2018. Screening of phytochemical, antimicrobial and antioxidant activities in extracts of some fruits and vegetables consumed in Turkey. *Celal Bayar University Journal of Science*, 14(1), 81-92.
[25] Hong, H., Lee, J.H. and Kim, S.K., 2018. Phytochemicals and antioxidant capacity of some tropical edible plants. *Asian-Australasian Journal of Animal Sciences*, 31(10), 1677-1684.
[26] Rochín-Medina, J.J., Sotelo-Castro, J.A., Salazar-Salas, N.Y., López-Valenzuela, J.A. and Ramírez, K., 2019. Antioxidant and anti-*Salmonella* activities of eggplant peel compounds obtained by solvent-free calcium-based extraction. *CYTA-Journal of Food*, 17(1), 873-881.
[27] Edmonds, J.M. and Chweya, J.A., 1997. *Black Nightshades Solanum nigrum L. and Related Species*. Rome: International Plant Genetic Resources Institute.
[28] FAO, 1999. *The Vegetable Sector in Thailand. A Review*. [online] Available at: http://www.fao.org/3/a-ac145e.pdf
[29] Tangkanakul, P., Trakoontivakorn, G., Auttaviboonkul, P., Niyomvit, B. and Wongkrajang, K., 2006. Antioxidant activity of Northern and Northeastern Thai foods containing indigenous vegetables. *Kasetsart Journal (Natural Science)*, 40(Suppl.), 47-58.
[30] Kasikawattana, C., Ketsakul, S., Pethpun, A., Ampoln, D. and Auvuchanon, A., 2017. Evaluation of 18 pumpkin cultivars in rainy season production. *Songklanakarin Journal of Plant Science*, 4(1), 2-7.
[31] Kumar, P., Kumar, J., Kumar, R. and Dubey, R.C., 2016. Studies on phytochemical constituents and antimicrobial activities of leaves, fruits and stems of *Solanum nigrum* L. *Asian Journal of Plant Science and Research*, 6(4), 57-68.
[32] Djaafar, Z. and Ridha, O.M., 2014. Phytochemical study of selected medicinal plant, *Solanum nigrum*, the Algerian desert. *International Letters of Chemistry, Physics and Astronomy* 1, 25-30.
[33] Suryawanshi, P. and Vidyasagar, G.M., 2016. Phytochemical screening for secondary metabolites of *Opuntia dillenii* Haw. *Journal of Medicinal Plants Studies*, 4(5), 39-46.
[34] Brand-Williams, W., Cuvelier, M.E. and Berset, C., 1995. Use of a free radical method to evaluate antioxidant activity. *LWT-Food Science and Technology*, 28(1), 25-30.
[35] Hammer, Ø., Harper, D.A.T., and Ryan, P.D., 2001. PAST: Paleontological statistics software package for education and data analysis. *Palaeontolgia Electronica*, 4(1), 1-9.
[36] Begum, F., Islam, A.K.M.A., Rasul, M.G., Mian, M.A.K. and Hossain, M.M., 2013. Morphological diversity of eggplant (*Solanum melongena*) in Bangladeesh. *Emirates Journal of Food and Agriculture*, 25(1), 45-51.
[37] Khafagi, A.A.F., El-Ghamery, A.A., Ghaly. O.N. and Ragab, O.G., 2018. Fruit and seed morphology of some species of Solanaceae. *Taeckholmia*, 38, 123-140.

[38] CIE, 1986. *CIE Publications Nos. 15.2, Colorimetry*. 2nd ed. Vienna: Central Bureau of the CIE.
[39] Gajewski, M. and Arasimowicz, D., 2004. Sensory quality of eggplant fruits (*Solanum melongena* L.) as affected by cultivar and maturity stage. *Polish Journal of Food and Nutrition Sciences*, 13/54(3), 249-254.
[40] Sękara, A., Cebula, S. and Kunicki, E., 2007. Cultivated eggplants-origin, breeding objectives and genetic resources, a review. *Folia Horticulturae*, 19(1), 97-114.
[41] Chattopadhyay, A., Seth, T., Dutta, S., Ghosh, P.P., Chattopadhyay, S.B., Majumder, D. and Hazra, P., 2012. Breeding eggplant for higher productivity and bacterial wilt tolerance. *International Journal of Vegetable Science*, 18(4), 376-392.
[42] Batu, A., 1998. Some factors affecting on determination and measurement of tomato firmness. *Turkish Journal of Agriculture and Forestry*, 22, 411-418.
[43] Koundinya, A.V.V., Pandit, M.K., Dolui, S., Bhattacharya, A. and Hegde, V., 2019. Multivariate analysis of fruit quality traits in brinjal. *Indian Journal of Horticulture*, 76(1), 94-103.
[44] Hamouz, K., Pazderui, K., Lachman, J., Orsák, M., Pivec, V., Hejtmánková, K., Tomášek, J. and Cížek, M., 2014. Effect of cultivar, flesh colour, location and year of cultivation on glycoalkaloid content in potato tubers. *Plant, Soil and Environment*, 60(11), 512-517.
[45] Fidrianny, I., Winarsih, S. and Ruslan, K., 2017. Phytochemical content and antioxidant potential of different organs of eggplant (*Solanum melogena* L.) grown in West Java-Indonesia. *Asian Journal of Pharmaceutical and Clinical Research*, 10(8), 144-149.
[46] Koomson, D.A., Kwakye, B.D., Darkwah, W.K., Odum, B., Asante, M. and Aidoo, G., 2018. Phytochemical constituents, total saponins, alkaloids, flavonoids and vitamin C contents of ethanol extracts of five *Solanum torvum* fruits. *Pharmacognosy Journal*, 10(5), 946-950.
[47] Sánchez-Mata, M.-C., Yokoyama, W.-E., Hong, Y.J. and Prohens, J., 2010. α-solasonine and α-solamargine contents of gboma (*Solanum macrocarpon* L.) and scarlet (*Solanum aethipicum* L.) eggplants. *Journal of Agricultural and Food Chemistry*, 58(9), 5502-5508.
[48] Sczkowski, C.P., Kalinowska, M. and Wojciechowski, Z., 1988. The 3-O-glucosylation of steroidal saponins and alkaloids in eggplant (*Solanum melongena*); evidence for two separate glycosyltransferases. *Phytochemistry*, 48, 1151-1159.
[49] Atul, T. and Ray, S., 2014. Certain medicinal plants of Solanaceae and their alkaloids screening. *International Research Journal of Medical Sciences*, 2(1), 4-6.
[50] Buzzini, P., Arapitsas, P., Goretti, M., Branda, E., Turchetti, B., Pinelli, P., Leri, F. and Romani, A. 2008. Antimicrobial and antiviral activity of hydrolysable tannins. *Mini-Reviews in Medicinal Chemistry*, 8(12), 1179-1187.
[51] Orlowski, P., Zmigrodzka, M., Tomaszewska, E., Ranoszek-Soliwoda, K., Czupryn, M., Antos-Bielska, M., Szemraj, J., Celichowski, G., Grobelny, J. and Krzyzowska, M., 2018. Tannic acid-modified silver nanoparticles for wound healing: the importance of size. *International Journal of Nanomedicine*, 13, 991-1007.
[52] Rao, A.V. and Sung, M.K., 1995. Saponins as anticarcinogens. *The Journal of Nutrition*, 125(3), 717-724.
[53] Xu, R., Zhao, W., Xu, J., Shao, B. and Qin, G., 1996. Studies on bioactive saponins from Chinese medicinal plants. *Advances in Experimental Medicine and Biology*, 404, 371-382.
[54] Khoo, H.E., Azlan, A., Tang, S.T. and Lim, S.M., 2017. Anthocyanidins and anthocyanins: colored pigments as food, pharmaceutical ingredients, and the potential health benefits. *Food and Nutrition Research*, 61, https://doi.org/10.1080/16546628.2017.1361779
[55] Liu, Y., Tikunov, Y., Schouten, R.E., Marcelis, L.F.M., Visser, R.G.F. and Bovy, A., 2018. Anthocyanin biosynthesis and degradation mechanisms in Solanaceous vegetables: A review. *Frontiers in Chemistry*, https://doi.org/10.3389/fchem.2018.00052
[56] Martín, J., Kuskoski, E.M., Navas, M.J. and Asuero, A.G., 2017. Antioxidant capacity of anthocyanin pigments. In: J.C. Justino, ed. *Flavonoids*. Rijeka: Intech, pp. 205-255.

[57] Tateyama, C. and Igarashi, K., 2006. Anthocyanin and chlorogenic acid contents of some selected eggplant (*Solanum melongena* L.) cultivars, and the radical scavenging activities of their extracts. *Nippon Shokuhin Kagaku Kogaku Kaishi*, 53(4), 218-224.
[58] Passam, H.C. and Karapanos, I.C., 2008. Eggplants, peppers and tomatoes: factors affecting the quality and storage life of fresh and flesh-cut (minimally processed) produce. *The European Journal of Plant Science and Biotechnology*, 2(1), 156-170.
[59] Do, Q.D., Angkawijaya, A.E., Tran-Nguyen, P.L., Huynh, J.H., Soetaredjo, F.E., Ismadji, S. and Ju, Y.H., 2014. Effect of extraction solvent on total phenol content, total flavonoid content, and antioxidant activity of *Limnophila aromatica*. *Journal of Food and Drug Analysis*, 22, 296-302.
[60] Somawathi, K.M., Rizliya, V., Wijesinghe, D.G.N.G. and Madhujith, W.M.T., 2014. Antioxidant activity and total phenolic content of different skin coloured brinjal (*Solanum melongena*). *Tropical Agricultural Research*, 26(1), 152-161.
[61] Nookaraju, A., Upadhyaya, C.P., Pandey, S.K., Young, K.E., Hong, S.J., Park, S.K. and Park, S.W., 2010. Molecular approaches for enhancing sweetness in fruits and vegetables. *Scientia Horticulturae*, 127, 1-15.
[62] Magwaza, L.S. and Opara, U.L., 2015. Analytical methods for determination of sugars and sweetness of horticultural products-a review. *Scientia Horticulturae*, 184, 179-192.
[63] Hallman, A., 1985. Plants and cardiac glycosides. *British Heart Journal*, 54, 258-261.
[64] Bartnik, M. and Facey, P.C., 2017. Glycosides. In: S. Badal and R. Delgoda, eds. *Pharmacognosy: Fundamentals, Applications and Strategies*. San Diego: Academic Press, pp. 101-161.
[65] Rashidi, M., Ranjbar, I., Gholami, M. and Abbassi, S., 2010. Prediction of total soluble solids and firmness of carrot based on carrot water content. *International Journal of Agriculture and Biology*, 12(2), 237-240.

UV-Vis Spectrophotometric Method Using Natural Reagent from *Vigna unguiculata* subsp. *sesquipedalis* for Tetracycline Determination in Pharmaceutical Samples

Senee Kruanetr[1] and Kanyarak Prasertboonyai[2]*

[1]Center of Excellence for Innovation in Chemistry, Department of Chemistry (PERCH-CIC), Faculty of Science, Mahasarakham University, Mahasarakham, Thailand
[2]Faculty of Science, Energy and Environment, King Mongkut's University of Technology North Bangkok (Rayong Campus), Rayong, Thailand

Received: 20 April 2020, Revised: 15 July 2020, Accepted: 4 August 2020

Abstract

The natural reagents from *Vigna unguiculata* subsp. *sesquipedalis* were studied and applied in the determination of tetracycline by UV-Vis spectrophotometry. The method was based on a complexation formation between tetracycline and iron (III) derived from natural plant extract in acetate buffer at pH 5 to give a yellow complex with the optimum absorption at 430 nm. Parameters related to the extraction efficiency of the natural reagent and the factors that affected the determination of tetracycline were examined. Under optimum conditions, linearity was obtained over the range of 1.00 - 20.00 mg l^{-1}. The limit of detection *(*LOD, 3σ*)* and limit of quantification *(*LOQ, 10σ*)*, calculated following IUPAC, were 0.65 and 2.15 mg l^{-1}, respectively. The repeatability and reproducibility for determining 10.00 mg l^{-1} of tetracycline (n=11) were 3.43%and 5.14%, respectively. The proposed method was successfully applied to the determination of tetracycline in pharmaceutical formulations. The results obtained by the proposed method were in good agreement with the label values verified by the student t-test at the 95% confidence level.

Keywords: *Vigna unguiculata* subsp. *sesquipedalis*; tetracycline; UV-Vis spectrophotometer
DOI 10.14456/cast.2021.8

1. Introduction

Tetracycline (TC) is an antibiotic that is used to treat various bacterial infections such as infections of the skin, intestines, respiratory tract and other body systems [1]. It is often used in treating severe acne, or sexually transmitted diseases such as syphilis, gonorrhea, and chlamydia. In some cases, tetracycline is used when penicillin or other antibiotics cannot be used to treat serious infections [2]. It can be seen that it is effective against a broad spectrum of bacteria, as well as other organisms, including some protozoan parasites. However, overdose with tetracycline can cause liver failure and even death [3].

*Corresponding author: Tel.: (+66) 856939614
E-mail: kanyarak.p@sciee.kmutnb.ac.th

The literature review demonstrated that a wide range of analytical methods, including high-performance liquid chromatography (HPLC) [4-6], capillary electrophoresis [7, 8], electrochemistry [9, 10], spectrofluorometry [11], and chemiluminescence [12], have been used to detect tetracycline in pharmaceutical formulations and environmental samples. Although these methods provide high sensitivity, high selectivity and high precision, they do not provide sufficiently low determination ranges. Moreover, they can be very time consuming and have high operating costs.

UV-Vis spectrophotometry is one option of analytical methods because it is fast, simple, low cost, and offers a wide range of applications that are commonly available in all laboratories set up for quality control for drug analysis. Many researchers have presented the complexation of tetracycline by using various metal ions for tetracycline analysis by UV-Vis spectrophotometric method, and ions used included as lanthanide (III) [13], Manganese (III) and copper (II) [14], aluminium (III) [15], uranium (VI) [16], platinum (II) [17], iron (III) [18]. Moreover, iron (III) is one of the metal ions that strongly chelates tetracycline and it has been shown that the determination of tetracycline was influenced by the presence of iron (III) [19]. In 1988, Sultan *et al.* [18] developed a spectrophotometric method for determining tetracycline that depended on the reaction between iron (III) and tetracycline in H_2SO_4 medium. This method was used for tetracycline detection in drug formulations. In 2008, Palamy and Ruengsitagoon [20] presented an applied flow injection spectrophotometric method for tetracycline detection based on the reaction of tetracycline and iron (III) in acidic medium, and the product was detected at the maximum absorption of 423 nm. However, wastes that result from the use of iron (III) as a chelating agent can be harmful to people and the environment.

Recently, researchers have focused on the design and development of method based on 'green' chemistry as processes that reduce or eliminate the generation of hazardous substances which are economically and environmentally friendly [21]. Natural reagent from plant extract is another alternative for green chemical analysis that is gaining attention. Therefore, plants that have high iron content are another option to develop as a natural extract for tetracycline analysis.

Vigna unguiculata subsp. *sesquipedalis* (Yard-long bean) is an important legume that is grown in tropical and subtropical areas [22]. It offers high nutritional value in both its leaves and seeds, and is resistant to drought and salinity [23]. Yardlong beans are mainly cultivated for their soft and long pods that can be eaten both fresh and cooked [24]. It is widely cultivated for its edible iron-protein-rich seeds, antioxidant capacity and tolerance to mild drought [25].

In this research, we presented a spectrophotometric method for the determination of tetracycline in pharmaceutical formulations by using the natural reagent from *Vigna unguiculata* subsp. *sesquipedalis.* The proposed method depended on the complex reaction between iron (III) content in plant extract and tetracycline in acetate buffer pH 5.0 to form a yellow complex with an optimum absorption at 430 nm. The complexation reaction was shown in Figure 1.

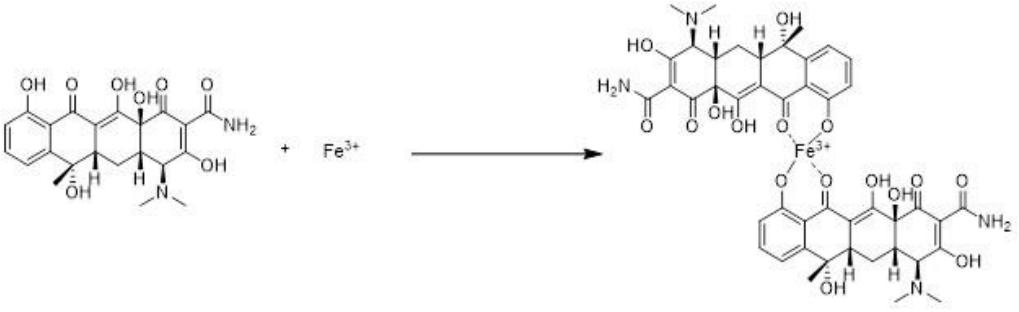

Figure 1. The possible reaction mechanism tetracycline reacts with iron **(**III**)**

2. Materials and Methods

2.1 Reagents and chemicals

All chemicals used in this study were of analytical reagent grade and were not further purified. Double-distilled deionized water (DI water) was used for diluting and adjusting volume of solution throughout the experiments.

Tetracycline standard was purchased from Fluka (Switzerland). Nitric acid (HNO_3) and hydrochloric acid (HCl) were purchased from Merck (Germany). A standard solution of tetracycline (10 mg l^{-1}) was prepared by dissolving 0.01 g of tetracycline in DI water and adjusting volume to 1000 ml.

Acetate buffer solution (0.10 mol l^{-1} at pH 5.0) was prepared by dissolving 5.772 g of sodium acetate in 500 ml of DI water solution. Acetic acid, 1.70 ml, was then added. Finally, a 10 N HCl solution was gently dropped into the solution.

2.2 Apparatus

A spectrophotometer (model Shimadzu 2600, Japan) was used for scanning the spectra of the complex and employed during the investigation for colorimetric studies. A pH meter (Metrohm, Switzerland) was used for measuring the pH of the solutions. A Microwave Plasma Atomic Emission Spectrometer (MP-AES) instrument (Model: 4100, Agilent Inc., Santa Clara, CA, USA) was used for iron (III) determinations (wavelength at 259.94 nm). The sample introduction system consisted of solvent-resistant tubing, a double-pass cyclonic chamber, and an inert flow blurring nebulizer (OneNeb). The wavelength for iron (III) determinations used was at 259.94 nm.

2.3 Plant extraction for iron (III) content

Vigna unguiculata subsp. *sesquipedalis* (collected from Rayong Province, Thailand) was cleaned by washing with tap water and cut into small-sized pieces. The selected plant in the experiment was dried under the sun light for a day. After that, it was stored in a desiccator at room temperature until the weight was constant to be certain that the prepared plant was dried before use in the extraction process.

The parameters that related to the efficiency of preparation of plant extract such as type of acid, volume ratio of acid, acid concentration, *Vigna unguiculata* subsp. *sesquipedalis* concentration and time of digestion were studied (as shown in section 3.1).

The extraction process was as follows; 5.00 g of dry plant was dissolved with acid mixture solution of 1.00 M HNO_3 and 1.00 M HCl at a ratio of 25:75, and heated for 1 h on a hot plate [20]. The solution was cooled down to room temperature and filtered through a Whatman No. 42 filter paper. The extract as natural reagent was then collected and adjusted to the volume of 100 ml with DI water. The amount of iron (III) in *Vigna unguiculata* subsp. *sesquipedalis* extract was analyzed using Microwave Plasma Atomic Emission Spectroscopy (MP-AES 4100, Algilent Technologies).

2.4 Procedure for tetracycline determination

Aliquots (1.00-5.00 ml) of standard tetracycline solution (10 mg l^{-1}) and 2.00 ml aliquots of plant extract were mixed together into 10 ml volumetric flasks. The contents of each flask were then adjusted to the mark with acetate buffer solution pH 5.0 to form a yellow color complex. The product solution was transferred into a cuvette and measured its absorption at 430 nm against a reagent blank using UV-Vis spectrophotometry.

2.5 Sample preparation

Sample was purchased from pharmacies in Rayong, Thailand. Twenty drugs (capsules or tablets containing 250 and 500 mg per capsule or tablet of tetracycline) were mixed together and then ground into a fine powder. A sample was accurately weighed to contain 100 mg of tetracycline and dissolved in DI water and filtered through Whatman No. 42 paper. The filtered solution was transferred to 100 ml volumetric flask and made up to the mark volume by DI water. An aliquot of the sample solution was determined by the proposed method.

3. Results and Discussion

The experiment was divided into 2 sections, the first section was concerned with studying the optimum conditions for preparing the natural reagent. The second part was an investigation of the suitable conditions for determining tetracycline by the prepared reagent using the univariation method. The parameters that affected the accuracy and sensitivity of analysis of tetracycline were varied while the other were fix constant. The parameter that gave the highest signal with low standard deviation was selected.

3.1 Studying the preparation of the plant extract

The process for the preparation of plant extract containing high amount of iron (III) was a considerable purpose. The highest iron (III) content led to obtain the highest complex resulting in a highest sensitivity. The sensitivity of each studied parameter was examined by selecting the highest slope from the linear relation graph plotted between the absorbance of the iron (III)-complex against three concentrations of the standard tetracycline (1, 2 and 3 mg l^{-1}). The parmeter that provided the highest sensitivity was selected as the optimum condition.

3.1.1 Effect of acid type

Using a suitable acid and/or acid mixture for extraction of plant led to obtain a high efficiency of iron(III) extraction for forming a complex with tetracycline resulting to high absorption signal and high sensitivity. Therefore, the effect of single acid and acid mixture on the plant extraction efficiency was investigated. In this work, 1.00 mol l^{-1} of HNO_3, HCl, H_2SO_4 and acid mixture; HNO_3-HCl were examined. Figure 2 showed that the acid mixture of HNO_3-HCl gave the highest sensitivity. Therefore, the acid mixture between HNO_3-HCl was selected for the plant extract preparation.

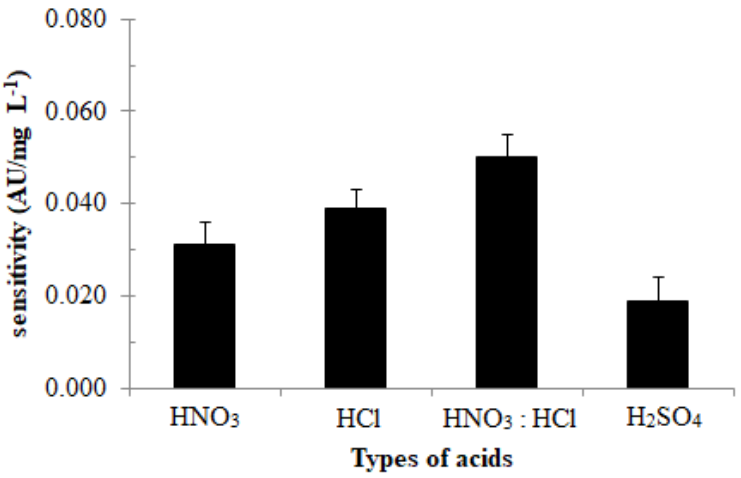

Figure 2. Effect of acid type on sensitivity (*n*=3)

3.1.2 Effect of volume ratio between HNO_3 and HCl

The ratio of mixed acid between HNO_3 and HCl affected the digestion of natural reagents that react with tetracycline to form complexes. Therefore, the ratio of mixed acid between HNO_3 and HCl (at 1.00 mol l^{-1} of each acid) in order to get the suitable acid ratio between HNO_3 and HCl in the determination of tetracycline content was studied. From the experiment, the mixed ratio of HNO_3 and HCl at 25:75, gave the highest sensitivity as showed in Figure 3. However, when the ratio of HNO_3 acid was more than 25, the sensitivity was decreased. Therefore, the mixture ratio of HNO_3 and HCl at 25:75 was chosen as the optimum condition.

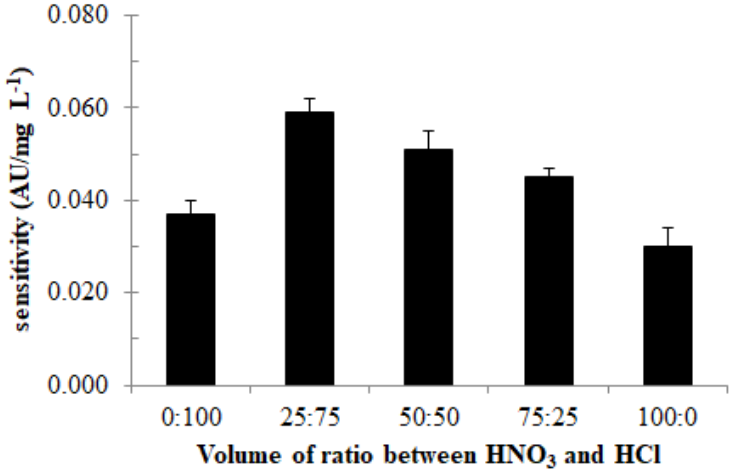

Figure 3. Effect of volume ratio between HNO_3 and HCl on sensitivity (*n*=3)

3.1.3 Effect of acid mixture between HNO_3 and HCl concentration

The concentration of the acid mixture between HNO_3 and HCl affected the digestion of natural reagents that reacted with tetracycline to form complexes. From Figure 4, the acid mixture concentration of HNO_3 and HCl at 1.00 mol l^{-1} provided the highest sensitivity. It can be seen that, the sensitivity was increased at the acid concentration range of 0.50-1.00 mol l^{-1}. However, the sensitivity was decreased at the acid concentration over 1.00 mol l^{-1}. Therefore, the concentration of HNO_3 and HCl at 1.00 mol l^{-1} was chosen as the optimum condition.

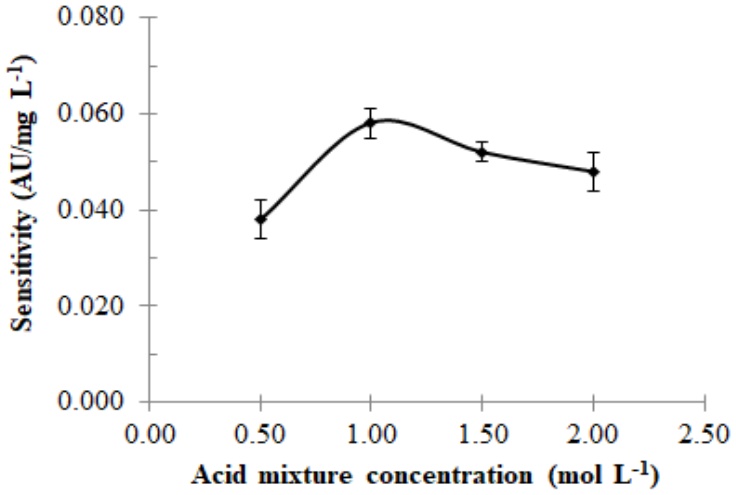

Figure 4. Effect of acid mixture between HNO_3 and HCl on sensitivity (*n*=*3*)

3.1.4 Effect of *Vigna unguiculata* subsp. *sesquipedalis* concentration

The study of the effect of *Vigna unguiculata* subsp. *sesquipedalis* concentration on sensitivity was studied by changing the weight of *Vigna unguiculata* subsp. *sesquipedalis* powder from 0.50-10.00 g (in 100 ml of DI water). Figure 5 showed that sensitivity increased when the weight of *Vigna unguiculata* subsp. *sesquipedalis* powder was increased to 5.00 g which was almost higher than its constant value. Therefore, 5.00 g of *Vigna unguiculata* subsp. *sesquipedalis* were selected.

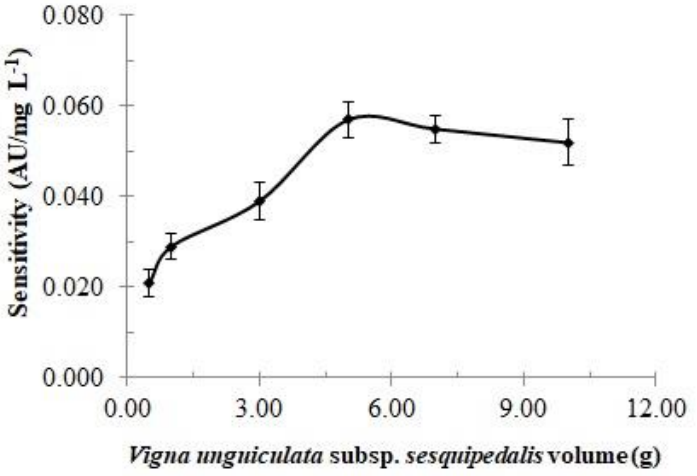

Figure 5. Effect of *Vigna unguiculata* subsp. *sesquipedalis* concentration on sensitivity (*n=3*)

3.1.5 Effect of digestion time for plant extract

The extraction time for the digestion of nature reagents, the type of acid, including the optimum conditions of the above acids affect the amount of iron (III) which is the main component of natural reagent extracts are digested. Therefore, the digestion time between 15-120 min was conducted. From the experimental results (Figure 6), it was found that the natural reagent digestion time at 60 min gave the highest sensitivity. It can be seen that between 15-60 min the sensitivity increased and after 60-120 min the sensitivity decreased. Therefore, the digestion time of 60 min was selected.

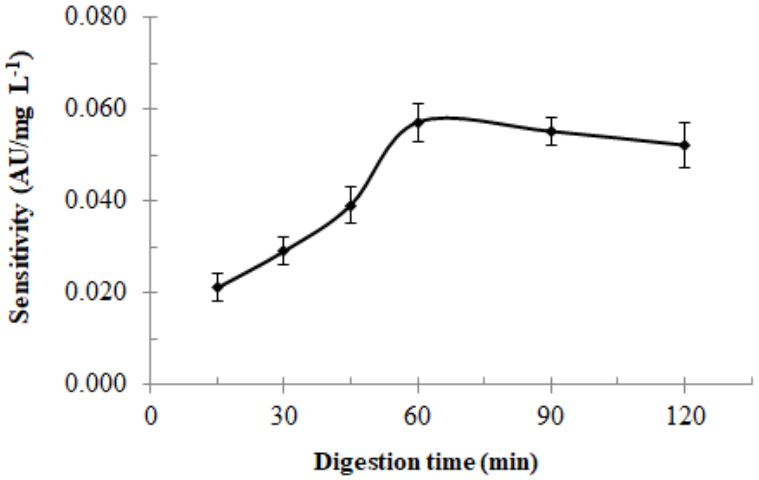

Figure 6. Effect of digestion time for plant extract on sensitivity (*n=3*)

Under the optimum condition, the amount of iron in *Vigna unguiculata* subsp. *sesquipedalis* extract were analyzed by using MP-AES. The results showed that the iron concentration in plant extracts used in the experiment was 49.56 mg l^{-1}.

3.2 Absorption spectra

The optimum absorption wavelength of a yellow color complex forming between tetracycline and iron contents in natural reagent extracts, pure tetracycline solution and standard iron (III) solution were measured over the range of 300-700 nm against reagent blank (acetate buffer pH 5.0). It was found that the maximum absorption signal of the complex was 430 nm while pure tetracycline solution and standard iron (III) solution were absorbed at 275 and 355 nm, respectively. Therefore, the absorption wavelength of 430 nm was selected.

3.3 Optimum conditions of reaction for tetracycline determination

3.3.1 Effect of pH

The stable yellow complex between tetracycline and iron (III) is pH dependent. Therefore, the acetate buffer pH range of 3.0-5.0 was studied. Figure 7 showed that, the sensitivity was increased at the pH range from 3.0-5.0, over of this pH the sensitivity was decreased. Therefore, the optimum pH of 5.0 was selected.

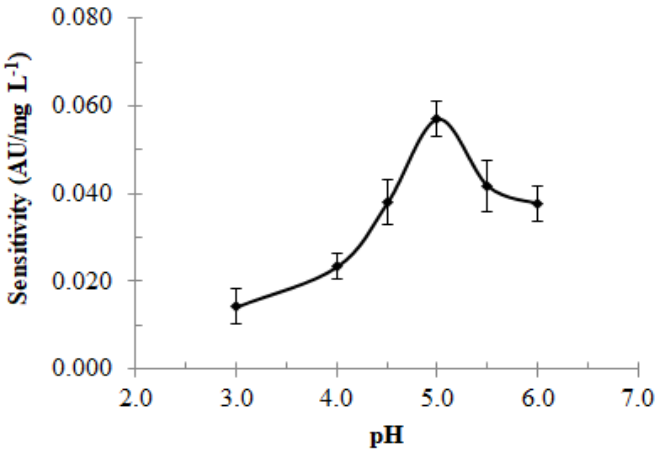

Figure 7. Effect of pH on sensitivity (*n*=3)

3.3.2 Effect of the volume of plant extract

The volume of plant extract affects the reaction because it acts as a reagent, which affects the distribution of the substance and affects the measured signal. In addition, finding the optimum condition in this variable reduces unnecessary use of the natural reagents while maintaining the best sensitivity, accuracy and reproducibility of the procedure for the drug of interest. Therefore, it is important to use the right volume of plant extract for the system environment. Figure 8 showed that the sensitivity increased with increasing volume of plant extract ranging from 1.00-2.00 ml. Above this volume, there was no significant change in sensitivity. So, the plant extract volume of 2.00 ml was selected for determining of tetracycline.

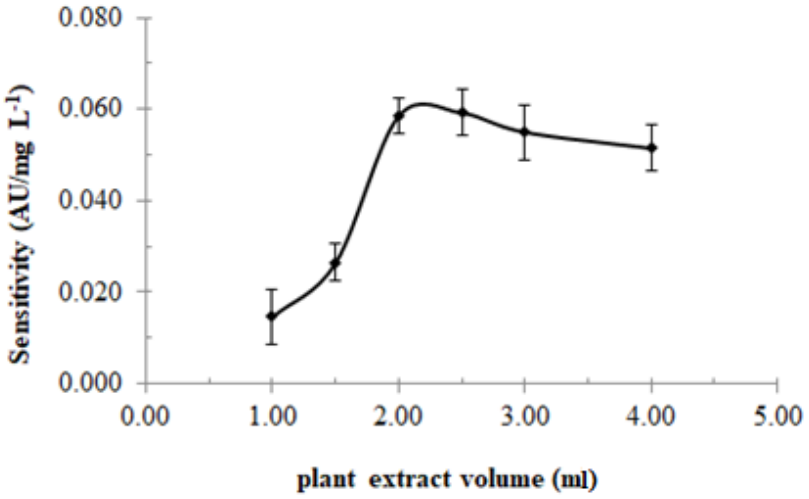

Figure 8. Effect of the volume of plant extract on sensitivity (*n*=*3*)

3.3.3 Effect of reaction time

The effect of reaction time on the sensitivity of the complex was investigated by studying the reaction time up to 60 min. Figure 9 showed that the reaction time did not affect the sensitivity of the complex.

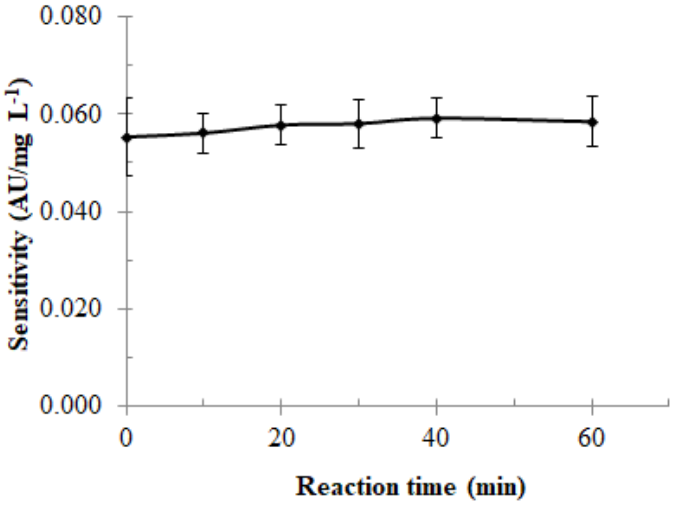

Figure 9. Effect of reaction time on sensitivity (*n*=*3*)

3.4 Validation method

The validation of the proposed method was evaluated under the optimum conditions (Table 1) obtained from the previous section. The results showed that the linearity range was in the range of 1.00-20.00 mg l^{-1} (Figure 10) with the regression equation: $y = 0.061x + 0.004$ (R^2= 0.9890), where Y and X present absorbance and TC concentrations in mg l^{-1}, respectively. The limit of detection (LOD, 3σ) and limit of quantification (LOQ, 10σ), calculated following IUPAC were 0.65 and 2.15 mg l^{-1}, respectively. The repeatability and reproducibility for 10.00 mg l^{-1} of tetracycline (n=11) was examined as the percentage relative standard deviation (%RSD), which was calculated using the equation ($SD/\bar{X}$) x 100, where SD is standard deviation and $\bar{X}$ is an average of the measurement data. It was found that the percentage relative standard deviations were 3.43% and 5.14%, respectively.

Table 1. Variable range studies and optimum conditions for tetracycline determination

Parameter studied	Range studied	Optimum level
- Effect of acid type	HNO_3, HCl, HNO_3 + HCl, H_2SO_4	HNO_3 + HCl
- Effect of volume ratio between HNO_3 and HCl (%v/v)	100:0, 75:25, 50:50, 25:75, 0:100	25:75
- Effect of acid mixture between HNO_3 and HCl concentration (mol l^{-1})	0.50 – 2.00	1.00
- Effect of *Vigna unguiculata subsp. sesquipedalis* concentration (g)	0.50-10.00	5.00
- Effect of digestion time (min)	15-120	60
Wavelength (nm)	350-700	430
- Effect of pH	3.00-7.00	5.00
- Effect of natural reagent volume (ml)	1.00-4.00	2.00
- Effect of reaction time (min)	0-60	0

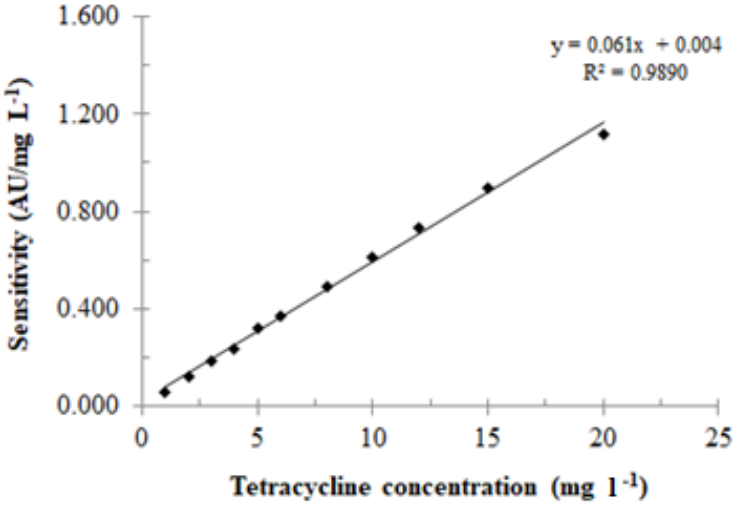

Figure 10. The calibration curve of spectrophotometric method for determination of tetracycline

3.5 Effects of interferences

Under the conditions selected above, the effects of many substances are used as generic excipients in drug preparation for this test method of tetracycline. The tolerance ratio was taken as the maximum amount causing an error not greater than 5% for determining the analyte of interest. The mixture of 5.00 mg l^{-1} tetracycline solutions with excipients at different concentrations were filtered if necessary before analysis. The tolerance values of the investigated species were >500 mg l^{-1} for starch; 400 mg l^{-1} for glucose, sucrose and lactose; 250 mg l^{-1} for fructose, citric acid and sodium benzoate. So, it could be considered that there was no interference and there was a specificity in drug analysis by the proposed method.

3.6 Application

The proposed method was applied for determination of tetracycline in pharmaceutical formulations available doses of 250 and 500 mg per capsule/tablet. The results obtained were satisfactory while compared to the label values (Table 2). Statistical analysis of the results from both values using the t-test [26] at the 95% confidence level were not significant. Indicating that this method was accurate.

Table 2. Accuracy of the proposed method compared with label value for determination of tetracycline in pharmaceutical sample

Pharmaceutical sample	**Tetracycline found (mg)**	
	Label value	**Proposed method[a]**
TC-1	250.00	242.11 ± 0.38
TC-2	250.00	247.21 ± 0.46
TC-3	250.00	241.09 ± 0.49
TC-4	250.00	245.25 ± 0.31
TC-5	500.00	496.02 ± 0.43

[a] = Average from three determinations

Table 3 showed the comparison of the analytical characteristics of the proposed method for determining tetracycline with the previous reports. The proposed method was provided a lower sensitivity than the previous report due to the limitation of the phototube detector in the UV-Vis spectrometer. Although this method was lower sensitivity than the previous reports, the advantages of this method was provided a wide linearity range, rapid and simple, using non-toxic natural reagent and environmentally friendly. To improve the sensitivity for further studies, it should be replaced with a high sensitivity detector such as photomultiplier tube or photodiode array detector.

Table 3. Comparison of the analytical characteristics of the proposed method for determining tetracycline with the previous reports

Analytical method	Linear range	LOD	%RSD	Reference
HPLC	50-5000 μg kg^{-1}	15.30 μg kg^{-1}	4.90%	[5]
CE	-	0.50 μg ml^{-1}	4.37%	[7]
Electrochemistry	2.0×10^{-5}-3.1×10^{-4} mol l^{-1}	3.6×10^{-7} mol l^{-1}	6.50%	[10]
Spectrofluorometry	0.05-100 μg ml^{-1}	0.029 μg ml^{-1}	3.53%	[11]
Chemiluminescence	5.0×10^{-5}-5.0×10^{-4} mol l^{-1}	2.0×10^{-6} mol l^{-1}	3.70%	[12]
This work	1.00 – 20.00 mg l^{-1}	0.65 mg l^{-1}	3.43%	

4. Conclusions

A simple, precise and green UV-Vis spectrophotometric method for tetracycline determination was demonstrated by the reaction between tetracycline and iron (III) contents in *Vigna unguiculata* subsp. *sesquipedalis* extraction as a natural reagent in an acetate buffer solution pH 5.0. The proposed method was successfully applied to the determination of tetracycline in pharmaceutical formulations. The results obtained by the proposed method were in good agreement with the assigned value from the label verified by student t-test at 95% confidence level. The benefit of the proposed method over the previous studies were used non-toxic/hazardous reagents, generates less waste, simple and cost-effective.

5. Acknowledgements

The authors would like to express their sincere gratitude and appreciation to the Faculty of Science, Energy and Environment, King Mongkut's University of Technology, North Bangkok (Rayong Campus) for providing all the necessary equipment and laboratory facilities. This research was funded by contract No. SciEE 01/61. Senee Kruanetr wishes to thank the Center of Excellence for Innovation in Chemistry, Department of Chemistry (PERCH-CIC), Faculty of Science, Mahasarakham University for facilities and financial support.

References

[1] Chopra, I. and Roberts, M., 2001. Tetracycline antibiotics: mode of action, applications, molecular biology, and epidemiology of bacterial resistance. *Microbiology and Molecular Biology Reviews*, 65(2), 232-260.

[2] Chopra, I., Hawkey, P.M. and Hinton, M., 1992. Tetracyclines, molecular and clinical aspects. *Journal of Antimicrobial Chemotherapy*, 29(3), 245-277.

[3] Katiyar, S.K. and Elend T.D., 1991. Enhanced antiparasitic activity of lipophilic tetracyclines: role of uptake. *Antimicrobial Agents and Chemotherapy*, 35, 2075-2080.

[4] Cinquina, A.L., Longo, F., Anastasi, G., Giannetti, L. and Cozzoani, R., 2003. Validation of a high-performance liquid chromatography method for the determination of oxytetracycline,

tetracycline, chlortetracycline and doxycycline in bovine milk and muscle. *Journal of Chromatography A*, 987(1-2), 227-233.

[5] Arabsorkhi, B. and Sereshti H., 2018. Determination of tetracycline and cefotaxime residues in honey by micro-solid phase extraction based on electrospun nanofibers coupled with HPLC. *Microchemical Journal*, 140, 241-247.

[6] Charoenraks, T., Chuanuwatanakul, S., Honda, K., Yamaguchi, Y. and Chailapakul, O., 2005. Analysis of tetracycline antibiotics using HPLC with pulsed amperometric detection. *Analytical Sciences*, 21(3), 241-247.

[7] Hsiao, Y.M., Ko, J.L. and Lo, C.C., 2001. Determination of tetracycline and streptomycin in mixed fungicide products by capillary zone electrophoresis. *Journal of Agricultural and Food Chemistry*, 49(4), 1669-1674.

[8] Islas, G., Rodriguez, J.A., Perez-Silva, I., Miranda, J.M. and Ibarra, I.S., 2018. Solid-phase extraction and large-volume sample stacking-capillary electrophoresis for determination of tetracycline residues in milk. *Journal of Analytical Methods in Chemistry*, 2018, 1-7.

[9] Palaharn, S., Charoenraks, T., Wangfuengkanagul, N., Grudpan, K. and Chailapakul, O., 2003. Flow injection analysis of tetracycline in pharmaceutical formulation with pulsed amperometric detection. *Analytica Chimica Acta*, 49, 191-197.

[10] Wong, A., Scontri, M., Materon, E.M., Lanza, M.R.V. and Sotomayor, M.D.P.T., 2015. Development and application of an electrochemical sensor modified with multi-walled carbon nanotubes and graphene oxide for the sensitive and selective detection of tetracycline. *Journal of Electroanalytical Chemistry*, 757, 250-257.

[11] Sun, C.Y., Su, R.F., Bie, J.X., Sun, H.J., Qiao, S.G., Ma, X.Y., Sun R. and Zhang, T.H., 2018. Label- free fluorescent sensor based on aptamer and thiazole orange for the detection of tetracycline. *Dyes and Pigments*, 149, 867-875.

[12] Townshend, A., Ruengsitagoon, W., Thongpoon, C. and Liawruangrath, S., 2005. Flow injection chemiluminescence determination of tetracycline. *Analytica Chimica*, 541, 103-109.

[13] Karthikeyan, G., Mohanraj, K., Elango, P.K. and Girishkumar, K., 2004. Synthesis, spectroscopic characterization and antibacterial activity of lanthanide-tetracycline complexes. *Transition Metal Chemistry*, 29(1), 86-90.

[14] Chen, R.W. and Huang, H.C., 2009. Transformation of tetracyclines mediated by Mn (II) and Cu (II) ions in the presence of oxygen. *Environmental Science and Technology*, 43, 401-407.

[15] Liawruangrath, S., Liawruangrath, B., Watanesk, S. and Ruengsitagoon, W., 2006. Flow injection spectrophotometric determination of tetracycline in a pharmaceutical preparation by complexation with aluminium (III). *Analytical Science*, 22(1), 15-19.

[16] Mahgoub, S.A., Khairy, M.E. and Kasem, A., 1974. Complex formation of uranyl acetate with tetracycline and its utilization for their microdetermination. *Journal of Pharmaceutical Sciences*, 63(9), 1451-1455.

[17] Silva, P. P., De Paula, F.C.S., Guerra, W., Silveira, J. N., Botelho, F.V., Vieira, L.Q., Bortolotto, T., Fischer, F.L., Bussi, G., Terenzi H. and Pereira-Maia, E.C. 2010. Platinum (II) compounds of tetracyclines as potential anticancer agents: cytotoxicity, uptake and interactions with DNA. *Journal of the Brazilian Chemical Society*, 21(7), 1237-1246.

[18] Sultan, M.S., Alzamil, Z.I. and Alarfaj, A.N., 1988. Complexometric-spectrophotometric assay of tetracyclines in drug formulations. *Talanta*, 35(5), 375.

[19] Grenier, D., Huot, M. and Mayrand, D., 2000. Iron-chelating activity of tetracyclines and its impact on the susceptibility of actinobacillus actinomycetemcomitans to these antibiotics. *Antimicrobial Agents and Chemotherapy*, 44(3), 763-766.

[20] Palamy, S. and Ruengsitagoon, W., 2017. A novel flow injection spectrophotometric method using plant extracts as green reagent for the determination of doxycycline. *Spectrochimica Acta Part A*, 171, 200-206.

[21] Settheeworrarit, T., Hartwell, S.K., Lapanatnoppakhun, S., Jakmunee, J., Christian, G.D. and Grudpan, K., 2005. Exploiting guava leaf extract as an alternative natural reagent for flow injection determination of iron. *Talanta*, 68, 262-267.

[22] Iriti, M. and Varoni, E., 2017. Pulses, healthy, and sustainable food sources for feeding the planet. *International Journal of Molecular Science*, 18(2), 1-8.

[23] Kongjaimun, A., Kaga, A., Tomooka, N., Somta, P., Vaughan, D.A. and Srinives, P., 2012. The genetics of domestication of yardlong bean, *Vigna unguiculata* (L.) Walp. ssp. *unguiculata cv.-gr. sesquipedalis. Annals of Botany*, 109 (6), 1185-1200.

[24] Kongjaimun, A., Somta, P., Tomooka, N., Kaga, A., Vaughan, A.D. and Srinives, P., 2013. QTL mapping of pod tenderness and total soluble solid in yardlong bean [*Vigna unguiculata* (L.) Walp. subsp. *unguiculata cv.-gr. sesquipedalis*]. *Euphytica*, 189(2), 217-223.

[25] Kumar, S., Yadav, S.S, Tripura, P. and Jatav, S.H., 2017. Use of phosphorus for maximization of mungbean (*Vigna radiata* L.) (Wilszeck) productivity under semi-arid condition of Rajasthan, India. *International Journal of Current Microbiology and Applied Sciences,* 6(2), 612-617.

[26] Miller, J.C. and Miller, J.N. 1993. *Statistics for Analytical Chemistry*, 3rd ed. New York: Ellis Horwood PTR Prentice Hall.

Biochemical Composition and Bioactive Properties of *Chlorella minutissima* (Chm1) as a Potential Source of Chemical Compounds for Nutritional Feed Supplement and Disease Control in Aquaculture

Eldrin DLR. Arguelles*

Philippine National Collection of Microorganisms, National Institute of Molecular Biology and Biotechnology (BIOTECH), University of the Philippine Los Baños, College, Laguna, Philippines

Received: 12 April 2020, Revised: 9 June 2020, Accepted: 7 August 2020

Abstract

Microalgae contain high levels of proteins, lipids, carbohydrates and other bioactive metabolites with direct relevance to aquaculture. This investigation was done to assess the bioactive properties and describe the neutraceutical and pharmacological benefits of a green microalga, *Chlorella minutissima* (Chm1). The alga has a total phenolic content of 30.94±0.06 mg GAE g^{-1}. Relative antioxidant efficiency showed that *C. minutissima* exerted potent ABTS scavenging activity and high ability of reducing copper ions in a concentration-dependent manner with IC_{50} values of 48.13 μg GAE ml^{-1} and 13.90 μg GAE ml^{-1}, respectively. Evaluation of antibacterial activities using microtiter plate dilution assay revealed that *C. minutissima* showed strong activity against *Aeromonas hydrophila* with a minimum inhibitory concentration (MIC) of 125 μg ml^{-1}. The algal extract is also effective against *Vibrio cholerae*, *Vibrio parahaemolyticus* and *Staphylococcus aureus* in each case with MIC value of 250 μg ml^{-1}. Also, *C. minutissima* extract was able to inhibit the growth of *Pseudomonas fluorescens* with MIC value of 500 μg ml^{-1}. Proximate composition of the dried microalga showed that *C. minutissima* consists of high protein, ash and crude fat content with values of 42.61±0.11%, 17.79 ± 0.04% and 11.70 ± 0.01%, respectively. The results show that *C. minutissima* is an excellent candidate organism as a potential source of chemical compounds important for feed formulation and disease control in aquaculture.

Keywords: Antibacterial activity; antioxidant activity; bioactive compounds; bacterial fish pathogen; *Chlorella*; microalgae; proximate analysis
DOI 10.14456/cast.2021.9

1. Introduction

Bacterial fish pathogens are regarded as principal causes of diseases in aquaculture occurring in nurseries and rear ponds that can cause massive fish mortalities leading to significant economic losses [1]. These bacterial fish infections are caused by several species of *Aeromonas* sp., *Vibrio* sp. and *Pseudomonas* sp. causing hemorrhages, lesions and ulceration in several fish species [2]. Antibiotics are being used in the aquaculture industry to prevent these infections. However, there is an increasing occurrence of antibiotic resistance in most aquaculture and thus antibiotics are becoming less effective. Also, the detection of drug

*Corresponding author: Tel.: +6349-536-2884 Fax: +6349-536-2721
E-mail: edarguelles@up.edu.ph

residues in aquatic animal tissues and the possibility of infection of drug-resistant bacteria to consumers (humans) have become major considerations for public health that result from the application of antibiotics in aquaculture [1, 3]. Thus, discovery of different mitigation strategies to solve such unforeseeable and unceasing occurrence of fish disease is considered an urgent need. The use of other existing natural resources such as microalgae is considered as one of the strategic solutions to address such issues. Microalgae are a natural source of food for animals (such as fish fry and larval shrimp) important in aquaculture, and some species (*Chlorella*, *Isochrysis*, *Tetraselmis*, *Chaetoceros*, *Nannochloropsis* and *Pavlova*) are being used commercially as dried algal feed or live prey [1, 2]. These organisms are known to have diverse bioactive metabolites with antioxidant, anticoagulant, antibacterial, antifungal, anticancer, and antiviral activities [1]. These organisms use inorganic nutrients and light to produce biomolecules with high nutritional value like lipids, carbohydrates, pigments, and proteins. Also, other chemical compounds such as polysaccharides, sterols, polyphenols, carotenoids, vitamins and polyunsaturated fatty acids are reported to have potential use in the prevention and reduction of fish disease [2, 4, 5].

The genus *Chlorella* is a group of unicellular, green-pigmented microalgae capable of synthesizing a wide array of bioactive chemical compounds using various pathways with good therapeutic effects. These microalgae are capable of exhibiting high growth rate, high adaptability to various environmental conditions with minimal media requirements. Also, some species such as *Chlorella vulgaris* are considered as Generally Regarded as Safe (GRAS) for consumption by animals and humans as alternative source of single cell proteins. Thus, the feasibility of these organisms as alternative source of beneficial biomolecules and chemical compounds for large-scale production are acknowledged. *Chlorella minutissima* is a coccoid green microalga that is characterized by having chlorophyll and parietal chloroplasts. This species is known to produce secondary metabolites when subjected to environmental stress like high temperature, high intensity of light, and nitrogen starvation. Substances derived from this microalga such as polyphenols, sterols, phycobilins, polysaccharides, carotenoids and bioactive peptides are reported to have antioxidant, antibacterial and anticholinesterase activities [6, 7].

The Philippine freshwater ecosystem is known to have a number of *Chlorella* species with functional and bioactive properties yet to be explored. However, only a few studies have been documented about the nutritional properties, antibacterial and antioxidant activities of these microalgae. Previously, a protein-rich strain of *Chlorella sorokiniana* was reported to contain bioactive peptides including phosphoglycerate kinase, Fe-superoxide dismutase and chloroplast Rubisco activase. These bioactive peptides were able to exhibit ACE inhibitory, anti-amnestic, antioxidant and antithrombotic activities that suggest the potential of this species as alternative source of high value natural product [8]. The present study is the first report in the Philippines exploring the bioactive properties of a green microalga, *Chlorella minutissima* Fott & Nováková with potential to be use as novel antibiotics for disease control in aquaculture and as an alternative source of protein rich biomass for feed formulation. The investigation was done to analyze the proximate composition, total phenolic content, antibacterial, and antioxidant (using ABTS radical scavenging and copper reduction antioxidant capacity (CUPRAC) assay) activities of *C. minutissima*. In addition, correlation analysis on the phenolic content of the microalgal extract and its antioxidant (ABTS radical scavenging and copper reducing capacity) activity was established.

2. Materials and Methods

2.1 Algal culture

The microalga, *Chlorella minutissima* was procured from the Philippine National Collection of Microorganisms, National Institute of Molecular Biology and Biotechnology (BIOTECH), University of the Philippine Los Baños. Culture of *C. minutissima* (100 ml) was inoculated into three sterile flasks containing one liter of BG 11 medium. The mass production set up was

cultivated for 24 days with mean temperature of 23 ± 2 °C. Three fluorescent white lamps (light intensity of 120 μmol photons m^{-2} s^{-1}) were utilized to provide illumination on a 16:8 light to dark cycle. The algal biomass was centrifuged at 10,000 rpm for 10 min and was rinsed with sterile distilled water. The rinsed biomass was centrifuged again and the biomass was freeze-dried using a Virtis Freeze mobile 25 SL lyophilizer [1, 5]. This freeze-dried biomass was used for determining the total phenolic content as well as antioxidant and antibacterial assays. In addition, algal biomass of *C. minutissima* obtained after centrifugation was oven dried at 60ºC for 24 h and used for determining the proximate composition [5].

2.2 Proximate composition analysis

The ash content was obtained by complete burning of the dried algal biomass in an oven at a temperature of 550°C for 4 h until an ash (grayish powder) was produced. Crude fiber content was analyzed using the Weende method [9]. Briefly, 0.3 g of the dried algal biomass was digested with 1.25% HCI followed by 1.25% NaOH. The residue obtained after the digestion process was dried at 105°C for 3 h and weighed. The protein content of *C. minutissima* was analyzed by Kjeldahl method [9]. The total amount of nitrogen in crude protein was determined using 6.25 as the conversion factor. The total crude fat concentration of the microalga was estimated using the Bligh and Dyer method. Ten grams of the dried algal biomass was mixed with the extraction solvent (1:2 chloroform/methanol) and kept overnight after addition of $CaCl_2$. The chloroform layer was separated from the algal sample and then evaporated to dryness (in an evaporator) and finally placed in an oven set at 105°C for 30 min. The total crude lipid concentration was obtained by calculating the weight differences between flasks [9]. The moisture content of *C. minutissima* was determined by subjecting the algal biomass (2 g) to dryness at 105°C until a constant weight was obtained [9]. The total carbohydrate concentration was estimated using the equation below:

$$\%\, Total\ Carohydrate\ = 100 - (\%\, Protein + \%\, Crude\ Fiber\ + \%\, Crude\ Fat + \%Ash)$$

2.3 Microalgal extract preparation

The lyophilized algal biomass was soaked overnight in methanol (1g biomass: 20 ml methanol) with stirring. The extract was filtered using a filter paper (Whatmann No. 1) and subjected to a rotary evaporator (at 40°C) under reduced pressure to concentrate the algal extract [1, 5].

2.4 Determination of total phenolic content

Analysis of the total phenolic content of *C. minutissina* was done using a Folin-Ciocalteau's reagent [10]. Briefly, a portion (0.5 ml) of the diluted algal extract (using distilled water as diluent) was added with equal volume of 10% sodium carbonate solution and Folin-Ciocalteau's reagent and set aside for 5 min. The solution was then added with 5 ml sterile distilled water. The optical density (OD readings) of the reaction mixture was measured at 720 nm using a Shimadzu UV-1601 spectrophotometer. The blank consisted of distilled water with other reagents used in the analysis. The standard gallic acid was used for the construction of the calibration curve. The total phenolic concentration of the extract was reported as mg gallic acid equivalents (GAE) g^{-1} of the algal sample [10].

2.5 ABTS radical scavenging assay

ABTS free radical scavenging activity of *C. minutissima* extract was done using a method that is based on the decolorization of 2,2-Azino-bis (3-ethylbenzothiazoline-6-sulfonic acid) diammonium salt [11]. In this method, ABTS chromophore is transformed to its radical cation upon addition of sodium persulfate. This radical cation (bluish in color) is converted to its neutral form (colorless) in the presence of antioxidants (such as phenolic compounds in the

extract) in the reaction mixture. Briefly, 40 µl of algal extract at different phenolic concentrations (diluted using distilled water) and 40 µl of 90% methanol for the control were mixed with 3 ml of ABTS radical mixture with a starting absorbance of 0.72±0.05 at 734 nm. The solutions were stirred and set aside for 5 min at ambient temperature. Then, optical density reading was read at 734 nm (water was used to zero the spectrophotometer) [11]. The blank consisted of distilled water with other reagents used in the assay. The percent ABTS inhibition was analyzed using the formula below:

$$\text{ABTS Inhibition (\%)} = \frac{\text{Abs}_{734}\,(\text{control}) - \text{Abs}_{734}\,(\text{sample})}{\text{Abs}_{734}\,(\text{control})} \times 100$$

2.6 Copper reduction antioxidant capacity (CUPRAC) assay

The cupric ion reducing capacity of the algal extract was analyzed by colorimetric method [12]. For this, 0.5 ml of the prepared algal extract concentrations (5, 10, 15, 20, and 25 µg GAE ml^{-1}) diluted using distilled water was mixed with 1 ml each of 0.0075 M neocuproine, ammonium acetate ($C_2H_3O_2NH_4$) buffer (1M, pH 7.0) solution, as well as 0.01 M $CuCl_2$ into a sterile test tube. The solutions were kept for 30 min at ambient temperature. The blank consisted of distilled water with other reagents used in the assay. The optical density (absorbance readings) of each reaction solution was noted at 450 nm and compared against a blank [12].

2.7 Test bacterial pathogens

The Philippine National Collection of Microorganisms, National Institute of Molecular Biology and Biotechnology (BIOTECH), University of the Philippines Los Baños (UPLB) provided the test organisms used in this study. Pathogenic strains of Gram-negative bacteria (*Pseudomonas aeruginosa* BIOTECH 1824, *Pseudomonas fluorescens* BIOTECH 1123, *Pseudomonas putida* BIOTECH 1506**,** *Vibrio cholerae* BIOTECH 1967, *Aeromonas hydrophila* BIOTECH 10089, and *Vibrio parahaemolyticus* BIOTECH 10210**)** and Gram-positive bacteria (*Listeria monocytogenes* BIOTECH 1958, *Staphylococcus epidermidis* BIOTECH 10098, and *Staphylococcus aureus* BIOTECH 1823) were pre-cultured using Luria Bertani (LB) broth or Marine broth (for *Vibrio* species) with shaking overnight at 35°C. The purity of each bacterial culture was maintained by continuously checking the biochemical tests and morphological characteristics of each pathogen [5, 13].

2.8 Micro-dilution antibacterial assay

The antagonistic activity of *C. minutissima* extract against the Gram-negative and Gram-positive pathogenic bacteria was analyzed using microtiter plate dilution assay [13]. Initially, bacterial stocks of each pathogenic bacterium with cell density of 1×10^5 cells ml^{-1} were prepared. Using a 96-well microtiter plate, 100 µl of the bacterial stock cultures were added with 100 µl of *C. minutissima* extract at different dilutions (1000 µg ml^{-1}-7.81 µg ml^{-1}). Methanol was also used in the assay as the negative control. The microtiter plate was incubated at 35°C for 12 h, after which minimum inhibitory concentration (MIC) for each bacterium was recorded. MIC of the *C. minutissima* extract is the minimum concentration capable of inhibiting bacterial growth after 12 h incubation period. To determine the minimum bactericidal activity (MBC) of the algal extract, a loopful of the sample from each MIC wells (that exhibited growth inhibition of bacteria) was streaked into freshly prepared culture (tryptic soy agar and marine agar) medium. The plates were kept at 35°C for 24 h and were evaluated for visible colony growth for each dilution subculturing. No visible bacterial growth meant that *C. minutissima* was bactericidal at that particular dilution [5, 13].

2.9 Statistical Analyses

The experimental assay in this study was done with three replicates and data were expressed as means ± standard deviations (mean ± SD). The statistical tests for the linear correlation between antioxidant activity and phenolic concentration of the algal extract using Pearson's correlation coefficient (R) were analyzed using MS Office Excel 2007.

3. Results and Discussion

3.1 Proximate composition analysis

The growing concern on the limitation of the use of arable land areas and the decrease in fish harvested from freshwater and open ocean highlights the need for sustainable animal feed source from aquaculture [14]. Microalgae are regarded as promising substitutes (to traditional plant-based feeds) for nutrient sources of protein, lipids and carbohydrates needed for partial replacement in animal feed formulation. These organisms are rich in protein (40-60% of dry biomass) as well as carbohydrates and lipids and their compositions vary depending on the species and growth condition [15-17]. Thus, evaluation of the chemical composition and assessing the possibility of several strains of microalgae for mass production will give baseline information needed for the development of new feed formulation essential in aquaculture.

The proximate composition analysis of the dried biomass of *C. minutissima* exhibited high nutritional value (Table 1). The algal strain possesses high concentration of protein with an estimated amount of 42.61 ± 0.11% of the total dried biomass. This result is comparable to other microalgae being used in feed formulation in aquaculture such as *Chlorella vulgaris* and *Spirulina platensis* which have protein contents of 55.70 ± 2.10% and 61.74 ± 1.06%, respectively [18]. Also, this microalga has a higher protein content than other traditional plant-based protein sources used in animal feed formulation such as *Azolla pinatta* (28.01 ± 1.15%) and soybean (37.69 ± 0.00%) [18, 19]. The study revealed that *C. minutissima* showed protein content that is higher than 40% of its total dry biomass proving its potential as alternative protein source in feed formulation for aquaculture [5]. Table 1 showed other dominant biochemical components like ash (17.79 ± 0.04%), carbohydrate (14.06 ± 0.03%) and crude fat (11.70 ± 0.01%). The ash content shows the concentration of inorganic substances found in the algal biomass. On the other hand, a low concentration of crude fiber (9.13 ± 0.15%) was observed in *C. minutissima* biomass. This value is good in feed formulation since animals do not a need high concentration of fiber in their diets [5, 14].

Table 1. Proximate composition of *Chlorella minutissima*

Proximate composition	Percent composition (%)
Moisture Content	4.71 ± 0.10
Ash Content	17.79 ± 0.04
Crude Protein	42.61 ± 0.11
Crude Fat	11.70 ± 0.01
Crude Fiber	9.13 ± 0.15
Carbohydrate	14.06 ± 0.03

3.2 Total phenolic content (TPC)

The amount and kind of phenolic compounds extracted from a sample are dependent on the polarity of the solvent and the binding (complex formation) of phenolic substance with the corresponding solvent (used for extraction) for it to become more soluble [13, 20]. Phenolic compounds have high solubility in polar solvents (such as methanol) giving a high concentration of these target compounds in the sample extract. The TPC of *C. minutissima* was analyzed using the Folin-Ciocalteu reagent [10] and is expressed in gallic acid equivalent (calibration curve equation: $y = 0.0682x - 0.0214$, $r^2 = 0.997$). The results showed that the total phenolic concentration in *C. minutissima* extract is 30.94 ± 0.06 mg GAE g^{-1}. The phenolic concentration obtained from methanol extract of *C. minutissima* is greater than that observed from other species of microalgae found in the Nile River in Egypt such as *Oscillatoria agardhii* and *Anabaena sphaerica* with 20.91 ± 0.21 mg GAE g^{-1} and 14.81 ± 0.02 mg GAE g^{-1}, respectively [21]. Likewise, lower TPC was also observed from previous studies using methanolic extract of *Chlorella marina* (0.647 ± 0.052 mg GAE g^{-1}) [22], *Scenedesmus quadricauda* (606.91 ± 0.028 μg GAE g^{-1}) [5] and *Desmodesmus* sp. (652.66±0.042 μg GAE g^{-1}) [3] in comparison with the current study.

3.3 Antioxidant activities

Microalgae have polyphenols with a wide range of antioxidant activities. Thus, utilization of these natural polyphenols for possible use in drug synthesis should be studied. The antioxidant activities of *C. minutissima* extract were evaluated using ABTS scavenging and CUPRAC assay. Two antioxidant assays were utilized in the study to better understand the antioxidant capacities of the microalgal extract.

3.3.1 ABTS radical scavenging activity

The ABTS radical scavenging assay is a spectrophotometric technique that uses the reduction of stable colored radicals to evaluate the antioxidant capability of a sample extract. In this assay, ABTS chromophore is generated through the reaction of sodium persulfate and ABTS, which changes ABTS into its radical cation. The radical cation is bluish in color and is capable of absorbing light at 734 nm [11]. The methanolic extract of *C. minutissima* exhibited a concentration-dependent inhibition of ABTS radical production (Table 2). The highest antioxidant activity (60.61%) for the algal extract was observed at 62.5 μg GAE ml^{-1} of the prepared concentration of the extract, whereas the standard, that is, ascorbic acid, exhibited the highest activity of 64.53% at 187.5 μg ml^{-1} concentration. This means that the antioxidant activity of the microalgal extract is thrice more effective than ascorbic acid (standard antioxidant) in scavenging ABTS free radical. *Chlorella minutissima* extract exerted a dose dependent ABTS free radical inhibition and scavenging activity (Table 2 and Figure 1). This activity can be ascribed to phenolic substances like flavonoids, vitamin C and carotenoids present in *C. minutissima* extract that serve as potent free radical scavengers which can be used as nutritional feed supplement in aquaculture for the control and prevention of fish diseases caused by bacteria and other external oxidative stressors. The activity of *C. minutissima* extract exhibited potent antioxidant activity when compared to ascorbic acid (positive control) with IC_{50} of 48.13 μg GAE ml^{-1} and IC_{50} = 147.9 μg ml^{-1}, respectively. Also, the effective concentration (IC_{50}) of *C. minutissima* extract showed greater antioxidant activity than other strains of microalgae from KwaZulu-Natal in South Africa such as *Chlorella sorokiniana* and *Chlorella minutissima* with IC_{50} values of 85.03 μg GAE ml^{-1} and 86.05 μg GAE ml^{-1}, respectively [7].

Table 2. ABTS radical scavenging activity and IC_{50} value of phenolics from *C. minutissima* and ascorbic acid

Sample	Phenolic concentration (μg GAE ml^{-1})					IC_{50}*
	12.5	25.0	37.5	50.0	62.5	
	ABTS Inhibition (%)					
Chlorella minutissima	16.38 ± 1.53	29.87 ± 0.00	40.62 ± 0.51	51.66 ± 0.82	60.61 ± 1.63	48.13 μg ml^{-1}
	Concentration (μg ml^{-1})					
	37.5	75.0	112.5	150.0	187.5	
	ABTS Inhibition (%)					
Ascorbic acid	11.70 ± 1.54	24.56 ± 0.62	36.70 ± 0.51	50.87 ± 0.82	64.53 ± 1.64	147.9 μg ml^{-1}

*IC_{50} is the effective concentration that inhibits the activity of ABTS (2,2-Azino-bis (3-ethylbenzothiazoline-6-sulfonic acid) diammonium salt) cation radical by 50%.

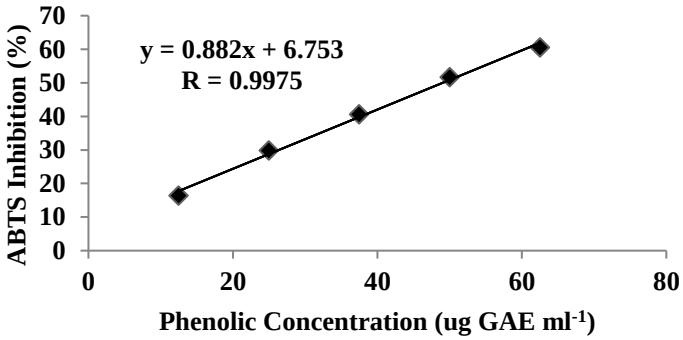

Figure 1. Correlation between the total phenolic content and antioxidant activity (ABTS radical scavenging assay) of *C. minutissima*

The coefficient of correlation (R) between phenolic concentration and antioxidant activity of *C. minutissima* using ABTS scavenging assay is presented in Figure 1. Based on the correlation analysis, a positive correlation (R=0.9975) exists between total phenolic concentration and ABTS antioxidant activity of the methanol extract of *C. minutissima*. This shows that the phenolic compound present in the algal extract enhances the antioxidant property of *C. minutissima*. Previous studies regarding antioxidant activity of green microalgae, *Scenedesmus quadricauda*, *Trentepohlia umbrina*, and *Desmodesmus* sp. showed positive correlation between antioxidant activities and phenolic contents of the algal extracts, a result that is in agreement in the current investigation [3, 5, 23].

3.3.2 Copper reduction antioxidant capacity (CUPRAC)

CUPRAC assay is a technique used in assessing the antioxidant capability of an extract by evaluating the capability of the algal extract to reduce (Cu (II)-Neocurpine) to colored Cu (I)-Neocurpine chelate, which exhibits a maximum absorbance at 450 nm. This method has unique advantages over other antioxidant assays such as the range of working pH near to physiological pH (as compared to the FRAP and Folin assay, which work at acidic and alkaline conditions, respectively) and efficient redox potential. Moreover, this assay is applicable in the detection of sulfhydryl (-SH) containing antioxidants (unlike FRAP method) as well as lipophilic and hydrophilic antioxidants (unlike other antioxidant assays such as

DPPH and Folin) in the sample extracts [24]. The presence of hydrophilic, lipophilic and sulfhydryl (-SH) containing antioxidants in the algal extract can exhibit promising biological activities that can be used for aquaculture [12]. *Chlorella minutissima* extract showed dose-dependent copper ion reduction ability. Table 3 shows the maximum absorbance of 0.860 of methanolic extract at 25 μg GAE ml^{-1} concentration, whereas the standard, that is, ascorbic acid, shows an absorbance of 0.542 at 50 μg GAE ml^{-1} concentration. In this method, a higher absorbance reading means greater antioxidant activity. The observed trend in this antioxidant assay is similar to that obtained from the ABTS assay in which 62.5 μg GAE ml^{-1} concentration showed the highest antioxidant activity. The study reveals that *C. minutissima* extract contains phenolic compounds having antioxidant properties that can be ascribed to its excellent copper reducing ability. Previous studies show that microalgal compounds such as tocopherol, carotenoids, polyphenolic compounds and pigments were observed to have reduction potential like antioxidant properties [3, 5]. Lipophilic antioxidants like tocopherols and carotenoids are highly effective in inhibiting nucleic acid formation and cytoplasmic leakage in bacteria. On the other hand, hydrophilic antioxidants such as flavonoids are capable of causing damage in bacterial cell wall by dissolving extracellular proteins [6, 23]. In this study, the presence of these compounds in the algal extract contributed to a stronger antioxidant property than that of the standard antioxidant (such as ascorbic acids) used in the food industry.

Table 3. Copper reduction antioxidant capacity (CUPRAC) and IC_{50} value of phenolics from *C. minutissima* and ascorbic acid

Sample	Phenolic concentration (μg GAE ml^{-1})					IC_{50}*
	5.0	10.0	15.0	20.0	25.0	
	CUPRAC (Absorbance at 450 nm)					
Chlorella minutissima	0.182 ± 0.001	0.389 ± 0.001	0.535 ± 0.004	0.635 ± 0.016	0.860 ± 0.002	13.90 μg ml^{-1}
	Concentration (μg ml^{-1})					
	10.0	20.0	30.0	40.0	50.0	
	CUPRAC (Absorbance at 450 nm)					
Ascorbic acid	0.112 ± 0.002	0.213 ± 0.007	0.328 ± 0.004	0.429 ± 0.012	0.542 ± 0.011	46.30 μg ml^{-1}

*IC_{50} is the effective concentration that gives CUPRAC value of 0.5 absorbance reading at 450 nm. Computed by interpolation.

The strong positive correlation (R) between the antioxidant activity of *C. minutissima* and the phenolic concentration using CUPRAC assay (R= 0.9927) shows that phenolic compounds present in the algal extract contributed significantly to the antioxidant activity of the microalga (Figure 2). In addition, *C. minutissima* extract exhibited potent antioxidant activity as compared to ascorbic acid (positive control) with IC_{50} of 13.90 μg GAE ml^{-1} and IC_{50} = 46.30 μg GAE mg ml^{-1}, respectively. The result of this analysis proves that the antioxidant activity of *C. minutissima* extract is stronger than ascorbic acid, which proves its promising characteristic as natural alternative source of bioactive compounds useful in drug discovery.

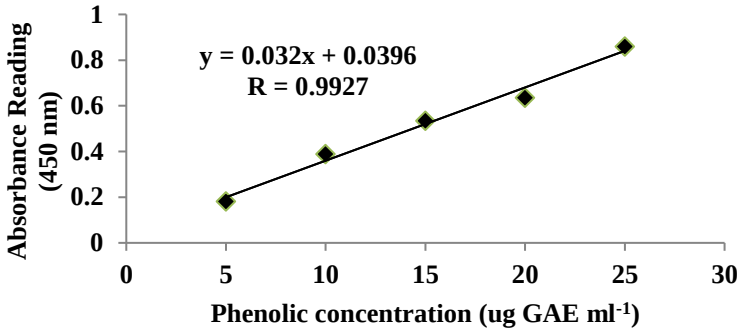

Figure 2. Correlation between the total phenolic content and antioxidant activity (copper reduction antioxidant capacity (CUPRAC) assay) of *C. minutissima*

3.4 Antibacterial activity

Chlorella is a common genera of microalgae widely used as feed supplement for aquaculture. These microalgae are being utilized as cultured microalgae in the rearing of the larvae of freshwater and marine fish, bivalves and other crustaceans. In addition, these cultured microalgae in ponds and culture tanks are reported to have a positive impact on the overall bacterial load of the aquaculture rearing system. These microalgae are capable of suppressing the growth and proliferation of opportunistic bacterial pathogens such as *Aeromonas* sp., *Pseudomonas* sp., and *Vibrio* sp., thus improving the survival rate of fish larvae [6, 25]. The enhanced effect of adding cultured microalgae in rearing tanks can be attributed to factors such as oxygen radicals produced during photosynthesis as well as other bioactive compounds produced by the microalgae [6].

The antibacterial activity of the *C. minutissima* extract against selected bacterial pathogen is shown in Table 4. The algal extract exhibited potent antibacterial effect against *A. hydrophila* with MIC and MBC values of 125 μg ml^{-1} and 250 μg ml^{-1}, respectively. The extract is also effective against *V. cholerae*, *V. parahaemolyticus* and *S. aureus*, each with MIC values of 250 μg ml^{-1}. Also, *C. minutissima* extract was able to prevent the growth of *P. fluorescens* with MIC value of 500 μg ml^{-1}. The minimum bactericidal concentration (MBC) value of the algal extract for *V. cholerae*, *V. parahaemolyticus* and *S. aureus* (each with MBC of 500 μg ml^{1}) was greater than that obtained for *P. fluorescens* (MBC of 1000 μg ml^{-1}). The antibacterial activity of the extract against *V. parahaemolyticus* is similar to an earlier study showing that axenic culture of *C. minutissima* when co-cultivated with other *Vibrio* species for 24-96 h exhibited antagonistic activity against the pathogens [6]. Bioactive substances such as polyphenols and bioactive peptides were detected in several *Chlorella* species that are capable of inactivating adhesins and other protein envelope of bacterial pathogens [5]. Antioxidants derived from microalgae such as flavones, astaxanthin, vitamin E, peptides, vitamin C, polyphenols, carotenoids, and amino acids are beneficial to aquatic animals by providing enhanced immune responses against pathogens via free radical neutralization and repair of membrane system and biomolecules due to oxidative damage. The use of these antioxidants has shown a great potential as nutritional and immunostimulating feed supplement by exhibiting antimicrobial activities against important disease causing bacterial pathogens in aquaculture. *Arthrospira platensis* fed to commercially important shrimp and fish, exhibited increased phagocytic activity and resistance against *Escherichia coli*, *Vibrio harveyii*, *Bacillus subtilis*, and *Salmonella typhimurium*. In addition, *Porphyridium* sp. supplemented in fish feed exhibited antiviral, antitumor, antioxidant, and anti-inflammatory activities, proving the important effect of microalgae on the survival and development of cultivated aquatic organisms [26, 27]. The amount and type of free fatty acids present in the algal extract can cause disruption in the efficiency of the oxidative phosphorylation and electron transport chain of bacterial cells, leading to cell lysis and death [28, 29].

Table 4. Antibacterial activities of *C. minutissima* extract

Bacterial Pathogen	Minimum inhibitory concentration (μg ml^{-1})	Minimum bactericidal concentration (μg ml^{-1})
Gram-positive bacteria		
Staphylococcus aureus BIOTECH 1823	250.00	500.00
Listeria monocytogenes BIOTECH 1958	>1000.00	ND
Staphylococcus epidermidis BIOTECH 10098	>1000.00	ND
Gram-negative bacteria		
Aeromonas hydrophila BIOTECH 10089	125.00	250.00
Vibrio cholerae BIOTECH 1967	250.00	500.00
Vibrio parahaemolyticus BIOTECH 10210	250.00	500.00
Pseudomonas fluorescens BIOTECH 1123	500.00	1000.00
Pseudomonas aeruginosa BIOTECH 1824	>1000.00	ND
Pseudomonas putida BIOTECH 1506	>1000.00	ND

*ND = Not detected

Several species of green microalgae, such as *Trentepohlia umbrina, Chlorococcum humicola, Chlorella vulgaris, Scenedesmus quadricauda, Desmococcus olivaceous* and *Desmodesmus sp.* were screened for antibacterial activities in search of new bioactive compounds effective in controlling bacterial pathogens [3, 5, 23, 30, 31], but in this investigation, for the first time in the Philippines, the antibacterial activities of *C. minutissima* methanolic extract against *A. hydrophila, V. cholerae, V. parahaemolyticus* and *P. fluorescens* were reported. Comparing the results obtained in this study with other microalgae, it seems that the methanolic extract of *Chlorella minutissima* showed relatively strong antibacterial activity against bacterial fish pathogen. Thus, *C. minutissima* is considered as a candidate freshwater microalgae with excellent biological activities that can be used for the development of new antibiotics. Further experiment should be conducted on the isolation, purification, chemical structure elucidation, and identification of these bioactive substances to better understand the mechanisms of antibacterial activity and its potential for large-scale production.

4. Conclusions

Chlorella minutissima (Chm1) possess bioactive metabolites with potential neutraceutical and pharmacological benefits. It is capable of producing chemical compounds in high concentration such as proteins, lipids and phenolic compounds with direct relevance to aquaculture application. The green microalga exhibits potent antioxidant and antibacterial activities as well as high protein content suitable for large-scale production. Further experiments focusing on the identification and characterization of the biologically active compounds using GC-MS analysis should be conducted to understand the mechanisms involving in the antibacterial and antioxidant properties of the algal extract. Also, studies on

the use of *C. minutissima* biomass as nutritional partial feed replacement in aquaculture feed formulation and feeding experiment should be conducted.

5. Acknowledgements

The author acknowledges the support of the Philippine National Collection of Microorganisms and Food Laboratory, National Institute of Molecular Biology and Biotechnology (BIOTECH), University of the Philippines Los Baños. The technical assistance of Mrs. Arsenia B. Sapin in the analysis of the algal sample and the constructive comments of the blind reviewer are acknowledged with gratitude.

References

[1] Falaise, C., François, C., Travers, M.A., Morga B., Haure, J., Tremblay, R., Turcotte, F., Pasetto, P., Gastineau, R., Hardivillier, Y., Liegnel, V. and Mouget, J.L., 2016. Antimicrobial compounds from eukaryotic microalgae against human pathogens and diseases in aquaculture. *Marine Drugs*, 14(9), 159, https://doi.org/10.3390/md14090159

[2] Charoonnart, P., Purton, S. and Saksmerprome, V., 2018. Applications of microalgal biotechnology for disease control in aquaculture. *Biology*, 7(2), 24, https://doi.org/10.3390/biology7020024

[3] Arguelles, E.D.L.R., Laurena, A.C., Martinez-Goss, M.R. and Monsalud, R.G., 2017. Antibacterial activity, total phenolic content and antioxidant capacity of a green microalga *Desmodesmus sp*. (U-AU2) from Los Baños, Laguna (Philippines). *Journal of Nature Studies*, 16(2), 1-13.

[4] de Morais, M.G., Vaz, B.S., de Morais, E.G. and Costa, J.A.V., 2015. Biologically Active Metabolites Synthesized by Microalgae. *BioMed Research International*, 2015, http://dx.doi.org/10.1155/2015/835761

[5] Arguelles, E.D.L.R., 2018. Proximate analysis, antibacterial activity, total phenolic content and antioxidant capacity of a green microalga *Scenedesmus quadricauda* (Turpin) Brébisson. *Asian Journal of Microbiology Biotechnology and Environmental Science*, 20(1), 150-158.

[6] Kokou, F., Makridis, P., Kentouri, M. and Divanach, P., 2012. Antibacterial activity in microalgae cultures. *Aquaculture Research*, 43, 1520-1527.

[7] Olasehinde, T.A., Odjadjare, E.C., Mabinya, L.V., Olaniran A.O. and Okoh, A.O., 2019. *Chlorella sorokiniana* and *Chlorella minutissima* exhibit antioxidant potentials, inhibit cholinesterases and modulate disaggregation of β-amyloid fibrils. *Electronic Journal of Biotechnology*, 40, 1-9.

[8] Tejano, L.A., Peralta, J.P., Yap, E.E.S., Panjaitan, F.J.A. and Chang, Y-W., 2019. Prediction of bioactive peptides from *Chlorella sorokiniana* proteins using proteomic techniques in combination with bioinformatics analyses. *International Journal of Molecular Sciences*, 20, 1786-1801.

[9] AOAC, 2011. *Official Methods of Analysis International*. 18th ed. Washington DC: Association of Official Analytical Chemists.

[10] Nuñez Selles, A., Castro, H.T.V., Aguero, J.A., Gonzalez, J.G., Naddeo, F., De Simone, F. and Pastrelli, L., 2002. Isolation and quantitative analysis of phenolic antioxidants, free sugars and polyols from mango (*Mangifera indica* L.) stem bark aqueous decoction used in Cuba as a nutritional supplement. *Journal of Agricultural and Food Chemistry*, 50, 762-766.

[11] Re, R., Pellegrine, N., Proteggente, A., Pannala, A., Yang, M. and Rice-Evans, C., 1999. Antioxidant activity applying an improved ABTS radical cation decolorization assay. *Free Radical Biology and Medicine*, 26, 1231-1237.

[12] Alpinar, K., Özyurek, M., Kolak, U., Guclu, K., Aras, Ç., Altun, M., Celik, S.E., Berker, K.I., Bektasoglu, B. and Ampal, R., 2009. Antioxidant capacities of some food plants

wildly grown in Ayvalik of Turkey. *Food Science and Technology Research*, 15(1), 59-64.

[13] Arguelles, E.D.L.R., Monsalud, R.G. and Sapin, A.B., 2019. Chemical composition and *in vitro* antioxidant and antibacterial activities of *Sargassum vulgare* C. Agardh from Lobo, Batangas, Philippines. *Journal of the International Society for Southeast Asian Agricultural Sciences (ISSAAS)*, 25(1), 112-122.

[14] Arguelles, E.D.L.R., Laurena, A.C., Monsalud, R.G. and Martinez-Goss, M.R., 2019. High-lipid and protein-producing epilithic microalga, *Desmodesmus* sp. (U-AU2): A promising alternative feedstock for biodiesel and animal feed production. *Philippine Journal of Crop Science*, 44(2), 13-23.

[15] Becker, E.W., 2007. Micro-algae as a source of protein. *Biotechnology Advances*, 25, 207-210.

[16] Arguelles, E.D.L.R., Laurena, A.C., Monsalud, R.G. and Martinez-Goss, M.R., 2018. Fatty acid profile and fuel-derived physico-chemical properties of biodiesel obtained from an indigenous green microalga, *Desmodesmus* sp. (I-AU1), as potential source of renewable lipid and high quality biodiesel. *Journal of Applied Phycology*, 30, 411-419.

[17] Arguelles, E.D.L.R. and Martinez-Goss, M.R., 2020. Lipid accumulation and profiling in microalgae *Chlorolobion* sp. (BIOTECH 4031) and *Chlorella* sp. (BIOTECH 4026) during nitrogen starvation for biodiesel production. *Journal of Applied Phycology*, https://doi.org/10.1007/s10811-020-02126-z

[18] Radhakrishnan, S., Bhavan, P.S., Seenivasan, C. and Muralisankar, T., 2017. Nutritional profile of *Spirulina platensis*, *Chlorella vulgaris* and *Azolla pinnata* to novel protein source for aquaculture feed formulation. *Austin Journal of Aquaculture and Marine Biology*, 2(1), 1005.

[19] Etiosa, O.R., Chika, N.B. and Benedicta, A., 2017. Mineral and proximate composition of soya bean. *Asian Journal of Physical and Chemical Sciences*. 4(3), 1-6.

[20] Arguelles, E.D.L.R. and Sapin, A.B. 2020. Bioactive properties of *Sargassum siliquosum* J. Agardh (Fucales, Ochrophyta) and its potential as source of skin-lightening active ingredient for cosmetic application. *Journal of Applied Pharmaceutical Science*, 10(7), 51-58.

[21] Abd El-Aty, A.M., Mohamed, A.A. and Samhan, F.A., 2014. *In vitro* antioxidant and antibacterial activities of two fresh water Cyanobacterial species, *Oscillatoria agardhii* and *Anabaena sphaerica*. *Journal of Applied Pharmaceutical Science*, 4(7), 69-75.

[22] Manivannan, K., Anantharaman, P. and Balasubramanian, T., 2012. Evaluation of antioxidant properties of marine microalga *Chlorella marina* (Butcher, 1952). *Asian Pacific Journal of Tropical Biomedicine*, 2(1), S342-S346.

[23] Simić, S., Kosanić, M. and Ranković, B., 2012. Evaluation of in vitro antioxidant and antimicrobial activities of green microalgae *Trentepohlia umbrina*. *Notulae Botanicae Horti Agrobotanici Cluj-Napoca*, 40(2), 86-91.

[24] Apak, R., Güclü, K., Demirata, B., Özyürek, Z., Çelik, S.E., Bektasoglu, B., Berker, K.I. and Özyurt, D., 2007. Comparative evaluation of various total antioxidant capacity assays applied to phenolic compounds with the CUPRAC assay. *Molecules*, 12, 1496-1547.

[25] Salvesen, I., Skjermo, J. and Vadstein, O., 1999. Growth of turbot (*Scophthalmus maximus* L.) during first feeding in relation to the proportion of r/K strategists in the bacterial community of the rearing water. *Aquaculture*, 175, 337-350.

[26] Aklakur, M., 2019. Natural antioxidants from sea: a potential industrial perspective in aquafeed formulation. *Reviews in Aquaculture*, 10(2), 385-389.

[27] Silveira Júnior, A.M., Faustino, S.M.M. and Cunha, A.C., 2019. Bioprospection of biocompounds and dietary supplements of microalgae with immunostimulating activity: a comprehensive review. *Peer Journal 7*, e7685, https//doi.org//10.7717/peerj.7685

[28] Desbois, A.P. and Smith, V.J., 2010. Antibacterial free fatty acids: activities, mechanisms of action and biotechnological potential. *Applied Microbiology and Biotechnology*, 85, 1629-1642.

[29] Shannon, E. and Abu-Ghannam, N., 2016. Antibacterial derivatives of marine algae: An overview of pharmacological mechanisms and applications. *Marine Drugs*, 14(4), 81, https://doi.org/10.3390/md14040081

[30] Seenivasan, R., Indu, H., Archana, G. and Geetha, S., 2010. The antibacterial activity of some marine algae from south east coast of India. *American-Eurasian Journal of Agricultural and Environmental Science*, 9(5), 480-489.

[31] Uma, R., Sivasubramanian, V. and Niranjali Devaraj, S., 2011. Preliminary phycochemical analysis and *in vitro* antibacterial screening of green micro algae, *Desmococcus olivaceous, Chlorococcum humicola* and *Chlorella vulgaris. Journal of Algal Biomass Utilization*, 2, 74-81.

Development of Fermented Prunus Vinegar: Chemical Characterization and Antioxidant Activity

Wilawan Boonsupa[1]* and Kittisak Kerdchan[2]

[1]Department of Biology, Faculty of Science and Technology, Rajabhat Maha Sarakham University, Mahasarakham, Thailand
[2]Faculty of Pharmacy, Maha Sarakham University, Mahasarakham, Thailand

Received: 15 January 2020, Revised: 22 July 2020, Accepted: 10 August 2020

Abstract

The purpose of this study was to examine the chemical properties, antioxidant activities and sensory test of a two-stage fermented vinegar that was produced from three Prunus species, namely *Prunus persica* L., *Prunus domestica* L., and *Prunus mume L.* Alcoholic fermentation was produced using *Saccharomyces cerevisiae* and acetous fermentation was achieved using *Acetobacter pasteurianus*. Samples taken during the alcoholic fermentation showed a continuous decrease in total soluble solids and an increase in alcohol content at the end of fermentation process. The result showed that the wine produced from *Prunus persica* L. exhibited the highest content of alcohol (13.81±0.04 %, w/v) and exhibited the highest content of antioxidant activity (45.21±0.06 mg/ml). In the acetous fermentation, alcohol content dropped continuously and acetic acid content elevated at the end of the process. The highest content of acetic acid (4.04 ± 0.19 %, v/v) was detected in the vinegar produced from *Prunus domestica* L., while the vinegar produced from *Prunus persica* L. exhibited the highest content of antioxidant activity (49.08 ± 8.49 mg/ml). The 9-point hedonic scale showed that the vinegar produced from *Prunus mume L.* exhibited the highest overall acceptability (7.83±1.02), a result that indicated that consumers rated it at the very pleasant level on the preference scale.

Keywords: chemical properties; antioxidant activity; fruit vinegar; Prunus; sensory evaluation
DOI 10.14456/cast.2021.10

1. Introduction

Thailand is a tropical country that has an abundance of tropical fruits such as bananas, tamarinds and pineapples, which can be preserved to add value to fruit production by transforming fruit into functional foods, for example, banana vinegar [1]. In the north of Thailand, a lot of prunus fruit are grown and can be processed into healthy beverages. Prunus fruits species, include peach (*Prunus persica* L.), red plum (*Prunus domestica* L.), and chinese plum (*Prunus mume* L.) are mostly processed as frozen, caned, and dried fruits, as well as fruit juice. Currently, there is an upsurge of interest in new healthy foods, and this has stimulated the development of innovations in food processing, such as the production of novel vinegar drinks from fruits. Vinegar is rich in nutrients

*Corresponding author: Tel.: +66 4 374 2620; fax: +66 4 373 2620.
E-mail: wilawanboonsupa@ymail.com

including amino acids, vitamins, sugars, organic acids, polyphenols, tetramethylpyrazine, and melanoidins [2]. The demand for fruit vinegars has increased because of its benefit as health food products, which offers various different kinds of beneficial effects to human such as having antibacterial, antidiabetic properties and lowering cholesterol levels by inhibiting the oxidation of low density lipoproteins (LDLs) [3].

Peach (*Prunus persica* L.) is a popular fruit appreciated by consumers for its odor and flavor and it is an excellent source of bioactive compounds such as phenolic compounds which show a variety portion of biological activities favorable to human health [4]. Red plum (*Prunus domestica* L.) is well-known worldwide because of its color, aroma, flavor and nutritional value. The main nutrition value of red plum comes from their phenolic compound such as phenolic acid and flavonoids, which decrease the risk of oxidative damage and cancer [5]. Chinese plum (*Prunus mume* L.) is a tree of genus Rosaceae. Chinese plum contains phenolic compounds, such as flavonoids and phenolic acids, which are involved in antioxidant activity. These phenolic compounds from Chinese plum also show an inhibitory effect against cancer cells [6].

Previously, bioactive compounds, volatile aroma compounds and antioxidant capacities of Sour cherry (*Prunus cerasus* L.) vinegars were studied [7]. However, there was not much information available in the literature concerning the production of vinegar from other prunus fruits. Therefore, the objective of the present work was to evaluate the chemical properties including alcohol contents, glucose and fructose contents, and acetic acid contents. Antioxidant activities were determined by DPPH radical assays, total phenolic contents and sensory scores of the Prunus vinegars was performed based on the 9-point hedonic scale test. Importantly, it was hoped that this research would enhance the utilization of the prunus fruits.

2. Materials and Methods

2.1 Chemicals and reagents

All the reagents and solvents used during these experiments were of analytical grade and were purchased from various suppliers, 2,2-diphenyl-1-picrylhydrazyl hydrate (DPPH) was purchased from Sigma-Aldrich (Steinheim, Germany). Gallic acid standard was supplied by Fluka (Buchs, Switzerland). Folin-ciocalteau reagent was from Merck (Darmstadt, Germany) and sodium carbonate (anhydrous) from Univar (Downers Grove, IL, USA).

2.2 Raw materials

Peach (*Prunus persica* L.), Red plum (*Prunus domestica* L.) and Chinese plum (*Prunus mume* L.) fruits were harvested during March in 2019 at Chiang Mai province.

2.3 Prunus vinegar production

For the vinegar fermentation process, Prunus fruits of each species were pickled with rock sugar at a ratio of 1:1 w/w for 7 days. After that, the juice was squeezed from the fruits. The sugar content of the juice was then adjusted down to 24 ºBrix by addition of water. The Prunus juice was pasteurized for 30 min at 60ºC. Alcoholic fermentation was conducted for 5 days at room temperature in plastic vessels containing 2 l of the Prunus juice inoculated with wine yeast, *Saccharomyces cerevisiae* (Wine & Scientific Equipment Ltd., Part) at a ratio of 0.75% (v/v). The preparation of yeast inoculum was carried out by mixing 5 g of yeast powder with 60 ml of warm water. At the end of the fermentation process, the wine was separated from the sediment by allowing

it to settle in glass bottles, followed by pasteurization for 30 min at 60 ºC and clarification for 45 days at 10 ºC. Then, the alcohol content of the obtained wine was adjusted to 7% (v/v) was inoculated with *Acetobacter pasteurianus* TISTR 102 (Thailand Institute of Scientific and Technological Research) which had been grown in glucose yeast extract broth at a ratio of 10% (v/v). The vinegar fermentation was carried out for 15 d at 30ºC on a shaker (150 g) in a glass flask containing 135 ml of the Prunus wine. The samples were allowed to settle in microtubes and storage at 4 ºC before the analyses.

2.4 Chemical analysis

The wine and vinegar samples were centrifuge and filtered through a 0.45 µm filter before injection into HPLC system. The analysis were performed on a Shimadzu HPLC-RID system (Shimadzu, Japan) consisting of Shimadzu LC-20AD pumps and RID-10A refractive index detector. The analytical columns used were Aminex HPX-87H column (300 mm × 7.8 mm i.d., 9 µm, Bio-Raand Laboratories, Inc., USA) coupled to a cationic exchange precolumn (Bio-Rad Laboratories, Inc., USA). H_2SO_4 (5 mM) was used as the mobile phase. The injection volume was 20 ml with a flow rate of 0.6 ml/min. The column temperature was set at 45ºC. [8]. A series of standard solutions (ranging from 0-12 % w/v of fructose, glucose and 0-16 % v/v alcohol, acetic acid) were prepared. A standard curve with R^2 greater than 0.99 was plotted, and then the concentrations of sugar, alcohol and acetic acid in wine and vinegar were quantified accordingly. The total soluble solids values of the wine were measured using refractometer (AllA France, France) calibrated with distilled water. The values were expressed as ^{O}Brix.

2.5 Antioxidant activity

The antioxidant activities of the sample were determined by DPPH radical assay [9] in which 2,2-diphenyl-1-picrylhydrazyl hydrate (DPPH) radical was used as a stable radical. In brief, 5 ml of each sample was added to 5 m of 0.1 mM DPPH radical solution prepared in ethanol, and the mixture was incubated for 20 min at room temperature in the dark. After incubation, absorbance was measured at 517 nm using a Shimadzu UV-1700 spectrophotometer (Shimadzu, Japan), and the DPPH radical scavenging activities were expressed as mg ascorbic acid equivalents in 1 ml of sample (mg/ml).

2.6 Total phenolic content analysis

Folin-Ciocalteu method was utilized for the determination of total phenolic contents of the Prunus vinegars [10]. Briefly, 1 ml of each sample was diluted with 9.5 ml of distilled water and was then mixed with 0.5 ml of Folin-Ciocalteu reagent and 2 ml of 10% Na_2CO_3 solution. After 30-min incubation at room temperature, absorbance was measured at 765 nm using a Shimadzu UV-1700 spectrophotometer (Shimadzu, Japan). Results were expressed as mg gallic acid equivalents in 1 l of sample (mg GAE/l).

2.7 Sensory evaluation

Drinking vinegar was prepared by 200 g of the Prunus vinegars, 150 g of honey and 150 g of water were mixed together to make drinking vinegars and the drinking vinegars were subjected to the sensory evaluation based on the 9-point hedonic scale by using 30 untrained panelists for 5 attributes of clarity, color, odor, taste and overall acceptance. A scale value of 9 represented like extremely, 5 represented neither like nor dislike and 1 represented dislike extremely.

2.8 Statistical analysis

The trials were carried out in triplicate. The results were given as the mean ± standard deviation (SD). The obtained data were analyzed by one-way analysis of variance (ANOVA) with Duncan multiple range test (DMRT) to determine the significance between samples. In all cases, $p < 0.05$ was considered significant.

3. Results and Discussion

3.1 Chemical properties of the Prunus wines and vinegars

The Prunus wines produced from three Prunus species via a 5-day alcoholic fermentation process using *Saccharomyces cerevisiae* as an inoculant were analyzed for their chemical compositions, and the results are presented in Tables 1-8. It was observed that at the end of the fermentation, high alcohol content was detected in peach wines, indicating that sugars in the peach juice had been rapidly converted to alcohol. The Prunus wine produced from 'peach' species contained the highest alcohol content of 13.81 ± 0.04 %, v/v which was similar to that (8.12 %) detected in peach wines produced from Redhaven variety [11]. As given in Table 2, glucose was rapidly utilized during the production of the Prunus wine as observed for peach. Notably, glucose was completely depleted in peach wine samples after 5 days of the fermentation. Fructose was likely to be utilized more slowly as compared to glucose (Table 3). The most rapid utilization of fructose was observed in the Prunus wine produced from peach, which was depleted in day 5 of the fermentation. Yeasts fermented only hexose sugars. Yeasts fermented sugars at quantity up to 20%; at higher concentrations the metabolism slow down. During alcoholic fermentation, sugars must be metabolized to pyruvate via the glycolytic pathway, which is then decarboxylated to acetaldehyde and finally reduced to ethanol. Glucose and fructose were the favored sugars of *S. cerevisiae* [12]. In Table 4, the total soluble solids of 3 wine were adjusted to 24 ^{o}Brix, and after fermentation for 5 days, the results showed that peach wine (7.30 ^{o}Brix) had less TSS than Chiness plum (14.50 ^{o}Brix) and Red plum (13.50 ^{o}Brix). From the experiment, it was found that the alcohol content in Peach wine was higher than Chinese Plum and Red plum wine because yeast had the ability to consume TSS in peach effectively. During a 15-day acetous fermentation process, oxidative fermentation is a fermentation process caused by bacteria that require oxygen for respiration at the cellular level. Acetic acid bacteria, for examples *Acetobacter pasteurianus*, were used as the starter cultures for producing vinegar. In acetous fermentation, the mechanism for the conversion of alcohol into acetic acid by alcohol dehydrogenase has pyroloquinoline quinone (PQQ) and acetaldehyde dehydrogenase (ALDH) as cofactors. Under these conditions, acetic acid will be excreted and accumulated in media culture until ethanol was completely oxidized [13]. In our work, the Prunus vinegars produced from the three Prunus wines using *A. pasteurianus* were analyzed for their chemical compositions, and the results are given in Tables 5-8. All the Prunus vinegars showed a significant decrease in the alcohol content as it was converted to acetic acid by acetic acid bacteria. However, the alcohols were not completely depleted, in which at the end of acetous fermentation the vinegar produced from peach contained the highest alcohol content of 3.35%, v/v while that produced from red plum had the lowest alcohol content of 1.14%, v/v. For the acetous fermentation, at the end of a 15-day acetous fermentation process, acetic acid content was found to range from 2.90% to 4.04%, v/v with the highest value of 4.04%, v/v, observed in the Prunus vinegar produced from Red Plum, a result which was much higher those found in mulberry vinegar (3.90%) [14] and banana vinegar (3.49%) [1].

Table 1. Changes in alcohol contents of the Prunus wines produced via alcoholic fermentation process

Species	**Alcohol content (%, v/v)**					
	Days after fermentation					
	0	1	2	3	4	5
Chinese plum	0	3.02 ± 0.24^{b}	3.94 ± 0.04^{c}	4.71 ± 0.01^{c}	6.20 ± 0.05^{c}	6.23 ± 0.01^{c}
Red plum	0	4.38 ± 0.03^{a}	5.59 ± 0.00^{b}	5.35 ± 0.00^{b}	6.71 ± 0.01^{b}	6.72 ± 0.01^{b}
Peach	0	2.53 ± 0.05^{c}	7.78 ± 0.02^{a}	10.29 ± 0.05^{a}	12.34 ± 0.23^{a}	13.81 ± 0.04^{a}

Values with various letters in the same column are significantly different according to Duncan's multiple range test ($p < 0.05$).

Table 2. Changes in glucose contents of the Prunus wines produced via alcoholic fermentation process

Species	**Glucose content (%, w/v)**					
	Days after fermentation					
	0	1	2	3	4	5
Chinese plum	17.67 ± 0.01^{a}	15.83 ± 0.12^{a}	10.5 ± 0.00^{a}	8.74 ± 0.00^{a}	6.83 ± 0.01^{a}	6.83 ± 0.01^{a}
Red plum	11.82 ± 0.01^{b}	9.92 ± 0.01^{b}	8.79 ± 0.01^{b}	7.79 ± 0.01^{b}	6.42 ± 0.01^{a}	5.79 ± 0.01^{b}
Peach	10.16 ± 0.02^{c}	8.91 ± 0.03^{c}	2.92 ± 0.01^{c}	1.83 ± 0.01^{c}	0.86 ± 0.29^{b}	0.00^{c}

Values with various letters in the same column are significantly different according to Duncan's multiple range test ($p < 0.05$).

Table 3. Changes in fructose contents of the four berry wines produced via alcoholic fermentation process

Species	**Fructose content (%, w/v)**					
	Days after fermentation					
	0	1	2	3	4	5
Chinese plum	21.00 ± 0.07^{a}	19.00 ± 0.01^{a}	16.43 ± 0.46^{a}	14.13 ± 0.09^{a}	12.7 ± 0.00^{b}	12.73 ± 0.02^{a}
Red plum	16.58 ± 0.48^{b}	14.74 ± 0.01^{b}	14.78 ± 0.65^{b}	14.29 ± 0.47^{a}	13.92 ± 0.15^{a}	12.17 ± 0.12^{b}
Peach	15.77 ± 0.03^{c}	14.11 ± 0.43^{b}	7.46 ± 0.01^{c}	4.50 ± 0.00^{b}	0.48 ± 0.36^{c}	0.00^{c}

Values with various letters in the same column are significantly different according to Duncan's multiple range test ($p < 0.05$).

Table 4. Changes in total soluble solid of the Prunus wines produced via alcoholic fermentation process

Species	Total soluble solid (ºBrix)					
	Days after fermentation					
	0	1	2	3	4	5
Chinese plum	24	23.00 ± 0.00^{a}	20.50 ± 0.71^{a}	18.80 ± 0.28^{a}	17.00 ± 0.00^{a}	14.50 ± 0.71^{a}
Red plum	24	21.50 ± 0.71^{b}	18.70 ± 0.14^{a}	16.50 ± 0.71^{b}	15.00 ± 0.00^{b}	13.50 ± 0.71^{a}
Peach	24	20.00 ± 0.00^{c}	13.50 ± 0.71^{b}	8.50 ± 0.71^{c}	8.00 ± 0.00^{c}	7.30 ± 0.14^{b}

Values with various letters in the same column are significantly different according to Duncan's multiple range test ($p < 0.05$).

Table 5. Changes in acetic acid contents of the Prunus vinegars produced via acetous fermentation

Species	Acetic acid content (%, v/v)			
	Days after fermentation			
	0	5	10	15
Chinese plum	0.24 ± 0.12	1.43 ± 0.12^{a}	2.06 ± 0.14^{a}	3.88 ± 0.70
Red plum	0.10 ± 0.00	1.03 ± 0.00^{b}	3.41 ± 0.18^{a}	4.04 ± 0.19
Peach	0.09 ± 0.00	0.20 ± 0.01^{c}	0.88 ± 0.68^{b}	2.90 ± 0.06

Values with various letters in the same column are significantly different according to Duncan's multiple range test ($p < 0.05$).

Table 6. Changes in alcohol contents of the Prunus vinegars produced via acetous fermentation

Species	Alcohol content (%, v/v)			
	Days after fermentation			
	0	5	10	15
Chinese plum	5.80 ± 0.00^{b}	3.70 ± 0.02^{b}	2.84 ± 0.12^{b}	1.61 ± 0.00^{b}
Red plum	6.49 ± 0.34^{b}	4.95 ± 0.03^{c}	2.40 ± 0.00^{c}	1.14 ± 0.02^{c}
Peach	8.14 ± 0.00^{a}	7.19 ± 0.03^{a}	5.34 ± 0.00^{a}	3.35 ± 0.01^{a}

Values with various letters in the same column are significantly different according to Duncan's multiple range test ($p < 0.05$).

Table 7. Changes in glucose contents of the Prunus vinegars produced via acetous fermentation

Species	Glucose content (%, w/v)			
	Days after fermentation			
	0	5	10	15
Chinese plum	$2.77 \pm 0.0.1^{a}$	2.96 ± 0.00^{a}	2.99 ± 0.01^{a}	3.14 ± 0.01^{a}
Red plum	2.45 ± 0.00^{b}	2.46 ± 0.00^{b}	2.41 ± 0.01^{b}	2.41 ± 0.00^{b}
Peach	0.00 ± 0.00^{c}	0.00 ± 0.00^{c}	0.00 ± 0.00^{c}	0.00 ± 0.00^{c}

Values with various letters in the same column are significantly different according to Duncan's multiple range test ($p < 0.05$).

Table 8. Changes in fructose contents of the Prunus vinegars produced via acetous fermentation

Species	Fructose content (%, w/v)			
	Days after fermentation			
	0	5	10	15
Chinese plum	5.80 ± 0.08^{a}	6.08 ± 0.07^{a}	6.06 ± 0.07^{a}	6.73 ± 0.15^{a}
Red plum	5.59 ± 0.02^{a}	5.77 ± 0.02^{b}	5.76 ± 0.07^{b}	5.90 ± 0.09^{b}
Peach	0.00 ± 0.00^{b}	0.00 ± 0.00^{c}	0.00 ± 0.00^{c}	0.00 ± 0.00^{c}

Values with various letters in the same column are significantly different according to Duncan's multiple range test ($p < 0.05$).

3.2 Total phenolic contents and antioxidant activities

The antioxidant activity of fruit is attributed to the presence of phytochemical compounds such as ascorbic acid and carotenoids. The polyphenols are the primary antioxidant compounds of various fruits [15]. Two roles of antioxidants are to inhibit lipid oxidation and to scavenge free radicals, and methods used to determine the antioxidant activity in wine and vinegar are based on the free radical scavenging activity with DPPH. The levels of antioxidant activities of the Prunus vinegars are presented in Table 9. The results showed that the Prunus wine derived from peach exhibited the highest antioxidant activity of 75.21 mg/ml which was less than that produced from Redhaven cultivar peach (387.95 mg/ml) [11]. Similarly, the vinegar produced from peach species was observed to exhibit the highest antioxidant activity of 49.08±8.49 mg/ml which was much higher than that detected in Rich Lady Peach (3.50 g/kg) [16]. The levels of total phenolic contents detected in the Prunus vinegars produced from different Prunus species via the two-stage fermentation process are given in Table 10. It was noted that the Prunus wine derived from Red plum contained the highest levels (215.85±1.43 mg/l) of total phenolics. Similar results were observed for the Prunus wine produced from the same species, in which the vinegar measured at the end of acetous fermentation exhibited the highest total phenolic content of 133.08±0.76 mg/l, which was much less than that detected in prune juice (441±59 mg/l), in which the main polyphenol in prunes juice were hydroxycinnamates, neochlorogenic acid and chlorogenic acid [17]. The antioxidant activity and total phenolic content were decreased in vinegar, and this result was in agreement with an earlier study of Towantakavanit *et al*. [18] that demonstrated that the decrease in total phenol level could have been due to fermentation process condensation and polymerization reactions as well as the formation of oxidative products and precipitations.

Table 9. Antioxidant activities of the three Prunus wine and vinegars produced via a two-stage fermentation process

Species	DPPH (mg/ml)	
	Wine	Vinegar
Chinese Plum	5.42 ± 0.00^{c}	25.83 ± 0.00^{b}
Red Plum	14.96 ± 0.18^{b}	27.67 ± 0.82^{b}
Peach	45.21 ± 0.06^{a}	49.08 ± 8.49^{a}

Values with various letters in the same column are significantly different according to Duncan's multiple range test ($p < 0.05$).

Table 10. Total phenolic contents of the three Prunus wine and vinegars produced via a two-stage fermentation process

Species	Total phenolic content (mg/l)	
	Wine	Vinegar
Chinese Plum	66.39 ± 0.67^{c}	36.66 ± 0.29^{c}
Red Plum	215.85 ± 1.43^{a}	133.08 ± 0.76^{a}
Peach	140.51 ± 0.38^{b}	80.78 ± 0.57^{b}

Values with various letters in the same column are significantly different according to Duncan's multiple range test ($p < 0.05$).

3.3 Sensory evaluation

The levels of consumers' preference based on the 9-point hedonic scale of the vinegar drinks, a blend of the vinegars made from different Prunus species and honey, are depicted in Table 11. The results show that significant ($p < 0.05$) differences in clarity, color, odor taste and overall acceptability were observed among the drinking vinegars produced from different Prunus species. The drinking vinegar produced from Chinese plum displayed the highest level of consumers' preference, with the mean overall acceptability score of 7.83 ± 1.02, which was equivalent to the hedonic scale of 9. In our study, the high levels of consumers' preference were for the Chinese plum vinegar, and this might be because the taste of the vinegar was sweet blended with sour and because the flavor included some alcohol odor.

Table 11. Sensory scores of the drinking vinegars blended from the three fermented Prunus vinegars

Species	Clarity	Color	Odor	Taste	Overall acceptability
Chinese Plum	6.70 ± 1.21^{ns}	6.77 ± 1.33^{ns}	7.20 ± 1.37^{ns}	7.27 ± 1.41^{ns}	7.83 ± 1.02^{a}
Red Plum	6.80 ± 1.42^{ns}	6.50 ± 1.25^{ns}	6.67 ± 1.60^{ns}	6.70 ± 1.29^{ns}	7.03 ± 1.30^{b}
Peach	6.40 ± 1.52^{ns}	6.53 ± 1.83^{ns}	6.57 ± 2.03^{ns}	6.77 ± 1.98^{ns}	6.57 ± 1.79^{b}

Values with various letters in the same column are significantly different according to Duncan's multiple range test ($p < 0.05$).

4. Conclusions

This study was conducted in order to compare the levels of acetic acid, total phenolics, antioxidants and consumers' preference of the Prunus vinegars produced from three Prunus species via a two-stage fermentation process. The results showed that the vinegars produced from Red plum species exhibited the highest level of acetic acid (4.04 %, v/v), while those produced from peach displayed the highest antioxidant activities (49.08 mg/ml), as measured by means of DPPH radical assay. Meanwhile, the vinegars produced from Red plum were observed to have the highest total phenolics

(133.08 mg/l). Sensory test based on the 9-point hedonic scale using untrained panelists showed that the drinking vinegars made from Chinese plum had the highest overall preference (7.83).

5. Acknowledgements

The authors would like to thank the Laboratory Equipment Center of Mahasarakham University for the laboratory facilities.

References

[1] Boonsupa, W., Pimda, W., Sreeninta, K., Yodon, C., Samorthong, N., Bou-on, B. and Hemwiphat, P., 2019. Development of fermented banana vinegar: Chemical characterization and antioxidant activity. *Journal of Food Health and Bioenvironmental Science*, 12(1), 21-27.

[2] Xia, T., Zhang, B., Duan, W., Zhang, J. and Wang, M., 2020. Nutrients and bioactive components from vinegar: A fermented and functional food. *Journal of Functional Foods*, 64, 1-14.

[3] Chen, Y., Huang, Y., Bai, Y., Fu, C., Zhou, M., Gao, B., Wang, C., Li, D., Hu, Y. and Xu, N., 2017. Effects of mixed cultures of *Saccharomyces cerevisiae* and *Lactobacillus plantarum* in alcoholic fermentation on the physicochemical and sensory properties of citrus vinegar. *LWT Food Science and Technology*, 84, 753-763.

[4] Aubert, C. and Chalot, G., 2020. Physicochemical characteristics vitamin c and polyphenolic composition of four European commercial blood- flesh peach cultivars (*Prunus persica* L.Batsch). *Journal of Food Composition and Analysis*, 86, 1-11.

[5] Nourbakhas, H., Emam-Djomeh, Z. and Mirsaeedghazi. H., 2015. Effect of operating parameters on physicochemical properties of red plum juice and permeate flux during membrane clarification. *Desalination and Water Treatment*, 54(11), 3094-3105.

[6] Lee, J.A., Ko, J.H., Jung, B.G., Kim, T.H., Hong, J.I., Park, Y.S. and Lee, B.J., 2013. Fermented *Prunus mume* with probiotics inhibits 7,12-dimethylbenz[a] anthracene and 12-O-tetradecanoyl phorbol-13-acetate induced skin carcinogenesis through alleviation of oxidative stress. *Asian Pacific Journal of Cancer Prevention*, 14, 2973-2978.

[7] Ozen, M., Ozdemir, N., Filiz, B.E., Budak, N.H. and Kok-Taş, T., 2020. Sour cherry (*Prunus cerasus* L.) vinegars produced from fresh fruit or juice concentrate: Bioactive compounds, volatile aroma compounds and antioxidant capacities. *Food Chemistry*, 309, https://doi.org/10.1016/j.foodchem.2019.125664

[8] Aguiar, A., Nascimenta, R.A.D.A., Ferretti, L.P and Goncalves, A.R., 2005. Determination of organic acids and ethanol in commercial vinegars. *Brazilian Journal of Food Technology*, 5^0 SIPAL, Macro., 51-56.

[9] Brand-Williams, W., Cuvelier, M.E.and Berset, C., 1995. Use of a free radical method to evaluate antioxidant activity. *LWT-Food Science and Technology*, 28, 25-30.

[10] Singleton, V.L., Orthofer, R. and Lamuela-Raventós, R.M., 1999. Analysis of total phenols and other oxidation substrates and antioxidants by means of Folin-Ciocalteu reagent. *Methods in Enzymology*, 299, 152-178.

[11] Davidovic, S.M., Veljović, M.S., Pantelić, M.M., Baošić, R.M., Natić, M.M., Dabić, D.Č., Pecić, S.P.and Vukosavljevic, P.V., 2013. Physicochemical, antioxidant and sensory properties of peach wine made from Redhaven cultivar. *Journal of Agricultural and Food Chemistry*, 61(6), 1357-1363.

[12] Dynesen, J., Smits, H., Olsson, L. and Nielsen, J., 1998. Carbon catabolite repression of invertase during batch cultivations of *Saccharomyces cerevisiae*: the role of glucose, fructose, and mannose. *Applied Microbiology and Biotechnology*, 50, 579-582.
[13] Pongdam, S., 2017. Cellular respiration of acetic acid bacteria: Oxidative fermentation and applications. *SDU Research Journal*, 10(3), 203-236.
[14] Boonsupa, W., 2019. Chemical properties, antioxidant activities and sensory evaluation of berry vinegar. *Walailak Journal of Science and Technology*, 16(11), 887-896.
[15] Liu, H., Jiang, W., Cao, J. and Li, Y., 2019. Changes in extractable and non-extractable polyphenols and their antioxidant properties during fruit on-tree ripening in five peach cultivars. *Horticultural plant Journal*, 5(4), 137-144.
[16] Puerta-Gomez, A.F. and Cisneros-Zevallos, L., 2011. Postharvest studies beyond fresh market eating quality: Phytochemical antioxidant changes in peach and plum fruit during ripening and advanced senescence. *Postharvest Biology and Technology*, 60(3), 220-224.
[17] Donovan, J.L., Meyer, A.S. and Waterhouse, A.L., 1998. Phenolic composition and antioxidant activity of Prunus and prune juice (*Prunus domestica*). *Journal of Agricultural and Food Chemistry*, 46, 1247-1252.
[18] Towantakavanit, K., Park, Y.S. and Gorinstein, S., 2011. Bioactivity of wine prepared from ripened and over-ripened kiwifruit. *Central European Journal of Biology*, 6, 205-215.

The Anti-Diabetic Effect of Nano-Encapsulated Propolis from *Apis mellifera* on Type 2 Diabetes

Sarah S. Hegazy[1]*, Hanan Helmy[2], Mohamad S. Salama[1], Nadia M. Lotfy[1] and Dalia M. Mahmoud[1]

[1]Entomology Department, Faculty of Science, Ain Shams University, Cairo, Egypt
[2]Research and Training Center on Vectors of Disease, Ain Shams University, Cairo, Egypt

Received: 28 March 2020, Revised: 22 July 2020, Accepted: 10 August 2020

Abstract

Diabetes mellitus is viewed as a major disease and is among the most prevalent health problems globally. The goal of the present research was to evaluate the therapeutic efficiency of an ethanolic extract of Egyptian propolis (EEP) conjugated with chitosan polyacrylic (CS-PAA) nanoparticles against type 2 diabetes mellitus. Thirty Wistar rats were randomly categorized into 6 groups (5 animals/ group). Group I consisted of normal rats as a normal control. The remaining five groups were injected with streptozotocin (STZ), a diabetogenic agent, in order to induce diabetes. The experimental groups were treated for 4 consecutive weeks as follows: Group II included untreated diabetic rats, serving as a negative control. Group III consisted of diabetic rats treated with EEP. Group VI consisted of diabetic rats treated with Metformin. The findings of this work illustrated that no significant differences were noticed concerning the body weight of the treated groups compared to that of the normal control group. Blood glucose levels were significantly decreased in the diabetic rats treated with EEP and EEP encapsulated CS-PAA nanoparticles compared to the untreated diabetic rats. The results indicated that EEP encapsulated CS-PAA nanoparticles displayed a potential therapeutic effect against type 2 diabetes mellitus.

Keywords: diabetes mellitus; chitosan, polyacrylic acid; propolis; body weight
DOI 10.14456/cast.2021.11

1. Introduction

Diabetes is viewed as a chronic metabolic disease marked by high blood sugar (hyperglycemia) and is a leading global health problem. In addition, it is one of the most distressing medical problems of the century. Per the data described by the World Health Organization **(**WHO**)**, the global incidence rates of diabetes mellitus were 171,000,000, and this number is predicted to escalate up to 439,000,000 by 2030. Diabetes mellitus is distinguished by a deficiency regarding insulin secretion and/or action, associated with chronic hyperglycemia and disorders of carbohydrate, protein, and lipid metabolism [1].

Propolis is defined as a resinous substance gathered and produced by honeybee workers from various floral substances along with bees wax and salivary secretions. One of the unique

*Corresponding author: Tel.: (+20) 100 494 2997
E-mail: sarah.hegazy@sci.asu.edu.eg

characteristics of propolis is its high resin content (approx. 50%), in addition to wax (30%), essential oils, pollens, along with other organic components [2]. Noticeably, propolis composition differs according to its geographical area of origin, in addition to the type of flora in that region. Propolis, in particular, possesses an extensive variety of biological activities, including antioxidant, antiviral, anti-inflammatory, cytotoxic, antimicrobial, and immune-modulatory properties. In addition, some recent studies have revealed that propolis has hypoglycemic properties in addition to antioxidant capacity [3]. Preceding studies revealed that ethanol and water extracts of propolis exhibited positive effects in diabetic animals [4].

Nanoparticles have been used since the early 1990s. They have been used as drug delivery vehicles either by encapsulating the drugs or by the deposition of the drugs on the surface of the nanocarrier molecules [5]. Nonetheless, polymeric nanoparticles and liposomes are among the most recognized delivery vehicles of drugs with medical applications in the pharmaceutical area. Polymeric nanoparticles have achieved this standing due to their biocompatibility, non-toxicity to biological systems, biodegradability, long shelf life, controlled release, targeted delivery and therapeutic efficiency [6].

There has been a disastrous rise in diabetes across the world, paralleling the prevalence of obesity. More than 95 percent of obese/overweight people would develop type-2 diabetes (T2D) during their lifetime [7]. Moreover, the type-2-diabetic drug, metformin is being investigated for traces of a probable carcinogen in addition to other side effects hampering its therapeutic efficiency [8]. Consequently, it is an excessive insistence to find alternative treatments and innovative inhibition tactics for T2D. The present study investigated the effect of encapsulated propolis on the body weight and blood glucose level of type 2 diabetic rats.

2. Materials and Methods

2.1 Preparation of propolis samples

Egyptian propolis samples were harvested from local western honey bee workers (*Apis mellifera* Linnaeus) from Egyptian bee colonies located at the Agriculture Research Centre at Dokki, Giza Governorate, Egypt, according to the method of Souza *et al*. [9], using glass slides close to the internal and lateral walls of the rearing boxes.

The collection process involved using white glass slides (48 cm length, 5 cm width and 5 mm thickness), arranged contiguously to each other and put onto the top bar of the rearing combs, with an elevation at approximately 3 mm in between.

2.1.1 Preparation of ethanolic extract of propolis

The ethanolic extract of propolis (EEP) was formulated by the maceration of raw propolis at room temperature, usually accompanied by shaking, in the proportion of 10 g raw propolis to 100 ml of ethanol 80% (solvent). The propolis extracts were collected after 7 days of maceration and filtration by Whatman No. 1 filter paper per the procedure reported by Cunha *et al.* [10].

2.1.2 Characterization of propolis extract by Gas Chromatography-Mass Spectrometry (GC-MS)

The component detection was achieved using the database and software of the National Institute Standard and Technology (NIST) and Wiley Registry of Mass Spectral data's, New York (WILEY). The characterization data, including retention time and peak area percentages, were acquired using

th GC-MS chemical analysis to identify the major components present in the propolis sample. The components with percentage peak area greater than 0.07% were considered to be significant elements and were documented according to Usman *et al*. [11].

2.2 Preparation of nanoparticles

The chitosan**-**poly acrylic acid (CS-PAA) polymer was conjugated with the EEP according to the method of Braun *et al*. [12]. The CS-PAA nano-spheres were synthesized by polymerization. An amount of 100 g of chitin (Sigma Aldrich, USA) was converted to chitosan through a deacetylation process using 500 ml of saturated NaOH and glycerin bath at 160ºC-170ºC for 3 h [13]. Later the chitosan solution obtained was mixed with polyacrylic acid solution with stirring overnight.

The polymerization was accomplished by preheating 22 ml of distilled water to 70°C, with an inlet for nitrogen flow, and another one for a thermometer. At this temperature, a solution of potassium persulphate (KPS) (0.32 g/8 ml distilled water to produce 0.66 mM solution) was slowly introduced dropwise into the flask over a period of 5-10 min, while stirring at 300 rpm. The saturated solution of the EEP was introduced into the acrylic acid (AA) and the cross-linking agent KPS to produce EEP conjugated with CS-PAA polymer. After complete polymerization was reached, the temperature was kept at 80°C for another 30 min. Afterwards, the viscous polymer solution was added dropwise to 0.1 N hydrochloric acid (HCl), whereupon the polymer precipitated. The polymer was then incubated for 48 h at 60ºC. The resulting polymer was dried to constant weight at 50°C. After the drying process, each of the resulting polymer formulations (blank and EEP-conjugated CS-PAA) was rod-milled thoroughly for 1 h using a home-made rod mill (100 rpm), then sonicated (42 KHz, 15 min, CE-7200A, China) and finally centrifuged (12,000 ×*g*, 30 min) to remove insoluble materials. The nano-spheres were powdered by freeze-drying at -44ºC (LGJ-18C, China).

2.3 Characterization of the propolis conjugated with nanoparticles

2.3.1 Physicochemical characterization of the CS-PAA nanoparticles

Examination of propolis conjugated with nanoparticles by Transmission Electron Microscopy (TEM) was done according to Ray *et al*. [14] and Wang *et al*. [15]. Samples were sonicated for 30 min (42 KHz, CE-7200A, China) prior to being loaded on a TEM sample grid (silicon oxide supported by copper mesh) via standard fine tweezers. Afterward, the loaded TEM grids were left to dry in air.

The size distribution and mean diameter of the CS-PAA nanoparticles (hollow and EEP-loaded) were measured by dynamic light scattering (DLS) (Zetasizer 3000 HS, Malvern, UK) in pH 4 buffer solution according to the method described by Kao *et al*. [16]. The nanoparticles' samples were diluted, and then the DLS measurements were done with a wavelength of 633 nm at 25ºC with an angle detection of 90º**.** The measurements were done in triplicates and the mean diameter ± SD was calculated**.**

2.3.2 Determination of the EEP encapsulation efficiency of the CS-PAA nanoparticles

The amount of EEP encapsulated into the CS-PAA nanoparticles was calculated by determining the difference between the total EEP amount used to prepare the nanoparticles and the amount of EEP present in the aqueous phase, according to the method described by Andrade *et al*. [17].

After the preparation, the EEP-loaded nanoparticles were separated from the aqueous suspension medium by centrifugation at 50,000 ×*g* for 2 h. After centrifugation, the amount of free propolis in the clear supernatant was measured using a UV spectrophotometer (LS-50B, Perkin

Elmer) at the wavelength of 425 nm. All analyses were carried out in triplicates and blank nanoparticles were used as control. Encapsulation efficiency was calculated using equation (1).

$$\text{Encapsulation Efficiency} = \frac{\text{Total amount of propolis} - \text{Free amount of propolis}}{\text{Total amount of propolis}} \times 100 \quad (1)$$

2.3.3 *In vitro* release of propolis from the CS-PAA nanoparticles

The release of propolis from CS**-**PAA nanoparticles was carried out in an aqueous phosphate buffer solution at pH 4 (to simulate the gastric environment) and 37◦C, according to Zhu *et al*. [18]. The EEP**-**loaded nanoparticles were placed into 60 ml of aqueous buffer solution. Each 10 min, 3 ml samples of the aqueous buffer solutions were withdrawn and replenished by 3 ml fresh buffer solution to maintain a constant volume. The amount of the released propolis in the withdrawn buffer samples was determined by UV-vis absorbance at 425 nm. All EEP release data were performed in triplicate and averaged. The release percentage of the propolis was plotted against time in minutes.

2.3.4 Fourier transform infrared (FT-IR, Thermo Nicolet 6700, UK) spectroscopy

This technique was applied according to Ray *et al*. [14] and Wang *et al*. [15] to determine the chemical structure and functional groups of surface-modified nanoparticles revealing interactions at the nanoparticle surface.

The procedure involved taking FT-IR spectra of CS-PAA polymer and propolis conjugated with CS-PAA using the potassium bromide (KBr) pellet technique, which involved crushing the different samples in a mortar, then mixing each of the crushed materials with KBr (IR spectroscopy grade). Afterwards, the mixture was compressed to 12 mm diameter semi-transparent disk by applying a pressure of 65 kN (pressure gauge, Shimadzu, China) for two min. The FT-IR was verified in the range of 400-4000 cm^{-1} via FT-IR spectrophotometer. To know if there was any chemical interaction between propolis and polymer nanoparticles, IR spectra of the previously mentioned specimens were compared together.

2.4 The experimental induction of diabetes

The rats, serving as the experimental study samples, were procured from the lab animals house at the medical research center (MRC), Ain Shams University, and then were divided into two main groups, experimental or treatment and control. The induction of type-2 diabetes (T2D) in the studied rats was achieved by intoxicating their pancreatic β-cells using streptozotocin (STZ), a potent diabetogenic agent.

The rats (treatment and control) were allowed a standard formulated pellet diet and water access, *ad libitum*, during the duration of the experiment and were maintained at 24 ± 2◦C, 60-70% humidity, <50 dB noise level, and 12 h dark/12 h light cycles. All animal maintenance and experimentation procedures were done in accordance with the Ethical Principles of Animal Research adopted by the Faculty of Science, Ain Shams University.

In this study, a mixture of high fat diet (HFD) for 2 weeks and a single dose intraperitoneal injection (35 mg/ kg STZ) for 3 successive days were used to induce T2D in the rat models according to Vatandoust *et al*. [19]. The components of the HFD diet (as a percentage of total kcal) were 41% fat, 18% protein, and 41% carbohydrates. Rats were fed on their corresponding diets for 2 weeks before injection of STZ, according to Dranse *et al*. [20]. The STZ agent was dissolved in a sterile biological citrate buffer (0.05 M, pH 4.5). After 72 h, all rats were fasted for 16 h and their blood glucose levels were checked from the tail vein using a glucose analysis kit and an auto-analyzer (ACCU-CHEK Active, Roche diagnostics). After 1 week of the last STZ injection, the blood of the

studied groups was collected from the caudal vein (groups II-VI) in a fasting state. After plasma separation, an aliquot was taken for the measurement of insulin by ELISA test (Linco Research, Inc), to confirm the development of T2D (evident by insulin resistance) [21, 22]. The rats used in the experiments were regarded as diabetic when their fasting blood glucose (FBG) levels were more than 200 mg/dl [23]. The treatment was made available to the diabetic study sample through an oral gavage, on a daily basis for 30 days.

2.4.1 Experimental design

Male Wister albino (30) rats were used in this research and categorized into 6 groups (5 animals/ group), as follows:
Group I: Included non-diabetic rats that received only 0.9% NaCl saline solution as a normal control.
Group II: Included diabetic rats without treatment as a negative control.
Groups III: Included diabetic rats treated with EEP at dosage levels of 300 mg/kg.
Groups IV: Included diabetic rats treated with CS-PAA nanoparticles at dosage levels of 300 mg/kg.
Groups V: Included diabetic rats treated with EEP conjugated with CS-PAA nanoparticles at dosage levels of 300 mg/kg.
Groups VI: Included diabetic rats treated with Metformin (Met) at dosage levels of 100 mg/kg.

Bodyweight and blood glucose were recorded every week for diabetic- related measurements. The selected dose of propolis was according to the reported guidelines of Al-Hariri *et al*. [24] and Usman *et al*. [25].

2.4.2 Blood sampling and analysis

At the termination of the experiment, rats were fasted 14-16 h after their last meal, and then blood samples were harvested under diethyl-ether-induced anesthesia, from the heart of each rat. The blood samples were then centrifuged for 10 min at 2,000 ×*g* and 4°C, and afterwards, the serum was separated and stored at -80°C until further analysis.

2.5 Statistical analysis

Analysis of variance (ANOVA) and Tukey statistical tests were employed. Data were shown as means ± standard deviation ($P < 0.05$).

3. Results and Discussion

3.1 Gas chromatography-mass spectrometry (GC-MS)

The GC-MS spectrum of propolis extract confirmed the presence of a number of components, as illustrated in Figure 1. The peak numbers in Table 1 were designated according to the retention time of the major peaks, corresponding to the main 26 compounds identified and listed in Table 1. Flavonoids in propolis are classified into flavones, flavonols, flavanones, flavanonols, chalcones as 2'-Hydroxy-2,3,4',6'-tetramethoxychalcone, dihydrochalcones, according to their chemical structure, in addition to sugars (like fructose), mannitol, esters, and glycerol.

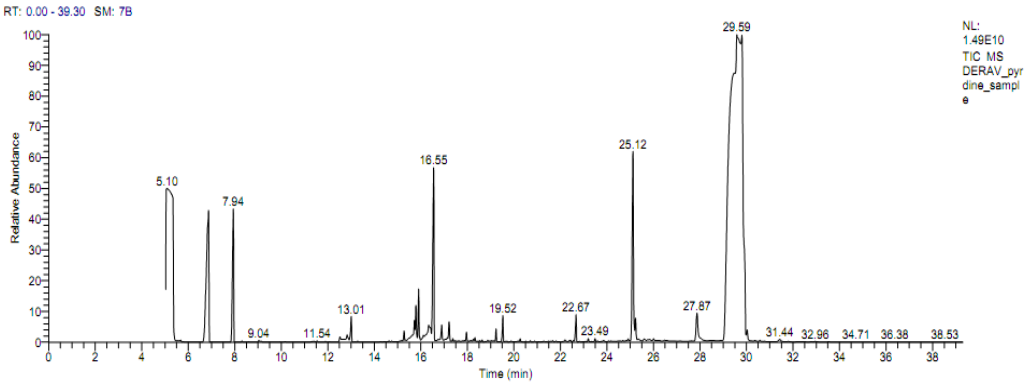

Figure 1. Gas chromatography-mass spectrometry (GC-MS) of ethanolic extract of propolis (EEP)

Table 1. Chemical composition of ethanol extracts of Egyptian propolis sample by GC-MS

Peak area (%)	Retention time (min.)	Compound name	Molecular formula	Molecular weight (u)
24.55	5.33	2-[3,4-(Methylenedioxy) Phenyl]-1-Cyclopentanone	$C_{12}H_{12}O_3$	204
		3(2h)-Pyridazinone, 4,5-Dihydro-4-(4-Methoxyphenyl)-	$C_{11}H_{12}N_2O_2$	204
		7-Methoxy-3,6-Dimethyl-2-Tetralone	$C_{13}H_{16}O_2$	204
		2'-Hydroxy-2,3,4',6'-Tetramethoxychalcone	$C_{19}H_{20}O_6$	344
8.95	6.87	4(Pentadeuterio)Phenylazulene	$C_{16}H_{12}$	204
		1[(Hexadeuterio)Phenyl]Naphthalene	$C_{13}H_{24}N_2$	208
		1h-Pyrrole, 2-(5-Chloro-2-Methoxyphenyl)-	$C_{16}H_6D_6$	210
5.47	7.93	Glycerol, Tris (Trimethylsilyl) Ether4	$C_{12}H_{32}O_3Si_3$	308
0.81	13.01	Sulfamic Acid, 3TMS Derivative Tris(Trimethylsilyl)Sulfamate	$C_9H_{27}NO_3SSi_3$	313
0.26	15.28	Levoglucosan, 3TMS Derivative Levoglucosan, Tris(Trimethylsilyl)-1H-INDOLE	$C_{15}H_{34}O_5Si_3$	378
1.26	15.91	D-Psicofuranose, Pentakis(Trimethylsilyl) Ether (Isomer 2)	$C_{21}H_{52}O_6Si_5$	540
0.43	16.34	Quinic Acid-Pentatms	$C_{22}H_{52}O_6Si_5$	552
		Chlorogenic Acid (6TMS)	$C_{34}H_{66}O_9Si_6$	786
6.85	16.55	9,9'(10h,10'h)-Spirobiacridine	$C_{25}H_{18}N_2$	346

Table 1. (cont.)

Peak area (%)	Retention time (min.)	Compound name	Molecular formula	Molecular weight (u)
0.67	17.21	3,6-Heptanooxepin-4,5-Dicar Bonsaure-Dimethylester	$C_{17}H_{22}O_5$	306
0.29	17.96	D-Glucopyranose, 5TMS Derivative	$C_{21}H_{52}O_6Si_5$	540
		Glucopyranose, 1,2,3,4,6-Pentakis-O-(Trimethylsilyl)-,		
0.31	19.23	Myo-Inositol, 6TMS Derivative	$C_{24}H_{60}O_6Si_6$	612
		Myo-Inositol, 1,2,3,4,5,6-Hexakis-O-(Trimethylsilyl)		
0.75	19.52	Caffeic Acid, 3TMS Derivative	$C_{18}H_{32}O_4Si_3$	396
		Trimethylsilyl3,4-Bis(Trimethylsiloxy)Cinnamate		
0.86	22.67	5á-Androstan-7á,17à-Dimethyl-3à,17á-Diol, Di-Trimethylsilyl	$C_{27}H_{52}O_2Si_2$	464
		Pregnan-11-One, 3,17,20-Tris[(Trimethylsilyl)Oxy]-, (3à,5á,20s)-	$C_{30}H_{58}O_4Si_3$	566
		Sucrose, 8TMS Derivative	$C_{36}H_{86}O_{11}Si_8$	918
0.61	25.23	Maltitol, Nonakis(Trimethylsilyl) Ether	$C_{39}H_{96}O_{11}Si_9$	992
		Cis-5-O-Feruloylquinic Acid, 5TMS	$C_{32}H_{60}O_9Si_5$	728
		17-Phenyl Trinor Prostaglandin E2	$C_{23}H_{30}O_5$	386
0.80	29.93	3-O-Coumaroyl-D-Quinic Acid, 5TMS	$C_{31}H_{58}O_8Si_5$	698
0.21	30.03	1,3-Benzodioxole, 3a,6,7,7a-Tetrahydro-2,2,3a,7-Tetramethyl-5 (Phenylsulfonyl),[3AS(3Aà,7á,7Aà)]	$C_{17}H_{22}O_4S$	322

The GC-MS analytical data demonstrated the existence of 26 compounds in Egyptian EEP. This result is to some degree in contrast with analysis of Malaysian propolis, which described 36 compounds by GC-MS analysis when extracted with ethanol. This difference may have been due to the fact that the chemical make-up of propolis is affected by the geographical locale, botanical origin, and bee species, according to Usman *et al.* [11].

The Egyptian EEP was found to be rich in phenolic compounds including cinnamic acid, caffeic acid, coumaric acid, and their derivatives. This result was in agreement with the study of Huang *et al.* [26] and that of Huang *et al.* [27].

3.2 Characterization and propolis-polymer biocompatibility

3.2.1 Physicochemical characterization, size distribution and encapsulation efficiency of EEP-loaded CS-PAA nanoparticles

The TEM photomicrographs elaborated the morphology of CS-PAA polymer and propolis conjugated CS-PAA nanoparticles. In addition, the size distribution (in terms of diameter) of the resultant propolis conjugated CS-PAA nanoparticles along with their topography was also revealed.

The blank CS-PAA polymer nanoparticles were shown to be approximately 24-32 nm spheres as illustrated in Figure 2a and Table 2.

The propolis conjugated CS-PAA polymer nanoparticles ranged in size between 40 nm and they were in the form of encapsulated spheres according to the data revealed by Figure 2b and Table 2. The encapsulation efficiency assay showed that propolis was efficiently core-encapsulated within the CS-PAA nanoparticles, evidenced by a 90.2 ± 2.3% encapsulation efficiency.

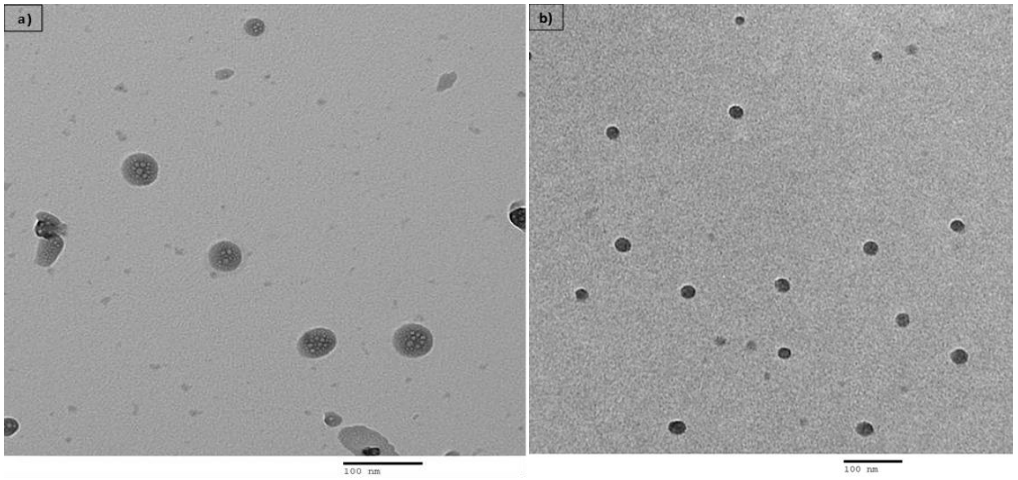

Figure 2. Transmission electron microscope micrograph showing a magnified view of the morphology and topography of: (a) the blank CS-PAA nanoparticles, size 24-32 nm; and (b) the EEP encapsulated in CS-PAA nanoparticles, size 40 nm

Table 2. Size distribution of the blank and EEP-loaded CS-PAA nanoparticles

	Hollow	**EEP-loaded**
Diameter of Nanoparticles (Mean ± SD)	29 ± 10	40 ± 12

The morphology and topography of the individual polymer and propolis conjugated nanoparticles was found to be regularly spherical with a diameter of 24-32 nm and around 40 nm, respectively. In addition, the propolis was observed to be encapsulated within the core of the CS-PAA nanoparticles at a level of 90.2 ± 2.3%. The encapsulated propolis was easily absorbed throughout the polymer matrix crystalline structures. These results are in agreement with Cevher *et al.* [28] and Seven *et al.* [29].

Additionally, this size range was in accordance with the study conducted by Omidirad *et al.* [30] on doxorubicin-loaded poly AA-coated magnetite nanoparticles, where the particles were 6-15 nm. On the other hand, this range was not in agreement with the study conducted by Guo *et al.* [31], in which the size range of the resulting EEP-loaded nanoparticles was between 1-100 nm. This discrepancy in the size range of the resulting particles may have been due to the variation in the synthesis process and type of the nanoparticles.

3.2.2 *In vitro* EEP release from CS-PAA nanoparticles

The *in vitro* release of EEP from the CS-PAA nanoparticles, as illustrated in Figure 3, showed that nearly 60% of the propolis payload was released within the first 800 min. The release profile involved a brief initial burst release in the first 40 min, followed by a slower release rate, and then another release burst was detected still within the first 200 min. Afterwards, the release occurred at a slow but constant rate. This observation could be due to a rapid degradation of the polymer outer shell in the first 40 min, followed by partial degradation of the initial CS layer beneath the PAA outer shell. These findings are in accordance with the study of Dounighi *et al.* [32].

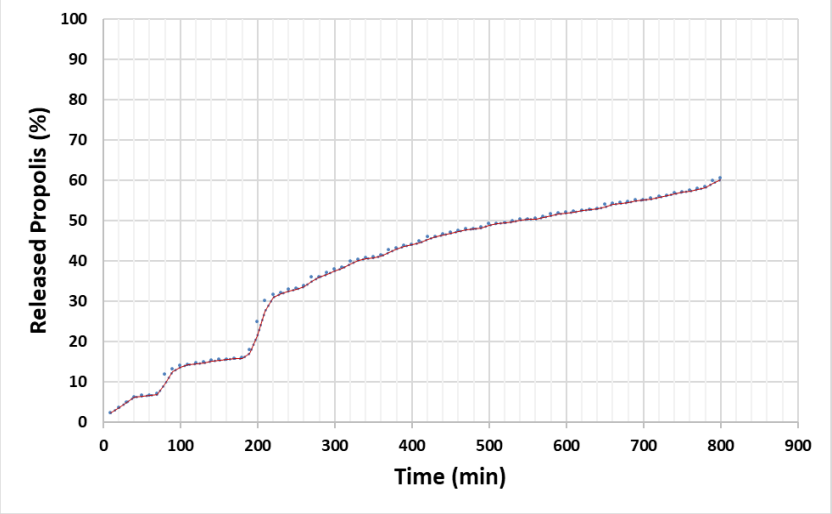

Figure 3. Propolis release profile from CS-PAA nanoparticles at pH 4

3.2.3 Fourier transform infrared (FT-IR)

Figure 4 showed the results obtained from the comparative FT-IR study between CS-PAA polymer, and propolis conjugated CS-PAA nanoparticles. The characteristic absorption bands of CS-PAA polymer displayed peaks in the 500, 1000, 1500, 2000, 2500, 3000 and 3500 cm^{-1} regions. The peaks shown by the propolis conjugated nanoparticles were found to be nearly identical to those produced by the blank CS-PAA polymer. The results showed a slight difference in the chemical group bands between CS-PAA polymer and EEP-conjugated CS-PAA nanoparticles.

The FT-IR data illustrated the appearance of spectroscopic peaks characteristic for the chosen parent polymer, CS-PAA, in the propolis conjugated CS-PAA samples without showing any traces for those characteristics for propolis (i.e. propolis was completely masked). This result strongly suggests the complete and successful physical encapsulation of propolis by CS-PAA without forming any chemical bonding. Otherwise, the chemical conformations of the polymer and the encapsulated propolis would have been altered and this would have accordingly resulted in the appearance of new FT-IR peaks, different from those of both the polymer and propolis.

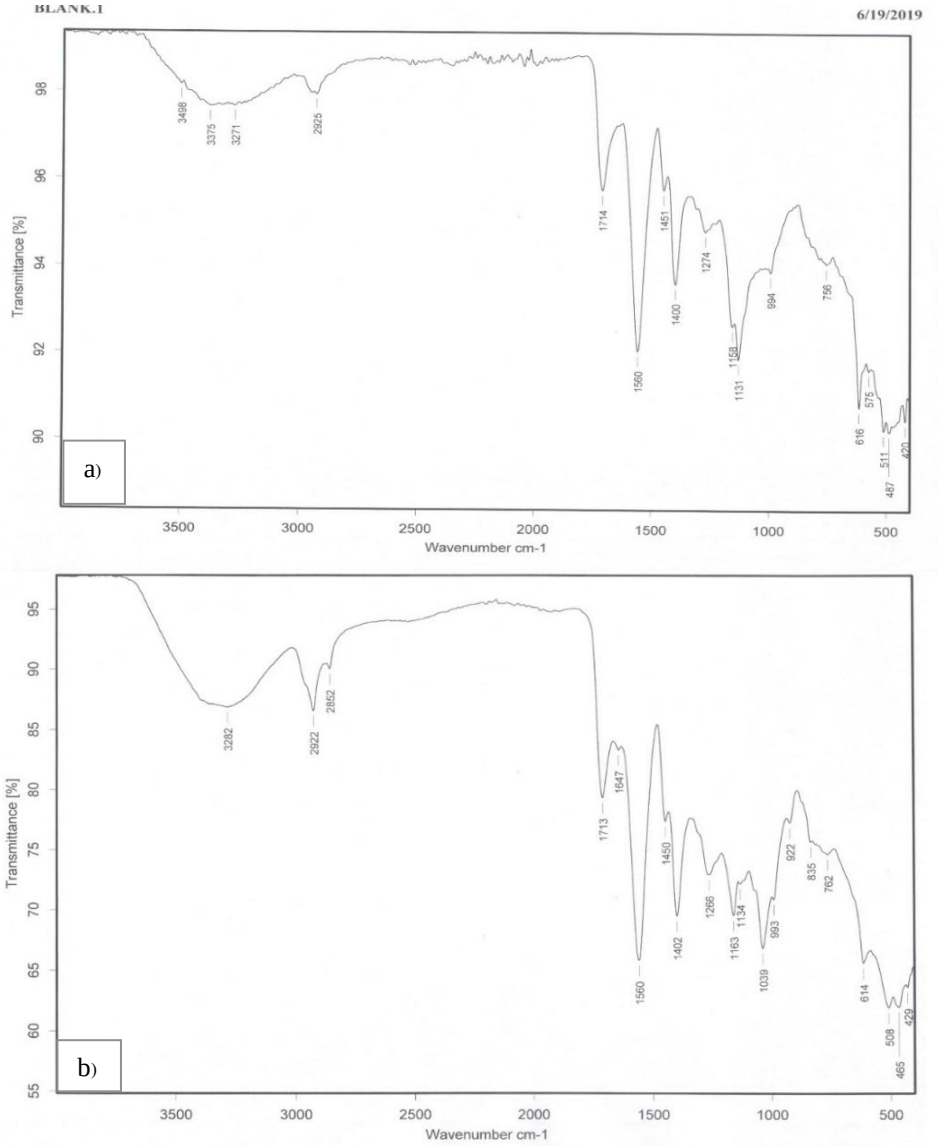

Figure 4. Fourier transforms infra-red spectrographs for (a) the CS-PAA polymer, and (b) the EEP-conjugated with CS-PAA polymer

For the pure propolis, the peaks produced were in the 400-4000 cm^{-1} regions according to Hussein *et al.* [33]. A comparison between the characteristic peaks was performed in the region of 2500-3500cm^{-1} to determine the efficiency of CS-PAA polymer nanoparticles encapsulation of propolis without any chemical interactions. Peres *et al.* [34] mentioned that the strong and broadband at 3445 cm^{-1} is associated with the −OH hydrogen bonds between the polyphenol rings.

3.3 Effect of EEP and EEP conjugated with CS-PAA nanoparticles on type 2 diabetes mellitus

3.3.1 The experimental induction of type-2 diabetes

The initiation of experimental T2D in the rats via diabetogenic chemicals is very convenient and simple to use, and a famous example of such chemicals is STZ. In the current work, induction of T2D via STZ at a dosage of 35mg/kg in rats was conducted according to El Rabey *et al.* [35], and the experimental animals showed a notable rise in the serum glucose levels in comparison to those in the normal control group. Moreover, the results of fasting serum insulin (FSI), evident in Table 3, illustrated that all the studied groups showed normal insulin range, with an emphasis that the groups II-VI showed lower values than the normal control (group I).

Table 3. Fasting serum insulin (FSI) for the studied rat groups

Weeks	Groups*					
	I	**II**	**III**	**IV**	**V**	**VI**
FSI (ng/ml) (Mean ± SD)	$1.12^{a} \pm 0.07$	$0.94^{a} \pm 0.04$	$1.01^{a} \pm 0.06$	$0.97^{a} \pm 0.03$	$0.88^{a} \pm 0.08$	$0.99^{a} \pm 0.06$

*Means that do not share a letter are significantly different.

3.3.2 Changes in body weight

Figure 5 shows the changes in bodyweight of the studied groups. The results did not show notable differences with respect to the body weight at the initiation of drug administration ($P>0.05$), however during the following 4 weeks of drug administration, the bodyweight of each studied group increased gradually. The bodyweight of all treated groups increased at an equal rate compared to the control groups.

Data revealed no marked differences with respect to the body weight of all the diabetes-afflicted groups compared to that of the normal control group. These findings came in agreement with those of Holmes *et al*. [36] and El Rabey *et al*. [35], who suggested that at the end of the study period, experimental rats weighed the same as the control rats.

3.3.3 Changes in blood glucose level

As shown in Figure 6, diabetic rats served as a negative control (group II) and showed increasing hyperglycemia from week 1 until week 4, whereas the groups of diabetic rats treated with EEP (group III) and EEP conjugated with CS-PAA (group IV) showed significantly reduced blood glucose levels from week 1 till the end of the treatment period. The group of diabetic rats treated with EEP conjugated with CS-PAA showed a three-fold significant decrease in blood glucose level compared to the diabetic positive control, EEP group and metformin group ($P < 0.05$). In the healthy rats, constant glucose levels were maintained below 200 mg/dl.

These results, combined with those of FSI values indicate that the type of diabetes developed in the diabetic rats (groups II-VI) is type 2, indicated by normal serum insulin accompanied with hyperglycemia, a strong indicator of insulin resistance [24].

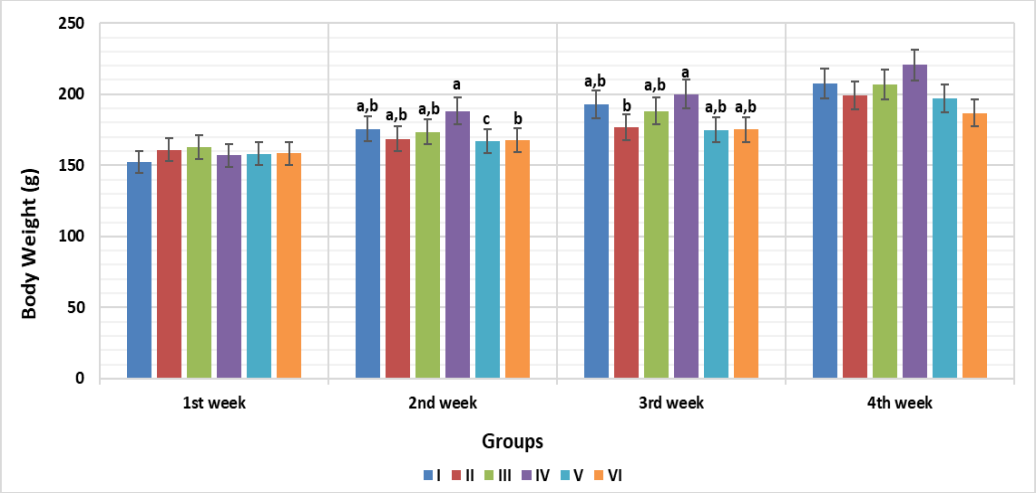

Figure 5. Changes in body weight (g) of rats with induced T2D and normal rats treated for 4 weeks after STZ administration where means that do not share a letter are significantly different. I: non-treated non-diabetic group (normal control), II: non-treated diabetic group (negative control), III: diabetic group treated with EEP, IV: diabetic group treated with CS-PAA nanoparticles, and V: diabetic group treated with (EEP) conjugated with (CS-PAA) nanoparticles, VI: diabetic group treated with metformin

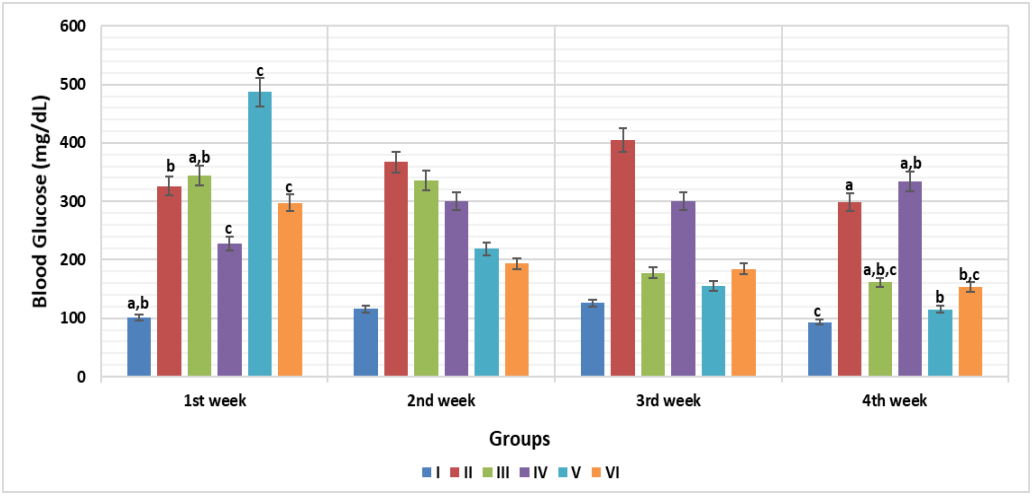

Figure 6. Changes in serum glucose (mg/dl) of rats with induced T2D and normal rats treated for 4 weeks after STZ administration where means that do not share a letter are significantly different. I: non-treated non-diabetic group (normal control), II: non-treated diabetic group (negative control), III: diabetic group treated with EEP, IV: diabetic group treated with CS-PAA nanoparticles, V: diabetic group treated with (EEP) conjugated with (CS-PAA) nanoparticles, VI: diabetic group treated with metformin

The findings of the current study illustrated that the blood glucose levels in T2DM rats were significantly higher than those in normal ones ($P<0.05$). These findings supported those of previous studies which concluded that healthy rats fed on a high-fat diet and later injected with low-dose STZ developed insulin resistance. In addition, hyperglycemia was later induced due to the aforementioned insulin resistance, and not due to a reduced insulin secretion, according to the findings of Li *et al.* [37].

The group of diabetic rats treated with EEP and EEP conjugated CS-PAA nanoparticles showed significantly reduced blood glucose levels from week 1 till the end of the treatment period. These findings were in agreement with the results of El Rabey *et al.* [35] and Kurek-Górecka *et al.* [38], who found that the oral administration of propolis to diabetic rats for 4 weeks expressively reduced glucose levels. The decrease in the blood glucose levels could have been a consequence of some bioactive constituents of propolis that had a protective effect on pancreatic β-cells as suggested in the study of Usman *et al.* [25] or due to increased peripheral utilization of glucose by direct stimulation of glucose uptake and inhibition of glucose transporter activity from the intestine, as proposed by Jadhav and Puchchakayala [39]. Past research suggested that propolis contains bioactive elements such as phenolic acids with hypoglycemic properties, and also indicated that propolis could improve blood glucose levels by promoting insulin secretion *in vivo* in STZ-induced diabetic rats [11].

In addition, treatment of diabetic rats with EEP conjugated CS-PAA nanoparticles for 4 weeks significantly decreased blood glucose levels by nearly three-folds compared with the untreated diabetic rats. This result came in agreement with Rivera-Yañez *et al*. [1]. Consequently, the results displayed that EEP conjugated with CS-PAA nanoparticles could almost regulate the hyperglycemia in the STZ-induced diabetic rats. The glycemic control realized by EEP treatment could have been due to the stimulation of glucose uptake by peripheral tissues, prevention of its release in circulation, or decreased glucose captivation in the gut [40]. Other explanations were presented by Mohammed *et al*. [41] who suggested chitosan nanoparticles could effectively deliver the loaded drugs at specific sites by locally retaining the drug to permit an extended time for drug absorption.

4. Conclusions

In conclusion, findings from the present study suggest that propolis conjugated with CS**-**PAA nanoparticles show a promising potential to control blood glucose in type 2 diabetic rats**.** However, more research is still needed to estimate the long**-**term effects of the proposed nano**-**therapy using propolis as an alternative type**-**2**-**diabetes therapy**.**

5. Acknowledgements

The authors would like to thank the Dean of the Faculty of Science and the Head of Entomology Department, Ain Shams University for giving permission to carry out our experiments in the Faculty of Science, Ain Shams University.

References

[1] Rivera-Yañez, N., Rodriguez-Canales, M., Nieto-Yañez, O., Jimenez-Estrada, M., Ibarra-Barajas, M., Canales-Martinez, M.M. and Rodriguez-Monroy, M.A., 2018. Hypoglycaemic and antioxidant effects of propolis of Chihuahua in a model of experimental diabetes. *Evidence-based Complementary and Alternative Medicine*, 2018, https://doi.org/10.1155/2018/4360356

[2] El-Awady, M.S., El-Agamy, D.S., Suddek, G.M. and Nader, M.A., 2014. Propolis protects against high glucose-induced vascular endothelial dysfunction in isolated rat aorta. *Journal of Physiology and Biochemistry*, 70(1), 247-254.

[3] Al-Hariri, M.T., 2011. Propolis and its direct and indirect hypoglycemic effect. *Journal of Family and Community Medicine*, 18(3), 152-154.

[4] Zhang, J., Cao, X., Ping, S., Wang, K., Shi, J., Zhang, C., Zheng, H. and Hu, F., 2015. Comparisons of ethanol extracts of Chinese propolis (poplar type) and poplar gums based on the antioxidant activities and molecular mechanism. *Evidence-Based Complementary and Alternative Medicine*, 2015, https://doi.org/10.1155/2015/307594

[5] Ali, I., Lone, M.N., Suhail, M., Mukhtar, S.D. and Asnin, L., 2016. Advances in nanocarriers for anticancer drugs delivery. *Current Medicinal Chemistry*, 23(20), 2159-2187.

[6] Rizvi, S.A.A. and Saleh, A.M., 2018. Applications of nanoparticle systems in drug delivery technology. *Saudi Pharmaceutical Journal*, 26(1), 64-70.

[7] Pulgaron, E.R. and Delamater, A.M., 2014. Obesity and type 2 diabetes in children: Epidemiology and treatment. *Current Diabetes Reports*, 14(8), 508, https://doi.org/10.1007/s11892-014-0508-y

[8] U.S. Food and Drug Administration, 2019. *Statement of Janet Woodcock, MD, Director of FDA's Center for Drug Evaluation and Research, on Impurities found in Diabetes Drugs Outside the U.S. States*. Available at: https://www.fda.gov/news-events/press-announcements/statement-janet-woodcock-md-director-fdas-center-drug-evaluation-and-research-impurities-found

[9] Souza, E.A., Zaluski, R., Veiga, N. and Orsi, R.O., 2016. Effects of seasonal variations and collection methods on the mineral composition of propolis from *Apis mellifera* Linnaeus Beehives. *Brazilian Journal of Biology*, 76(2), 396-401.

[10] Cunha, I.B.S., Sawaya, A.C.H.F., Caetano, F.M., Shimizu, M.T., Marcucci, M.C., Drezza, F.T., Povia, G.S. and Carvalho, P. de O., 2004. Factors that influence the yield and composition of Brazilian propolis extracts. *Journal of the Brazilian Chemical Society*, 15(6), 964-970.

[11] Usman, U.Z., Bakar, A.B.A. and Mohamed, M., 2016. Phytochemical composition and activity against hyperglycaemia of Malaysian propolis in diabetic rats. *Biomedical Research (India)*, 27(1), 46-51.

[12] Braun, D., Cherdron, H., Rehahn, M., Ritter, H. and Voit, B., 2013. *Polymer Synthesis: Theory and Practice.* Berlin: Springer-Verlag.

[13] Abou El Fadl, F.I., 2016. Synthesis and characterization of chitosan-poly(acrylamide-co-acrylic acid) magnetic nanocomposite hydrogels for use in catalysis. *Russian Journal of Applied Chemistry*, 89(10), 1673-1680.

[14] Ray, D., Mohanta, G.P., Manavalan, R. and Sahoo, P.K., 2009. Synthesis and characterization of acrylic based copolymeric hydrogel nanoparticles: An approach to drug delivery. *International Journal of ChemTech Research*, 1(3), 627-633.

[15] Wang, X., Chen, C., Huo, D., Qian, H., Ding, Y., Hu, Y. and Jiang, X., 2012. Synthesis of β-cyclodextrin modified chitosan-poly(acrylic acid) nanoparticles and use as drug carriers. *Carbohydrate Polymers*, 90(1), 361-369.

[16] Kao, H.J., Lo, Y.L., Lin, H.R. and Yu, S.P., 2006. Characterization of pilocarpine-loaded

chitosan/Carbopol nanoparticles. *Journal of Pharmacy and Pharmacology*, 58(2), 179-186.
[17] Andrade, Â.L., Manzi, D. and Domingues, R.Z., 2006. Tetracycline and propolis incorporation and release by bioactive glassy compounds. *Journal of Non-Crystalline Solids*, 352(32-35), 3502-3507.
[18] Zhu, A., Luo, X. and Dai, S., 2009. Chitosan-poly(acrylic acid) complex modified paramagnetic Fe_3O_4 nanoparticles for camptothecin loading and release. *Journal of Materials Research*, 24(7), 2307-2315.
[19] Vatandoust, N., Rami, F., Salehi, A.R., Khosravi, S., Dashti, G., Eslami, G., Momenzaden, S. and Salehi, R., 2018. Novel high-fat diet formulation and streptozotocin treatment for induction of prediabetes and type 2 diabetes in rats. *Advanced Biomedical Research*, 7(1), 107, https://doi.org/10.4103/abr.abr_8_17
[20] Dranse, H.J., Waise, T.M.Z., Hamr, S.C., Bauer, P.V., Abraham, M.A., Rasmussen, B.A. and Lam, T.T., 2018. Physiological and therapeutic regulation of glucose homeostasis by upper small intestinal PepT1-mediated protein sensing. *Nature Communications*, 9, 1118, https://doi.org/10.1038/s41467-018-03490-8
[21] Zhang, F., Ye, C., Li, G., Ding, W., Zhou, W., Zhu, H., Chen. G., Luo, T., Guang, M. Liu, Y., Zhang, D., Zheng, S., Yang, J., Gu, Y., Xie, X. and Luo, M., 2003. The rat model of type 2 diabetic mellitus and its glycometabolism characters. *Experimental Animals*, 52(5), 401-407.
[22] Sendrayaperumal, V., Pillai, S.I. and Subramanian, S., 2014. Design, synthesis and characterization of zinc-morin, a metal flavonol complex and evaluation of its antidiabetic potential in HFD-STZ induced type 2 diabetes in rats. *Chemico-Biological Interactions*, 219, 9-17.
[23] Motyl, K. and McCabe, L.R., 2009. Streptozotocin, Type I diabetes severity and bone. *Biological Procedures Online*, 11, 296-315.
[24] Al-Hariri, M., Eldin, T. and Al-Harb, M., 2016. Protective effect and potential mechanisms of propolis on streptozotocin-induced diabetic rats. *Journal of Taibah University Medical Sciences*, 11(1), 7-12.
[25] Usman, U.Z., Bakar, A.B.A. and Mohamed, M., 2018. Propolis improves pregnancy outcomes and placental oxidative stress status in streptozotocin-induced diabetic rats. *BMC Complementary and Alternative Medicine*, 18(1), 324, https://doi.org.//10.1186/s12906-018-2391-6
[26] Huang, S., Zhang, C.-P., Wang, K., Li, G. and Hu, F.-L., 2014. Recent advances in the chemical composition of propolis. *Molecules*, 19(12), 19610-19632.
[27] Huang, X.-Y, Guo, X.-L, Luo, H.-L, Fang, X.-W, Zhu, T.-G, Zhang, X.-L., Chen, H.W. and Luo, L.-P., 2015. Fast differential analysis of propolis using surface desorption atmospheric pressure chemical ionization mass spectrometry. *International Journal of Analytical Chemistry*, 2015, https://doi.org/10.1155/2015/176475
[28] Cevher, E., Salomon, S.K., Makrakis, A., Li, X.W., Brocchini, S. and Alpar, H.O., 2015. Development of chitosan-pullulan composite nanoparticles for nasal delivery of vaccines: Optimisation and cellular studies. *Journal of Microencapsulation*, 32(8), 755-768.
[29] Seven, P.T., Seven, I., Baykalir, B.G., Mutlu, S.I. and Salem, A.Z.M., 2018. Nanotechnology and nano-propolis in animal production and health: an overview. *Italian Journal of Animal Science*, 17(4), 921-930.
[30] Omidirad, R., Rajabi, F.H. and Farahani, B.V., 2013. Preparation and in vitro drug delivery response of doxorubicin loaded PAA coated magnetite nanoparticles. *Journal of the Serbian Chemical Society*, 78(10), 1609-1616.
[31] Guo, L., Liu, G., Hong, R.Y. and Li, H.Z., 2010. Preparation and characterization of chitosan poly(acrylic acid) magnetic microspheres. *Marine Drugs*, 8(7), 2212-2222.
[32] Dounighi, N.M., Eskandari, R., Avadi, M.R., Zolfagharian, H., Sadeghi, A.M.M. and Rezayat, M., 2012. Preparation and in vitro characterization of chitosan nanoparticles containing

Mesobuthus eupeus scorpion venom as an antigen delivery system. *The Journal of Venomous Animals and Toxins including Tropical Diseases*, 18(1), 44-52.

[33] Hussein, U., Hassan, N.Y., Elhalwagy, M.E.A., Zaki, A.R., Abubakr, H.O., Venkata, K.C.N., Jang, K.Y. and Bishayee, A., 2017. Ginger and propolis exert neuroprotective effects against monosodium glutamate-induced neurotoxicity in rats. *Molecules*, 22(11), 1928, https://doi.org/10.3390/molecules 22111928

[34] Peres, R.S., Zmozinski, A.V., Brust, F.R., Macedo, A.J., Armelin, E., Alemán, C. and Ferreira, C.A., 2018. Multifunctional coatings based on silicone matrix and propolis extract. *Progress in Organic Coatings*, 123, 223-231.

[35] El Rabey, H.A., Al-Seeni, M.N. and Bakhashwain, A.S., 2017. The antidiabetic activity of *Nigella sativa* and propolis on streptozotocin-induced diabetes and diabetic nephropathy in male rats. *Evidence-Based Complementary and Alternative Medicine*, 2017, https://doi.org/ 10.1155/2017/5439645

[36] Holmes, A., Coppey, L.J., Davidson, E.P. and Yorek, M.A., 2015. Rat models of diet-induced obesity and high fat/low dose streptozotocin type 2 diabetes: Effect of reversal of high fat diet compared to treatment with Enalapril or Menhaden oil on glucose utilization and neuropathic endpoints. *Journal of Diabetes Research*, 2015, https://doi.org/10.1155/2015/307285

[37] Li, Y., Chen, M., Xuan, H. and Hu, F., 2012. Effects of encapsulated propolis on blood glycemic control, lipid metabolism, and insulin resistance in type 2 diabetes mellitus rats. *Evidence-Based Complementary and Alternative Medicine*, 2012, https://doi.org/10.1155/ 2012/981896

[38] Kurek-Górecka, A., Rzepecka-Stojko, A., Górecki, M., Stojko, J., Sosada, M. and Świerczek-Zięba, G., 2013. Structure and antioxidant activity of polyphenols derived from propolis. *Molecules*, 19(1), 78-101.

[39] Jadhav, R. and Puchchakayala, G., 2012. Hypoglycemic and antidiabetic activity of flavonoids: Boswellic acid, Ellagic acid, Quercetin, Rutin on streptozotocin-nicotinamide induced type 2 diabetic rats. *International Journal of Pharmacy and Pharmaceutical Sciences*, 4(2), 251-256.

[40] Al-Hariri, M., Eldin, T.G., Abu-Hozaifa, B. and Elnour, A., 2011. Glycemic control and anti-osteopathic effect of propolis in diabetic rats. *Diabetes, Metabolic Syndrome and Obesity: Targets and Therapy*, 4, 377-384.

[41] Mohammed, M.A,, Syeda, J.T.M., Wasan, K.M. and Wasan, E.K., 2017. An overview of chitosan nanoparticles and its application in non-parenteral drug delivery. *Pharmaceutics*, 9(4), 53, https//doi.org//10.3390/pharmaceutics9040053

Deterministic and Stochastic Models of the Spread of Streptococcal Disease and Its Sequel

Nichaphat Patanarapeelert[1], Natsuda Yokchoo[1] and Klot Patanarapeelert[2]*

[1]Department of Mathematics, Faculty of Applied Science, King Mongkut's University of Technology North Bangkok, Bangkok, Thailand
[2]Department of Mathematics, Faculty of Science, Silpakorn University, Nakhon Pathom Province, Thailand

Received: 13 April 2020, Revised: 10 July 2020, Accepted: 17 August 2020

Abstract

The beta-hemolytic group A *Streptococcus* (GAS) is responsible for its sequel, acute rheumatic fever (ARF), which may lead to the more serious condition on other heart diseases. To gain a better understanding of the transmission in a population, we formulated epidemic models using a standard compartmental model and a continuous-time Markov chain. The models allow for the contribution of disease carrier and the effect of treatment. The equilibrium points and stability are analyzed in relation to the basic reproduction number based on the deterministic model. For the stochastic model, numerical simulation of sample paths is performed. The results indicate that the dynamic behavior for the two approaches depends on the epidemic threshold. Under stable endemic condition, most sample paths fluctuate around its mean and deterministic curve. On the other hand, when the basic reproduction number is less than one, the stochastic system undergoes a minor outbreak, while the deterministic curve approaches zero. The results are expected to be the first step of a deeper analysis of stochastic treatment linked to its deterministic counterpart.

Keywords: group A *Streptococcus*; acute rheumatic fever; deterministic model; stochastic model; carriers
DOI 10.14456/cast.2021.12

1. Introduction

The beta-hemolytic group A *Streptococcus* (GAS) bacteria [1] is the main cause of infections of the throat and skin such as pharyngitis, tonsillitis, sinusitis, impetigo, rheumatic fever, and meningitis. These can occur in any gender and at any age. The most common of GAS occurs in children ages 5-15 [2-8]. GAS are carried in the throat or on the skin of individuals where the individuals may have no symptoms of illness [9-11] and infections can be spread from person to person by direct contact or inhalation of the secretions in the nasopharynx such as mucus and saliva [8]. Treatment of a GAS with an antibiotic such as penicillin can reduce the risk of ARF by about 90%. In about 10% of cases, GAS still remain in the throat even though the individual has had a full course of treatment [12]. Treatment failures of GAS may arise from the ineffectiveness of antibiotic therapy

*Corresponding author: Tel.: (+66) 94 264 8255
E-mail: klotpat@gmail.com

or an incomplete course of the prescribed antibiotic. The patients who failed from these treatments may be asymptomatic or classified as carriers, which can be a significant impact on the GAS epidemic, since they do not take any special precautions to prevent transmission [1, 13-15].

Untreated GAS pharyngitis or treatment failures may develop into acute rheumatic fever (ARF), which is a non-communicable disease caused by disorders of an autoimmune [16]. ARF is most common in 5-15 years old [4]. The symptoms of ARF are swelling, skin inflammation, blisters or bulges underneath the skin, heart tissue damage, and inflammation of the brain, which causes a movement disorder called Chorea. About 0.3%-3.0% of people will develop ARF following a GAS infection. In addition, patients who have had previous attacks of ARF have a recurrence of ARF following a GAS infection in 30%-80% of cases [12]. There are about 5 million individuals worldwide with rheumatic heart disease and there are about 282,000 new cases per year and 233,000 deaths from this disease each year due to lack of proper infection prevention of GAS [16-18].

Mathematical models have been used widely as a tool to study the propagation of diseases [1, 12]. In addition to deterministic formulation, stochastic model can be used to treat the realistic contact pattern given by unpredictable individual behaviors. In this research, we study the dynamics of infectious and asymptomatic GAS infections that affect the dynamics of ARF. Deterministic and associated stochastic models are constructed to compare the system behaviors. An analytic framework is based on the deterministic analysis while a numerical simulation is the main approach used to solve the stochastic model.

2. Materials and Methods

2.1 Basic assumptions and the deterministic model

We employ the standard compartmental SIS model for the models of GAS and ARF [19]. The model is formulated under the assumption that individuals infected with GAS can be treated by using an antibiotic such as penicillin or amoxicillin [5]. In addition to the possible failure of antibiotic treatment with several reasons [18, 20-23], we assume that even if a full course of the antibiotic is taken, a small fraction of GAS may remain in the throat. Therefore, asymptomatic carriers will be defined as errors of treatment which is different from the previous study [24]. By the term 'error of treatment', we mean that some treated patients may have not complied with the treatment steps or may not have completed the full course of drug administration and dosage.

Suppose that the total population, N is constant. We denote S as the number of susceptible individuals, I as the number of symptomatic GAS individuals, C as the number of asymptomatic GAS individuals or carriers and, A as the number of individuals that develop ARF. Figure 1 shows the flow diagram of GAS infection and ARF development. Since both I and C individuals have positive throat cultures for GAS [23, 25], new ARF patients may develop from these two groups [26]. The differential equations describing the transition rates are given by

$$\frac{dS}{dt} = \Lambda - (\beta_1 I + \beta_2 C)S + \gamma_2 A + \theta\gamma_1 I - \mu S \tag{1}$$

$$\frac{dI}{dt} = (\beta_1 I + \beta_2 C)S + \text{ò}C - (\gamma_1 + \delta_1 + \mu)I \tag{2}$$

$$\frac{dC}{dt} = (1-\theta)\gamma_1 I - (\text{ò} + \delta_2 + \mu)C \tag{3}$$

$$\frac{dA}{dt} = \delta_1 I + \delta_2 C - (\gamma_2 + \mu)A \tag{4}$$

where the definitions of the parameter values used in the above model and their corresponding values are given in Table 1. Since carriers are thought to have a lower density of GAS in their pharynx, compared to those with an acute infection [25-28], and GAS carriers are at little risk for developing acute rheumatic fever [26], we presume that $\beta_2 < \beta_1$ and $\delta_2 < \delta_1$. We note that given the nonnegative initial conditions, the solutions are nonnegative for all time, and if the initial condition is positive, then the set

$$\Omega = \left\{ \left(S(t), I(t), C(t), A(t) \right) \in \text{¡}^4_+ : 0 \le S, I, C, A \le \Lambda / \mu \right\}$$

is a positively invariant.

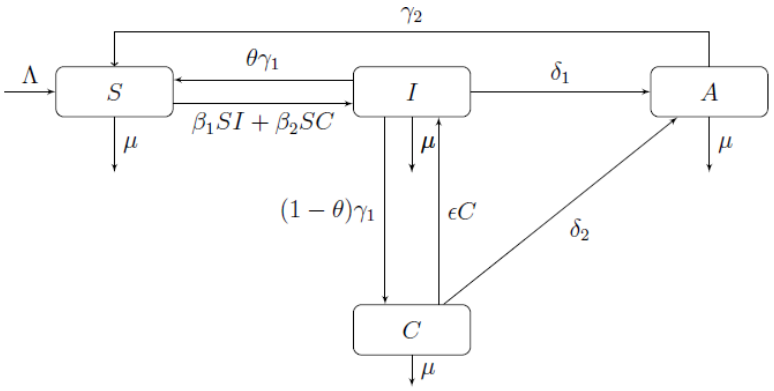

Figure 1. Flowchart describing the transition between compartments

Table 1. Symbols and definition of the parameters

Parameters	Description
Λ	recruitment rate of susceptible class
γ_1	rate at which the infectious individual gets antibiotic treatment
θ	proportion of effectiveness of antibiotic treatment
γ_2	per capita recovery rate of ARF individual
β_1	rate at which a symptomatic GAS individual can infect a susceptible
β_2	rate at which a GAS carrier can infect a susceptible
μ	per capita natural death rate of all compartment
Ò	rate at which a carrier becomes symptomatic GAS individual
δ_1	rate at which a symptomatic GAS individual develops ARF
δ_2	rate at which a carrier develops ARF

2.2 Stochastic model

A continuous time Markov chain (CTMC) associated with the deterministic counterpart is presented. As opposed to the deterministic model, the stochastic model better explains the uncertainty and variability in a real epidemic due to the complex pattern of human contact, which is unpredictable [29-31]. In this study, however, the aim is to demonstrate the random nature via the simulated trajectories which can be compared with the numerical solution of the deterministic model, while we left the stochastic analysis as the future extension.

The multivariate random process is assumed to obey the Markov property where the meaning is the same as in the deterministic model. Hence, we denote $S(t), I(t), C(t)$ and $A(t)$ as the stochastic processes that have a common state space $\{1,2,3,...,N\}$ where $t \in [0,\infty)$. We note that the values of discrete random variables are denoted by the lower case. The transition probabilities related with a small period of time $\Delta t > 0$ is given by

$$P\Big(\big(S(t+\Delta t), I(t+\Delta t), C(t+\Delta t), A(t+\Delta t)\big) = (s+j, i+k, c+m, a+n) \,|\, \big(S(t), I(t), C(t), A(t)\big) = (s,i,c,a)\Big). \tag{5}$$

The transition probability is time-homogeneous and satisfies the Markov property. Summarized in Table 2 are the changes, $\Delta S, \Delta I, \Delta C$ and ΔA associated with thirteen events. Given $I(0) = i > 0$ and $C(0) = c > 0$, the state (s,i,c,a), where $I = 0$ and $C = 0$ refer to absorbing states; the epidemic ends at time t when an absorbing state is reached.

Table 2. Model assumptions

Event	Change ($\Delta S, \Delta I, \Delta C, \Delta C$)	Probability
Infection to I	$(-1,1,0,0)$	$s(\beta_1 i + \beta_2 c)\Delta t + o(\Delta t)$
Death of S	$(-1,0,0,0)$	$\mu s \Delta t + o(\Delta t)$
Recruitment	$(1,0,0,0)$	$\Lambda \Delta t + o(\Delta t)$
Recover from A to S	$(1,0,0,-1)$	$\gamma_2 a \Delta t + o(\Delta t)$
Recover from I to S	$(1,-1,0,0)$	$\theta \gamma_1 i \Delta t + o(\Delta t)$
Recover from I to C	$(0,-1,1,0)$	$(1-\theta)\gamma_1 i \Delta t + o(\Delta t)$
Recover from I to A	$(0,-1,0,1)$	$\delta_1 i \Delta t + o(\Delta t)$
Death of I	$(0,-1,0,0)$	$\mu i \Delta t + o(\Delta t)$
Moving from C to I	$(0,1,-1,0)$	$\grave{\alpha} c \Delta t + o(\Delta t)$
Develop from C to A	$(0,0,-1,1)$	$\delta_2 c \Delta t + o(\Delta t)$
Death of C	$(0,0,-1,0)$	$\mu c \Delta t + o(\Delta t)$
Death of A	$(0,0,0,-1)$	$\mu a \Delta t + o(\Delta t)$

For any event other than in Table 2, we let $(\Delta S, \Delta I, \Delta C, \Delta A) = (0,0,0,0)$.

2.3 Simulation and the basic reproduction number

Here, we implement numerical simulation for stochastic realization (sample path) of the process. Gillespie [29] developed a numerical method for the simulation of CTMC models, which is known as the Gillespie algorithm or the stochastic simulation algorithm. The Markov property implies that

inter-event time is exponentially distributed, where a parameter λ is the sum of the rates for all possible events:

$$\lambda = \Lambda + s\left(\beta_1 i + \beta_2 c\right) + \gamma_2 a + \theta\lambda_1 i + \left(1-\theta\right)\gamma_1 i + \delta_1 i + \grave{o}c + \delta_2 c + \mu\left(s + i + c + a\right), \tag{6}$$

where (s, i, c, a) is specific for the state of (S , I , C , A) at a given time t. From the inverse method, we obtain the value of the inter-event time τ by

$$\tau = -\frac{\ln u_1}{\lambda} \tag{7}$$

where u_1 is a uniform random generator. To determine which event will occur, we construct a probability distribution of twelve events, i.e., $p_i, i = 1, 2, \text{K}\ 12$, and hence apply the inverse method by generating a second uniform random value, u_2 such that if u_2 lies in k-th subinterval among [0, p_1], ($p_1, p_1 + p_2$] ,…, ($p_1 + p_2 + ... + p_{11}, 1$], then the k-th event occurs.

Since $A = N - S - I - C$, we denote the disease-free equilibrium of the model as

$$E_0 = (S_0, I_0, C_0) = (\Lambda / \mu, 0, 0) .$$

We then derive the basic reproduction number, R_0 by using the next generation method [32]. Therefore, we obtain

$$R_0 = \frac{\Lambda}{\mu}\left\{\frac{\beta_1(\grave{o} + \delta_2 + \mu) + \beta_2(1-\theta)\gamma_1}{\gamma_1(\delta_2 + \mu + \grave{o}\theta) + (\delta_1 + \mu)(\grave{o} + \delta_2 + \mu)}\right\}. \tag{8}$$

3. Results and Discussion

3.1 Stability analysis

Let us begin with the existence and uniqueness of the endemic equilibrium $E^* = (S^*, I^*, C^*)$. By solving the system of algebraic equations, and rewriting in terms of R_0 , we have

$$S^* = \frac{\Lambda}{\mu R_0}, \tag{9}$$

$$I^* = \frac{\Lambda}{\mu}\left(1 - \frac{1}{R_0}\right)(\grave{o} + \delta_2 + \mu)\eta, \tag{10}$$

and

$$C^* = \frac{\Lambda}{\mu}\left(1 - \frac{1}{R_0}\right)(1-\theta)\gamma_1\eta \tag{11}$$

where

$$\eta = \frac{(\grave{o} + \delta_2 + \mu)}{(\gamma_2 + \delta_1 + \mu)(\grave{o} + \delta_2 + \mu) + \gamma_1(1-\theta)(\gamma_2 + \delta_2 + \mu)}.$$

Since the endemic equilibrium is biological meaningful when all variables are positive, from above expression, E^* can be uniquely determined when $R_0 > 1$.

The stability of E_0 can be determined by calculating the Jacobian matrix

$$J(E_0)=\begin{pmatrix} -(\gamma_2+\mu) & \theta\gamma_1-\gamma_2-\dfrac{\beta_1\Lambda}{\mu} & -\left(\dfrac{\beta_2\Lambda}{\mu}+\gamma_2\right) \\ 0 & \dfrac{\beta_1\Lambda}{\mu}-(\gamma_1+\delta_1+\mu) & \dfrac{\beta_2\Lambda}{\mu}+\grave{o} \\ 0 & (1-\theta)\gamma_1 & -(\grave{o}+\delta_2+\mu) \end{pmatrix}. \tag{12}$$

The characteristic equation is given by

$$(\lambda+\gamma_2+\mu)\left(\lambda^2+c_1\lambda+c_2\right)=0 \tag{13}$$

where

$$c_1=2\mu+\grave{o}+\delta_1+\delta_2+\gamma_1-\frac{\beta_1\Lambda}{\mu}, \tag{14}$$

$$c_2=-(\grave{o}+\delta_2+\mu)\left(\frac{\beta_1\Lambda}{\mu}-\gamma_1-\delta_1-\mu\right)-\gamma_1(1-\theta)\left(\frac{\beta_2\Lambda}{\mu}+\grave{o}\right). \tag{15}$$

Due to the presence of trivial eigenvalue, the problem is reduced to the second order equation. Suppose that $R_0<1$, from equation (15), we find $c_2>0$. Hence, it follows that $c_1>0$. Therefore, we find that the disease-free equilibrium E_0 is locally asymptotically stable if $R_0<1$.

Next, we will derive the conditions for which the endemic is stable. Let us suppose that $R_0>1$, and define

$$R_0^{(1)}=\frac{1}{(\grave{o}+\delta_2+\mu)\eta}, \qquad R_0^{(2)}=\frac{1}{(1-\theta)\gamma_1\eta}.$$

We calculate a Jacobian matrix at $E^*=(S^*,I^*,C^*)$,

$$J=\begin{pmatrix} -\beta_1I^*-\beta_2C^*-\gamma_2-\mu & -\beta_1S^*-\gamma_2+\theta\gamma_1 & -\beta_2S^*-\gamma_2 \\ \beta_1I^*+\beta_2C^* & \beta_1S^*-(\gamma_1+\delta_1+\mu) & \beta_2S^*+\grave{o} \\ 0 & (1-\theta)\gamma_1 & -(\grave{o}+\delta_2+\mu) \end{pmatrix},$$

and hence obtain the characteristic equation

$$\lambda^3+a_1\lambda^2+a_2\lambda+a_3=0 \tag{16}$$

where

$$a_1=\beta_1(I^*-S^*)+\beta_2C^*+\gamma_2+\mu+\gamma_1+\delta_1+\mu+\grave{o}+\delta_2+\mu,$$

$$a_2=\beta_1I^*\left(\delta_1+(1-\theta)\gamma_1\right)+\beta_1\left(I^*-S^*\right)\left(2\mu+\gamma_2+\grave{o}+\delta_2\right)+\beta_2C^*\left(\delta_1+\mu+\gamma_2\right)+\left(\gamma_2+\mu\right)\left(\gamma_1+\delta_1+\mu\right)$$
$$+\left(\beta_2C^*+\gamma_2+2\mu+\delta_1\right)\left(\grave{o}+\delta_2+\mu\right)+\gamma_1\left(\delta_2+\mu+\grave{o}\theta\right)+(1-\theta)\gamma_1\beta_2\left(C^*-S^*\right),$$

$$a_3=\beta_1I^*(1-\theta)\gamma_1\left(\delta_2+\mu\right)+\beta_2C^*(1-\theta)\gamma_1\delta_2+\beta_2\left(C^*-S^*\right)(1-\theta)\gamma_1+\left(\beta_1I^*+\beta_2C^*\right)\delta_1\left(\grave{o}+\delta_2+\mu\right)$$
$$+\left(\beta_1\left(I^*-S^*\right)+\beta_2C\right)\left(\grave{o}+\delta_2+\mu\right)\left(\mu+\gamma_2\right)+\left(\mu+\gamma_2\right)\left(\gamma_1\left(\delta_2+\mu\right)+\left(\delta_1+\mu\right)\left(\grave{o}+\delta_2+\mu\right)\right)$$
$$+\gamma_2(1-\theta)\gamma_1\left(\beta_1I^*+\beta_2\left(C^*-S^*\right)+\grave{o}\theta\gamma_1\left(\mu+\gamma_2\right)\right).$$

According to Routh-Hurwitz criteria [33], the necessary condition for the real parts of all eigenvalues are negative is that the coefficients of the characteristic equation (16) must be positive.

Observe that if $R_0 > R_0^{(1)}$, then $I^* - S^* > 0$ leads to $a_1 > 0$, and hence $C^* - S^* > 0$ which leads to $a_3 > 0$. Thus, it is immediate that if $R_0 > R_0^{(1)}$, and $R_0 > R_0^{(2)}$ then $a_2 > 0$. Finally, after some tedious work, it can be verified that if such two conditions hold, then we find $a_1 a_2 - a_3 > 0$. The last condition fulfills the necessary and sufficient conditions in Routh-Hurwitz criterion.

In summary, we have that the endemic equilibrium is asymptotically stable if

$$R_0 > 1 + \max\left\{R_0^{(1)}, R_0^{(2)}\right\}.$$

In order to assure the stability of the endemic state, the value of the basic reproduction number must satisfy the above condition. The additional parameters, such as $R_0^{(1)}$ and $R_0^{(2)}$, merely provide the sufficient conditions for this to happen. Further analysis, such that the above condition does not hold while $R_0 > 1$, requires a deeper investigation into the parameter relationship which is beyond the scope of this study.

3.2 Numerical results

To support our theoretical results, we present numerical results where the total population is assumed as $N = 1000$ and other parameter values, including the references are provided in Table 3. In this section, the numerical solutions of deterministic models will be compared with the sample paths of the stochastic model.

From the range of parameter values, we first choose $\beta_1 = 0.00089$, $\beta_2 = 0.000001$, $\grave{o} = 0.0027$ and $\gamma_1 = 0.8$. From the analytic results, it follows that $E_0 = (1,000, 0, 0)$ and $R_0 = 0.8926$. Thus, these parameter values combined with the rest in Table 3, form a set of parameters at which the disease will eventually die out. Figure 2 (a) illustrates the time-dependent solutions of the deterministic model confirming the accordance with theoretical prediction.

Table 3: The values of the parameters

Parameters	Values	Units	Reference
γ_1	0.1−1	day^{-1}	[12]
θ	0.9	-	[12]
γ_2	0.8 0.8	day^{-1}	[12]
μ	0.00004	day^{-1}	[1]
$\grave{o}$	0.0027 − 0.0110	day^{-1}	[1]
δ_1	0.2	day^{-1}	[12]
δ_2	0.1	day^{-1}	Estimated
Λ	0.04	$\text{person}\cdot\text{day}^{-1}$	[1]
β_1	0.00089 − 0.0099	$\text{person}^{-1}\cdot\text{day}^{-1}$	[1]
β_2	0.000001 − 0.0005	$\text{person}^{-1}\cdot\text{day}^{-1}$	[1]

The graph of the solutions shown in Figure 2 (b) illustrates the dynamic behavior of deterministic model when we choose $\beta_1 = 0.00356, \beta_2 = 0.000004$, and The difference from the previous case is that we increase the contact rates from both infected groups and reduce the treatment rate. Based on these parameter values, we find that $E^* = (252.1, 370.9, 252.7, 124.3)$ $R_0^{(1)} = 2.0162$,

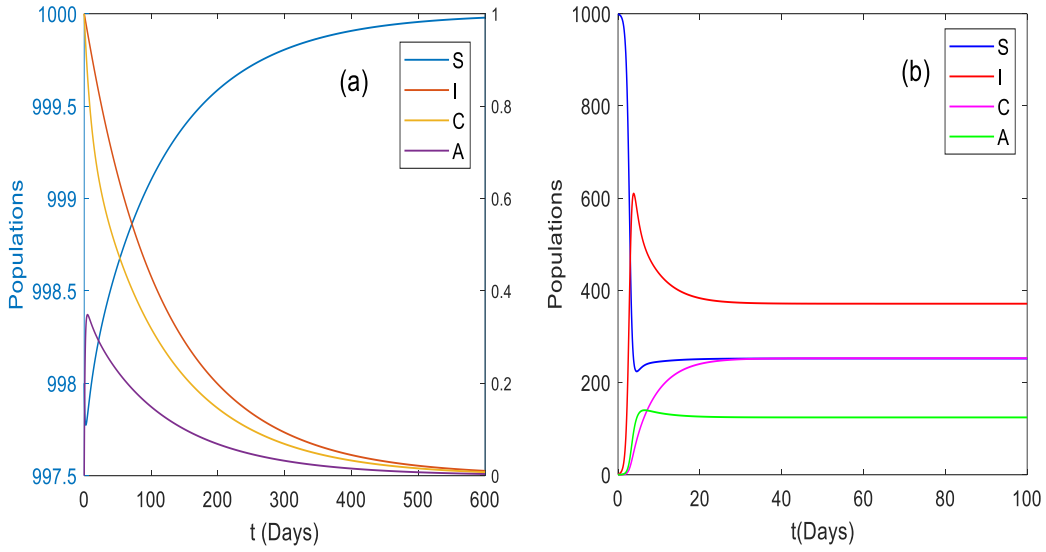

Figure 2. The solution curves of deterministic model with initial conditions $S(0)=999$ and $I(0)=1$. (a) Disease-free equilibrium E_0 is asymptotically stable when $R_0<1$ and (b) endemic equilibrium E^* is asymptotically stable when $R_0>1+\max(R_0^{(1)},R_0^{(2)})$.

$R_0^{(2)}=2.5903$ and $R_0=3.9666$, respectively. To consider the long-term epidemic pattern, we see that, on average, there will be about 37% who have symptomatic infections, and about 12.43% are expected to develop the ARF condition in the future. We note that rate of increase of the force of infection by the contact rates from each infectious group is the same at 300%, while the treatment rate is reduced by only 12.5%.

Let us now focus on the sample paths of the stochastic model. As in the deterministic case, the graph will be plotted in the case $R_0<1$ and $R_0>1+\max(R_0^{(1)},R_0^{(2)})$ using the same parameter values and initial conditions. In the absence of the theoretical conjecture, it can be argued that, for $R_0<1$, a minor outbreak may exist with a positive probability [24]. This implies that under the small number of infectious individuals, there is a fraction of realizations that indicates the presence of successful transmission of a small magnitude and a finite time interval, while the remaining paths are instantly extinct in the successive step by chance. This is referred to as the minor epidemic. In our case, the minor outbreak is observed in Figure 3 (a).

In contrast to the minor outbreak, the system may possess the major outbreak or endemic persistence. The fifty sample paths are plotted in Figure 3 (b), demonstrating a random fluctuating pattern around its mean. In this case (but not always), the paths also fluctuate around the solution of deterministic model. It is possible that the more samples, the more deviation is observed. However, most of the paths fluctuate around the endemic level under the degree of variability.

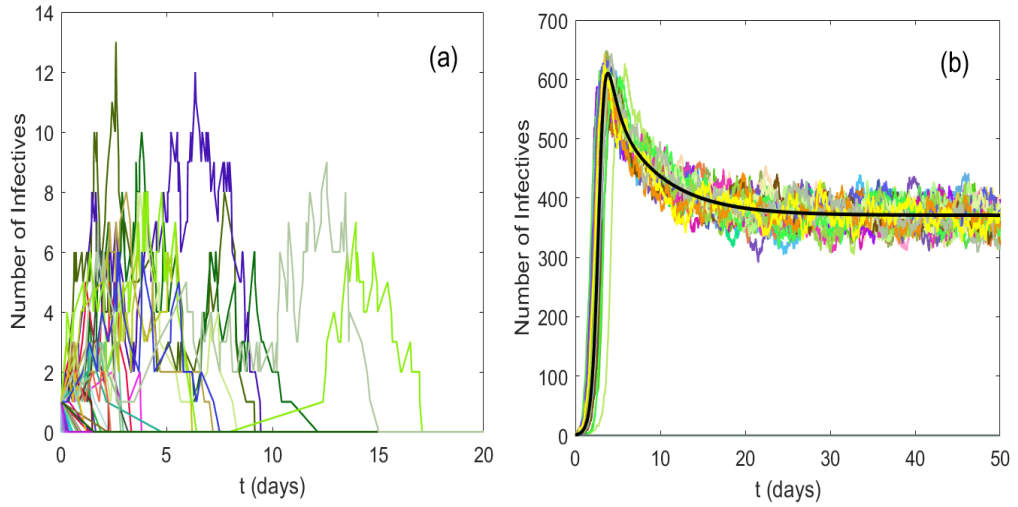

Figure 3. Simulations of ample paths. (a) The fifty sample paths when $R_0 < 1$. (b) The dashed curve is the ODE solution (black solid line) and the other curves are fifty sample paths when $R_0 = 3.9666$.

4. Conclusions

In the deterministic model, we found two equilibrium points. The disease-free equilibrium is locally asymptotically stable when the basic reproduction number less than one. The endemic equilibrium is locally asymptotically stable when the basic reproduction number is greater than one plus the maximum of two additional parameters. Due to the complexity of parameter relations, these two parameters are difficult to interpret in terms of biological meaning. In fact, further analysis to establish the stronger stability condition is required.

Qualitative comparison between deterministic and stochastic dynamics can be made via numerical simulations. Although the trend of stochastic realizations behaves in the similar fashion with the deterministic solutions subject to the stable condition of endemic state, when the basic reproduction number is less than one, their behaviors are quite different. This is because of the stochastic nature of individuals. The further extension should be determination of the probability of extinction and the probability of the outbreak, analysis of the stochastic fade out, and quantification of variance.

From sensitivity analysis, the most effective parameter relevant to the outbreaks of disease is the rate at which an infected individual can infect a susceptible one. From sensitivity index, we note that the parameter that can be practically controlled to directly reduce the outbreak of disease is β_1 . While these analyses can be easily done for the deterministic model, the role of parameter variation can alter the stochastic behaviors if they are quantified. We conclude that the cooperation between the two approaches may be mutually supportive and produce insight into the disease dynamics, knowledge that can facilitate disease management and control.

5. Acknowledgements

This work is supported by Grant No. 6242102, Faculty of Applied Science, King Mongkut's University of Technology North Bangkok.

References

[1] Doura, K., Melendez-Morales, J.D, Meyer, G.G. and Perez, L.E.,1999. *An SIS Model of Streptococcal Disease with a Class of Beta-Hemolytic Carriers*. Biometrics Unit Technical Reports, Number BU-1524-M.

[2] Armstrong, C., 2010. AHA guidelines on prevention of rheumatic fever and diagnosis and treatment of acute streptococcal pharyngitis. *American Family Physician*, 81(3), 346-359.

[3] Fauci, A.S., Braunwald, E., Kasper, D.L., Hauser, S.L., Longo, D.L., Jameson, J.L. and Loscalzo, J., 2008. *Harrison's Principles of Internal Medicine*. *Vol II*. 17th ed. New York: McGrow-Hill.

[4] Mayo Clinic, 2017. *Rheumatic Fever*. [online] Available at: https://www.mayoclinic.org/diseases-conditions/rheumatic-fever/symptoms-causes/syc-20354588

[5] Choby, C., 2009. Diagnosis and treatment of streptococcal pharyngitis. *American Family Physician*, 79(5), 383-390.

[6] National Heart Foundation of New Zealand, 2019. *Group A Streptococcal Sore Throat Management Guideline*. Auckland: National Heart Foundation of New Zealand.

[7] Wessels, M.R., 2011. Streptococcal pharyngitis. *The New England Journal of Medicine*, 364 (7), 648-655.

[8] Chauhan, S., Kashyap, N., Kanga, A., Thakur, K., Sood, A. and Chandel, L., 2016. Genetic diversity among group a streptococcus isolated from throats of healthy and symptomatic children. *Journal of tropical pediatrics*, 62(2), 152–157.

[9] Weber, R., 2014. Pharyngitis. *Primary Care: Clinics in Office Practice*, 41(1), 91-98.

[10] Department of Health, 2011. Streptococcal Infections (Invasive Group A Strep, GAS). [online] Available at: https://www.health.ny.gov/diseases/communicable/streptococcal/group_a/ fact_ sheet.htm

[11] Martin, J.M., Green, M., Barbadora, K.A. and Wald, E.R., 2004. Group A streptococci among school-aged children: clinical characteristics and the carrier state. *Pediatrics*, 114(5), 1212–1219.

[12] McGuinness, M., Sibanda, N. and Welsh, M., 2015. Modeling acute rheumatic fever. *Mathematical Population Studies*, 22(4), 187-208.

[13] Barreto, M. L., Teixeira, M.G., and Carmo, E.H., 2006. Infectious diseases epidemiology. *Journal of Epidemiology and Community Health*, 60(3), 192-195.

[14] Centers for Disease Control and Prevention, 2012. *Principles of Epidemiology in Public Health Practice, Third Edition an Introduction to Applied Epidemiology and Biostatistics*. [online] Available at: https://www.cdc.gov/ophss/csels/dsepd/ss1978/lesson1/section10.html

[15] Bargh, G.J.M., Hoch, J.S., Hwang, S,W., Speechley, M., Willey, B.M. and McGeer, A., 2007. Group A streptococcal carriage among residents of an urban homeless shelter. *Infectious Diseases and Medical Microbiology*, 18(5), 316-317.

[16] PRINTO, 2016. *Information on Pediatric Rheumatic Diseases*. [online] Available at: https://www.printo.it/pediatric-rheumatology/TH/info/10/

[17] Sika-Paotonu, D., Beaton, A., Raghu, A., Steer, A. and Carapetis, J., 2017. Acute Rheumatic Fever and Rheumatic Heart Disease. In: J.J. Ferretti, D.L. Stevens and V.A. Fischetti, eds.

Streptococcus pyogenes : Basic Biology to Clinical Manifestations [Internet]. Oklahoma City: : University of Oklahoma Health Sciences Center.

[18] RHD Australia, 2020. What is Acute Rheumatic Fever? [online] Available at: https://www.rhdaustralia.org.au/what-acute-rheumatic-fever

[19] Bagnall, E.M., Ho, M.J. and McCormick, I.A., 2015. A 39-year-old man with recurrent rheumatic fever. *CMAJ*, 187(1), 50-54.

[20] Verkaeren, E., Epelboin, L., Epelboin, S., Boddaert, N., Brossier, F. and Caumes, E. 2014. Recurrent *Streptococcus pyogenes* genital infection in a woman: test and treat the partner! *International Journal of Infectious Diseases*, 29, 37-39.

[21] Passali, D., Lauriello, M., Passali, G.C., Passali, F.M. and Bellussi, L., 2017. Group A Streptococcus and its antibiotic resistance. *Acta Otorhinolaryngologica Italica*, 27(1), 27-32.

[22] Sela, S. and Barzilai, A., 1999. Why do we fail with penicillin in the treatment of group A streptococcus infections? *Annals of Medicine*, 31(5), 303-307.

[23] Olivier, C., 2000. Rheumatic fever-is it still a problem? *Journal of Antimicrobial Chemotherapy*, 45(suppl.1), 13-21.

[24] Yokchoo, N., Patanarapeelert, N. and Patanarapeelert, K., 2019. The effect of group A streptococcal carrier on the epidemic model of acute rheumatic fever. *Theoretical Biology and Medical Modelling*, 16(1), 1-9.

[25] Martin, J., J.J. Ferretti, D.L. Stevens and V.A. Fischetti, ed., 2016. The *Streptococcus pyogenes* carrier state. In *Streptococcus pyogenes: Basic Biology to Clinical Manifestations [Internet]*. Oklahoma: University of Oklahoma Health Sciences Center.

[26] DeMuri, G.P. and Wald, E.R., 2014. The group A streptococcal carrier state reviewed: still an enigma. *Journal of the Pediatric Infectious Diseases Society*, 3(4), 336-342.

[27] Gerber, M.A., Baltimore, R.S., Eaton, C.B., Gewitz, M., Rowley, A.H., Shulman, S.T. and Taubert, K.A., 2009. Prevention of rheumatic fever and diagnosis and treatment of acute *Streptococcal pharyngitis*: a scientific statement from the American Heart Association Rheumatic Fever, Endocarditis, and Kawasaki Disease Committee of the Council on Cardiovascular Disease in the Young, the Interdisciplinary Council on Functional Genomics and Translational Biology, and the Interdisciplinary Council on Quality of Care and Outcomes Research: endorsed by the American Academy of Pediatrics. *Circulationaha*, 119(11), 1541-1551.

[28] Krause, R.M., Rammelkamp, C.H., Denny, F.W. and Wannamaker, L.W., 1962. Studies of the carrier state following infection with group A streptococci. I. Effect of climate. *The Journal of Clinical Investigation*, 41(3), 568-574.

[29] Gillespie, D.T., 1997. Exact stochastic simulation of coupled chemical reactions. *The Journal of Physical Chemistry*, 81(25), 2340-2361.

[30] Ayoub, E.M., 1992. Resurgence of rheumatic fever in the United States: The changing picture of preventable disease. *Postgraduate Medicine*, 92(3), 133-142.

[31] Spencer, S., 2008. *Stochastic Epidemic Models for Emerging Diseases*. Ph.D. University of Nottingham.

[32] van den Driessche, P. and Watmough, J., 2002. Reproduction numbers and sub-threshold endemic equilibria for compartmental models of disease transmission. *Mathematical Biosciences*, 180(1-2), 29-48.

[33] Suli, E., 2014. Numerical Solution of Ordinary Differential Equations. [online] Available at: https://people.maths.ox.ac.uk/suli/nsodes.pdf

Design of Ni-based Bulk Metallic Glasses with Improved Mechanical and Corrosion Properties

Gayatri Tanuja Guddla[1], Suman Gandi[2], Satyadevi Ambadipudi[1] and Balaji Rao Ravuri[2]*

[1]Department of Mechanical Engineering, School of Technology, GITAM (Deemed to be University), Hyderabad, India
[2]Department of Physics, School of Science, GITAM (Deemed to be University), Hyderabad, India

Received: 30 January 2020, Revised: 11 August 2020, Accepted: 20 August 2020

Abstract

Bulk metallic glasses (BMGs) are synthesized using high energy mechanical ball milling technique with the general formula, $[Ni\text{-}Cr\text{-}Si]_{100-x}:Nb_x$ (x = 0, 3, 6 and 9 at.%, labelled as $NCSNb_0$, $NCSNb_3$, $NCSNb_6$, $NCSNb_9$). Interestingly, all the thermal, mechanical and corrosion properties are greatly enhanced with increase in Niobium (Nb) content up to 6 at.% ($NCSNb_6$). XRD analysis shows that the phase attribution over all the BMGs is due to Nickel (Ni, 98-006-0833), Chromium (Cr, 98-002-1500), Silicon (Si, 98-001-2990) and Niobium (Nb, 98-002-3331). The values of the largest super-cooled liquid region width and plastic strain attained are 232 K and 0.94±0.1%, for the $NCSNb_6$ BMG sample. The considerable addition of Niobium (Nb ~ 6 at.%) content in [Ni-Cr-Si] BMG network ($NCSNb_6$) is anticipated to have the best glass-forming ability, mechanical and corrosive resistant properties and is expected to be used as potential material for lightweight vehicle applications.

Keywords: glass-forming ability; bulk metallic glass; super-cooled liquid region
DOI 10.14456/cast.2021.13

1. Introduction

Initially, the research area of amorphous glasses was focused on the scientific curiosity of how deeply nucleation and crystal growth could be arrested by under cooling liquids below their glass transition temperature, until 1960 when the metallic glass system, AuSi was first introduced [1]. After two decades of further research, the development of multi-component compositions with large atomic size mismatches between constituent elements with deep eutectics was proposed [2]. The discovery of bulk metallic glasses (BMGs) instigated a widespread research interest owing to their technological and scientific importance towards glass formation phenomena. Among the extensive family of glasses, BMGs are possibly the youngest, owing to a number of special characteristics like amorphocity, high strength, etc [3]. BMGs have attracted great attention, owing to their unique properties attained due to different atomic configuration. In recent investigations, significant advances in enhancing glass-forming abilities (GFA) have paved the way for their

*Corresponding author: Tel.: (+91) 08455221307
E-mail: balajirao.ravuri@gitam.edu

potential applications as functional and structural materials [4-8]. Perker and Johnson reported on the excellent glass-forming ability of the bulk metallic glass: $Zr_{41.2}Ti_{13.8}Cu_{12.5}Ni_{10.0}Be_{22.5}$, prepared by the metal casting method [9]. As per Park and Kim, by successfully designing the BMG matrix, the plasticity can be controlled effectively [10].

Feng *et al*. designed a new matrix by proportional mixing of binary alloys $Cu_{50}Zr_{50}$ and $Cu_{73}Ti_{27}$ and investigated their thermal, mechanical and corrosion properties including glass-forming abilities [11]. Similarly, Wang and Li investigated bulk metallic glass formation in the binary Cu-Zr system, prepared by the copper mould casting system [12]. Furthermore, Xia *et al*. [13] reported $Ni_{62}Nb_{38}$ as the best glass former composition upon investigating binary Ni-Nb bulk metallic glasses. Several studies reported the glass-forming abilities and thermal stability of ternary Ca-Mg-Zn BMG [14, 15]. Sun *et al*. [16] introduced Zr-Cu-Ni-Al quaternary amorphous alloy compositions with super high glass-forming ability. Liu and Lu [17] provided a comprehensive review of the effect of minor doping on the glass-forming properties in BMGs and stated that the glass-forming ability was enhanced considerably using small amounts (usually < 2 at. %) of B, Si, Y and Sc.

Kui *et al*. [18] found that there was no crystallinity found in the glass alloy $Pd_{40}Ni_{40}P_{20}$ that had been consistently undercooled, via X-ray diffraction, SEM studies and calorimetry. Several researchers studied the microstructure and corrosion behavior of extruded Mg-4Zn-2Gd-0.5Ca Alloy [19-24]. Many studies have proposed a parameter γ to quantify the glass-forming ability of BMGs. They have also discussed the limitations of all the discussed GFA parameters [25-28]. Many research findings reported the improvements in the mechanical and corrosion properties of Ni-Mo coatings through the incorporation of Y_2O_3 nanoparticles [29-36]. Trexler and Thadhani [37] studied the mechanical properties of bulk metallic glasses in detail, including their superior strength, hardness, excellent wear and corrosion resistance. Wang *et al.* [38] reported the effects of Cr contents in Fe-based bulk metallic glasses $Fe_{69.9-x}C_{7.1}Si_{3.3}B_{5.5}P_{8.7}Cr_xMo_{2.5}Al_{2.0}Co_{1.0}$ (x = 0.0, 2.3-12.3) (fabricated using industrial raw materials) on the glass-forming ability and corrosion resistance. They found that the GFA decreases and corrosion resistance increases with the addition of Cr content.

Chang *et al*. [39] studied the microstructure and mechanical properties of Ni-Cr-Si-B-Fe composite coating that had been fabricated by laser additive manufacturing and found that this composite exhibited excellent wear resistance. Qiu *et al*. [40] concluded that addition of small amounts of Niobium, Nb (0, 2, 5 at.%) enhances the strength and plasticity of the base alloy $Zr_{65-x}Nb_xCu_{17.5}Ni_{10}Al_{7.5}$ as a result of the rapid formation of a highly protective passive film.

Inspired by all these results, we have examined the glass-forming abilities, thermal properties, mechanical and corrosion properties of the ternary BMG matrix [Ni-Cr-Si], which was doped with Niobium at various concentrations, Nb_x (x = 0, 3, 6 and 9 at.%) and characterized by XRD, DTA, Vicker's hardness test, Uniaxial compression test, Polarization test and then SEM before and after corrosion test. It is understood that minor alloying can greatly affect the performance of BMGs. Doping with Niobium (Nb) offers excellent resistance to oxidation and corrosion and even 0.1% Niobium (Nb) can significantly enhance the performance characteristics of metals.

2. Materials and Methods

The base metal matrix [Ni-Cr-Si] was prepared with pure metal powders of high purity: Nickel (Ni, 99.99 Wt.%), Chromium (Cr, 99.99 Wt.%) and Silicon (Si, 99.99 Wt.%), each with 33.33 At. Wt.%, which were mixed well in an agate mortar, for a period of 30 min to form a homogenous mixture. This base metallic powder (BMG) was doped with Niobium (Nb, 99.99 Wt.%) using the general formula, $[Ni\text{-}Cr\text{-}Si]_{100-x}$:$[Nb]_x$, (x = 0, 3, 6 and 9 at.% and labelled as $NCSNb_0$, $NCSNb_3$,

$NCSNb_6$ and $NCSNb_9$). Further synthesis of this metal composition was carried out using a high energy mechanical ball milling apparatus in which it was further mixed and crushed to micro size, using a tungsten crucible, with powder to balls ratio taken as 1:10 with a rotation speed of 300 rpm, for about 30 h. The tungsten carbide vials were initially evacuated and purged under pressure of $3x10^5$ Pa. In order to control the agglomeration of the particles, the entire milling process was carried out in a wet medium using 30 ml hexane. At the end of successful ball milling, the samples were dried for about 5 h using a vacuum oven (i-therm, AI-7981Model) at 350 K and collected in powdered form and then analyzed with the help of ICP Spectroscopy. The amorphous nature of the sample and phase analysis was studied via XRD analysis and this was carried out using an Empyrean PANalytical X-rays diffractometer instrument using Co-Kα radiation with a step size of 0.02o with 60 kV tube voltage and 5 mA of tube current for a period of 20 s/step, prior to and post ball milling. A Jeol JEM-1010 electron microscope was used to obtain TEM-scanned images to analyze the surface morphologies. In order to be sure that the samples to be tested were electrically conductive and dry, some sample preparation was done by embedding the BMG powder sample in a copper foil at first, using electrodeposition for mechanical thinning. For electron transparency, ion milling was used and a high energy electron beam was focused on the sample to achieve highly magnified and complex images to better understand the topography of the sample.

The thermal properties were characterized using a Thermo-Gravity/ Differential Thermal Analysis (TG/DTA) analysis (CMET, Pan: Alumina). It was carried out with nitrogen gas at a heating rate of 40 K/min for 0.5s and 10 cel./min and a temperature range of 300 K-1300 K. Through this process, sharp endothermic peaks indicated any phase changes such as melting or fusion, and broad exothermic peaks revealed any dehydration reactions or chemical reactions including oxidation [41]. Then the BMG samples were put n into a vacuum hot-pressing machine and the pressing was carried out with a pressure of 1.2 GPa at its T_c for about an hour, to obtain green pellets of 10mm X 2mm size.

Vickers indenter (Wolpert Wilson, Universal 930/250 N DigiTestor) was used to measure the microhardness of the samples under a load of 1 kg with a dwell time of 10s. A 3369 Uniaxial Compression testing machine was used to perform compression tests with a loading rate of 2X10-4/s and an aspect ratio of 2:1. The corrosive nature of the prepared samples was investigated using an electrochemical polarization technique with RST500F device in 0.5 M HCL aqueous solution from -2.5V-5.5V at a potential sweep rate of 0.05mV/s. This test was done with a standard SCE (Saturated Calomel Electrode) as a reference electrode. The counter electrode was a three-electrode cell, with a platinum foil. The samples were exposed to open air for about 20 min prior to the electrochemical measurements set up, to stabilize the open-circuit potentials [42]. SEM, JEOL, and JSM-6700F instruments were used to study the structural morphologies and find the crystallite sizes of the samples at 20kV, prior to and post corrosion test.

3. Results and Discussion

From XRD studies, we obtained the crystallite sizes, lattice strains and phase identifications of the BMG powder mixtures before and after ball milling for 30 h, using X'pert high score plus software. The energy utilized throughout the milling process depends on the degree of crystalline and amorphous phases present in the BMG matrix. The XRD profiles of all synthesized BMG samples ($NCSNb_0$, $NCSNb_3$, $NCSNb_6$, and $NCSNb_9$), prior to the ball milling process, are displayed in Figure 1. The peak positions of the diffraction peaks, aroused due to Nickel (Ni, 98-006-0833), Chromium (Cr, 98-002-1500), Silicon (Si, 98-001-2990) and Niobium (Nb, 98-002-3331) crystalline phases, at 0 h of ball milling are shown in Figure 1.

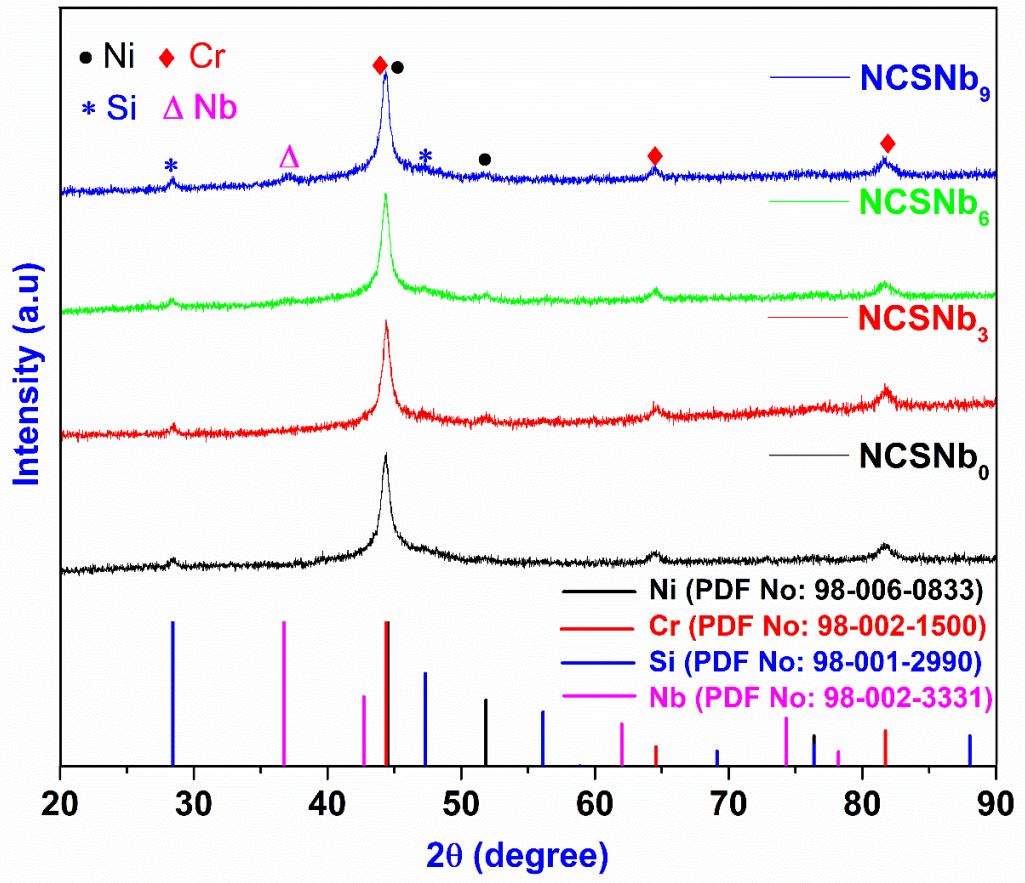

Figure 1. XRD profile of all $NCSNb_x$ BMG samples ($NCSNb_0$, $NCSNb_3$, $NCSNb_6$ and $NCSNb_9$) before ball milling

Upon subsequent prolonged hours of milling, from 0 to 30 h most of the crystalline peak intensities start decreasing and almost disappeared at 30 h milling time. However, few broad peaks that conform to a typical amorphous state are retained (Figure 2). Hence, it is expected that 30 h milling time is adequate to obtain the amorphization phase of the $NCSNb_x$ BMG samples. Furthermore, the broad peaks of the sample containing 6 at.% of Nb content ($NCSNb_6$), slightly shift to a lower position compared to the other prepared BMG samples ($NCSNb_0$, $NCSNb_3$, and $NCSNb_9$) owing to the degree of amorphous nature that develops due to the nucleation process of Nb content [43]. This tendency reveals that the $NCSNb_6$ BMG sample comprises more than 95% of the original compound and is expected to possess the best glass-forming ability (GFA).

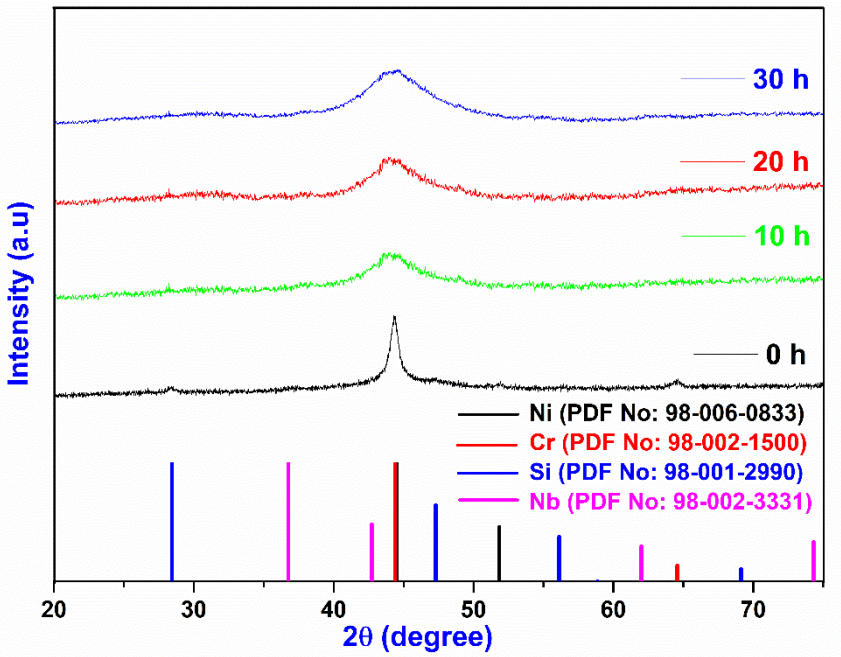

Figure 2. XRD peak patterns of the composition $[Ni\text{-}Mo\text{-}Si]_{94}$:$[Nb]_6$ ($NCSNb_6$ BMG Matrix), as a function of milling time

To further justify the amorphous nature of the $NCSNb_6$ BMG sample, the TEM bright-field image at 30 h milling time is displayed in Figure 3. An interesting blend of the crystalline phase, which is precipitated together with an amorphous phase is seen in Figure 3. This can be attributed to the active participation of Niobium (Nb) nano-crystallites in the nucleation process so as to promote the rate of crystallization during the hot-pressing process. The overall XRD analysis can be summarized as follows: i) All prepared BMG samples, $NCSNb_0$, $NCSNb_3$ and $NCSNb_9$ have shown considerable crystalline peaks that are higher than $NCSNb_6$ sample, ii) Also, $NCSNb_0$, $NCSNb_3$ and $NCSNb_9$ BMG samples exhibited poor amorphization tendencies when compared to $NCSNb_6$ sample. This shows that the BMG sample containing Niobium (Nb) composition of 6 at.% ($NCSNb_6$) exhibits superior glass-forming abilities and a decrease in surface roughness because of the incorporation of Niobium (Nb) into the Ni-Mo-Si matrix. This is attributed to the aggregation of Niobium (Nb) nano-crystallites which are expected to create an impact on improved corrosion resistance properties [44]. As such, more emphasis is laid on the structural properties, mechanical and corrosion behavior of $NCSNb_6$ BMG sample in coming up sections. Using the Scherer formula, the average sizes of the crystallites were found to vary from 41 nm to 60 nm as a function of Niobium (Nb) content (Table 1).

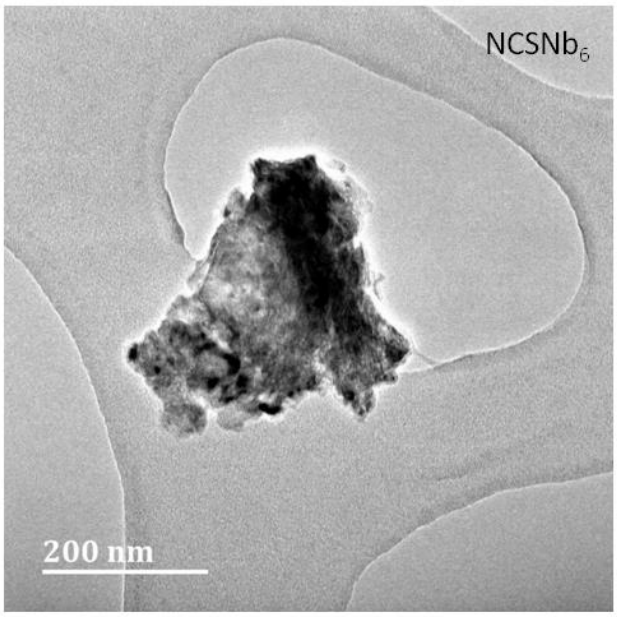

Figure 3. TEM bright-field image of $NCSNb_6$ BMG sample

Table 1. Crystallite size and lattice strain of all as-prepared $NCSNb_x$ BMG samples at 30 h of ball milling

BMG	Crystallite size (nm)	Lattice strain (%)
$NCSNb_0$	60	1.5
$NCSNb_3$	49	0.9
$NCSNb_6$	**41**	**0.4**
$NCSNb_9$	47	1.1

Based on the XRD analysis, the thermal stability and the glass-forming ability of all prepared $NCSNb_x$ BMG samples were measured at 30 h of ball milling and examined via DTA studies at a heating rate of 10 K/min and the results are shown in Figure 4. The endothermic profile of the DTA images is a primary characteristic that shows a glass transition phase, followed by a super-cooled liquid region and an exothermic crystalline reaction. As an example, for the Niobium free ($NCSNb_0$) sample, the glass transition temperature (T_g) is 627 K, and the crystallization temperature (T_c) is 764 K. Similarly, the super-cooled liquid region (ΔT) and liquidus temperature (T_l) are recorded to be 121 K and 1127 K respectively. Based on these studies, the thermal properties (T_g, T_c, T_l, $\Delta T=T_c-T_g$) and the parameter, γ ($=T_c/(T_g+T_l)$)) for all the as-prepared BMG samples are calculated after 30 h of ball milling and are tabulated in Table 2. From Table 2, the decreasing trend of ΔT values are found to be $NCSNb_6 > NCSNb_9 > NCSNb_3 > NCSNb_0$, which implies that $NCSNb_6$ sample possesses the best glass-forming characteristics when compared to all other BMG samples

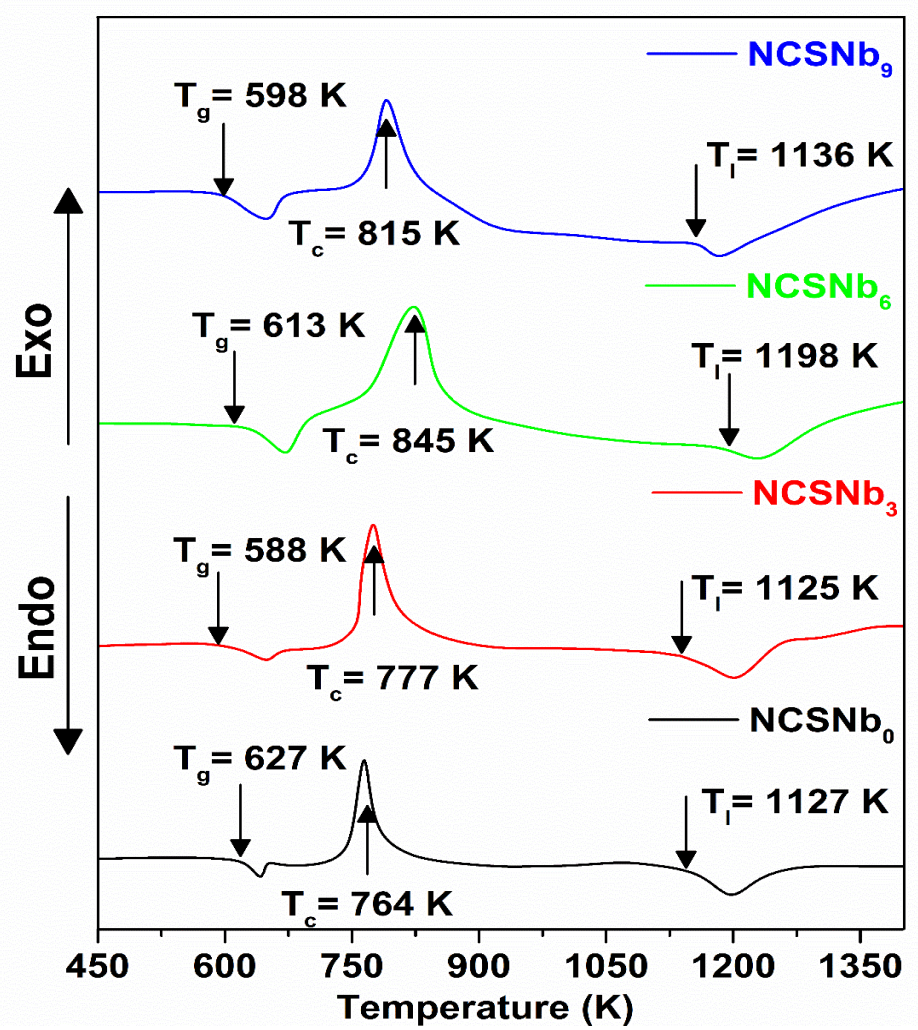

Figure 4. DTA profiles of all as-prepared $NCSNb_x$ BMG samples at 30 h of ball milling

Table 2. DTA parameters of all as-prepared $NCSNb_x$ BMG samples at 30 h of ball milling

BMG	T_g (K)	T_c (K)	T_l (K)	$\Delta T = T_c - T_g$ (K)	$\gamma = T_c/(T_g+T_l)$
$NCSNb_0$	627	764	1127	137	0.435
$NCSNb_3$	588	777	1125	189	0.453
$NCSNb_6$	**613**	**845**	**1198**	**232**	**0.466**
$NCSNb_9$	598	815	1136	217	0.470

under investigation. A higher ΔT represents higher thermal stability. As indicated in Figure 5 and Table 2, the addition of Nb strongly affects the thermal stability of BMGs. The value of ΔT increases from 137 K to a maximum value of 232 K with increasing Niobium content from 0 to 6

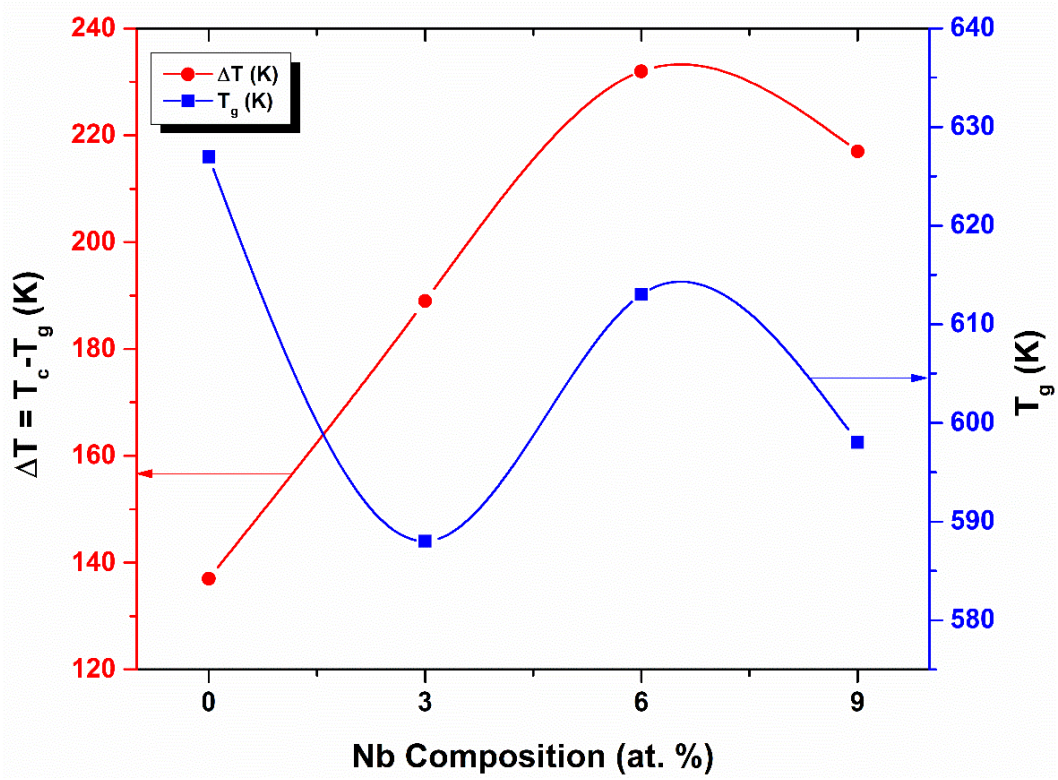

Figure 5. Variations of ΔT and T_g with Nb content of all as-prepared $NCSNb_x$ BMG samples

at.%, then decreases with increasing Niobium content from 6 at.% to 9 at.%. It is well known that γ and ΔT are important parameters for estimating glass-forming ability, and therefore higher γ and ΔT corresponds to higher glass forming ability [45].

The correlation behavior of T_g Vs ΔT with the Niobium (Nb) composition (at.%) is shown in Figure 5. The super-cooled liquid region, ΔT and γ are found to be highest for the sample having 6 at.% of Niobium ($NCSNb_6$). These results are in good agreement with the XRD studies. Additionally, the correlation between Vickers hardness values and plastic strain with respect to Niobium (Nb) composition is depicted in Figure 6. It is noteworthy that the sample with the best glass-forming ability ($NCSNb_6$) displayed the highest plastic strain and hardness, which is a significant contribution of this present family of BMG network (Figure 6 and Table 2). This could be due to the large negative heating effect generated with substantial doping of Niobium (Nb) content with base BMG matrix, [Ni-Cr-Si]. The other mechanical properties of all the as-prepared $NCSNb_x$ BMG samples were studied with the help of compressive stress-strain curves, and the results are shown in Figure 7. All the BMG samples exhibit a unique behavior of increasing stress with the increase of strain, which is in accordance with the law of elasticity and is also referred as work hardening. All the curves undergo an elastic deformation followed by a serrated plastic deformation before fracture failure occurs. The yield strength (σ_y), fracture strength (σ_f) and ε_p for all $NCSNb_x$ BMG samples are calculated from the stress-strain curves and are listed in Table 3. Nevertheless, the values of σ_y, σ_f and ε_p for the Niobium free ($NCSNb_0$) BMG sample are found to be 1701±27, 1732±12 and 0.33±0.1% respectively.

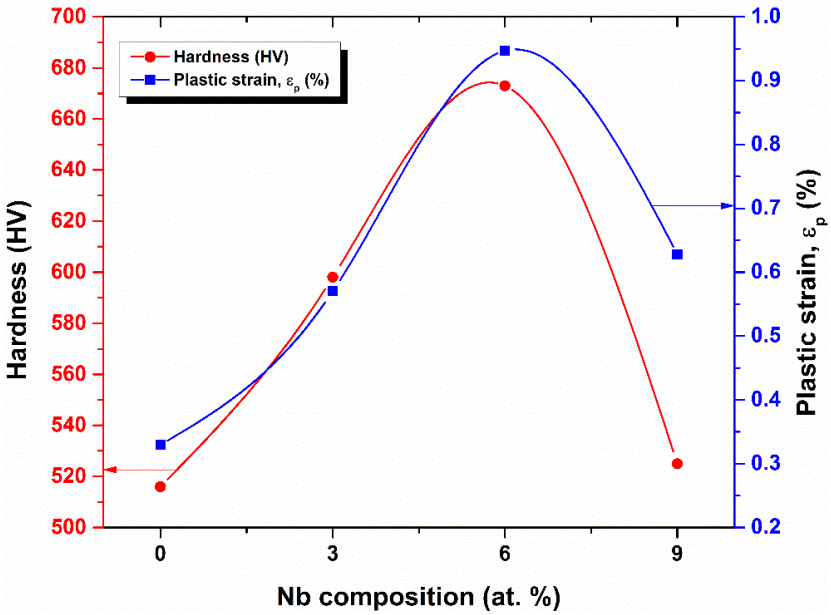

Figure 6. Correlation between Vickers hardness and plastic strain values of all prepared $NCSNb_x$ BMG samples

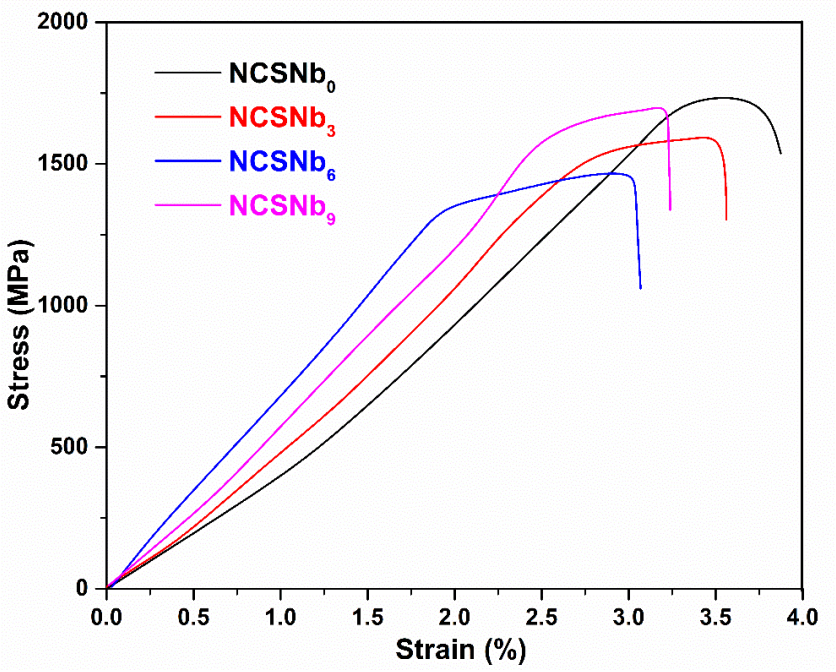

Figure 7. Engineering Stress-Strain curves of all $NCSNb_x$ BMG samples at 30 h of ball milling

Table 3. Yield strength (σ_y), fracture strength (σ_f), plastic strain (ε_p), and hardness values of all as-prepared $NCSNb_x$ BMG samples

BMG	σ_y (MPa)	σ_f (MPa)	ε_p (%)	Hardness (HV)
$NCSNb_0$	1701±27	1732±12	0.33±0.1	516
$NCSNb_3$	1549±35	1595±22	0.57±0.1	598
$NCSNb_6$	**1363±43**	**1467±45**	**0.947±0.1**	**673**
$NCSNb_9$	1605±23	1699±15	0.628±0.1	525

Figure 8 displays the compressive plasticity of all the as-prepared $NCSNb_x$ BMG samples and it is observed from Table 3 and Figure 8 that among all the prepared samples, the ε_p is maximum for $NCSNb_6$. Indeed, the yield strength (σ_y) and compressive strength (σ_f) values are found to be minimum for the Nb composition of 6 at.% ($NCSNb_6$) and the plastic strain (ε_p) value is also found to be maximum for the same. In general, during the blending of different elements with different atomic weights, there is every possibility for generating positive heating effect. This effect will create a heterogeneous atmosphere in the BMG matrix over the entire amorphous phase that can lead to the formation of a large number of shear bands across the whole volume, which results in an improvement of the plastic strain of BMG sample up to a certain extent [46, 47]. Also, the excess quantities of Niobium (Nb) doping of the base matrix may lead to the aggregation of Nb particles causing repulsive forces among the blended elements that may definitely hamper the plastic strain (ε_p) values of the BMG samples [47].

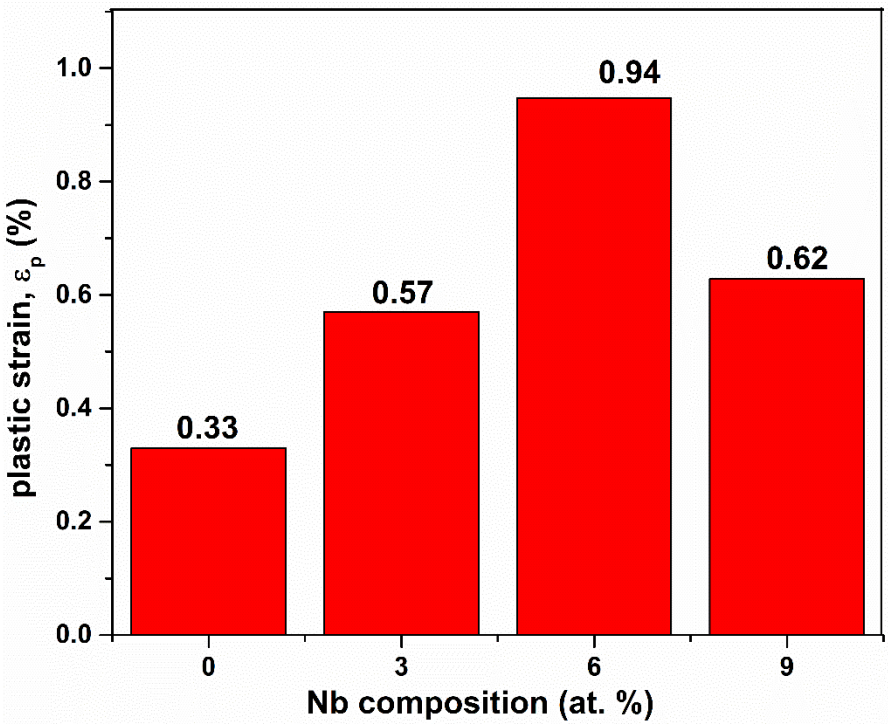

Figure 8. Compressive plasticity of all $NCSNb_x$ BMG samples

To further investigate the evidence of the deformation nature of as-prepared $NCSNb_x$ BMG samples, SEM analysis was done on these samples after the compression test and the results are displayed in Figure 9 (a-d). The images reveal that the homogeneity of the amorphous nature is retained even after 30 h of ball milling and the presence of Nb nano-crystallites can be seen in all the images as depicted in the TEM image of $NCSNb_6$ sample (Figure 3). From Figure 9 (a), a single-clustered morphology along with a considerable amount of porosity can be seen. However, this nature is gradually minimized with the doping of Niobium (Nb) content up to 6 at.% ($NCSNb_6$) (Figure 9 (c)). Moreover, uncontrolled aggregation of Nb nano-crystallites and cracks can be observed above 6 at.% (Figure 9 (d)). Therefore, it can be inferred that the structural morphology of $NCSNb_6$ can be the best plastic and also the best corrosive resistant sample when compared to the other BMGs under investigation.

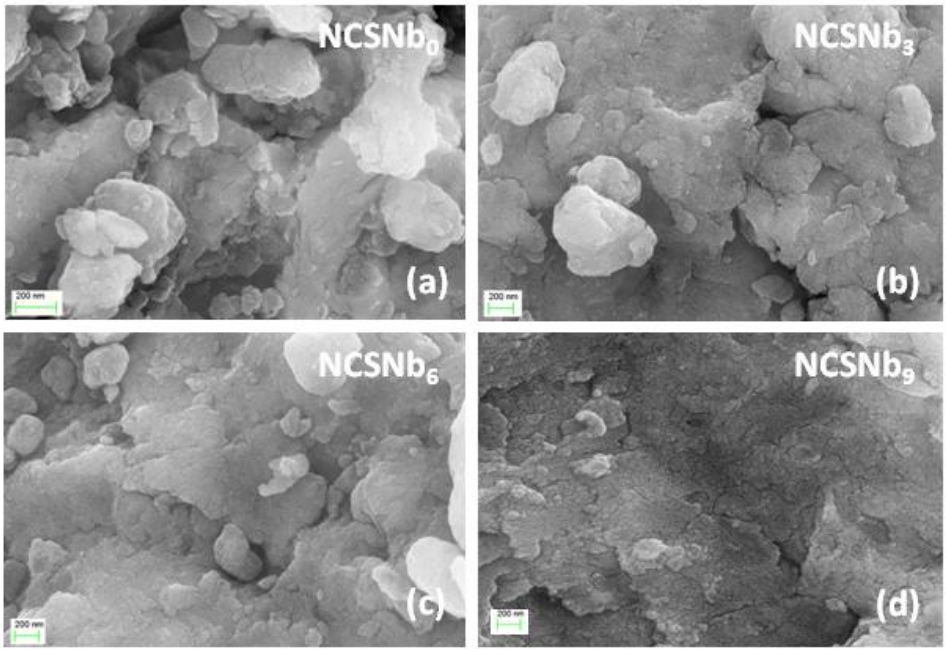

Figure 9. SEM Image Analysis of all $NCSNb_x$ BMG samples at 30 h of ball milling after compression tests: (a) A single-crystal morphology of Nb free BMG sample ($NCSNb_0$), (b) $NCSNb_3$ BMG sample, (c) $NCSNb_6$ BMG sample, and (d) $NCSNb_9$ BMG sample

Further, to study the corrosive properties of the as-prepared $NCSNb_x$ BMG samples, a potentio-dynamic polarization test was also performed from -2.5V~5.5V in 0.5 M HCl solution, with a potential sweep rate of 0.05mV/s. The anodic and cathodic polarization curves from Figures 10 (a) and (b), exhibit similar polarization tendency. From Figure 10 (a), it is noticed that the anodic curve does not hold good Tafel curve, which means that these curves for all the present BMG samples exhibit active or passive transition. However, their slopes can be extrapolated back to the open-circuit corrosion potential. From Figure 10 (b), the anodic current density (i_p) is calculated by summing the experimental anodic current density with extrapolated cathodic current density (i_c) (Table 4). It is noticed from Table 4 that the anodic current density (i_p) increases sharply before reaching a stable value, with a slight increase in the anodic polarization. This might

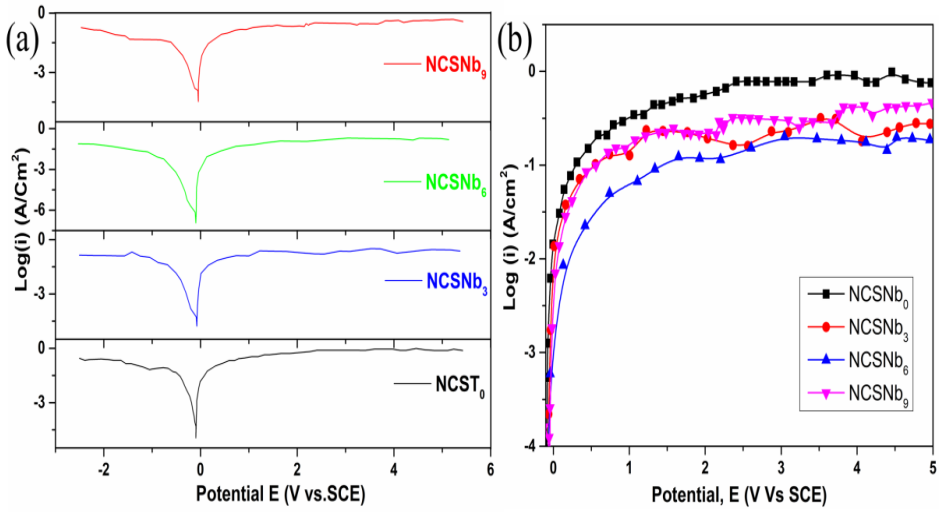

Figure 10. (a) Potentio-metric analysis of all $NCSNb_x$ samples at 30 h of ball milling-anodic current density with corrosion potential, (b) Potentio-metric analysis of $NCSNb_x$ BMG samples at 30 h of ball milling-magnification images of Figure 10 (a)

Table 4. Corrosion potential (E_c), passive potential (E_p), corrosion current density (i_c), and passive current density (i_p) of all $NCSNb_x$ BMG samples

BMG	E_c (mV)	E_p (V)	i_c (A/cm^2)	i_p (A/cm^2)
$NCSNb_0$	-107.1	1.2093	$3.8x10^{-2}$	0.5785
$NCSNb_3$	-80.2	0.7321	$1.7x10^{-2}$	0.7529
$NCSNb_6$	-65.4	0.5120	$5.2x10^{-3}$	0.0062
$NCSNb_9$	-94.7	1.1025	$4.1x10^{-2}$	0.4512

be due to the corrosion tendency of the BMG network. It is also known that for the best corrosive resistant sample, the corrosive current density should be smaller. The i_c ($5.2x10^{-3}$ A/cm^2) and i_p (0.0062 A/cm^2) values of the $NCSNB_6$ BMG sample are expected to be smaller when compared with the other prepared samples of BMGs under investigation which shows its active nature towards corrosion resistance. On the other hand, the step height and serration fluctuation and the corrosion potential value, E_c is highest for the best corrosion-resistant sample ($NCSNb_6$) (Figure 10 (b)). The results show that all the prepared samples of $NCSNb_x$ BMGs exhibit self-passivization behavior. Additionally, E_p value is found to increase at first until x = 6 at.%, indicating a chance of self-passivization and then decreases after x>6 at. %. As the i_p value of $NCSNb_6$ is of two orders of magnitude lesser than the other prepared samples of Ni-based BMGs, this would make it clear that the $NCSNb_6$ sample is comparatively less prone to passive film formation and is the best corrosion-resistant BMG sample. The compositional correlation curves of E_c Vs i_c and E_p Vs i_p are depicted in Figures 11 (a) and (b), respectively, show and prove the active nature of $NCSNb_6$ BMG sample towards corrosion resistance and self-passivization behaviour.

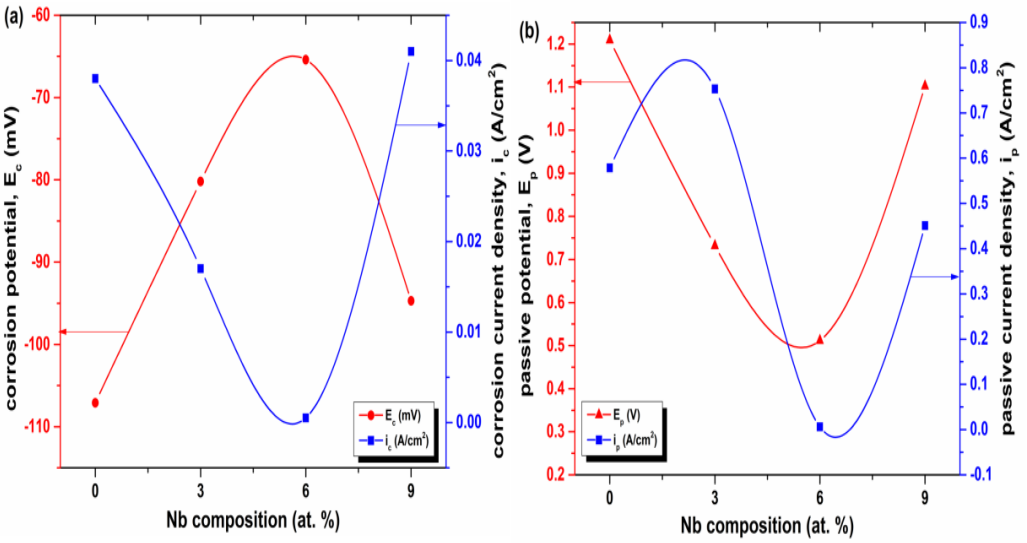

Figure 11. (a) Compositional dependence between corrosion current density (i_c) and corrosion potential (E_c) values of all $NCSNb_x$ BMG samples, (b) Compositional dependence between passive current density (i_p) and passive potential (E_p) values of all $NCSNb_x$ BMG samples

Lastly, to better understand the corrosion properties, the SEM morphologies of the prepared BMG samples after potentio-dynamic polarization tests are taken (Figure 12). It can be observed that Niobium free ($NCSNb_0$) BMG sample (Figure 12 (a)) is more prone to corrosion. It can be seen that sufficient doping of the base metal BMG matrix, with Niobium (Nb), definitely produces an improvement in the surface film structure (Figures 12 (b-d)). The images show the separation of passive films from the standard matrix, which may be caused by corrosion attack. Doping with Niobium (Nb) builds a protective surface film with more chemical stability and more corrosive resistance with a chloride medium. It is also clearly seen that the corroded surface of $NCSNb_6$ (Figure 12(c)) is more unstable and looser than the other BMGs.

The corrosion behavior of all the $NCSNb_x$ BMGs can be related to the variable content of alloying elements. For the prepared samples of BMGs, the atomic percentages of Nickel (Ni), Chromium (Cr) and Silicon (Si), decrease as x increases from 0 at.% to 9 at.%. But, the Niobium (Nb) atomic percentage increases with increasing x. A larger electrochemical potential discrepancy of the alloying elements allows the selective dissolution of Chromium (Cr) in [Ni-Cr-Si] BMG. With the increase of potential, the Chromium (Cr) found on the surface could be re-deposited into the pits, a process that accelerate pits propagation [48, 49]. Even though Ni can form oxides, Cr and Si are chemically more stable and structurally denser. A good corrosion-resistant BMG always has a dense uniform passive film that contains strong passive elements [50-52]. The i_p value indicates corrosion rate and E_c value indicates corrosion tendency. So, the higher corrosive resistance and low E_c and i_p of $NCSNb_6$ BMG sample would be a potential candidate for light-weight vehicle applications.

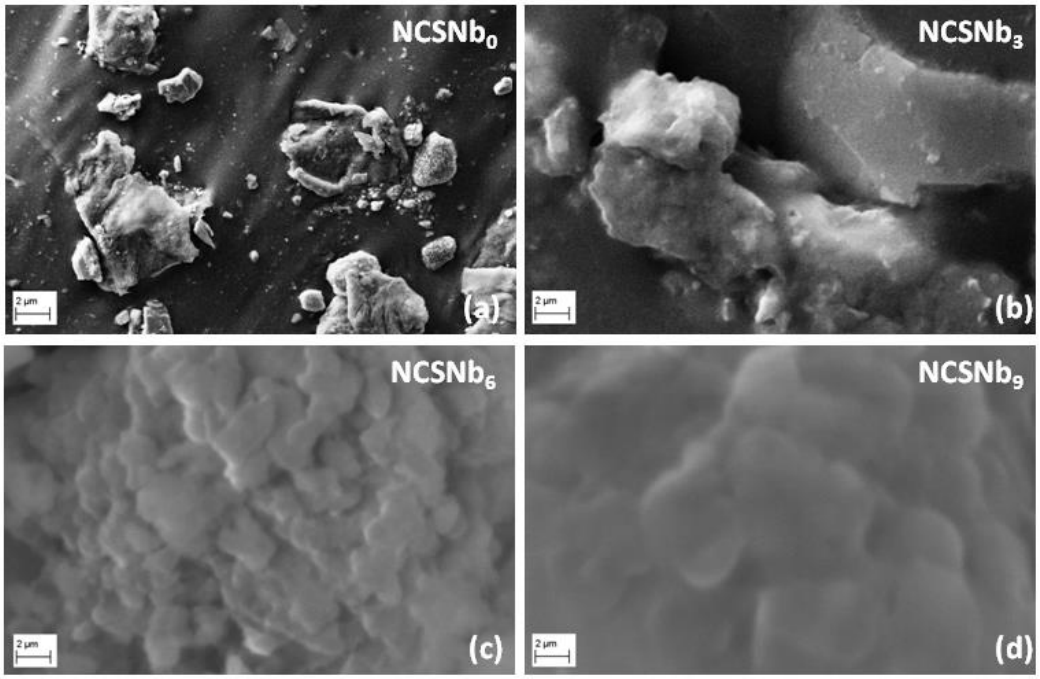

Figure 12. SEM micrographs of the corroded surfaces of all prepared $NCSNb_x$ BMG samples

4. Conclusions

The XRD results reveal that $NCSNb_6$ BMG contains more than 95% of the original compound and can be considered as the BMG with the best glass-forming ability (GFA). The greater the values of the super-cooled liquid region, ΔT and the GFA parameter, γ, the higher will be the glass-forming ability. So, the DTA reports are also in accordance with XRD results. The Vickers hardness test and the Uniaxial compression test confirm that all the prepared samples show work hardening behavior and is comparatively lesser for $NCSNb_6$ and also have high hardness value compared to all the other BMG samples. The σ_y (yield strength), σ_f (fracture strength) are respectively, in the range of 1.3-1.7 Gpa and 1.4-1.73 Gpa. The plastic strain value, ε_p of $NCSNb_6$ is the highest among all the studied $NCSNb_x$ BMG samples and reaches a maximum of 0.947±0.1%. Potentio-dynamic polarization tests also report lower values of i_p and i_c, further confirming that $NCSNb_6$ is the best corrosive resistant sample. The final SEM micrographs, after the corrosion test, show more unstable and looser patterns of the corroded surface of $NCSNb_6$, which further agrees with the results of potentio-dynamic test. This confirms that $NCSNb_6$ is the best corrosive resistant sample with good glass-forming abilities and mechanical strength.

5. Acknowledgements

The author wishes to thank Prof. Jonnalagadda B. Srikanth, School of Chemistry and Physics, University of KwaZulu Natal (UKZN), Westville Campus, Durban, South Africa for his kind support to carry out electron microscopy images and analysis.

References

[1] Klement, W., Willens, R.H. and Duwez, P.O.L., 1960. Non-crystalline structure in solidified gold-Silicon alloys. *Nature*, 187(4740), 869-870.

[2] Hofmann, D.C., 2013. Bulk metallic glasses and their composites: a brief history of diverging fields. *Journal of Materials*, 2013, https://doi.org/10.1155/2013/517904

[3] Chen, M. 2011. A brief overview of bulk metallic glasses: A review. *NPG Asia Materials*, 3, 82-90.

[4] Choi-Yim, H. and Johnson, W.L., 1997. Bulk metallic glass matrix composites. *Applied Physics Letters*, 71(26), 3808-3810.

[5] Inoue, A., 1998. Bulk Amorphous *Alloys: Preparation and Fundamental Characteristics*. Uetikon-Zürich: Trans Tech Publications.

[6] Inoue, A., 1999. *Bulk Amorphous Alloys: Practical Characteristics and Applications.* Vol. 6. Uetikon-Zürich: Trans Tech Publications.

[7] Suryanarayana, C. and Inoue, A., 2011. *Bulk Metallic Glasses*, 208-211. Boca Raton: CRC Press.

[8] Lu, Z.P. and Liu, C.T., 2004. Role of minor alloying additions in formation of bulk metallic glasses: A review. *Journal of Materials Science*, 39(12), 3965-3974.

[9] Peker, A. and Johnson, W.L., 1993. A highly processable metallic glass: $Zr_{41.2}Ti_{13.8}Cu_{12.5}Ni_{10.0}Be_{22.5}$. *Applied Physics Letters*, 63(17), 2342-2344.

[10] Park, E.S. and Kim, D.H., 2005. Design of bulk metallic glasses with high glass forming ability and enhancement of plasticity in metallic glass matrix composites: A review. *Metals and Materials International*, 11(1), 19-27.

[11] Feng, Y., Cai, A.H., Ding, D.W., Liu, Y., Wu, H., An, Q., Ning, H., Zhou, G.J. and Peng, Y.Y., 2019. Composition design and properties of Cu-Zr-Ti bulk metallic glass composites. *Materials Chemistry and Physics*, 232, 452-459.

[12] Wang, D., Li, Y., Sun, B.B., Sui, M.L., Lu, K. and Ma, E., 2004. Bulk metallic glass formation in the binary Cu-Zr system. *Applied Physics Letters*, 84(20), 4029-4031.

[13] Xia, L., Li, W.H., Fang, S.S., Wei, B.C. and Dong, Y.D., 2006. Binary Ni-Nb bulk metallic glasses. *Journal of Applied Physics*, 99, 026103-026106.

[14] Senkov, O.N. and Scott, J.M., 2005. Glass forming ability and thermal stability of ternary Ca-Mg-Zn bulk metallic glasses. *Journal of Non-crystalline Solids*, 351(37-39), 3087-3094.

[15] Schuster, B.E., Wei, Q., Hufnagel, T.C. and Ramesh, K.T., 2008. Size-independent strength and deformation mode in compression of a Pd-based metallic glass. *Acta Materialia*, 56(18), 5091-5100.

[16] Sun, Y.J., Qu, D.D., Huang, Y.J., Liss, K.D., Wei, X.S., Xing, D.W. and Shen, J., 2009. Zr-Cu-Ni-Al bulk metallic glasses with superhigh glass-forming ability. *Acta Materialia*, 57(4), 1290-1299.

[17] Liu, C.T. and Lu, Z.P., 2005. Effect of minor alloying additions on glass formation in bulk metallic glasses. *Intermetallics*, 13(3-4), 415-418.

[18] Kui, H.W., Greer, A.L. and Turnbull, D., 1984. Formation of bulk metallic glass by fluxing. *Applied Physics Letters*, 45(6), 615-616.

[19] Niu, H.Y., Cao, F.F., Deng, K.K., Nie, K.B., Kang, J.W. and Wang, H.W., 2020. Microstructure and corrosion behavior of the As-extruded Mg-4Zn-2Gd-0.5 Ca alloy. *Acta Metallurgica Sinica (English Letters)*, 33(3) 362-374.
[20] Warren, B.E., 1990. *X-ray Diffraction*. North Chelmsford: Courier Corporation.
[21] Egami, T., 2010. Understanding the properties and structure of metallic glasses at the atomic level. *Journal of Materials*, 62(2), 70-75.
[22] Wang, X.D., Bednarcik, J., Franz, H., Lou, H.B., He, Z.H., Cao, Q.P. and Jiang, J.Z., 2009. Local strain behavior of bulk metallic glasses under tension studied by in situ x-ray diffraction. *Applied Physics Letters*, 94(1), 011911-011913
[23] Stoica, M., Das, J., Bednarčik, J., Wang, G., Vaughan, G., Wang, W.H. and Eckert, J., 2010. Mechanical response of metallic glasses: Insights from in-situ high energy x-ray diffraction. *Journal of Materials*, 62(2), 76-82.
[24] Zhou, W., Zhang, C., Sheng, M. and Hou, J., 2016. Glass forming ability and corrosion resistance of Zr-Cu-Ni-Al-Ag bulk metallic glass. *Metals*, 6(10), 230- 236
[25] Lu, Z.P., Bei, H. and Liu, C.T., 2007. Recent progress in quantifying glass-forming ability of bulk metallic glasses. *Intermetallics*, 15(5-6), 618-624.
[26] Kivelson, D., Kivelsonb, S.A., Zhao, X., Nussinovb, Z. and Tarjusc, G., 1995. A thermodynamic theory of supercooled liquids. *Physica A: Statistical Mechanics and Its Applications*, 219(1), 27-38
[27] Debenedetti, P.G. and Stillinger, F.H., 2001. Supercooled liquids and the glass transition. *Nature*, 410(6825), 259-267.
[28] Li, Y.H., Zhang, W., Dong, C., Qiang, J.B., Xie, G.Q., Fujita, K. and Inoue, A., 2012. Glass-forming ability and corrosion resistance of Zr-based Zr-Ni-Al bulk metallic glasses. *Journal of Alloys and Compounds*, 536, S117-S121.
[29] Fathi, M., Safavi, M.S., Mirzazadeh, S., Ansariyan, A. and Ahadzadeh, I., 2020. A promising horizon in mechanical and corrosion properties improvement of Ni-Mo coatings through incorporation of Y_2O_3 nanoparticles. *Metallurgical and Materials Transactions A*, 51(2), 897-908.
[30] Maddin, R. and Masumoto, T., 1972. The deformation of amorphous palladium-20 at.% Silicon. *Materials Science and Engineering*, 9, 153-162.
[31] Argon, A.S., 1979. Plastic deformation in metallic glasses. *Acta Materilia.*, 27(1), 47-58.
[32] Hufnagel, T.C., Ott, R.T. and Almer, J., 2006. Structural aspects of elastic deformation of a metallic glass. *Physical Review B*, 73(6), 064204.
[33] Schuh, C.A., Hufnagel, T.C. and Ramamurty, U., 2007. Mechanical behavior of amorphous alloys. *Acta Materialia*, 55(12), 4067-4109.
[34] Tian, L., Cheng, Y.Q., Shan, Z.W., Li, J., Wang, C.C., Han, X.D., Sun, J. and Ma, E., 2012. Approaching the ideal elastic limit of metallic glasses. *Nature Communications*, 3(1), 1-6.
[35] Egami, T., Iwashita, T. and Dmowski, W., 2013. Mechanical properties of metallic glasses. *Metals*, 3(1), 77-113.
[36] Langer, J.S., 2008. Shear-transformation-zone theory of plastic deformation near the glass transition. *Physical Review E*, 77(2), 021502.
[37] Trexler, M.M., and Thadhani, N.N., 2010. Mechanical properties of bulk metallic glasses. *Progress in Materials Science*, 55(8), 759-839.
[38] Wang, S.L., Li, H.X., Zhang, X.F. and Yi, S., 2009. Effects of Cr contents in Fe based bulk metallic glasses on the glass forming ability and the corrosion resistance. *Materials Chemistry and Physics*, 113(2-3), 878-883.
[39] Chang, Z., Wang, W., Ge, Y., Zhou, J. and Cui, Z., 2018. Microstructure and mechanical properties of Ni-Cr-Si-B-Fe composite coating fabricated through laser additive manufacturing. *Journal of Alloys and Compounds*, 747, 401-407.

[40] Qiu, C.L., Liu, L., Sun, M. and Zhang, S.M., 2005. The effect of Nb addition on mechanical properties, corrosion behavior, and metal-ion release of ZrAlCuNi bulk metallic glasses in artificial body fluid. *Journal of Biomedical Materials Research Part A*, 75(4), 950-956.

[41] Pang, S.J., Zhang, T., Asami, K. and Inoue, A., 2002. Bulk glassy Fe-Cr-Mo-C-B alloys with high corrosion resistance. *Corrosion Science*, 44(8), 1847-1856.

[42] Naka, M., Hashimoto, K. and Masumoto, T., 1976. High corrosion resistance of Chromium-bearing amorphous iron alloys in neutral and acidic solutions containing chloride. *Corrosion*, 32(4), 146-152.

[43] Adylov, G.T., Voronov, V.G. and Sigalov, L.M., 1987. The system Nd_2O_3-Y_2O_3. *Inorganic Materials*, 23(11), 1644-1646.

[44] Shibli, S.M.A., Chinchu, K.S. and Sha, M.A., 2019. Development of nano-tetragonal Zirconia-Incorporated Ni-P coatings for high corrosion resistance. *Acta Metallurgica Sinica (English Letters)*, 32(4), 481-494.

[45] Lu, Z.P. and Liu, C.T., 2002. A new glass-forming ability criterion for bulk metallic glasses. *Acta Materialia*, 50(13), 3501-3512.

[46] Nieh, T.G., Yang, Y., Lu, J. and Liu, C.T., 2012. Effect of surface modifications on shear banding and plasticity in metallic glasses: An overview. *Progress in Natural Science: Materials International*, 22(5), 355-363.

[47] Park, E.S., Kim, D.H., Ohkubo, T. and Hono, K., 2005. Enhancement of glass forming ability and plasticity by addition of Nb in Cu-Ti-Zr-Ni-Si bulk metallic glasses. *Journal of Non-Crystalline Solids*, 351(14-15), 1232-1238.

[48] Pang, S.J., Zhang, T., Asami, K. and Inoue, A., 2002. Synthesis of Fe-Cr-Mo-C-B-P bulk metallic glasses with high corrosion resistance. *Acta Materialia*, 50(3), 489-497.

[49] Souza, C.A.C., Ribeiro, D.V. and Kiminami, C.S., 2016. Corrosion resistance of Fe-Cr-based amorphous alloys: An overview. *Journal of Non-Crystalline Solids*, 442, 56-66.

[50] Qin, C.L., Zhang, W., Asami, K., Kimura, H., Wang, X.M. and Inoue, A., 2006. A novel Cu-based BMG composite with high corrosion resistance and excellent mechanical properties. *Acta Materialia*, 54(14), 3713-3719.

[51] Asami, K., Qin, C.L., Zhang, T. and Inoue, A., 2004. Effect of additional elements on the corrosion behavior of a Cu-Zr-Ti bulk metallic glass. *Materials Science and Engineering: A*, 375, 235-239.

[52] Tang, J., Wang, Y., Zhu, Q., Chamas, M., Wang, H., Qiao, J., Zhu, Y. and Normand, B., 2018. Passivation behavior of a $Zr_{60}Cu_{20}Ni_8Al_7Hf_3Ti_2$ bulk metallic glass in sulfuric acid solutions. *International Journal of Electrochemical Science*, 13, 6913-6929.

Current Applied Science and Technology Vol. 21 No. 1 (January-March 2021)

Morphological Characterization and Phylogeny of *Pythium* and Related Genera in Rayong Province, Thailand

Rattasit Saelee[1], Kanungnid Busarakam[2] and Prommart Koohakan[1]*

[1]Department of Plant Production Technology, Faculty of Agricultural Technology, King Mongkut's Institute of Technology Ladkrabang, Bangkok, Thailand
[2]Biodiversity Research Centre, Thailand Institute of Scientific and Technological Research, Pathum Thani, Thailand

Received: 12 March 2020, Revised: 5 August 2020, Accepted: 21 August 2020

Abstract

Most well-known microorganisms in the class Oomycetes (notably genera *Phytophthora* and *Pythium*) are pathogenic to both animals and plants due to their diverse lifestyle patterns. This study was designed to recover *Pythium* from composite soils (cultivated and forest soils) and water sources (fresh and brackish water) from Rayong Province. Twenty isolates of hyaline and non-septate fungal-like organisms were isolated from those sources. The primer pair ITS4 and ITS6 were used to amplify approximately 900 bp products from Internal transcribed spacer (ITS) region and morphological characteristics including sporangium, oogonium, antheridium and oospore, were noted. Morphological characteristics data of recovered *Pythium* strain can be classified into 12 source groups. ITS sequencing results revealed that eight closely related species had been recovered: *Globisporangium splendens*, *Pythium cucurbitacearum*, *Pythium acanthichum*, *Pythium deliense*, *Pythium diclinum*, *Pythium torulosum*, *Phytopythium vexans* and *Phytopythium helicoides*, which had similarities in the range 94.67-100% values at between 656 and 922 locations. Most of these species were reported as plant pathogens. Therefore, this report can be used as a guide for disease control planning.

Keywords: Oomycetes; identification; phylogeny; Rayong Province; *Pythium*
DOI 10.14456/cast.2021.14

1. Introduction

The microbes in class Oomycetes are classified in kingdom Chromista and subphylum Oomycota. Some species: like *Pythium* sp., live in many types of ecosystems, including a wide range of soil and water sources [1]. Many species in this class affect the environment and economy due to their capability to be plant and animal pathogens [2, 3]. *Pythium* and related genera in family Pythiaceae are one of the most important Oomycete distributed worldwide. They can survive under different location and environments such as tropical forests, natural and agricultural ecosystems, arid zones, temperate zones or even polar regions [4], because they have an ability to produce thick-walled resting spore or sexual reproductive structure called oospore, and asexual reproductive structure called sporangium which form zoospore inside which can be released through vesicle discharge tube

*Corresponding author: E-mail:prommart.ko@kmitl.ac.th

[1]. *Pythium* and related genera can be isolated from both terrestrial and aquatic habitats, and many of them are plant pathogens. Oomycetes have a high distribution rate, which results in a infecting a wide range of host plants, notably succulent plants causing pre- and post- emergence damping off disease [1, 5, 6]. Moreover, *Pythium* can infect mammals, mainly in tropical and subtropical area, and causes pythiosis disease [7-9]. However, there were many reports about the capability of *Pythium* spp. as biological control agent (BCA), for example: *Pythium oligandrum* [10], *Pythium periplocum* and *Pythium acanthicum* [11]. Moreover, there have been a few reports that indicated that *Pythium* could also produce cellulolytic enzymes [12, 13]. Then, it can be seen that *Pythium* exists in every type of ecosystems, and can cause both positive and negative effects on a wide range of hosts. Therefore, good cultivation plan and pathogenicity data are necessary for disease control measures. Simultaneously, it can be applied as additional data for *Pythium* and related genera distribution in Thailand. Generally, a conventional procedure such as morphological study has been widely used to identify Oomycetes genera and the internal transcribed spacer (or ITS) sequences have also been used to classify to species level [1]. Thus, the purpose of this investigation was to study the diversity group of *Pythium* spp. that could be isolated from cultured-dependent methods. The samples were collected from cultivated areas, natural forests, mangrove forests and rivers in Rayong province <12.686277, 101.271261>. All *Pythium* isolates in this study were classified using morphological characteristics and ITS sequence data.

2. Materials and Methods

2.1 Sampling and isolation

Vertical soil samples (300 mm soil depth) were obtained from a cultivated field<12.85099178, 101.55733498>, a natural forest <12.849345, 101.555479>, a mangrove soil <12.698767, 101.707131> and a river <12.776806, 101.714779>. Moreover, plant debris from river and mangrove were also collected. Three techniques were used for isolation:

1) Modified soil plate technique [14]: Approximately 1g of soil sample was put on the surface of selectiveagar media (CMA (corn meal agar) + BNPRA (benomyl 10 ppm, Nystatin 25 ppm, Pentachloronitrobenzene 25 ppm, Rifampicin 10 ppm and Amplicillin 500 ppm) media + Rose Bengal(0.05 g/liters) [15]. Then an agar plug was transferred onto new agar media (CMA, potato dextrose ager (PDA) and V8 juice agar) to obtain a pure culture.

2) Soil baiting technique [16]: Approximately 1g soil or 1ml water sample was mixed with 9 ml sterile distilled water in a Petri dish, then 10 cucumber seeds were added and spread carefully. The sample was incubated (room temperature, 24 h), and a seed was transferred onto selective agar media. Then again an agar plug was transferred onto CMA, PDA and V8 agar media to obtain a pure culture.

3) Soil dilution technique [17]: Approximately 1g soil sample was mixed with 9 ml of sterile distilled water in a test tube and serially diluted to obtain a 10^{-4} dilution. One milliliter of the soil suspension was then pipetted onto Petri dishes containing CMA + BNPRA + Rose Bengal media and then an agar plug was transferred to CMA, PDA and V8 agar media to obtain a pure culture.

2.2 Morphology identification

Water culture, grass blade culture and low nutrient media were used to study asexual reproduction (Sporangium development) [18]. All techniques used were as follows:

1) The water culture technique: an agar plug of pure culture was placed on a Petri dish filled with sterile distilled water.

2) Grass blade culture technique: a boiled grass leaf was placed in a Petri dish and sterile distilled water was then added.

3) Low nutrient media culture: each isolate was cultured in CMA and then checked for asexual structures under a light microscope.

4) Checking for sporangium and zoospore formation within 24-48 h to study sexual reproduction: each isolate was cultured in V8 juice agar and the sexual organs (antheridia, oogonia, and oospores) were observed under a light microscope. All experiments were performed with 3 replicates and observed within 7 days. The taxonomic key used for identification was referred to Van der Plaats-Niterink [19]

2.3 DNA extraction, PCR amplification and sequencing

Oomycetes strains were cultured in PDA at room temperature and genomic DNA was extracted according to Ivors protocol [20]. The internal transcribed spacer (ITS) regions were amplified using the primer ITS6 (5'-GAAGGTGAAGTCGTAACAAGG-3') and ITS4 (5'-TCCTCCGC TTATTGATATGC-3) [21]. The PCR conditions were the same as those used by Cooked *et al.* [22]. The PCR products were analyzed by gel electrophoresis. Gels were extracted and purified using GeneJET Gel Extraction Kit (Thermo scientific). The purified products were stored at -20C° until required. The sequencing of ITS region was determined by Bionics Co. Ltd.

2.4 Phylogenetic analyses

Sequences were determined by the Basic Local Alignment Search Tool (BLAST) at the National Center for Biotechnology (NCBI; Bathesda, USA). The aligned sequences were used to construct phylogenetic trees. The neighbour-joining algorithm [23] was from the MEGA X program. The resultant tree was evaluated in bootstrap analyses [24] based on 1000 resamplings of the neighbour-joining dataset from the PHYLIP package. All DNA sequences were submitted to GenBank (NCBI database).

3. Results and Discussion

3.1 Isolation and morphological identification

Twenty isolates containing 2 genera, *Pythium* and *Phytopythium*, were obtained from soil and water samples and could be classified into 8 species. They were well delineated into 12 groups based on the origin (cultivated field, degraded forest, fresh water or marine). Most isolates produced both asexual and sexual structures, but some isolates did not. RYS-13, RYS-6, RYS- 7, RYS- 13 and RYS- 16 showed no asexual organs, while RYS-9, RYS-10, RYS-12, RYS-13, RYS-14, RYS-15, RYS-16 and RYS-17 presented no sexual organs (Table 1, Figures 1-12). However, in mangrove soil, there were no isolates of Oomycetes found.

Group 1: No zoospoarangia, produce only sexual reproductive structure obtained from cultivated soil (Figure 1).
Group 2: Subglobose or pyriform proliferating zoosporangia and smooth wall oospores obtained from natural forest soil (Figure 2).
Group 3: No zoosporangia formation, produced only sexual reproductive organs obtained from natural forest soil (Figure 3).
Group 4: Oomycete with non-internal and internal proliferating subglobose or pyriform zoosporangia, acute spines oospore obtained from natural forest soil (Figure 4).
Group 5: Subglobose or pyriform zoosporangia with papillae and smooth wall oospores obtained from natural forest soil (Figure 5).
Group 6: Subglobose or pyriform of non-papillate zoosporangia obtained from natural forest soil (Figure 6).
Group 7: Non- inflated zoosporangia obtained from river water (Figure 7).
Group 8: Inflated zoosporangia with smooth wall oospore obtained from river leaf debris (Figure 8).
Group 9: Papillate subglobose or pyriform zoosporangia obtained from river leaf debris (Figure 9).
Group 10: Inflated filamentous sporangia (Figure 10)
Group 11: Non-internal and internal proliferating subglobose or pyriform zoosporangia, acutely spine oospores obtained from river soil (Figure 11).
Group 12: Subglobose or pyriform zoosporangia with papillae and smooth wall oospores obtained from river soil (Figure 12). The distribution of all isolates is shown in Figure 15.

Table 1. Morphology of Oomycetes isolates

Isolate	**Full growth (days)**			**Sporangia**	**Oogonia**	**Antheridia**	**Oospores (µm)**	**Source group**
	PDA	CMA	V8					
RYS-1	2	2	2	-	Smooth wall, intercalary	3-4 monoclinous antheridia per oogonia	Aplerotic (68.76)	1
RYS-2	2	2	2	Subglobose or pyriform proliferating	Smooth wall, terminal or intercalary	1 monoclinous or hypogynous antheridia per oogonia	Nearly Plerotic (47.31)	2
RYS-3	2	2	2	-	Smooth wall, intercalary	1 monoclinous or hyphogynous antheridia per oogonia	Aplerotic (56.38)	3
RYS-4	5	5	4	Subglobose with discharge tube	Ornamented, terminal or intercalary	1-2 monoclinous antheridia per oogonia	Plerotic (44.42)	4

Table 1. (cont.)

RYS-5	5	5	5	Subglobose with discharge tube	Ornamented, terminal or intercalary	1-2 monoclinous antheridia per oogonia	Plerotic (42.53)	4
RYS-6	4	4	5	-	Ornamented, terminal or intercalary	1 monoclinous of hyphogynous antheridia per oogonia	Plerotic (39.65)	4
RYS-7	7	7	6	-	Ornamented, terminal or intercalary	1-2 monoclinous antheridia per oogonia	Plerotic (44.64)	4
RYS-8	6	6	6	Subglobose or pyriform, papillate	Smooth wall, terminal or intercalary	-	Plerotic (32.48)	5
RYS-9	2	2	2	Subglobose or pyriform	Smooth wall, terminal or intercalary	1 monoclinous antheridia per oogonia	-	6
RYS-10	5	5	5	Non-inflated filamentous	-	-	-	7
RYS-11	2	2	2	Inflated filamentous with vesicle	Smooth wall, terminal and intercalary	1 monoclinous antheridia per oogonia	Aplerotic (50.81)	8
RYS-12	2	2	2	Subglobose or pyriform	Smooth wall, terminal and intercalary	1 monoclinous antheridia per oogonia	-	9
RYS-13	2	2	2	-	-	-	-	9
RYS-14	5	5	4	Inflated filamentous	-	-	-	10
RYS-15	2	2	2	Subglobose or pyriform	Smooth wall, terminal and intercalary	-	-	9
RYS-16	4	4	3	-	-	-	-	10
RYS-17	2	2	2	Subglobose or pyriform	-	-	-	9
RYS-18	5	5	4	Subglobose	Ornamented, terminal or intercalary	1 monoclinous antheridia per oogonia	Plerotic (28.11)	11

Table 1. (cont.)

RYS-19	3	3	3	Subglobose	Ornamented, terminal or intercalary	1 monoclinous antheridia per oogonia	Plerotic (42.75)	11
RYS-20	5	5	5	Pyriform	Smooth wall, terminal or intercalary	1-2 monoclinous antheridia per oogonia	Plerotic (34.11)	12

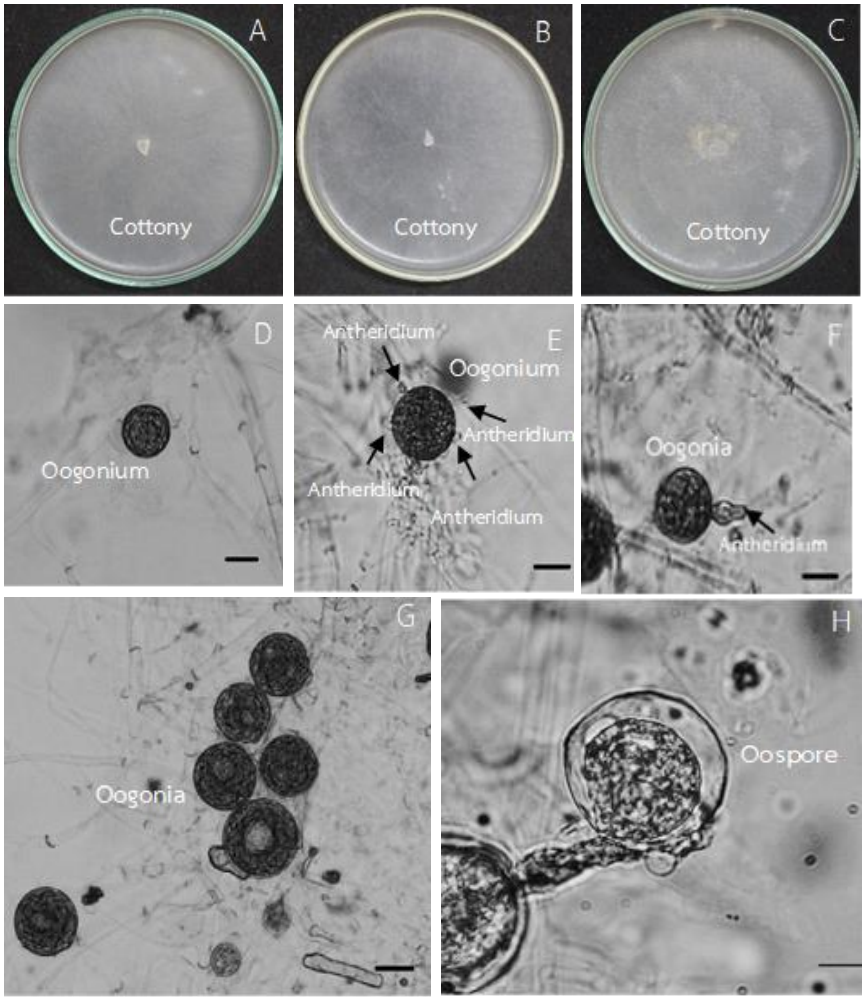

Figure 1. Morphology of an isolate obtained from cultivated soil (group 1: RYS-1). A-C: Colony patterns on CMA (A), PDA (B) and V8 agar (C); D-G: 10×; H: 40× (scale bars D-H: 20 µm); black arrows indicate antheridia.

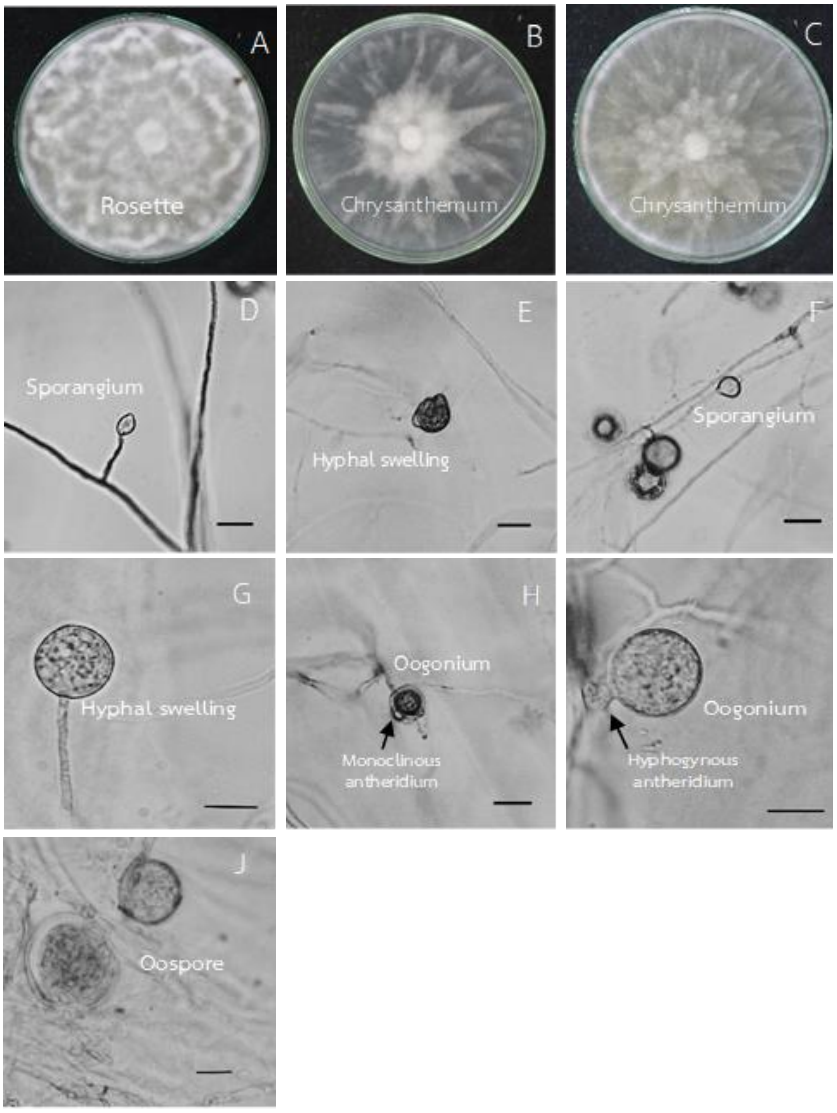

Figure 2. Morphology of an isolate obtained from natural forest soil (group 2: RYS-2). A-C: Colony patterns on CMA (A), PDA (B) and V8 a gar (C); D-F and H: 10×; G, I and J: 40× (scale bars D-J: 20 μm); black arrows indicate antheridia.

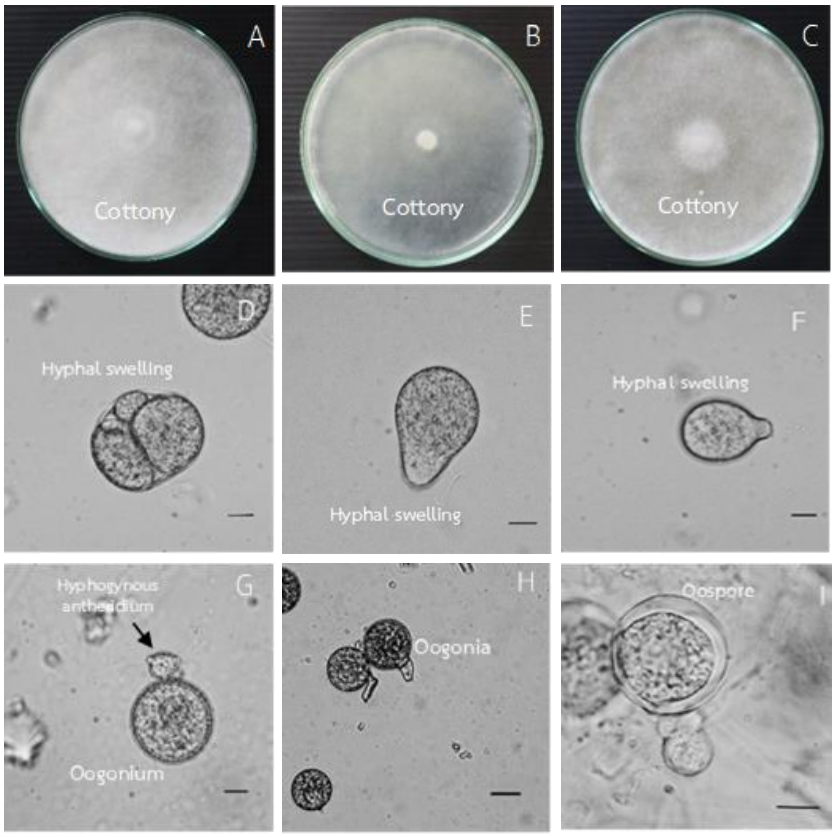

Figure 3. Morphology of an isolate obtained from natural forest soil (group 3: RYS-3). A-C: Colony patterns on CMA (A), PDA (B) and V8 agar (C); D-H: 10×; I: 40× (scale bars D-I: 20 µm); black arrows indicate antheridia.

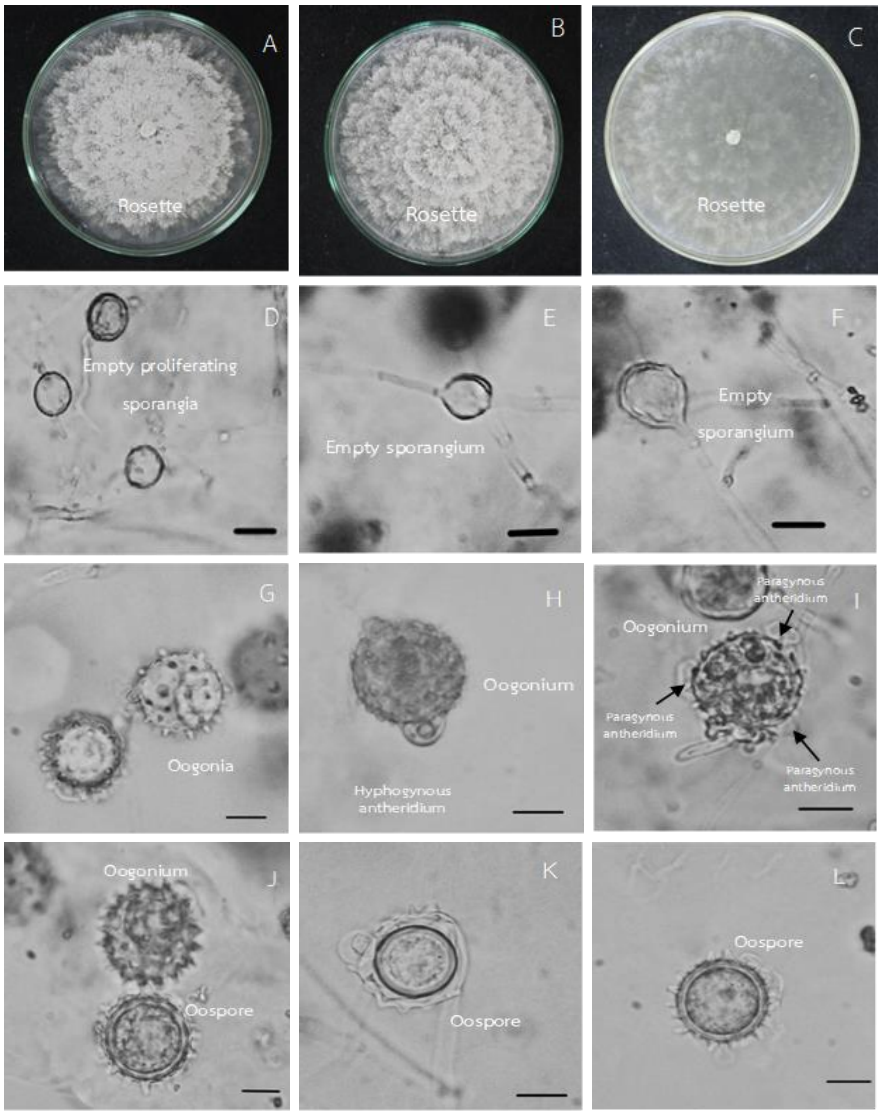

Figure 4. Morphology of an isolate obtained from natural forest soil (group 4: RYS-4, RYS-5, RYS-6 and RYS-7).A-C: Colony patterns on CMA (A), PDA (B) and V8 agar (C); D-F: 10×; G-L: 40× (scale bars D-L: 20 µm); black arrows indicate antheridia.

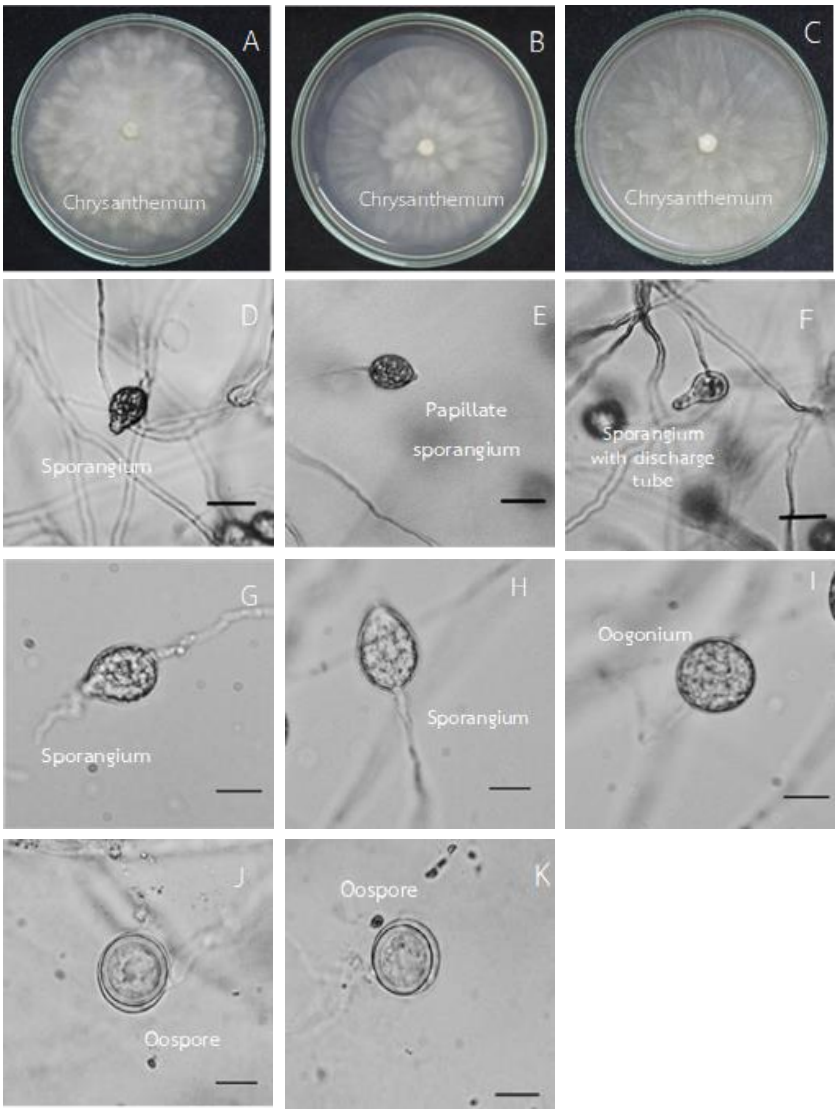

Figure 5. Morphology of an isolate obtained from natural forest soil (group 5: RYS-8). A-C: Colony patterns on CMA (A), PDA (B) and V8 agar (C); D-F: 10×; G-K: 40× (scale bars D-K: 20 µm)

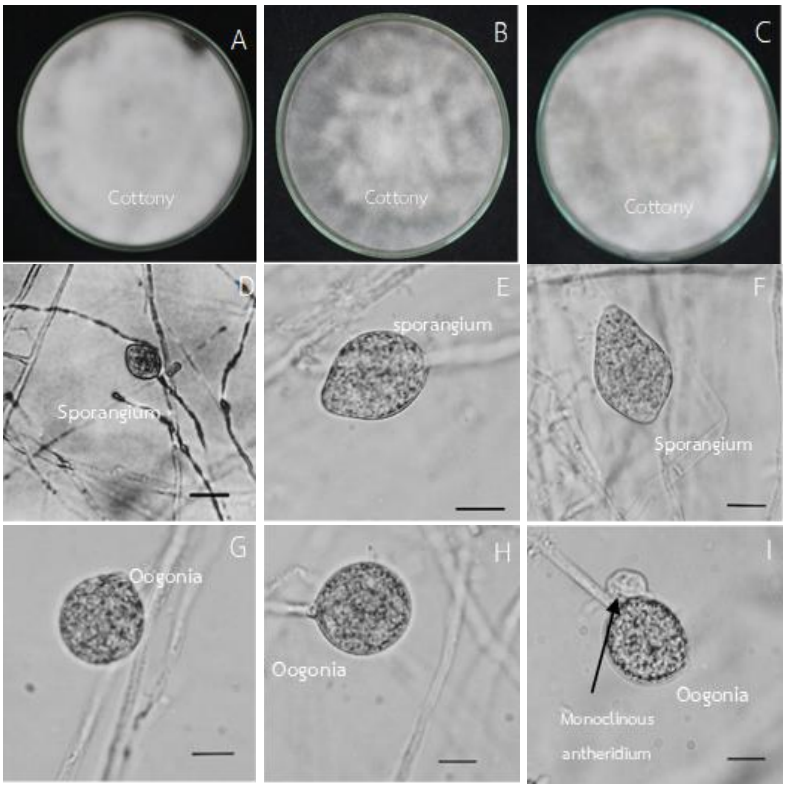

Figure 6. Morphology of an isolate obtained from natural forest soil (group 6: RYS-9). A-C: Colony patterns on CMA (A), PDA (B) and V8 agar (C); D and G: 10×; E-I: 40× (scale bars D-I: 20 µm); black arrows indicate antheridia.

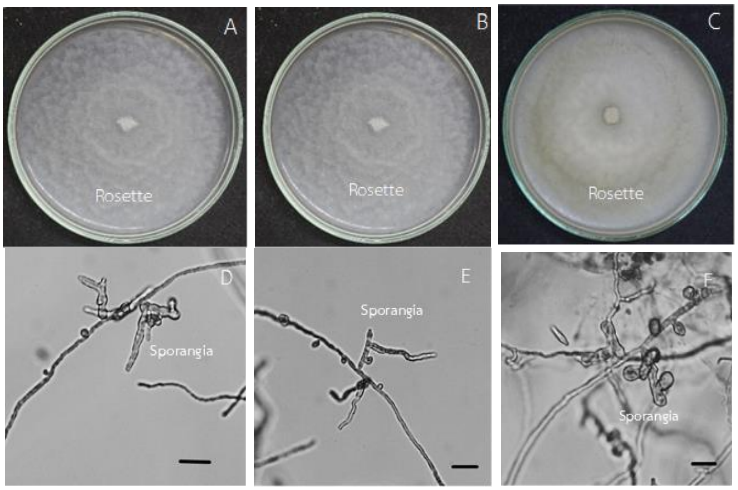

Figure 7. Morphology of an isolate obtained from river (fresh water; group 7: RYS-10).A-C: Colony patterns on CMA (A), PDA (B) and V8 agar (C); D-F: 10×; (scale bars D-F: 20 µm)

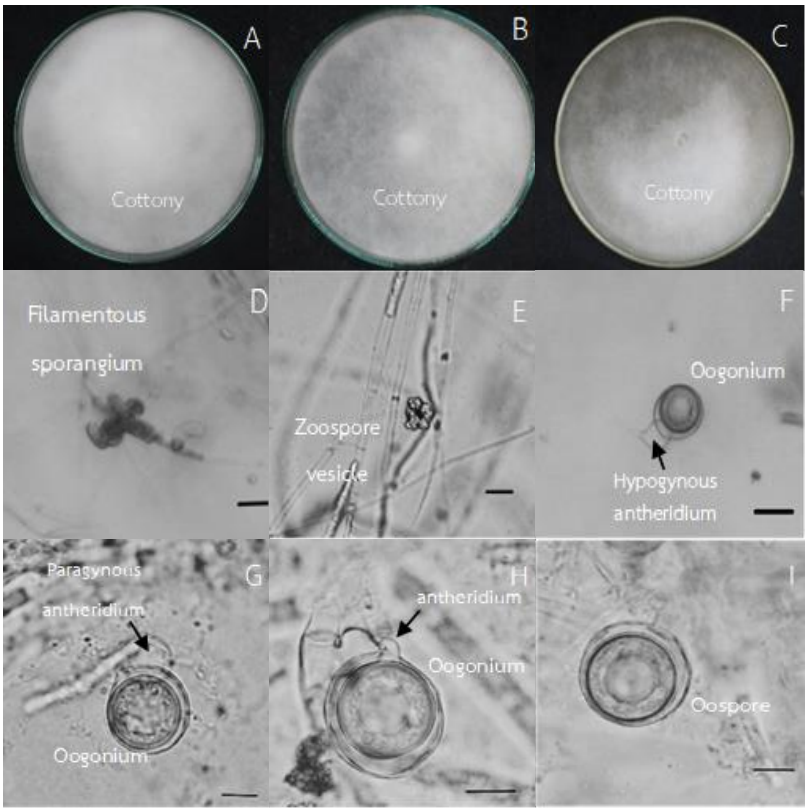

Figure 8. Morphology of an isolate obtained from river debris (group 8: RYS-11). A-C: Colony patterns on CMA (A), PDA (B) and V8 agar (C); D-F: 10×; G-I: 40× (scale bars D-I: 20 µm); black arrows indicate antheridia.

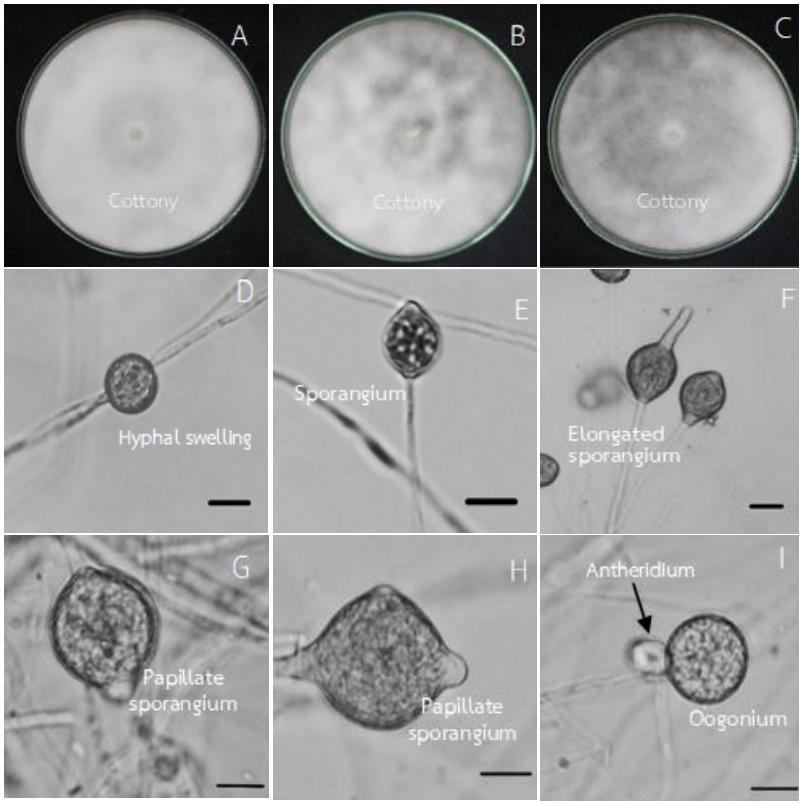

Figure 9. Morphology of an isolate obtained from river debris (group 9: RYS-12, RYS-13, RYS-15 and RYS-17). A-C: Colony patterns on CMA (A), PDA (B) and V8 agar (C); D-F: 10×; G-I: 40× (scale bars D-I: 20 µm); black arrows indicate antheridia.

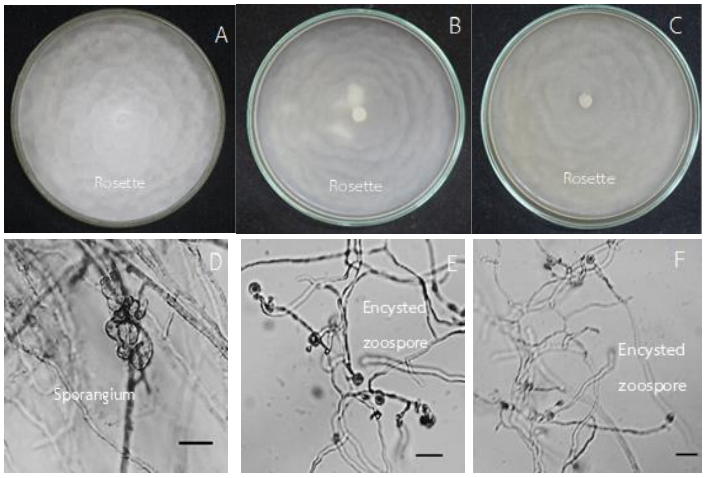

Figure 10. Morphology of isolate obtained from river debris (group 10: RYS-14 and RYS-16). A-C: Colony patterns on CMA (A), PDA (B) and V8 agar (C); D-F: 10×; (scale bars D-J: 20 µm)

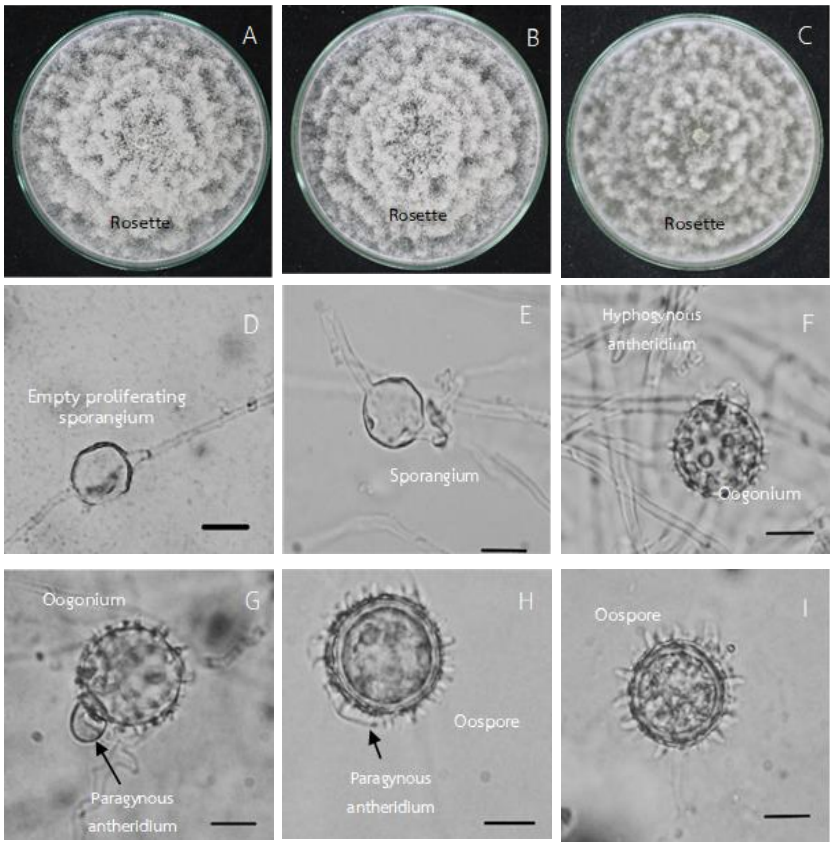

Figure 11. Morphology of an isolate obtained from river soil (group 11: RYS-18 and RYS-19). A-C: Colony patterns on CMA (A), PDA (B) and V8 agar (C); D: 10×; F-I: 40× (scale bars D-I: 20 µm); black arrows indicate antheridia.

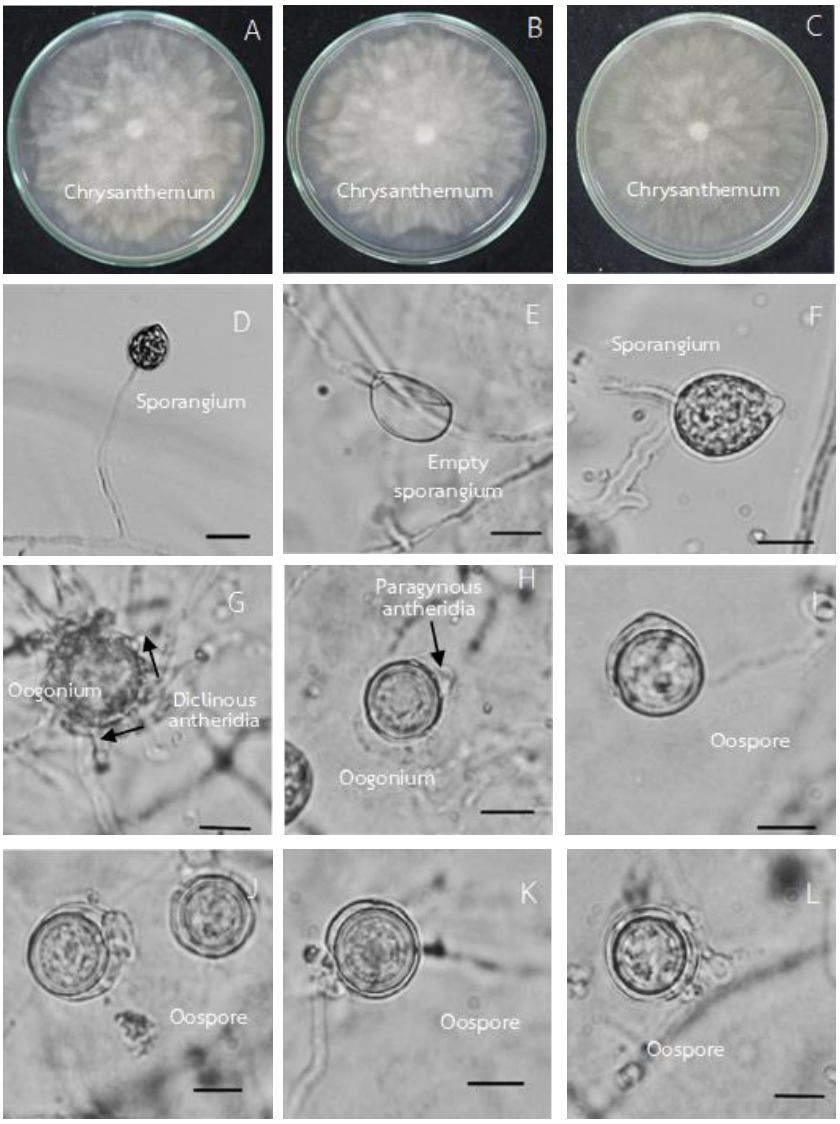

Figure 12. Morphology of an isolate obtained from river soil (group 12: RYS-20). A-C: Colony patterns on CMA (A), PDA (B) and V8 agar (C); D: 10×; E-L: 40× (scale bars D-I: 20 µm); black arrows indicate antheridia.

3.2 Phylogenetic analysis

After amplification of DNA sequence at ITS region using primers ITS4 and ITS6, approximately ~900 bp of PCR products were obtained (Figure 13). The comparison data between this study and the databases from NCBI found that the studied isolates were defined into eight Oomycetes species: *Globisporangium splendens* (formerly called *P. Splendens* [25], clade I), *Pythium cucurbitacearum* (clade K), *Pythium acanthichum* (clade D), *Pythium deliense* (clade A), *Pythium diclinum* (clade B), *Pythium torulosum* (clade B), *Phytopythium vexans* and *Phytopythium helicoides* (clade K) (Table

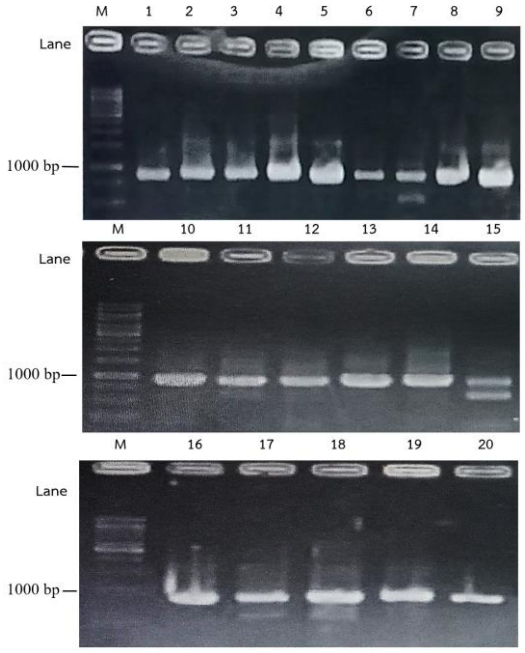

Figure 13. The primer pair ITS4 and ITS6 were used to amplified a 900 bp product compared with 1 kb marker (lane M); Lane 1-20: RYS-1 ~ RYS-20

2). All species showed the common morphological traits of each clade as reported by Lévesque and de Cock [26] and de Cock *et al.* [27]. It was found that *G. splendens* is a member of clade I in which most species in this clade do not produce zoospores. *Pythium cucurbitacearum* belongs to clade K with some common characteristics between *Pythium* and *Phytophthora* sp. like papillae sporangia, *Phytopythium* also belongs to this clade. *Pythium acanthichum* is in clade D, the members of which have oogonia with spines. Most of the species in this clade are mycoparasites, such as *P. oligandrum*. *Pythium deliense* belongs to clade A, which produce filimentous sporangia with intercalary antheridia. *Pythium diclinum* and *P. torulosum* are in clade B, which produce filimentous sporangia with smooth wall oogonia. Most species in this study are waterborne Oomycetes [28] (Figure 14). As stated, *Pythium* and related genera in the same class exist in many types of ecosystems. Therefore, the same genus can be found in a variety of habitats. A good example of this is *P. aphanidermatum*, now known to live in sea water [29] although this species was mostly found in cultivation area.

Table 2. Similarity and origin of each isolate

Species	GenBank Accession no. (ITS)	Origins	Hits	Seqence length (bp)	Similar (%)
G. splendens RYS-1	MT758164	Cultivated soil	*P. splendens* AY598655.2	853	98.71
P. vexans RYS-2	MT758165	Forest soil	*P. vexans* MK011121.1	922	99.21
G. splendens RYS-3	MT758166	Forest soil	*P. splendens* KU724186.1	793	99.62
P. acanthicum RYS-4	MT758167	Forest soil	*P. acanthicum* LC332027.1	772	98.71
P. acanthicum RYS-5	MT758168	Forest soil	*P. acanthicum* KU210470.1	863	98.61
P. acanthicum RYS-6	MT758169	Forest soil	*P. acanthicum* KU210470.1	871	98.74
P. acanthicum RYS-7	MT758170	Forest soil	*P. acanthicum* KU210470.1	858	98.49
P. cucurbitacearum RYS-8	MT758171	Forest soil	*P. cucurbitacearum* KP183959.1	856	99.42
P. helicoides RYS-9	MT758172	Forest soil	*P. helicoides* KT750954.1	797	99.75
P. torulosum RYS-10	MT758173	Fresh water	*P. torulosum* MK015674.1	877	99.42
P. deliense RYS-11	MT758174	Leaf debris	*P. deliense* MN365090.1	823	99.88
P. helicoides RYS-12	MT758175	Leaf debris	*P. helicoides* KT595686.1	656	96.68
P. helicoides RYS-13	MT758176	Leaf debris	*P. helicoides* KY084740.1	793	94.67
P. diclinum RYS-14	MT758177	Leaf debris	*P. diclinum* MK015676.1	782	99.22
P. helicoides RYS-15	MT758178	Leaf debris	*P. helicoides* KT750954.1	819	99.63
P. diclinum RYS-16	MT758179	Leaf debris	*P. diclinum* MK015676.1	774	99.21
P. helicoides RYS-17	MT758180	Leaf debris	*P. helicoides* KT750954.1	841	99.88
P. acanthicum RYS-18	MT758181	River soil	*P. acanthicum* AY598617.2	822	99.03
P. acanthicum RYS-19	MT758182	River soil	*P. acanthicum* HQ643411.1	770	98.83
P. cucurbitacearum RYS-20	MT758183	River soil	*P. cucurbitacearum* MK416211.1	868	100.00

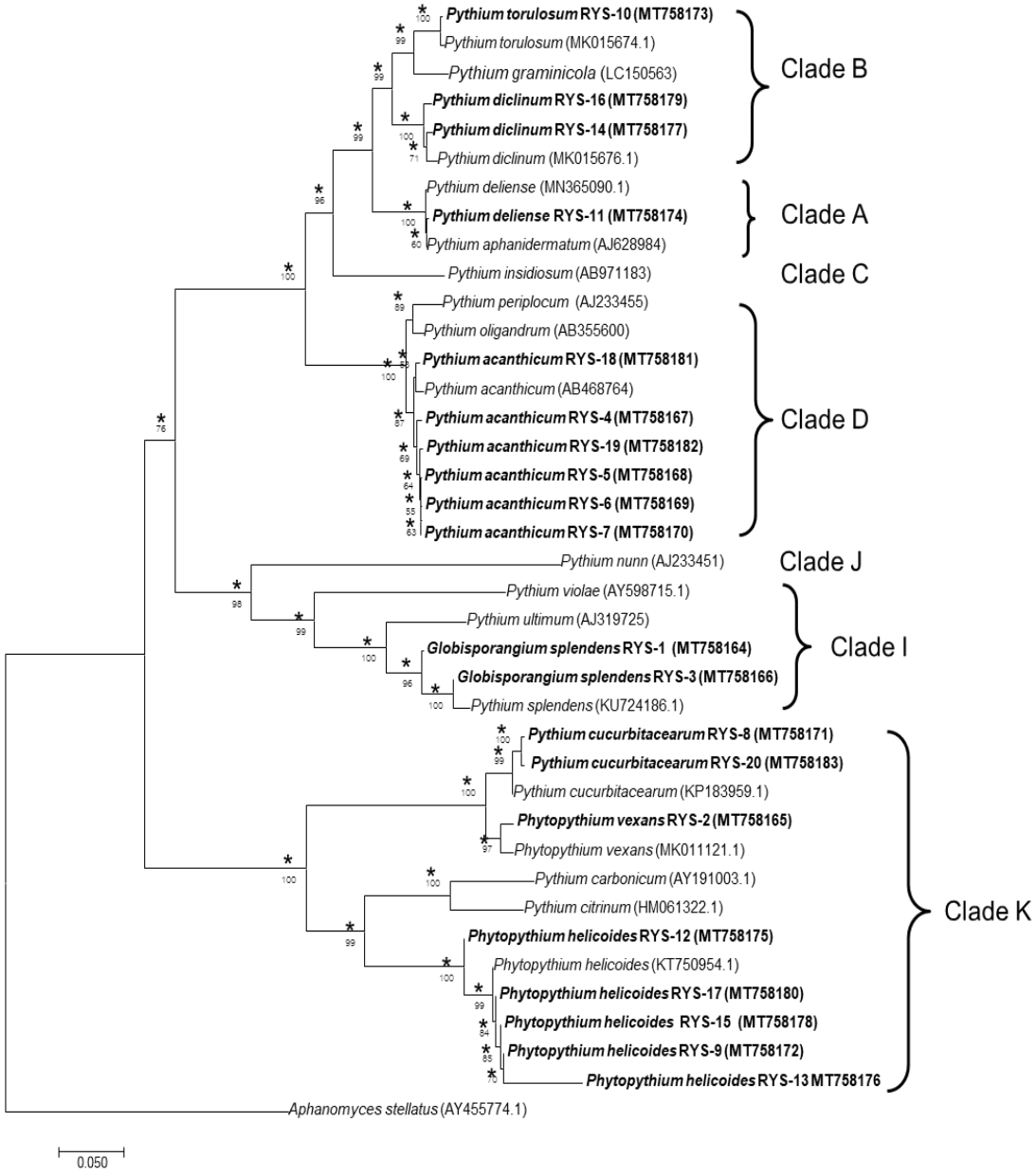

Figure 14. Neighbour-joining tree based on ITS region sequences (~900 bp) showing relationships between the studied-isolates and related *Pythium* species. Asterisks indicate branches of the tree that were also found using the maximum-likelihood and maximum-parsimony tree-making algorithms. Numbers of the nodes are percentage bootstrap values based on a neightbour-joining analysis of 1,000 sampled datasets. The root postion of the tree was determined using *Aphanomyces stellatus* AY455774.1. Bar, 0.05 substitutions per nucleotide position.

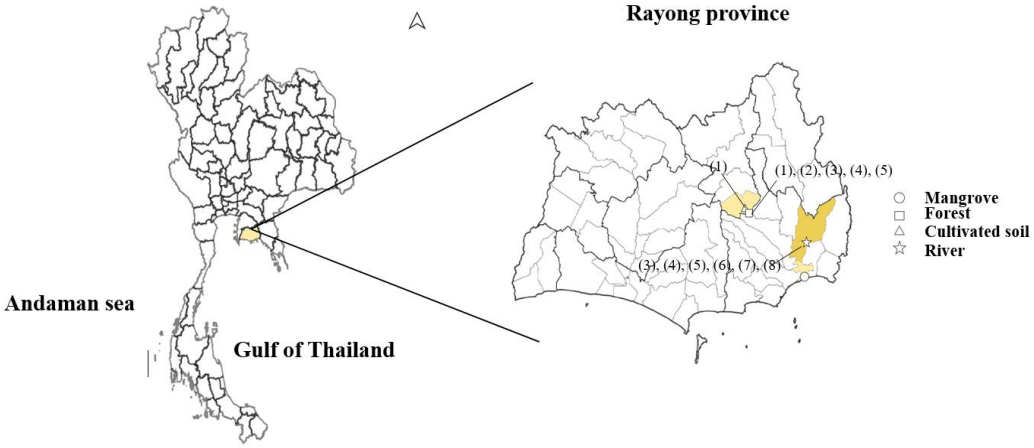

Figure 15. The distribution of *Pythium* and related genera in class Oomycetes; 1: *Globisporangium splendens*; 2: *Phytothora vexans*; 3: *Pythium acanthicum*; 4: *Pythium cucurbitacearum*; 5: *Phytothora helicoides*; 6: *Pythium torulosum*; 7: *Pythium deliense* and 8: *Pythium diclinum*

It can be seen that all strains of *Pythium* and related genera found in this study are more diverse in marginally disturbed or undisturbed habitats like natural forests or rivers, and less diverse in cultivated soil. Detection of these species was not that unexpected because there had been many reports of the discoveries of *Phytophthora* and *Pythium* species in similar locations. For example, *Phytophthora gonapodyides*, *Phy. lacustris*, *Pythium oopapillum*, etc., were discovered in rivers crossing the Polish-Ukrainian border area [30], *Pythium sukuiense*, from undisturbed natural forest in Taiwan [31], and *P. Aphanidermatum* was discovered a decades ago [32]. However, there have still been no discoveries of any Oomycetes species in mangrove soil. This might be because the condition of mangrove soil with obviously high salinity limits the diversity of soil and fresh-waterborne Oomycetes. There was a report about specific halotolerant *Pythium* species being able to inhabit in salt water and infect algae, but as mentioned, only a few particular species, such as *Pythium porphyrae*, can live in such conditions. However, there was also the discovery of *P. aphanidermatum* strain that inhabited leaf debris in sea water [29]. Based on this observation, the possibilities of finding well known plant or animal pathogenic Oomycetes in mangrove forests can not be ignored. A pathogenicity test can be carried out in a future study.

4. Conclusions

Fungal-like microorganisms in class Oomycetes are important in cultivation and environmental stability in many ways. Here, this paper provided new and detailed information about the distribution of *Pythium* and related genera in Rayong Province, Thailand. Eight *Pythium* species and related genera were identified, i.e. *Globisporangium splendens, Pythium cucurbitacearum, Pythium acanthichum, Pythium deliense, Pythium diclinum, Pythium torulosum, Phytopythium vexans* and *Phytopythium helicoides.* Moreover, it was found that Oomycetes in the undisturbed locations were more diverse than those found in disturbed locations. From the results, the distribution data can be used for advanced study or further field investigation. However, futher study of the obtained isolates is needed, and in particular further studies of pathogenicity and environmental factors that affect

Pythium and related genera will be required to formulate a universal overview of Oomycetes representives in Thailand.

5. Acknowledgements

This study was funded and supported by the Faculty of Agricultural Technology, King Mongkut's Institute of Technology Ladkrabang (KMITL) and Thailand Institute of Scientific and Technological Research (TISTR).

References

[1] Schroeder, K.L., Martin, F.N., De Cock, Arthur, W.A.M., Lévesque, C.A., Spies, C.F.J., Okubara, P.A. and Paulitz, T.C., 2013.Molecular detection and quantification of *Pythium* species: Evolving Taxonomy, New Tools, and Challenges. *Plant Disease*, 97(1), 4-20.

[2] Phillips, A.J.M., Anderson, V.L., Robertson, E.J., Secombes, C.J. and West, P.V., 2007. New insights into animal pathogenic Oomycetes. *TRENDS in Microbiology*, 16, 13-19.

[3] Kamoun, S., Furzer, O., Jones, J.D.G., Judelson, H.S., Ali, G.S. , Dalio, R.J.D., Roy, S.G., Schena, L., Zambounis, A., Panabières, F., Cahill D., Ruocco, M., Figueiredo, A., Chen, X.R., Hulvey, J., Stam, R., Lamour, K., Gijzen, M., Tyler, B.M., Grünwald, N.J., Mukhtar, M. S., Tomé, D.F.A., Tör, M. , Ackerveken, G.V.D, McDowell, J., Daay, F., Fry, W.E., Kreuze, H.L., Meijer, H.J.G., Petre, B., Ristaino, J., Yoshida, K., Birch, P.R.J. and Govers, F., 2016. The top 10 Oomycete pathogens in molecular plant pathology. *Molecular in Plant Pathology*, 16(4), 413-434.

[4] Tojo, M., van West, P., Hoshino, T., Kida, K., Fujii, H., Hakoda, A., Kawaguchi, Y., Mühlhauser, H.A., Van Den Berg, A.H., Küpper, F.C., Herrero, M.L., Klemsdal, S.S., Tronsmo, A.M. and Kanda H., 2012. *Pythium polare*, a new heterothallic oomycete causing brown discolouration of *Sanioniauncinata* in the Arctic and Antarctic. *Fungal Biology*, 116(7), 756-768.

[5] Navi, S.S., Huynh, T., Mayers, C.G. and Yang, X.B., 2019. Diversity of *Pythium* spp. associated with soybean damping-off, and management implications by using foliar fungicides as seed treatments. *Phytopathology Research*, 1, https://doi.org/10.1186/s 42483-019-0015-9

[6] Qiu, L., Mao, Y., Tang, L., Tang, X., and Mo, Z., 2018. Characterization of *Pythium chondricola* associated with red rot disease of *Pyropiayezoensis* (Ueda) (Bangiales, Rhodophyta) from Lianyungang, China. *Journal of Oceanology and Limnology*, 37, 1102-1112.

[7] Phillips, A.J.M., Anderson, V.L., Robertson, E.J., Secombes, C.J. and West, P.V., 2007. New insights into animal pathogenic Oomycetes. *Trends in Microbiology*, 16, 13-19.

[8] Bernheim, D., Dupont, D., Aptel, F., Dard, C., Chiquet, C., Normand, A.C., Piarroux, R., Cornet, M. and Maubon, D., 2019. Pythiosis: case report leading to new features in clinical and diagnostic management of this fungal-like infection. *International Journal of Infectious Diseases*, 86, 43-46.

[9] Gaastra, W., Lipman, L.J.A., De Cock, A.W.A.M., Exel, T.K., Pegge, R.B.G., Scheurwater, J., Vilela, R. and Mendoza, L., 2010. *Pythium insidiosum*: an overview. *Veterinary Microbiology*, 146, 1-16.

[10] Benhamou, N., Rey, N., Picard, K. and Tirilly, Y., 1999. Ultrastructural and cytochemical aspects of the interaction between the mycoparasite *Pythium oligandrum* and soilborne plant pathogens. *Phytophatology*, 89(6), 506-517.

[11] Ali-Shtayeh, M.S. and Saleh, A.S.F., 1999. Isolation of *Pythium acanthicum, P. oligandrum*, and *P. periplocum* from soil and evaluation of their mycoparasitic activity and biocontrol efficacy against selected phytopathogenic *Pythium* species. *Mycopathologia*, 145, 143-153.

[12] Deacon, J.W., 1979. Cellulose decomposition by *Pythium* and its relevance to substrate-group of fungi. *The British Mycological Society*, 77(3), 469-477.

[13] Park, D., 1980. A two-year study of numbers of cellulolytic *Pythium* in river water. *The British Mycological Society*, 74(2), 253-258.

[14] Warcup, J. H., 1950. The soil-plate method for isolation of fungi from soil. *Nature*, 166(4211), 117-118.

[15] Masago, H., Yoshikawa, M., Fukada, M. and Nakanishi, N., 1977. Selective inhibition of *Pythium* spp. on a medium for direct isolation of *Phytophthora* spp. from soils and plants. *Phytopathology*, 67, 425-428.

[16] Dhingra, O.D. and Sinclair, J.B., 1994. *Basic Plant Pathology Methods*. 2nd ed. Florida: CRC Press.

[17] Stanghellini, M.E. and Kronland, W.C., 1985 Bioassay for quantification of *Pythium aphanidermatum* in soil. *Phytopathology*, 75, 1242-1245.

[18] Abad, Z.G., Shew, H.D. and Lucas, L.T. 1994. Characterization and pathogenicity of *Pythium* species isolated from turfgrass with symptoms of root and crown rot in North Carolina. *Phytopathology*, 84, 913-921.

[19] Van der Plaats-Niterink, A.J., 1981. Monograph of the genus *Pythium*. *Studies in Mycology*, 21, 1-242.

[20] Ivors, K.L., 2015. *Laboratory Protocols for Phytophthora Species*. St. Paul: The American Phytopathological Society (APS).

[21] Hung, P.M., Pongnak. W., Soytong, K. and Poeaim, S., 2015. Efficacy of *Chaetomium* species as biological control agents against *Phytophthora nicotianae* root rot in citrus. *Mycobiology*, 43(3), 288-296.

[22] Cooke, D.E.L., Drenth, A., Duncan, J.M., Wagels, G. and Brasier, C.M., 2000. A molecular phylogeny of *Phytophthora* and related Oomycetes. *Fungal Genetics and Biology*, 30, 17-32.

[23] Saitou, N. and Nei, M., 1987. The neighbor-joining method: a new method for reconstructing phylogenetic trees. *Molecular Biology* and *Evolution*, 4, 406-425.

[24] Felsenstein, J., 1985. Confidence limits on phylogenies: An approach using the bootstrap. *Evolution*, 39, 783-791.

[25] Uzuhashi, S., Ikeda, H., Kamekawa, A., Radmer, L. E., Kobayashi-Yamazaki, S., Kuroda, K., Funakubo, T., Ichikawa, K. And Tojo, M., 2019. Presence of two species-level groups in *Globisporangium splendens* isolates in Japan. *European Journal of Plant Pathology*, 154, 751–766.

[26] Lévesque, C.A. and de Cock A.W.A.M., 2004. Molecular phylogeny and taxonomy of the genus *Pythium*. *Mycological Research*, 108, 1363-1383.

[27] de Cock, A.W.A.M., Lodhi, A.M., Rintoul, T.L., Bala, K., Robideau, G.P., Abad, Z.G., Coffey, M.D., Shahzad, S. and Lévesque, C.A., 2015. *Phytopythium*: molecularphylogeny and systematics. *Persoonia*, 34, 25-39.

[28] Nam, B. and Choi, Y.J., 2019. *Phytopythium* and *Pythium* species (Oomycota) isolated from freshwater environments of Korea. *Mycobiology*, 47(3), 261-272.

[29] Ho, H.H., Chen, X.X., Zeng, H.C., and Zheng, F.C., 2012. The occurrence and distribution of *Pythium* species on Hainan Island of South China. *Botanical Studies*, 53, 525-534.

[30] Matsiakh, I., Oszako, T., Kramarets, V. and Nowakowska, J.A., 2016. *Phytophthora* and *Pythium* species detected in rivers of the Polish-Ukrainian border areas. *Baltic Forestry*, 22(2), 230-238.
[31] Ko, W.H., Wang, S.-Y. and Ann, P.-J., 2004. *Pythium sukuiense*, a new species from undisturbed natural forest in Taiwan. *Mycologia*, 96(3), 647-649.
[32] Burr, T.J. and Stanghellini, M.E., 1973. Propagule nature and density of *Pythium aphanidermatum* in field soil. *Phytopathology*, 63, 1499-1501.

Effect of Subcritical Solvent Extraction Conditions on Amount of γ-Oryzanol and γ-Tocopherol in Dawk Pa-Yom Rice Bran Oil

Duangkamol Ruen-ngam[1,2*], Chitti Thawai[2], Sujitra Sukonthamut[3] and Kittisak Khuwaranyu[4]

[1]Rattanakosin College for Sustainable Energy and Environment (RCSEE), Rajamangala University of Technology Rattanakosin, Nakhon Pathom, Thailand
[2]Department of Biology, Faculty of Science, King Mongkut's Institute of Technology Ladkrabang, Bangkok, Thailand
[3]Department of Statistics, Faculty of Science, King Mongkut's Institute of Technology Ladkrabang, Bangkok, Thailand
[4]Department of Mechanical Engineering, Faculty of Engineering and Industrial Technology, Silpakorn University, Nakhon Pathom, Thailand

Received: 13 April 2020, Revised: 10 August 2020, Accepted: 24 August 2020

Abstract

This research focused on the subcritical solvent extraction of phytochemicals γ-oryzanol and γ-tocopherol from upland rice bran (Dawk Pa-yom variety, DY). Subcritical solvent extraction was conducted using a batch reactor. The temperature was varied in range from 80 to 120°C for 20 to 60 min. The solvents in use were ethanol, methanol, and water. γ-Oryzanol and γ-tocopherol were simultaneously analyzed by HPLC. Antioxidant activity was determined by a DPPH radical assay. Methanol was able to extract a higher level of γ-tocopherol than ethanol and water. Extraction by methanol gave higher antioxidant activity than ethanol. Even though water could not extract γ-oryzanol, it was able to extract substances with higher yield of antioxidant activity than either methanol and ethanol. Increasing the extraction temperature increased the oil yield, γ-oryzanol and γ-tocopherol in parallel with an increased antioxidant activity. During the extraction process, some degradation of antioxidants was observed, and this showed the importance of kinetics parameters in this research.

Keywords: extraction; kinetics; oil recovery; solvent extraction; γ-oryzanol; γ-tocopherol; rice bran
DOI 10.14456/cast.2021.15

*Corresponding author: E-mail: duangkamolruen@gmail.com, duangkamol.ru@kmitl.ac.th, duangkamol.rue@rmutr.ac.th

1. Introduction

Nowadays, many people have concerns about health, and therefore there is great interest in valuable food products and food supplements. Especially sources of vitamin and supplement are from nature or biological source. Other than the source of raw material, the extraction method used is also a crucial part of getting high quality of supplement. There are many interesting extraction methods; soxhlet extraction, maceration, subcritical solvent extraction, and supercritical carbon dioxide extraction. The last two methods are expensive to operate; however, they are efficiency ways of extracting high quality of product. Liquefied solvent extraction or subcritical solvent extraction involves a solvent heated under pressure that depends on the solvent type. Such condition has changed the solvent properties; they generally decrease permittivity (polarity), increase diffusion rate, and decrease viscosity and surface tension. In addition, extraction under subcritical condition differs quite significantly from conventional extraction methods; it is very fast and of a hydrolytic nature [1-3].

Rice bran is a by product of the milling process and is a well-known source of phytochemicals. Bran contains large numbers of vitamins, minerals, and other nutritious items including phenolic compounds, vitamin E, and its associated components: tocols, tocopherol, tocotrienol and γ-oryzanol, which are substanes that can reduce Alzheimer's disease, cholesterol, cancer and heart disease [4-8]. Oryzanol and tocopherol are famous antioxidants and have often been found in rice. A group of ferulic acid esters of phytosterols, called γ-oryzanol and α-tocopherol, are responsible for the antioxidant activities of flavonoids and are considered excellent antioxidants. Jasmine rice, or in common name, Dawk-Mali (MA), is a famous, conventional rice variety that grows in lowland areas where flooding is regular in Thailand. Because of the drought that occurred in 2015 in the middle part of Thailand, it was impossible to grow jasmine rice. Rice variety, Dawk Pa-yom variety (DY), was able to withstand drought were grown in its place. The color of DY rice bran is dark and purplish-red color. Previous research studies have shown that the color of a bran is correlated to its phytochemical content. Specifically, the genotypes of a purple bran are significantly correlated with higher total flavonoid content (TFC) and total phenolic content (TPC), and oxygen radical absorbance capacity value than a red rice bran (attributed mainly to its flavonoid content) [6-9]. Moreover, previous researchers found that DY had higher antioxidant activity than Iranian rice bran oil and wheat oil; however, it had less activity compared to rice oil from Pone-Sai district, Thailand [1, 10, 11].

There is some previous research on plant extraction under subcritical water and subcritical organic solvent extraction [12, 13]; however, there are no reports concerning rice bran extraction. A subcritical solvent can be defined as hot solvent put under high pressure to maintain it in its liquid state. Under subcritical condition, the ion product increase and dielectric constant decrease in which non-polar bioactive compounds can be extracted. However, this could be the effect of the degradation of bioactive compound during the extraction under limited temperature. Previous reseach discussed the degradation kinetics of substances that occurred during extraction [14-16]; however, no information relevant to rice bran oil extraction was mentioned, and thus there exists the need for research into the kinetics of rice brand extraction. This research will examine subcritical extraction of rice bran under three solvent types; ethanol, methanol and water in order to increase the extracted yield of rice bran oil, γ-oryzanol and α-tocopherol. In addition, their antioxidant ability would be evaluated by DPPH assay. This research should provide new knowledge in the area of subcritical extraction.

2. Materials and Methods

2.1 Upland rice bran

Upland rice bran was used as material in this research. Upland rice bran from Dawk Pa-yom variety (DY) was obtained from the southern part of Thailand, Suratthani province. The rice bran was sieved through a standard mesh (ASTM-E11-09, Endecotts, Endecotts Logistic Center, Inc.) with a mesh size of 850 µm, then kept at -20˚C until use.

2.2 Chemicals and materials

AR grade hexane, ethyl acetate, acetone, isopropanol and ethanol were used for extraction. HPLC grade methanol, isopropanol, ethyl acetate were used for HPLC analysis. Solvents of all types were ordered from RCI Labscan Limited, Bangkok, Thailand. For antioxidant activity assay, 2,2-diphenyl-1-picrylhydrazyl (DPPH) from Sigma-Aldrich, St.Louis, Missouri was used. γ-Oryzanol was purchased from Wako, Japan. γ-Tocopherol standard grade was purchased from Wako Pure Chemical Industries Ltd, Japan.

2.3 Subcritical solvent extraction

The subcritical solvent extraction was conducted using a 500-ml SS-316 batch reactor (Parr Instrument Co., Moline, IL, USA), as shown in Figure 1. A pressure limit was set with and protected by a rupture disc. The temperature and pressure were measured and recorded over time with Parr software. A constant ratio of bran sample and solvent at 1:10 (w/v) with solvent volume of 100 ml was maintained. The mixture was placed in the pressure vessel. Solvents in use were water, methanol and ethanol. After the lid had been tightly closed, oxygen gas in the reactor was replaced with nitrogen gas, and the reactor was warmed up until the pressure reached about 1 MPa, and then the extraction began. The extraction was performed for 20-60 min under various temperatures ranging from 80 to 120°C. Although some extraction had occurred during heating, the extraction time was recorded when the temperature had already reached the desired level. After the desired extraction time was achieved, the vessel was immediately removed from the oven and cooled down for 5 min. The mixture was then filtered through a 45 µm filter paper. The solvent in the extract was evaporated with a rotary evaporator (Hei-Vap Precision, Heidolph, Germany), and then the extract was kept in a refrigerator at -20°C until further analysis. Oil yield was determined by determining the ratio between grams of crude oil and grams of dried rice bran, and expressed in dimension (g/g dried rice bran).

2.4 γ-Oryzanol and γ-tocopherol determination

The γ-oryzanol and γ-tocopherol contents were simultaneously determined with RP-HPLC system following the procedure reported in Ruen-ngam [17] and Chen and Bergman [18]. The determination system consisted of a Shimadzu 2690 Alliance separation module and a Waters 2487 dual wavelength UV/Vis absorbance detector. Chromatograms were recorded and processed with LC Solution Chromatography Software (Shimadzu, Japan). The extracted crude oil was prepared into a concentration of 30 µg/ml by using a mobile phase of 47.5% methanol, 40% isopropanol, and 12.5% ethyl acetate. Then, a volume of 20 µl was injected into ACE 5 C18 column (250×4.6 mm, ACE, Scotland), which was the stationary phase. The mobile phase flow

rate was 1.0 ml/min. The contents were detected at the wavelength of 330 nm. The γ-oryzanol concentration was calculated based on the area under the peak of a standard of known concentration, which had been prepared in the range of 0.05-50 µg/ml.

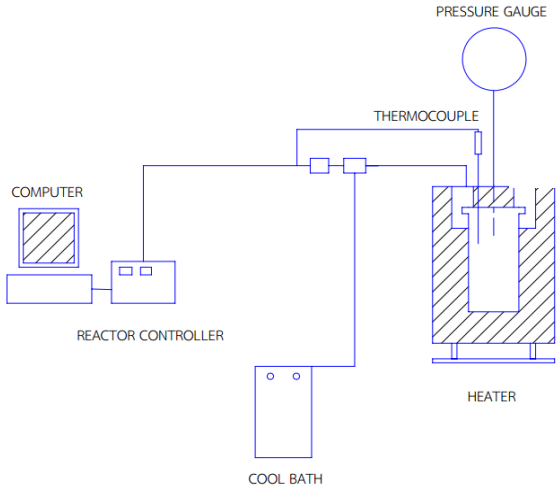

Figure 1. Experimental setup

2.5 Antioxidant activity assay

The free-radical scavenging activity of the rice bran extract was determined by DPPH radical assay according to previous research [6]. An aliquot of the sample solution was adjusted into a 0.2 mM ethanolic solution of DPPH at a ratio of 1:1 (v/v) in a 96-well plate. The well-mixed solution was then incubated for 30 min in the dark at room temperature. The absorbance was measured at 517 nm against a blank, using a UV-Vis microplate reader (EMS Reader MF, Labsystems). The results were expressed as half maximal inhibitory concentration (IC_{50}). A lower value of IC_{50} indicates a higher antioxidant activity. Percentage of inhibition of the DPPH radical was calculated by the following equation;

$$\%\ Inhibition\ = \frac{(A_{DPPH} - A_{Blank\ DPPH}) - (A_{Sample} - A_{Blank\ sample})}{(A_{DPPH} - A_{Blank\ DPPH})} \times 100 \qquad (1)$$

Where A_{Sample} is the absorbance of the extract in DPPH solution; $A_{Blank\ Sample}$ is the absorbance of the extract; A_{DPPH} is the absorbance of the DPPH solution; and $A_{Blank\ DPPH}$ is the absorbance of the solvent without DPPH.

The IC_{50} values obtained were compared to high-activity antioxidant standards: Ascorbic acid (Vit C), Trolox and BHT.

2.6 Statistical analysis

All experiments were performed in three replicates, and the mean and standard deviation were calculated. The significant differences between extraction conditions-solvent, temperature and time-were analyzed by one-way ANOVA and Duncan's new multiple range test at a significant level of 95% ($p < 0.05$).

3. Results and Discussion

3.1 Effect of solvent type

The effect of different solvent types on the amounts of extracted oil and the nutrients it contained at 100ºC subcritical extraction temperature and 40 min extraction time were tested. The preliminary results showed that methanol gave a higher (but not significantly higher at the 95% significance level) oil yield than ethanol did, which in turn, gave a higher yield than water did. In addition, the effect of solvent type on oil yield was also tested at various extraction temperatures (80, 100 and 120°C). It was found that methanol gave a higher oil yield than the other solvents did for every other temperature except at 100°C. At 100°C, methanol and ethanol gave higher ranges of yield and their yields were in the same range.

Both methanol and ethanol have similar dielectric constant values which are lower than that of water (as shown in Table 1). Therefore, they should be able to extract oil, a non-polar substance, better than water can. In general, dielectric constant, viscosity, and density of a solvent all strongly affect extraction efficiency. However, the results from this study indicate that the dielectric constant was a more predominant property than viscosity and density with regard to our extraction procedure, as methanol and ethanol (oil like non-polar solvents) with low dielectric constants produced higher oil yields than water did (polar solvent). Moreover, even though ethanol has a higher viscosity than water, it gave a higher oil yield than water did. Additionally, even though the density of water is the highest among the three solvents, it was not able to pull out the oil as well as the other two solvents.

At extraction temperature higher than 100°C, ethanol gave nearly the same range of γ-oryzanol yield as methanol did, whereas at an extraction temperature of 80°C, the ranges were quite different. It was astonishing that no content of γ-oryzanol was extracted by water as solvent even at different extraction temperatures. It might be that γ-oryzanol has a low polar structure of an alkyl group, but water does not have an alkyl group (like dissolves like). In the case of γ-tocopherol yield, methanol gave the significantly highest yield at a significant level of 95% among the the three solvents tested. Previous studies have found that both γ-oryzanol and γ-tocopherol showed a DPPH radical scavenging capability, and one substance was more dominant than the other depending on the type of the biological system [19, 20].

3.2 Effect of temperature

The extraction yield results of bran oil, γ-oryzanol and γ-tocopherol in previous sections demonstrated that methanol was able to achieve the highest yield of these compounds. Therefore, in the investigation of the effect of temperature, the focus was on methanol. Increasing the extraction temperature increased the oil yield because doing so decreased the density and viscosity of methanol (results not show here). Moreover, its dielectric constant seems to be decreased, as shown in the properties of water in Table 1. The lower density and viscosity of methanol enabled it to easily penetrate through the porous material, pull the oil out, and make the oil dissolved in the solvent on the outside. At the same time, the substances that were dissolved in the oil-γ-oryzanol and γ-tocopherol also came out. The highest amounts of γ-oryzanol and γ-tocopherol achieved by methanol extraction were around 12.12±0.48 and 397.70±2.82 mg/g dried rice bran, respectively. When the extraction temperature was increased up to 120°C, the extract still had good quality as shown in Figure 2. The IC_{50} values at 100 and 120°C were in almost the same range which were due to nearly the same amounts of γ-oryzanol extracted out at these temperatures (1.74±0.14 mg/ml). It was expected that with further increase of extraction temperature over 120°C,

Table 1. Solvent properties

Solvent types	T (°C)	p_v[1]	ρ_l[2]	ρ_v[3]	μ_l[4]	μ_v[5]	σ_l[6]	ε_r[7]
Ethanol	80	1.086	0.757	1.43	0.432	1.03	17.3	25.3 (20°C)
	100	2.26	0.73	3.41	0.318	1.092	15.5	
	120	4.29	0.71	6.01	0.243	1.157	13.4	
Methanol	80	1.819	0.7355	0.00208	0.271	115	17.5	33.0 (20°C)
	100	3.731	0.714	0.00398	0.214	123	15.7	
	120	6.551	0.69	0.00714	0.17	130	13.6	
Water	80	0.47359	0.97182	0.2932	0.351	113	62.69	80.1 (20°C)
	100	1.01325	0.95877	0.5974	0.279	121	58.91	10 (360°C)
	120	1.9854	0.94339	1.121	0.23	128	54.96	

Remarks: Ethanol: Boiling point = 78.1°C, Critical point = 241°C, 6.3 MPa
Methanol: Boiling point = 64.7°C, Critical point = 240°C, 7.7 MPa
Water: Boiling point = 100°C, Critical point = 374°C, 21.3 MPa
Data in Table were available from https://www.engineeringtoolbox.com/liquid-dielectric-constants-d_1263.html
[1]Saturation pressure (10^5 Pa)
[2]Liquid density (10^3kg/m³)
[3]Vapor density (kg/m³)
[4]Liquid viscosity (10^{-3}N-s/m²)
[5]Vapor viscosity (10^{-5}N-s/m²)
[6]Liquid surface tension (10^{-3}N/m)
[7]Dielectric constant

the antioxidant activity from γ-oryzanol might be degraded. At 120°C, γ-tocopherol might be the dominant substance that provided the antioxidant activity which was the reason that the IC_{50} value at this temperature did not decrease.

Therefore, for energy saving, the extraction temperature at 100°C was deemed to be the optimum temperature for extraction of this bran oil extraction. However, the γ-oryzanol concentration achieved was low for the material pretreated, implying some degradation, while other studies report that the amount of γ-oryzanol remained quite constant as the heating temperature was increased from 60°C to 110°C. Thus, it was expected that with the extraction temperature of more than 120°C, degradation of γ-oryzanol would be pronounced [21, 22]. This research also demonstrated the γ-oryzanol degradation kinetics in Section 3.4.

3.3 Effect of time

The amounts of rice bran oil, γ-oryzanol, γ-tocopherol yield and IC_{50} values for different periods of extraction time and at each temperature in methanol are shown in the extraction curves in Figures 2 (a)-(d). The oil yield increased sharply with time for the first 20 min and the rate of increase gradually slowed until the final yield. This behavior was the same for all temperatures. However, the extraction time of 60 min gave the significantly highest oil yield at the level of 95%.

The amounts of γ-oryzanol and γ-tocopherol followed a similar trajectory to the oil yield and reached the maximum at 60 min at the significant level of 95% as shown in Figures 2 (b)-(c). This behavior might be because initially the oil was extracted out easily from the immediate mass with which the solvent was in contact, but as time passed, it was difficult for the subcritical solvent to reach the inside mass of the material, and this corresponded to the period of gradual increase after the first 20 min.

In addition, the overall extraction curve in Figure 2 was used to calculate the solubility of the oil by dynamic method from the slope of the initial part of the overall extraction curve. The solubilities of all of the extracted substances—oil, γ-oryzanol and γ-tocopherol—increased when a higher extraction temperature was used. Initially, the γ-oryzanol yield increased sharply with time and then changed to more gradual increase in the second section, and this curve will be further used in the activation energy calculation in the following section. This increase in the solubility increased the driving force in the fluid phase. The maximum solubility of all substances were found at 120°C and the solubilities of oil, γ-oryzanol and γ-tocopherol were 0.0185, 0.4275 and 9.080 mg/g dried rice bran, respectively. It is surprising that the amount of γ-tocopherol continuously increased at extraction time longer than 40 min at the temperature of 120°C. It might be that the increased extraction temperature softened the hard mass of the rice bran and decreased the viscosity of the solvent so that it was able to penetrate deeply and easily into the material inside [22-25].

The amount of antioxidants increased significantly with time at120°C; howver, they contrasted with IC_{50} value which gradually increased. The IC_{50} at 120°C was in the same range as the IC_{50} at 100°C. This may indicate some degradation of substance. The IC_{50} antioxidant activity of extracted oil (1.74 mg/ml) was lower compared to other well-known antioxidants; Vit C (5.99 $\times 10^{-3}$ mg/ml), Trolox (14.47 $\times 10^{-3}$ mg/ml) and BHT (0.18 mg/ml).

3.4 Overall degradation of substances

The overall extraction curve in Figure 2 shows that for extraction times longer time than 20 min, the amounts of oil, γ-oryzanol and γ-tocopherol gradually decrease because of substance degradation. Therefore, this section offers information about the kinetic of degradation of such compounds. The graph plotted according to equation (2) shows that the fraction of γ-oryzanol is linearly related to time at constant temperature ranging from 80 to 120°C as shown in Figure 3. The trend of the curve was similar to that found by Debnath *et al*. [26]. The previous section in this work demonstrated the high extraction rate of γ-oryzanol in the first 20 min of extraction, which was followed by a decreased extraction rate. There was a similar trend occurred in the cases of the oil and γ-tocopherol. This indicates that the degradation process can be expressed by pseudo-first order kinetics. Activation energy and pre-exponential factor were calculated according to a pseudo-first order reaction kinetics by plots based on the natural logarithm of a Arrhenius equation as follows:

A pseudo-first order reaction:
$$\ln\left(\frac{C}{C_0}\right) = -kt \quad (2)$$

Arrhenius equation:
$$k = \mathrm{A}e^{\frac{-E_a}{RT}} \quad (3)$$

Taking the natural logarithm of (3):
$$\ln(k) = \frac{-E_a}{R}\left(\frac{1}{T}\right) + \ln(A) \quad (4)$$

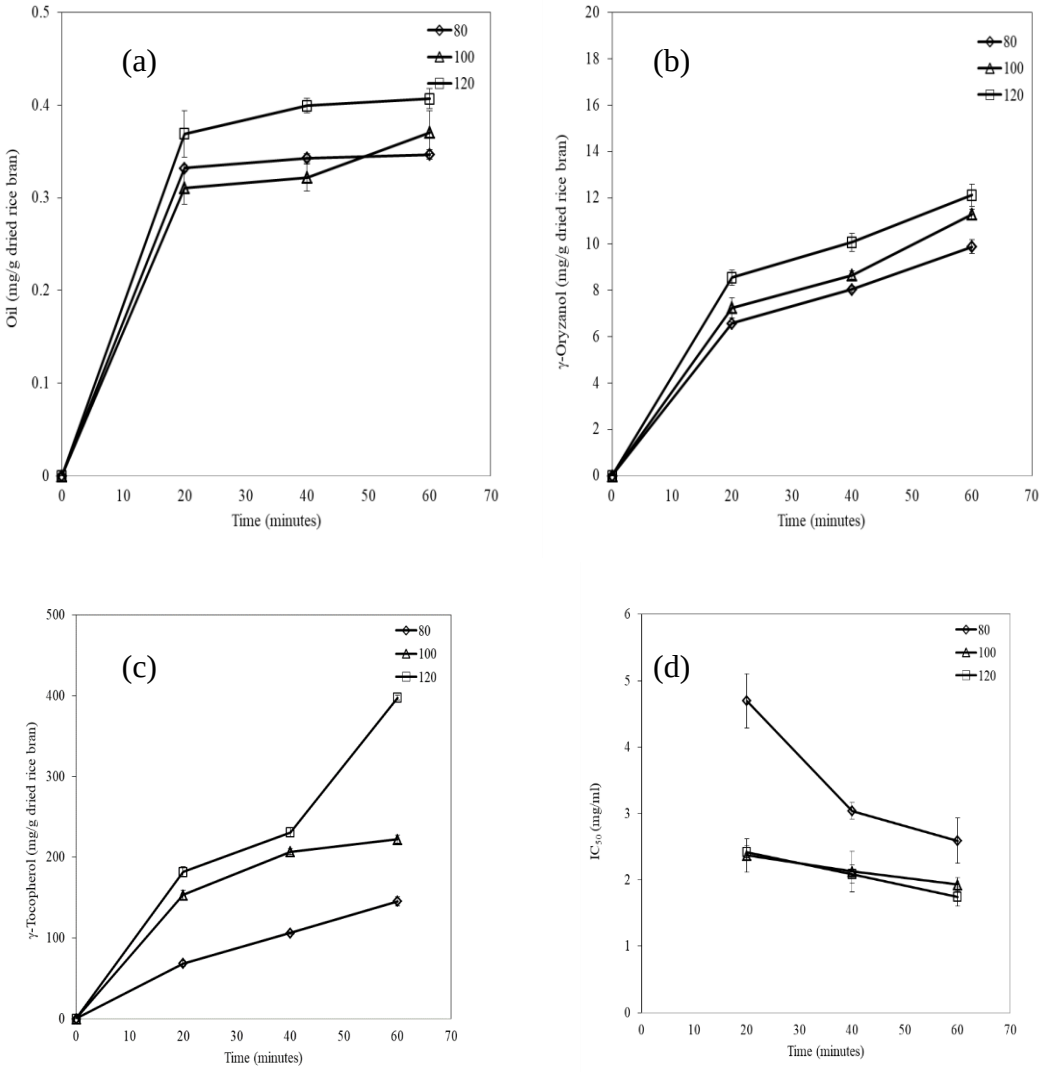

Figure 2. Effect of time and temperature on the yields in extracted DY rice bran oil under subcritical methanol; (a) oil, (b) γ-oryzanol, (c) γ-tocopherol, and (d) IC_{50}

Where C is concentration of γ-oryzanol in the solvent, C_o is initial concentration of γ-oryzanol in rice bran (mg/g rice bran), t is time, T is temperature, E_a is activation energy (kJ/mole) and A is pre-exponential factor (min^{-1})

The kinetic parameters are demonstrated in Table 2. The values of the kinetic parameters in Table 2 are in the same range as those for the degradation of folic acid (Ea = 69.9 kJ/mole) [24].

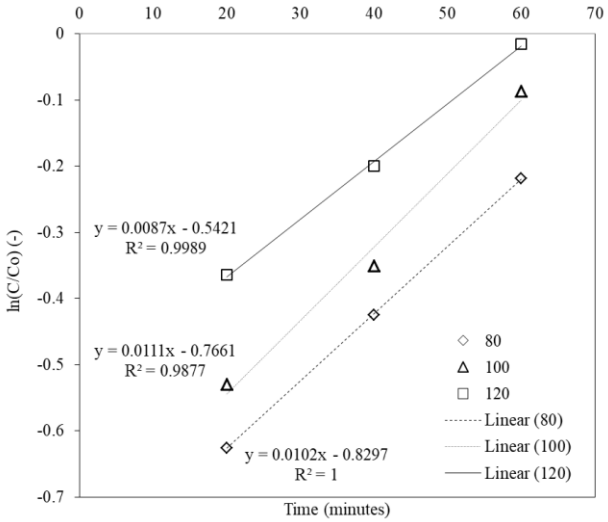

Figure 3. Plots of $\ln(C/C_o)$ vs. time for determining Arrhenius parameters of γ-oryzanol

Table 2. Activation energy (E_a) and pre-exponential factor (A) for pseudo-first order degradation kinetics of components in rice bran oil

Compositions	A (min^{-1})	E_a (kJ/mole)
Oil	0.0023	23.500
γ-Oryzanol	0.0024	4.413
γ-Tocopherol	0.0170	0.299

3.5 Comparison of conventional extraction

The results of extracted yield under methanolic subcritical extraction were then compared to the extraction results when using a soxhlet apparatus and done by ethanol extraction for 8 h at boiling point (78°C). The oil and γ-oryzanol were lower than those obtained from soxhlet extraction. The oil yield from methanolic subcritical extraction ranged from 81.03 to 99.25% of that produced by soxhlet extraction, and γ-oryzanol came in at 58.88 to 91.75% of Soxhlet extraction yield, a result with a wide range that might have been due to extraction time. The amount of γ-tocopherol at 60 min was higher (106.66%) than that obtained from soxhlet extraction. This experimental method used less time than did the conventional extraction method. Solvent type and solvent properties effected the amount of substance extracted. Solvent properties, especially viscosity and surface tension, seemed to be more effective at elevated temperatures as shown in the properties in Table 1. Moreover the solvent under high pressure changed phase to be ionic in nature, and therefore it could more easily penetrate and flow through the material than fluid phase [25, 26].

4. Conclusions

Subcritical solvent extraction was investigated as an alternative extraction method. Methanol produced the highest yield of oil, γ-oryzanol, and γ-tocopherol. The temperature and the time of 100°C and 60 min were optimal conditions for obtaining the highest yield of such compounds that also had the highest antioxidant activity. The highest oil yield obtained around 0.40±0.01 mg/g dried rice bran. γ-Oryzanol and γ-tocopherol had the highest value at around 12.12±0.48 and 397.70±2.82 mg/g dried rice bran, respectively. When extraction temperature was increased in range 80 to 120°C, there was some degradation of substance observed and the kinetics of degradation was also noted. Although methanol is not a green solvent, this research demonstrated its potential its potential use as a subcritical solvent that may be applied in further specific use.

5. Acknowledgements

This research was supported by research funding with Grant number KREF025603 from King Mongkut's Institute of Technology Ladkrabang.

References

[1] Butsat, S. and Siriamornpun, S., 2010. Antioxidant capacities and phenolic compounds of the husk, bran and endosperm of Thai rice. *Food Chemistry*, 119, 606-613.

[2] Chia, S.L., Boo, H.C., Muhamad, K., Sulaiman, R., Umanan, F. and Chong, G.H., 2015. Effect of subcritical carbon dioxide extraction and bran stabilization methods on rice bran oil. *Journal of the American Oil Chemists' Society*, 92, 393-402.

[3] Ravber, M., Knez Z. and Škerget, M. 2015. Simultaneous extraction of oil- and water-soluble phase from sunflower seeds with subcritical water. *Food Chemistry*, 166, 316-323.

[4] Xu, Z. and Godber, J.S., 2001. Antioxidant activities of major components of γ-oryzanol from rice bran using a linoleic acid model. *Journal of the American Oil Chemists' Society*, 78, 645-649.

[5] Zigoneanu, I.G., Williams, L., Xu, Z. and Sabliov, C.M., 2008 Determination of antioxidant components in rice bran oil extracted by microwave assisted method. *Bioresource Technology*, 99(11), 4910-4918.

[6] Ruen-ngam, D., Thawai, C., Sukonthamut, S., Nokkoul, R. and Tadtong, S., 2018. Evaluation of nutrient content and antioxidant, neuritogenic and neuroprotective activities of upland rice bran oil. *Journal of the Science Society of Thailand*, 4(4), 257-267.

[7] Bao, J.S., Cai, Y., Sun, M., Wang, G.Y. and Corke, H., 2005. Anthocyanins, flavonoids, and free radical scavenging activity of Chinese bayberry (*Myrica rubra*) extracts and their colour properties and stability. *Journal of Agricultural and Food Chemistry*, 53, 2327-2332.

[8] Shen, Y., Jin, L., Xiao, P., Lu, Y. and Bao, J., 2009. Total phenolics, flavonoids, antioxidant capacity in rice grain and their relations to grain color, size and weight. *Journal of Cereal Science*, 49, 106-111.

[9] Chen, M., McClung, A.M. and Bergman, C.J., 2016. Concentrations of oligomers and polymers of proanthocyanidins in red and purple rice bran and their relationships to total phenolics, flavonoids, antioxidant capacity and whole grain color. *Food Chemistry*, 208, 279-287.

[10] Araba, F., Alemzadehb, I. and Maghsoudi, V., 2011. Determination of antioxidant component and activity of rice bran extract. *ScientiaIranica C*, 18(6), 1402-1406.
[11] Brewer, L.R., Kubola, J., Siriamornpun, S., Herald, T.J. and Shi, Y.C., 2014. Wheat bran particle size influence on phytochemical extractability and antioxidant properties. *Food Chemistry*, 152, 483-490.
[12] Piñeiro, Z., Palma, M. and Barroso, G.C., 2004. Determination of catechins by means of extraction with pressurized liquids. *Journal of Chromatography A*, 1026, 19-23
[13] Marcus, Y., 2018. Review extraction by subcritical and supercritical water, methanol, ethanol and their mixtures. *Separations*, 5, 4, https://doi.org.10.3390/separations5010004
[14] Delchier, N., Ringling, C., Maingonnat, J., Rychlik, M. and Renard, M.G.C.C., 2014. Mechanisms of folate losses during processing: Diffusion vs. heat degradation. *Food Chemistry*, 157, 439-447.
[15] Tangboontina, A., 1986. *Kinetics of Folic Acid Degradation during Heat Processing*. M.Sc. Faculty of Science, Chulalongkorn University.
[16] Suganya, T. and Renganathan, S., 2012. Optimization and kinetic studies on algal oil extraction from marine macroalgae *Ulva lactuca*. *Bioresource Technology*, 107, 319-326.
[17] Ruen-ngam, D., Thawai, C., Nokkoul, R. and Sukonthamut, S., 2014. Gamma-oryzanol extraction form upland rice bran. *International Journal of Bioscience and Biochemistry*, 4(4), 252-255.
[18] Chen, M.H. and Bergman, C.J., 2005. A rapid procedure for analysing rice bran tocopherol, tocotrienol and g-oryzanol contents. *Journal of Food Composition and Analysis*, 18, 139-151.
[19] Juliano, C., Cossu, M., Alamanni, M.C. and Piu, L., 2005. Antioxidant activity of gamma-oryzanol: mechanism of action and its effect on oxidative stability of pharmaceutical oils. *International Journal of Pharmaceutics*, 299(1-2), 146-54.
[20] Cocero, J.M., Cabeza, Á., Abad, N., Adamovic, T., Vaquerizo, L., Martínez, C.M. and Pazo-Cepeda, M.V., 2018. Understanding biomass fractionation in subcritical&supercritical water: Review. *Journal of Supercritical Fluid*. 133, 550-565.
[21] Malekian, F., Rao, R.M., Prinyawiwatkul, W., Marshall, W.E., Windhauser, M. and Ahmedna, M., 2000. *Lipase and Lipoxygenase Activity, Functionality, and Nutrient losses in Rice Bran during Storage*. Louisiana: Louisiana State University Agricultural Center and Louisiana Agricultural Experiment Station.
[22] Kim, M., Park, J.W., Kim, J.Y., Park, K.W., Lee, S., Jang, J. and Lee, J.H., 2013. Effects of heat treatment and visible light exposure on the oxidative stability of rice bran and of rice bran oil. *Food Science and Biotechnology*, 22, 1223-1228.
[23] Pourali, O., Asghari, F.S. and Yoshida, H., 2010. Production of phenolic compounds from rice bran biomass under subcritical water conditions. *Chemical Engineering Journal*, 160, 259-266.
[24] Thanonkaew, A., Wongyai, S., McClements, D.J. and Decker, E.A., 2012. Effect of stabilization of rice bran by domestic heating on mechanical extraction yield, quality, and antioxidant properties of cold-pressed rice bran oil (*Oryzavsaltiva* L.). *LWT-Food Science and Technology*, 48, 231-236.
[25] Shin, T., Godber, S.J., Martin, D.E. and Wells, J.H., 1997. Hydrolytic stability and changes in E vitamers and oryzanol of extruded rice bran during storage. *Journal of Food Science*, 62, 704-708.
[26] Debnath, S., Rastogi, N.K., Krishna, A.G.G. and Lokesh, B.R., 2012. Effect of frying cycles on physical, traditional fried food. *Food and Bioproducts Processing*, 90, 249-256.

Current Applied Science and Technology Vol. 21 No. 1 (January-March 2021)

Adsorption of Dye Over Lignin Obtained from Wastewater Separation

Pummarin Khamdahsag[1], Thitisuda Jarichanon[2], Jakkapop Phanthasri[2], Suttikorn Suwannatrai[2], Bhuckchanya Pangkumhang[3] and Visanu Tanboonchuy[2,4,5]*

[1]Environmental Research Institute, Chulalongkorn University, Bangkok, Thailand
[2]Department of Environmental Engineering, Faculty of Engineering, Khon Kaen University, Khon Kaen, Thailand
[3]Chronic Kidney Disease Preventing in the Northeast of Thailand (CKDNET), Faculty of Medicine, Khon Kaen University, Khon Kaen, Thailand
[4]Research Center for Environmental and Hazardous Substance Management (EHSM), Khon Kaen University, Khon Kaen, Thailand
[5]Research Program on Development of Appropriate Technologies for Coloring Agent Removal from Textile Dyeing, Pulp & Paper, and Sugar Industries for Sustainable Management, Center of Excellence on Hazardous Substance Management (HSM), Chulalongkorn University, Bangkok, Thailand.

Received : 22 January 2020, Revised: 5 August 2020, Accepted: 24 August 2020

Abstract

Lignin is a major by-product problem for the pulp and paper industry. In our previous work, lignin was successfully separated from alkali lignin wastewater using iron (III) trimesic (Fe-BTC). This separation resulted in three layers: supernatant, lignin sludge, and Fe-BTC powder. In this study, the lignin separated by Fe-BTC (LSF) was expected to be used as an adsorbent for reactive red-120 dye (RR-120) removal. The LSF morphology was characterized by scanning electron microscope and energy dispersive X-ray spectrometer (SEM-EDS), the specific surface area was analyzed by Brunauer-Emmett-Teller (BET) method, and the functional groups were investigated by Fourier transform infrared (FTIR) spectrometer. The removal performance of LSF over RR-120 was approximately 35% in 60 min. The maximum adsorption capacity of LSF for RR-120 was found to be 10.363 mg/g. The adsorption kinetic of RR-120 removal fitted well with the pseudo-second-order kinetic model. The adsorption isotherm model of LSF also fitted with the Langmuir isotherm model. This research suggests the high potential of LSF as a lignin-based adsorbent agent for RR-120 removal in water.

Keywords: adsorption; dye; iron (III) trimesic; lignin; reactive red-120
DOI 10.14456/cast.2021.16

*Corresponding author: Tel.: +664-336-2140 Fax: +664-320-2571
E-mail: visanu@kku.ac.th

1. Introduction

Dyes are commonly used in industry, and in particular the textile industry consumes a large amount of water and discharges dyes as its main pollutant. These dyes are predominantly organic compounds that are difficult to be degraded and have strong toxicity. Therefore, when the dyes enter the environment, they may accumulate in some aquatic organisms [1]. Generally, synthetic dyes are divided into acidic, reactive, direct, basic, and other groups. Although different dyes are used in industries, azo and reactive classes are by far the most commonly used dyes [2]. Reactive dyes are typically azo-based chromophores combined with different types of reactive groups such as vinyl sulfone, chlorotriazine, trichloropyrimidine, and difluorochloropyrimidine [1]. Therefore, these dyes must be removed from industrial wastewater before discharging into recipient waters. Among the reactive dyes in the textile industry, reactive red-120 (RR-120) is one of the often-used dyes being hardly biodegradable associated with having aromatic rings in its structure [3]. Therefore, it must be removed from industrial wastewater before the wastewater is discharged into receiving waters.

There are several treatment technologies such as ion-exchange, adsorption, chemical precipitation, membrane filtration, flocculation, coagulation, and electrochemical methods that have been employed to treat dye-contaminated effluents [4]. Of these techniques, adsorption is one of the most common processes used in water and wastewater treatment. It is more productive in terms of economy, design and operation, and high efficiency. Mostly, adsorption is reversible because of the weak Van der Waals bonds between adsorbent and adsorbate [5].

Currently, novel materials are being investigated for their adsorptive potentiality, which obtain from agriculture by-products, industrial by-products, industrial waste biomass, and natural materials. In this study, a by-product from pulp and paper industry or lignin was tested for use as an adsorbent due to its primary properties: accessibility, high porosity, and high specific surface, which are characteristics that point to it being very beneficial in adsorption process [6].

Special attention was paid to lignin obtained from a pulp and paper wastewater treatment by iron (III) trimesic (Fe-BTC), which was used as coagulant-flocculant in a former study by our team [7]. After the treatment, three layers including supernatant, alkaline lignin sludge, and Fe-BTC powder occurred, and were simply separated [7]. Typically, in the pulp and paper industry, lignin is burned and used as not only a fuel source but also as an added value adsorbents because of its its high porosity and specific surface area [8]. Moreover, lignin has a variety of functional groups that give it the necessary characteristics to be an adsorbent [9, 10].

This research aimed to investigate the utilization of alkaline lignin separated with Fe-BTC (LSF) for use as an RR-120 adsorption. Experiments with various operating parameters such as RR-120 initial concentration and contact time of RR-120 adsorption were conducted. The adsorption kinetics and adsorption isotherm results were used to estimate the potential of LSF as an adsorbent agent for RR-120 removal.

2. Materials and Methods

2.1 Materials

Alkaline lignin (CAS no.: 8068-05-1) was purchased from Tokyo Chemical Industry CO., LTD. Ferric chloride hexahydrate ($FeCl_3.6H_2O$) was a QRëC New Zealand product. Benzene-1,3,5-tricarboxylic acid (H_3BTC) was purchased from Sigma-Aldrich. Ethanol was purchased from RCI Labscan. RR-120 was an analytical grade. Deionized (DI) water and reverse osmosis (RO) water were lab grade.

2.2 Lignin adsorbent and wastewater preparation

2.2.1 Adsorbent preparation

LSF as an adsorbent was obtained from wastewater via a coagulation process using Fe-BTC as coagulant-flocculant following our previous report [7]. As shown in Figure 1, Fe-BTC powder and LSF sludge settled separately; Fe-BTC at the bottom, LSF in the middle, and clear supernatant at the top. Then, LSF and Fe-BTC powder were separated by centrifuge and washed with RO water for several times. Next, LSF was dried in a hot air oven at 103 ℃ for 24 h. The dark-brown powder was collected and kept in a desiccator.

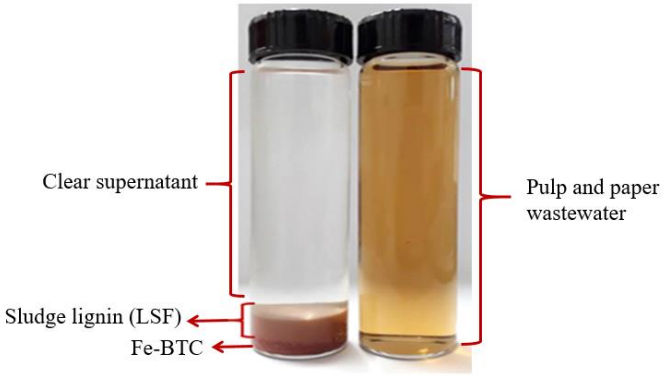

Figure 1. Separation of wastewater into layers: Fe-BTC powder at the bottom, LSF in the middle, and clear supernatant at the top

2.2.2 Wastewater preparation

The stock of synthetically colored wastewater was prepared by dissolving RR-120 in RO water. Likewise, the synthetic wastewater was prepared by dissolving LSF in DI water.

2.3 Characterization

The morphology of the LSF was recorded using a scanning electron microscopy and energy dispersive X-ray spectrometer (SEM-EDS) (LEO, 1450 VP) with a magnification of 5000x. A BET surface area pore size and pore volume distribution analyzer (BEL-Japan, BELSORP-mini II) was used to measure the specific surface area, pore-volume, and pore diameter of LSF. The degassing temperature was set at 150 °C. The functional groups of the LSF samples were investigated by Fourier transform infrared (FTIR) spectrometer (Bruker, TENSOR27) using the KBr pellet method and scanning over the range of 400 and 4000 cm^{-1}. The characteristics of LSF were compared to those of pristine alkaline lignin (PAL).

2.4 Adsorption kinetic models

The adsorption kinetic was conducted in a beaker with magnetic stirring to complete mixing at room temperature (30±1°C) in order to find the most suitable contact time. Based on the preliminary study, the adsorption kinetic was performed at the most suitable experimental conditions: an RR-120 initial concentration of 10 mg/l for 1 l, pH 6.5, and LSF dosage of 0.5 g/l. The sampling follows the

predetermined time until suitable contact time, and these samples were filtered using 0.45 μm-pore-size PTFE filters. The concentrations of the sample were analyzed by UV-vis spectrophotometer (HACH, DR 6000) under a maximum wavelength of 536 nm. The removal efficiency (R) and adsorption capacity of RR-120 (Q_e, mg of dye/g of adsorption) were calculated using the Equations (1) and (2) below,

$$R(\%)=\frac{C_0 - C_e}{C_0} x100 \quad (1)$$

$$Q_e=\frac{C_0 - C_e}{W} xV \quad (2)$$

where C_0 is the initial concentration (mg/l); C_e is the final concentration (mg/l); W is the mass of LSF (g); and V is the volume of RR-120 solution (l).

Adsorption kinetic models were proposed to understand the mechanism and to scale-up the efficiency of adsorption. To investigate the potential rate-determining step such as pseudo-first-order and pseudo-second-order kinetic models, the experimental data were tested. The linear form of the pseudo-first-order and pseudo-second-order models are given by the Equations (3) and (4),

$$\ln(q_e - q_t) = \ln q_e - k_1 t \quad (3)$$

$$\frac{t}{q_t}=\frac{1}{k_2 q_e^2}+\frac{t}{q_e} \quad (4)$$

where q_e and q_t are the amounts of RR-120 adsorbed by LSF at equilibrium and at various time t (mg/g); k_1 is the equilibrium rate constant of pseudo-first-order kinetics (min^{-1}); t is the contact time (min); k_2 is the equilibrium rate constant of the pseudo-second-order kinetics (g/mg-min) [11].

2.5 Adsorption isotherm models

Adsorption isotherms were conducted at different RR-120 initial concentrations from 0.5 to 30 mg/l at room temperature (30 ± 1 °C) for 60 min. In this process, the concentrations of RR-120 in the solution were always determined with a UV-Vis spectrophotometer (HACH, DR 6000) under a maximum wavelength of 536 nm. The analysis of equilibrium data by fitting to different isotherm models is important in the estimation of practical adsorption capacity and optimization of adsorption system design. The results from the study were therefore calculated using two models including Langmuir and Freundlich adsorption isotherm models, which are the most commonly used theoretical models. The models can be expressed by the Equations (5) and (6),

$$\text{Langmuir; } Q_e=\frac{Q_m K_L C_e}{1+K_L C_e} \quad (5)$$

$$\text{Freundlich; } Q_e=K_F C_e^{1/n} \quad (6)$$

where C_e is the RR-120 equilibrium concentration (mg/l) and Q_e is the adsorption amount of RR-120 after adsorption equilibrium (mg/g). Q_m is the theoretical saturated adsorption capacity (mg/g) and K_L is a Langmuir constant representing the affinity of adsorbate and adsorbent (l/mg). K_F is a

Freundlich constant indication of the relative adsorption capacity of adsorbent (mg/g) and 1/n is the adsorption intensity [12].

3. Results and Discussion

3.1 Characteristics of LSF

The morphologies of PAL and LSF from the SEM analysis technique is shown in Figure 2. PAL showed large particles with bare smooth surfaces, while LSF presented small fragments on the smooth surface of bulk particles. The semi-quantitative elemental results of PAL and LSF obtained from SEM-EDS analysis are presented in Table 1. The elements resulting in LSF held Fe about 5.74% whereas there was no Fe presented on PAL.

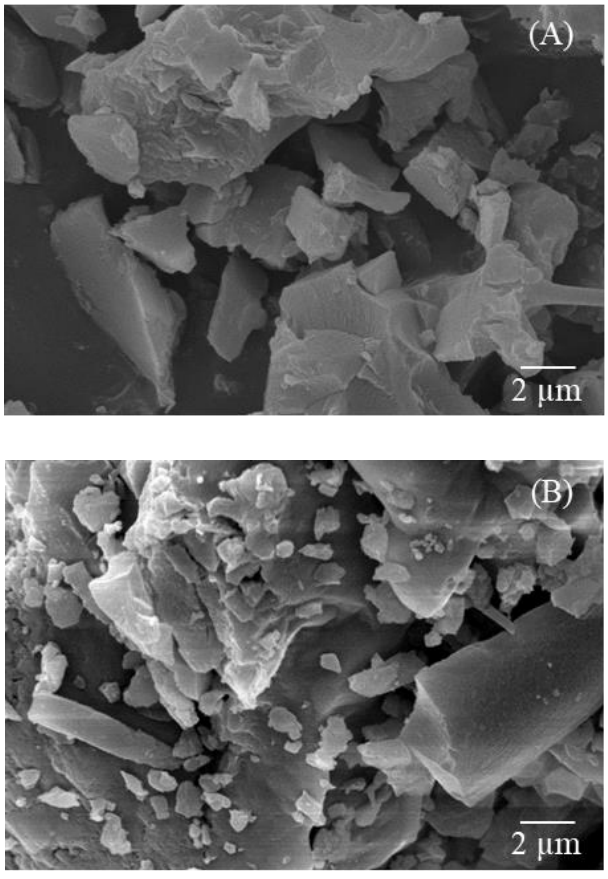

Figure 2. SEM images of (A) pristine alkaline lignin (PAL) and (B) lignin separated by Fe-BTC (LSF)

Table 1. Semi-quantitative elemental results of PAL and LSF obtained from SEM-EDS

	Weight (%)						
	C	**O**	**Na**	**Mo**	**Fe**	**Others**	**Total**
PAL	66.35	24.46	5.32	3.87	-	-	100
LSF	63.88	17.43	5.36	1.78	5.74	5.81	100

The specific surface area from the BET method (S_{BET}), total pore volume (V_p), and pore diameter (d_p) of PAL and LSF are shown in Table 2. The S_{BET} of LSF was found at 3.71 m^2/g and that was 3.37 times higher than that of PAL (1.10 m^2/g). The low value of PAL S_{BET} supported the interpretation of the material roughness observed from SEM. An increase in LSF S_{BET} could be related to the small fragments. The increase of LSF S_{BET} is supposed to be beneficial for an adsorbent. The total pore volume (V_p) of LSF was more than PAL, and the average pore size of LSF was also increased. Besides, the d_p of LSF (29.44 nm) is classified as a mesoporous material as recommended by IUPAC.

Table 2. Specific surface area from the BET method (S_{BET}), total pore volume (V_p), and pore diameter (d_p) of PAL and LSF

	S_{BET} (m^2/g)	**V_p (cm^3/g)**	**d_p (nm)**
PAL	1.10	0.01	17.00
LSF	3.71	0.02	29.44

FTIR spectra were recorded to identify functional groups in the lignin. The FTIR peaks of PAL and LSF are shown in Figure 3. The C-H stretching peaks at 2944 and 2842 cm^{-1} appeared only on the PAL as well as guaiacyl lignin units of C-C, C-O, C=O at 1604, 1127, and 823 cm^{-1}, respectively. The nitro compound stretching at 1523 cm^{-1} was also observed for the PAL. For LSF, the peak at 1706 cm^{-1} on LSF was interpreted as carboxylic acid. The LSF FTIR peak of 1625 to 700 cm^{-1} seemed to be the combination of FTIR from Fe-BTC and lignin [7]. The C=O bond at 1625 cm^{-1}, SO_3 groups stretching at 1042 cm^{-1}, C–O bond at 1381, 1220, and 1050 cm^{-1}, and C–H bond at 762 and 700 cm^{-1} were observed for LSF. The Fe-O at 611 and 478 cm^{-1} were also shown which were due to the Fe releasing from unsaturated sites of Fe-BTC [6, 13, 14]. The existence of Fe-O was associated with the results from SEM-EDS. Therefore, there was a good possibility to utilize the LSF as RR-120 adsorbent compared to the PAL.

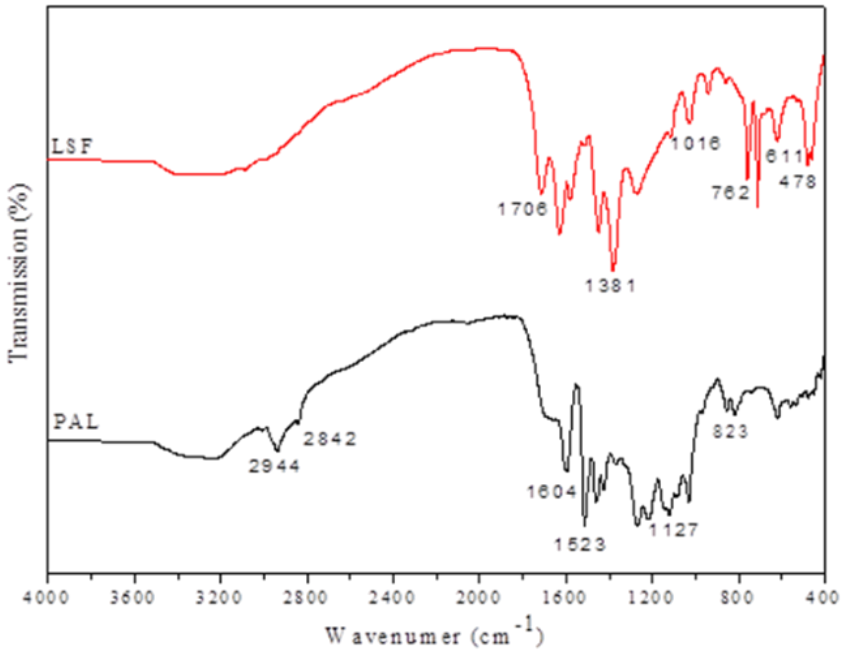

Figure 3. FTIR spectra of pristine alkaline lignin (PAL) and lignin separated by Fe-BTC (LSF)

3.2 Adsorption kinetics

The effect of contact time on the adsorption of RR-120 at room temperature (30 ± 1°C) by LSF was done under the RR-120 initial concentration of 10 mg/l, pH of 6.5, and LSF dosage of 0.5 g/l, as presented in Figure 4. It was found that approximately 35% of the equilibrium adsorption capacity for RR-120 occurred within 60 min. The adsorption ability of LSF is probably due to the Fe-O remaining in the LSF structure. The blank tests of LSF in DI water and RR-120 in RO water for interference and photolysis-volatilization, respectively, were found insignificantly.

To investigate the adsorption kinetics, pseudo-first-order and pseudo-second-order models were applied. Table 3 summarizes the calculated parameters of kinetic modeling. Based on the R^2 value, the kinetic of RR-120 adsorption fitted well with a pseudo-second-order model. This implies that the adsorption kinetic follows the pseudo-second-order rate mechanism with higher values of correlation coefficient ($R^2 = 0.983$), q_2 of 4.919 mg/g, and k^2 of 0.047 g/mg-min. Besides, this model assumes the rate-limiting step of adsorption as chemisorption between the molecules of RR-120 and the active sites of the LSF [15].

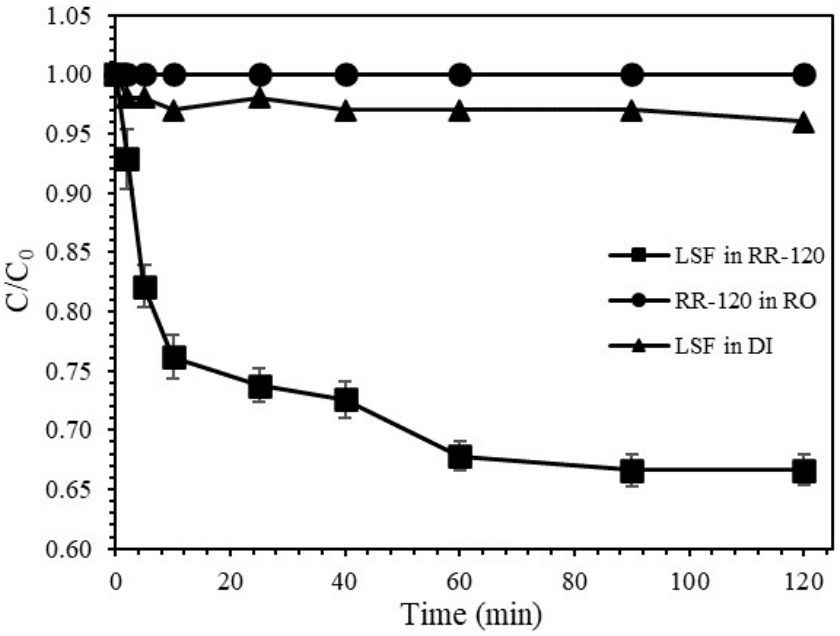

Figure 4. Effect of contact time on the adsorption of RR-120 on LSF

Table 3. Kinetic parameters of the pseudo-first-order and pseudo-second-order kinetic models for the adsorption of RR-120 on LSF

Pseudo-first-order	**q_1 (mg/g)**	**k_1 (min^{-1})**	**R^2**
	3.155	0.124	0.928
Pseudo-second-order	**q_2 (mg/g)**	**k_2 (g/mg-min)**	**R^2**
	4.919	0.047	0.983

3.3 Adsorption isotherm

The adsorption isotherms describe the distribution of adsorbate species between the liquid phase when the adsorption process reaches an equilibrium state. To obtain the adsorption capacity of LSF for RR-120, the experimental conditions were under pH 6.5, LSF dosage of 0.1 g/l, room temperature (30±1°C), and contact time of 60 min. The maximum adsorption capacity (Q_m) of RR-120 on LSF was found at 10.363 mg/g as presented in Table 4. In Figure 5, the higher correlation coefficient of the Langmuir isotherm model ($R^2 = 0.965$) means that the behavior adsorption RR-120 by LSF matched the isotherm which describes the homogeneous system. Moreover, the adsorption can be characterized as monolayer adsorption, and the adsorption equilibrium is steady-state [16].

Table 4. Langmuir and Freundlich isotherm model parameters for the adsorption of RR-120 on LSF

Langmuir isotherm	**Q_m (mg/g)**	**K_L (L/mg)**	**R^2**
	10.363	0.065	0.965
Freundlich isotherm	**K_F (mg/g)**	**n**	**R^2**
	1.015	1.695	0.938

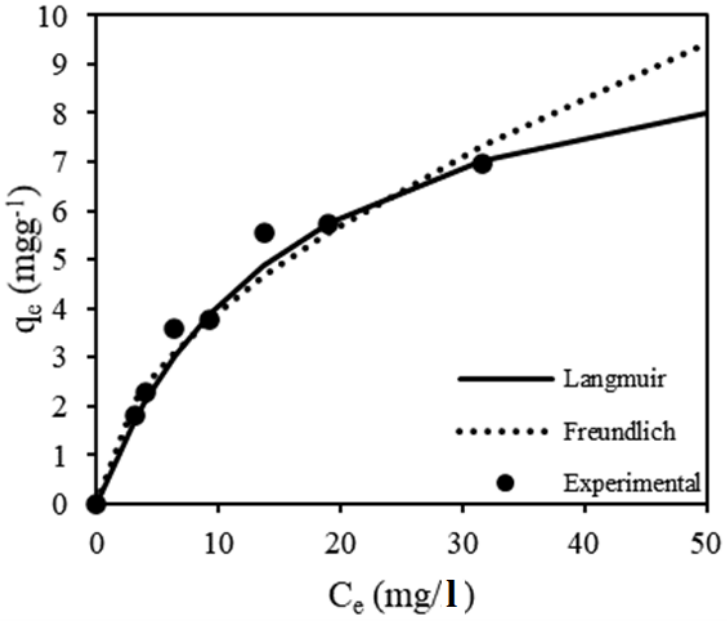

Figure 5. Adsorption isotherms of RR-120 onto LSF

4. Conclusions

LSF was used as an adsorbent for RR-120 removal and proved to be superior to PAL. The results showed that the adsorbent could effectively adsorb RR-120 dye. The adsorption kinetic of RR-120 fitted well with the pseudo-second-order kinetic model. The adsorption isotherm followed the Langmuir isotherm model. The overall result indicated the potential use of LSF as an adsorbent for adsorption of RR-120. There is an opportunity for further study to increase the specific surface area of LSF further promoting the utilization of LSF. It is expected to enhance the adsorption capacity of RR-120 as well as other dyes over the modified LSF.

5. Acknowledgements

This work was financially supported by Research Program on Development of Appropriate Technologies for Coloring Agent Removal from Textile Dyeing, Pulp & Paper, and Sugar Industries for Sustainable Management, Center of Excellence on Hazardous Substance Management (HSM), Chulalongkorn University and Reserch and Technology Transfer Affairs of Khon Kaen University.

References

[1] Bazrafshan, E., Ahmadabadi, M. and Mahvi, A.H., 2013. Reactive red-120 removal by activated carbon obtained from cumin herb wastes. *Fresenius Environmental Bulletin,* 22(2A), 584-590.

[2] Hossein, M.A. and Behzad, H., 2012. Removal of reactive red 120 and direct red 81 dyes from aqueous solutions by Pumice. *Research Journal of Chemistry and Environment,* 16(1), 62-68.

[3] Amran, M., Salleh, M., Khalid, D., Azlina, W., Abdul, W. and Idris, A., 2011. Cationic and anionic dye adsorption by agricultural solid wastes: A comprehensive review. *Desalination,* 280, 1-13.

[4] Leah, M.F., Love, M., Angela, D., Ruffel, R., Paoprasert, P. and Daniel, M., 2018. Adsorption of methylene blue dye and Cu (II) ions on EDTA-modified bentonite: Isotherm, kinetic and thermodynamic studies. *Sustainable Environment Research,* 28(5), 1-9.

[5] Kaykhaii, M., Sasani, M. and Marghzari, S., 2018. Removal of dyes from the environment by adsorption process. *Chemical and Materials Engineering,* 6(2), 31-35.

[6] Suteu, D., Malutan, T. and Bilba, D., 2010. Removal of reactive dye Brilliant Red HE-3B from aqueous solutions by industrial lignin: Equilibrium and kinetics modelling. *Desalination,* 255(1-3), 84-90.

[7] Pangkumhang, B., Jutaporn, P., Sorachoti, K., Khamdahsag, P. and Tanboonchuy, V., 2019. Applicability of iron (III) trimesic (Fe-BTC) to enhance lignin separation from pulp and paper wastewater. *Sains Malaysiana,* 48(1), 199-208.

[8] Feizi, Z. H. and Fatehi, P., 2018. Production of flocculants, adsorbents, and dispersants from lignin. *Molecules,* 23, 868-893.

[9] Tesfaw, B., Chekol, F., Mehretie, S. and Admassie, S., 2016. Adsorption of Pb (II) ions from aqueous solution using lignin from Hagenia abyssinica. *Bulletin of the Chemical Society of Ethiopia,* 30(3), 473-484.

[10] Xu, T., Zhang, N., Nichols, H.L., Shi, D. and Wen, X., 2007. Modification of nanostructured materials for biomedical applications. *Materials Science and Engineering: C,* 27(3), 579-594.

[11] Kajjumba, G.W., Emik, S., Özcan, A., Özcan, H.K. and Öngen, A., 2018. Modelling of adsorption kinetic processes-errors, theory and application. *Intech,* 1, 13, https://doi.org.10.5772/intechopen.80495

[12] Ali, I.H., Mesfer, M.K.A., Khan, M.I., Danish, M. and Alghamdi, M.M., 2019. Exploring adsorption process of lead (II) and chromium (VI) ions from aqueous solutions on acid activated carbon prepared from *Juniperus procera* leaves. *Processes,* 7(4), 217, https://doi.org/10.3390/pr7040217

[13] Kanna, R.R., Lenin, N., Sakthipandi, K. and Kumar, A.S., 2018. Structural, optical, dielectric and magnetic studies of gadolinium-added Mn-Cu nanoferrites. *Journal of Magnetism and Magnetic Materials,* 453, 78-90.

[14] Kerolli-Mustafa, M., Bačič, I. and Ćurkovič, L., 2013. Investigation of jarosite process tailing waste by means of raman and infrared spectroscopy. *Materialwissenschaft und Werkstofftechnik,* 44(9), 768-773.

[15] Li, Z., Xiao, D., Ge, Y. and Koehler, S., 2015. Surface-functionalized porous lignin for fast and efficient lead removal from aqueous solution. *Applied Materials & Interfaces,* 7(27), 15000-15009.
[16] Ge, Y., Qin, L. and Li, Z., 2016. Lignin microspheres: An effective and recyclable natural polymer-based adsorbent for lead ion removal. *Materials and Design,* 95, 141-147.

Spectrophotometric Determination of Zn(II) in Pharmaceutical Formulation Using a New Azo Reagent as Derivative of 2-Naphthol

Hawraa M. Alabidi[1], Ali M. Farhan[2] and Mohauman M. Al-Rufaie[1]*

[1]Department of Chemistry, Faculty of Science, University of Kufa, Najaf, Iraq
[2]Ministry of Education, Al-Najaf, Iraq

Received: 19 March 2020, Revised: 14 August 2020, Accepted: 27 August 2020

Abstract

For the fast investigation of Zn(II) using 2-hydroxy-5-(2-hydroxynaphthalen-1-yl) diazenyl benzoic acid, a specific novel spectrophotometric technique is suggested in this research. The interaction of the azo reagent with Zn(II) is instantaneous at pH 7, and the absorbance of the solution is stable for more than 24 h. The technique allows zinc levels of 1-18 ppm to be calculated, with a molar absorption of 1.516 $x10^4$ l mol^{-1} cm^{-1}. The suggested method for estimating zinc has been widely applied in many pharmaceutical formulations. The error of the determination does not exceed 4%.

Keywords: azo reagent; determination of zinc; spectrophotometry; pharmaceutical preparations
DOI 10.14456/cast.2021.17

1. Introduction

Zinc is commonly found in animal tissues at an average concentration of 20-30 mg/1 g of fresh tissue. Biochemically, zinc is a co-factor for several enzymes, for example carbonic anhydrase and alcohol dehydrogenase. Additionally, zinc is also attached to RNA. It is an essential element for healthy growth, and helps to maintain the plasma concentration of vitamin A, which has resulted in it being used in a large number of multi minerals preparations. In recent years, pharmaceutical preparations have incorporated a low concentration of zinc ion [1-3]. Many techniques for evaluating zinc (II) ions, particularly fluorometric techniques [4, 5], atomic absorption spectroscopy [6, 7] as well as spectrophotometric investigation [8, 9], have therefore been developed. In pharmaceuticals formulations, the zinc (II) ion has often been calculated through the use of azo dyes [10, 11]. The colored solutions of azo compounds have been widely studied in the field of inorganic and analytical chemistry and have generally been used during the spectrophotometric determination by UV-Vis spectra of metal ions in low concentration [12]. For example, the compound 2-carboxy-2'-hydroxy-5'-sulfoformazylbenzene, used as an analytical reagent, was observed to give a zinc complex that was stable over the pH range 8.5 to 9.5 and within the concentration range 0.1 to 2.4 ppm obeyed Beer's law [13]. Also, 4-(2-pyridylazo)

*Corresponding author: Tel.: 07809086646
E-mail: muhaimin.alrufaie@uokufa.edu.iq

resorcinol (PAR) was used in the determination of zinc (II) and produced a colored complex that obeyed Beer's law in the range 0.025-13 ppm, and the elaborated method was applied successfully in the determination of zinc ions in pharmaceutical preparations [14]. In this research, 2-hydroxy-5-(2-hydroxynaphthalen-1-yl) diazenyl benzoic acid (HNABA) is used as the reagent in a basic yet efficient spectrophotometric approach for evaluating the low concentrations of Zn(II) found in pharmaceutical formulations. The reagent undergoes a sensitive color producing reaction with Zn(II) in the presence of different pH values, and the prevailing color characteristic of the resulting zinc-complex solution and its stability are ideal for the determination of zinc ions. A solid zinc chelate with ligand was prepared and characterized to confirm the formation of zinc-azo complex in solution and to identify the structure of the formed complex by FT-IR and UV-Vis spectra.

2. Materials and Methods

A Shimdzu 1800 double beam spectrophotometer was used for all absorbances, whereas FT-IR spectra were obtained on Shimadzu 8400s double beam spectrophotometer in KBr disks, including spectra in ethanol with apparatus-digital. The pH measurements were made by using HI 9321 HANNA pH meter.

Reagents: The HNABA as azo reagent (Figure 1) was prepared by dissolving the amine (5-amino salicylic acid) in a mixture of hydrochloric acid and absolute ethanol and stirring for 15 min an ice bath and then an ice-cold solution of $NaNO_2$ (10 %) was added dropwise into the solution over a period of 30 min. The solution was brown, and an ice-cooled 2-naphthol solution in alkaline ethanol was added with continuous stirring at 0-5 ºC, and left overnight. The mixture was made neutral at pH=7 with dilute hydrochloric acid or ammonia solution. The solid product was filtered, washed with cold distilled water, and left to dry. The synthesis was performed following previous research [15].

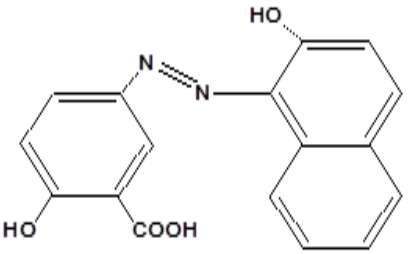

(*E*)-2-hydroxy-5-((2-hydroxynaphthalen-1-yl)diazenyl)benzoic acid

Figure 1. Structural formula of azo reagent

Zn(II) standard stock solution: Zn(II) standard stock solution (100 ppm) was obtained by dissolving Zn(II) in 100 ml volumetric flask for a precisely calculated amount of zinc sulphate. The zinc complex was then obtained by dispersing (2 mmol) ligand in 25 ml ethanol as well as mixing dropwise to a stoichiometric quantity of 1:2 (metal: ligand) molar ratio of zinc sulphate salt, and dissolved in 20 ml of hot distilled water. The pH of the reaction mixture for the complex was adjusted at optimum pH. The resulting solution was stirred for 2 h under reflux. The

complex's solid product was filtered, washed with distilled water, recrystallized using absolute ethanol, and dried overnight at 50ºC.

Buffer solution: Buffet solution was prepared by dissolution of 0.7708 g ammonium acetate into 95 ml of water followed by the addition of a few drops of acetic acid as well as ammonia to modify the pH.

Pharmaceutical samples: The contents of ten tablets and capsules containing the ion were weighed, processed into a fine powder, and the equivalent amounts of one capsule or tablet (0.015 g -0.025 g) of drug were dispersed in 70 ml buffer solution, filtered and then brought up to 100 ml. For syrup formulation, the content of 16.6 ml of the drug equivalent to 0.01g of zinc of the product tested, the volume was introduced to the buffer solution, and checked.

3. Results and Discussion

Zinc (II) ion reacts with 2-hydroxy-5-((2-hydroxynaphthalen-1-yl) diazenyl) benzoic acid (HNABA) and produces a red colored complex in neutral medium at pH=7. HNABA was selected as the molecule because it has more than one functional group that has the ability to form a chelating complex with the metal ion. It has been found that the reagent solutions are characterized by their rapid reaction with the metal ion solution in addition to their high stability of the resulting complex.

3.1 Absorption spectra of the reagent and Zn(II)- complex

Under optimal conditions, the absorbance spectra of the zinc (II) complex against blank as well as the reagent solution were measured over the range 200-800 nm. The reagent 's electronic spectra clearly show two main bands of absorption attributing to π-π * transitions at 198-216 nm and another band at 466 nm related to n-π* transitions [15]. It is noted that this solution showed a spectral color change from yellow to red and showed a peak absorption at 500 nm of the zinc-complex solution that is distinguished by its appearance in a location that differs from the location of the reagent spectra and this is clear evidence that there is coordination between Zn(II) ion and the reagent (Figures 2 and 3).

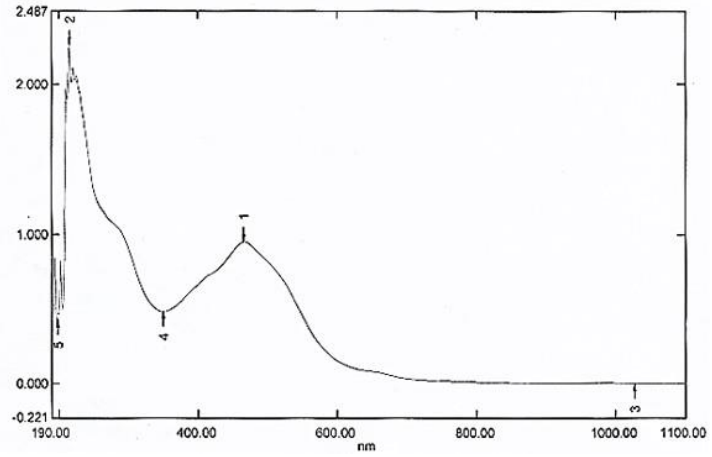

Figure 2. The absorption spectra of $1x10^{-4}$ M azo reagent

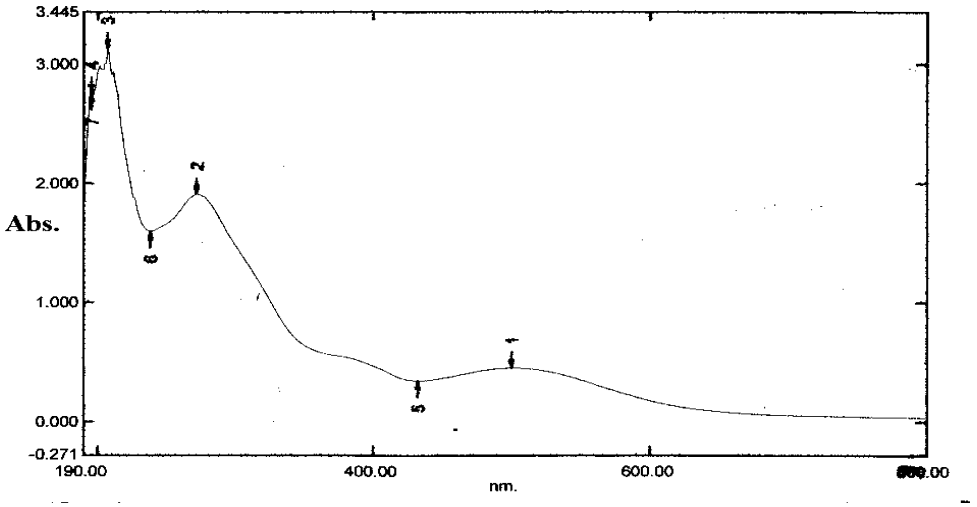

Figure 3. The absorption spectra of zinc-complex at pH 7 and 18 ppm (recorded against reagent blank)

3.2 Calibration curve

A wide range of concentrations (0.1-30 ppm) of mineral ions solutions were studied using the ligand, and it was observed during the preparation of mixing solutions with high concentrations (19-30 ppm) that precipitation occurred immediately after mixing the reagent and zinc ion solutions, which limited the spectral measurement process for these concentrations. As for the solutions that are less concentrated than the solutions mentioned, it has been shown that they obeyed the Lambert Bear law, but this did not apply right through the concentration range studied because some were almost colorless. The absorption values were measured at λ_{max} (500 nm), and the linear calibration curve followed the Lambert-Beer Law in a concentration range from 1 to 18 ppm. The coefficient (r^2) of 0.9988 and also the value of regression equation ($y = 0.0212x$) were noted and are shown in Figure 4. The analytical variables are described in Table 1.

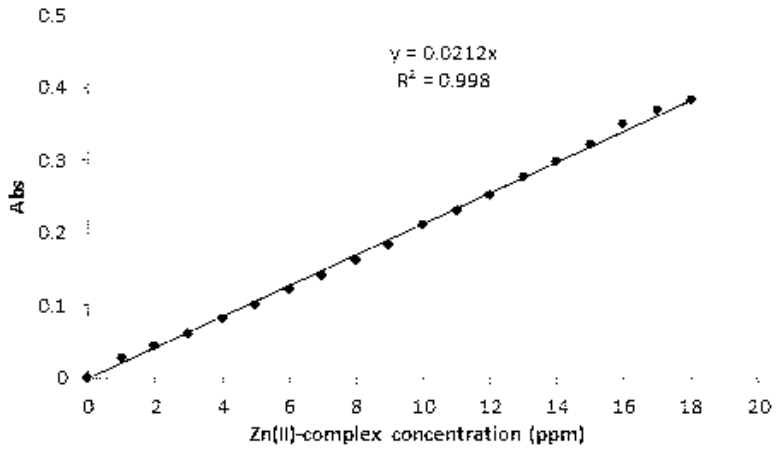

Figure 4. Linear relation between absorbance and Zn(II)-complex concentration (ppm)

Table 1. Analytical Parameters for Zn(II) - complex determination by azo reagent

Analytical Parameters	Value	Analytical Parameters	Value
λ_{max}(nm)	500	Sensitivity (µg cm^{-2})	0.003
Beers range (µg ml^{-1})	1-18	Coefficient (R^2)	0.998
Molar absorptivity (l mol^{-1} cm^{-1})	1.516 $x10^4$	(Metal: Ligand)	1:1
pH	7	Stability constant (β) (l mol^{-1})	6.5 $x10^5$
RSD%	0.433		

3.3 Optimum pH for formation of Zn(II)- complex

Appropriate pH levels were identified in the range of 5-10 for metal complex solutions. To assess the optimum pH value of metal-complex solutions, an ammonium acetate buffer solution was used. The pH against absorbance graph suggested that the optimal pH level for reagent-based Zn(II) complex forming was pH=7, as shown in Figure 5. and Table1. When the pH was increased to greater than 7, the probability of the formation of zinc hydroxide instead of zinc complex increased. The pH being lower than 7 led to the protonation of azo ligand and made the formation of complex difficult.

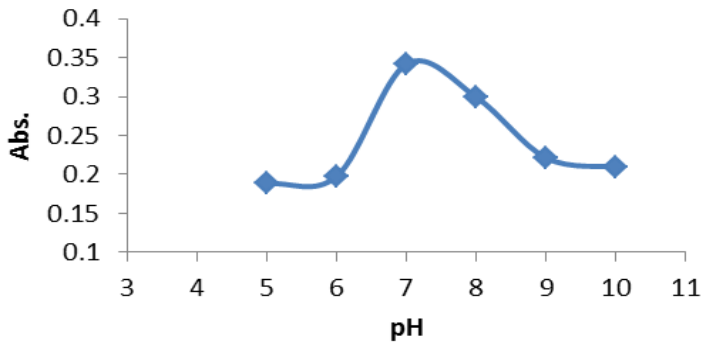

Figure 5. Effect of pH on the absorbance of Zn(II)-complex

3.4 Composition and stability constant for the complex

The formation of the complex was assessed by the molar ratio method [16] and under optimum conditions, the metal: ligand stoichiometry was determined to be 1:1. A stabilization constant was calculated from the absorbance data of ligand and metal ion mixture solutions at λ_{max} = 500 nm and pH=7, with the relationship $\beta=(1-\alpha)/(\alpha^2 c)$ for 1:1 metal complexes, where α=Am-As/Am. Am and As, in optimal level circumstance, are the absorbance values of the complete additionally partially formed-complex, respectively. Table 1 and Figure 6 display the measured (logβ) quantities for $[ZnL(H_2O)_2]$ complex. The reaction was performed at room temperature and its products stay stable for 24 h. This is due to the high stability of Zn(II)-complex as shown in Figure 7.

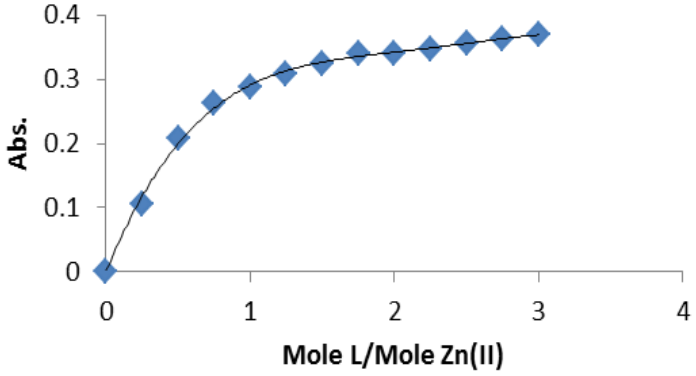

Figure 6. Mole ratio method for Zn(II)-complex

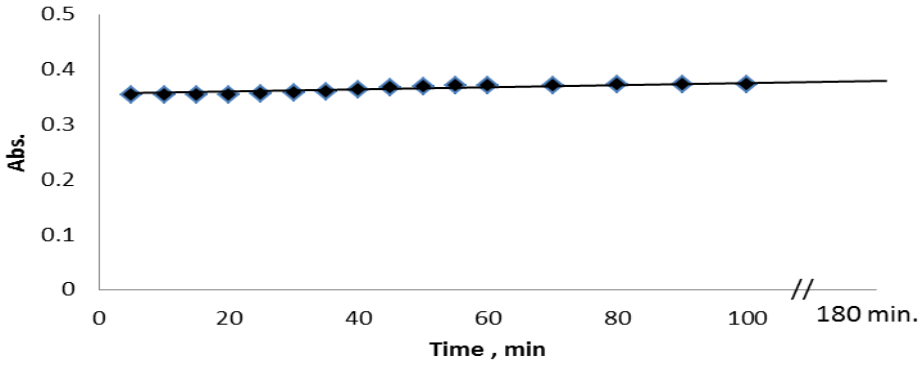

Figure 7. The Relation between absorbance and reaction time of Zn(II)-complex

3.5 Conductivity measurements

Table 2 describes the molar conductivity measurement data of 10^{-3} M Zn-complex in methyl alcohol and in DMF solvent, both at 25° C. The amount level for the molar conductance appears that the complex is non-electrolyte [17].

Table 2. Conductance measurements data of Zn-complex

Complex	**Λm(S.mol^{-1}.Cm^{2})**	
	In Methanol	In DMF
[ZnL $(H_2O)_2$]	10.54	12.16

3.6 Infrared spectra

The reagent FT-IR spectrum showed a wide band at 3419 cm^{-1} υ(O-H), and two more bands at 1666 υ(C=O), and 1489 cm^{-1} υ(N=N). For the zinc-complex spectra, it was found that the band of υ(C=O) at 1666 cm^{-1} had shifted to 1618 cm^{-1} and a new weak band at 623 cm^{-1} related to υ(M-O), suggesting that the carboxylic group and hydroxyl group had coordinated with Zn(II) ion [18]. On the other hand, the band of the azo group in the zinc-complex spectra appeared at the same frequencies that it had in the free reagent, suggesting that the N=N group had not coordinate with zinc ion (Figures 8-9 and Table 3).

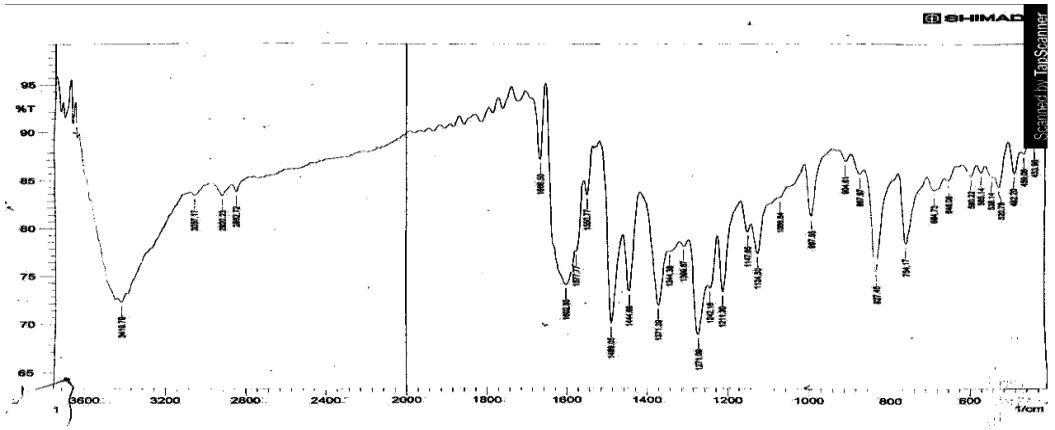

Figure 8. FT-IR spectra of the HNABA reagent

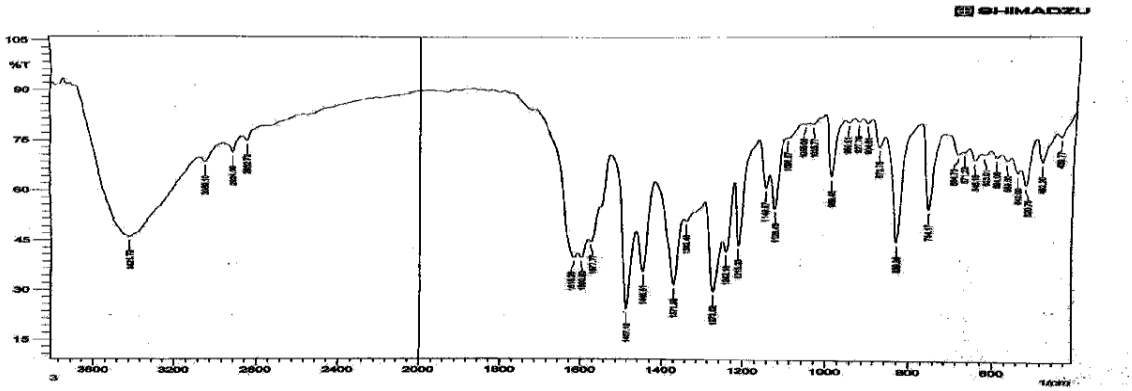

Figure 9. FT-IR spectra of Zn(II) complex

Table 3. FT-IR data of azo reagent and its complex with Zn(II) in cm^{-1} unit

Compound	υ(OH)	υ(C-H) arm.	υ(C=O)	υ(N=N)	υ(C=C)	υ(M-O)
Azo reagent	3419	3057	1666	1489	1602	----
$[ZnL(H_2O)_2]$	3421	3059	1618	1487	1602	623

3.7 Suggested structural formula of Zn- complex

Based on measurements, spectroscopic studies, and the molar conductivity for the reagent HNABA and its zinc-complex, we suggest that the reagent is a bidentate chelating moiety joined to Zn(II) metal ion through the O atoms of salicylic acid, with water molecules presenting as coordinating ions. These generate a tetrahedral structure (Figure 10).

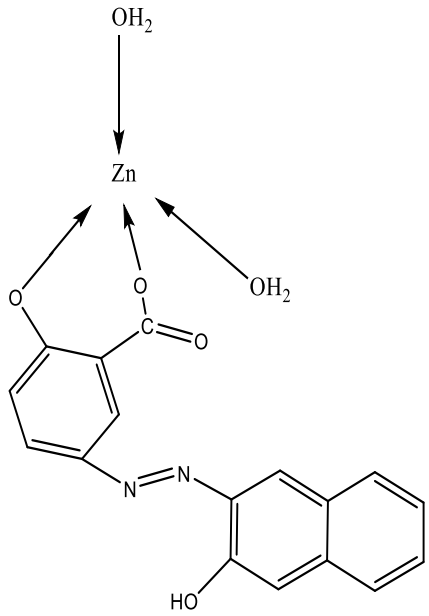

Figure 10. The suggested Zn(II)-complex fundamental formula

3.8 Effect of interference ions

The influence of different interference ions on the absorption of the solution comprising Zn(II) was calculated under optimal conditions. The different ions researched including Cu(II) as well as Fe(II), and the findings are described in Table 4. Foreign ions that do not interfere when introduce as masking agents (or not as masking agents) produce less than 4% error in an analytical recovery.

3.9 Identification of Zn(II) in pharmaceutical formulations

The described approach has indeed been extended to Zn(II) identification of Zn(II) in various pharmaceutical specimens (syrup, tablet and capsule) by spectrophotometric technique utilizing 2-hydroxy-5-(2-hydroxynaphthalen-1-yl) diazenyl benzoic acid as the azo reagent. The information collected in the evaluation is provided in Table 5, and the findings are described in comparison with other documented spectrophotometric technique (Table 6).

Table 4. Influence of interfering cations and anions as well as masking agent on Zn(II)'s relative error (E percent)

Foreign Ions	(E%)	Rec.%	R.S.D%
Fe(II)	2.09	102.09	0.70
Cu(II)	4	104	1.20
EDTA	1.16	101.16	0.90
Oxalate	3.5	96.5	1.30
Tartrate	0.24	99.76	0.88

Table 5. Evaluation of Zn(II) in Pharmaceutical formulations

Pharmaceutical formulations	(E%)	Rec.%	R.S.D%
Zinc tablet	-0.7	99.3	0.771
Zinc capsule	-1.2	98.8	0.562
Zinc plus with multivitamin syrup	1.6	101.6	0.812

Table 6. Comparison of chosen reagents utilized for Zn(II) spectrophotometric evaluation

Reagent	λ_{max} (nm)	pH	Ɛ(L mol^{-1} cm^{-1})	Linear rang (µg ml^{-1})	M:L	Reference
7-(4-nitrophenylazo)-8-hydroxyquinoline-5-sulphonic acid	520	9.2	3.75×10^4	0.05-1	1:2	[19]
3-(2,4-dihydroxy-1-phenylazo)-1,2,4-triazole)	490	10	4.86×10^4	2.6- 9	1:2	[20]
4-(2-arsonophenylazo) salicylic acid	525	6	1.36×10^4	0.5-7	1:1	[21]
2-(2,4-dihydroxyphenylazo) benzimidazole	540	9.23	----	0.06-1.44	1:2	[22]
3-(5-mercapto-1,2,4-triazolo-3-azo)-2,6-dihydroxybenzoas acid	480	7.35	----	0.05-2.25	1:2	[23]
HNABA (azo reagent)	500	7	1.516×10^4	1-18	1:1	P.M

4. Conclusions

The coloring-developing between HNABA azo reagent and Zn(II) was systematically investigated, as was the procedure for the assay of Zn(II) by using Zn(II)-complex coloring reaction. The proposed method showed that maximum absorbance was attained at 500 nm when using UV-Vis. Spectrophotometer, and optimum conditions at pH 7 and 1-18 ppm concentration. This new analytical method was relatively simple, rapid and sensitive in comparison with other spectrophotometric methods that involve the direct interaction between the zinc ion solution and the reagent solution used for estimation. In addition to the low limit of zinc that can be detected, the analysis of a wide range of concentrations follows the Lambert-Beer's Law, particularly in the concentration range from 1 to 18 ppm.

References

[1] Roohani, N., Hurrell, R., Kelishadi, R. and Schulin, R., 2013. Zinc and its importance for human health: An integrative review. *Journal of Research in Medical Sciences*, 18(2), 144-157.

[2] William, D. R., 1985. Analytical Methods in Human Toxicology. New York: Academic Press.

[3] Frassinetti, S., Bronzetti, G., Caltavuturo, L., Cini, M., and Croce, C.D., 2006. The role of zinc in life: a review. *Journal of Environmental Pathology, Toxicology and Oncology*, 25(3), 597-610.

[4] Maeda, M., Kinoshita, T. and Tsuji, A., 1970. A novel fluorophotometric method for determination of hexosamines using pyridoxal and zinc (II) ion. *Analytical Biochemistry*, 38(1), 121-129.

[5] Mahanand, D. and Houck, J.C., 1968. Fluorometric determination of zinc in biologic fluids. *Clinical Chemistry*, 14(1), 6-11.

[6] Tetsuo, M., Saito, M., Horiguchi, D. and Kina, K., 1982. A highly sensitive colorimetric determination of serum zinc using water-soluble pyridylazo dye. *Clinica Chimica Acta*, 120(1), 127-135.

[7] Smith, J.C., Butrimovitz, G.P. and Purdy, W.C., 1979. Direct measurement of zinc in plasma by atomic absorption spectroscopy. *Clinical Chemistry*, 25(8), 1487-1491.

[8] Tekale, P.P., 2012. Extractive spectrophotometric estimation of zinc from food and pharmaceutical samples using 1-phenyl-1-hydrazonyl-2-oximino propane-1, 2–dione reagent. *Der Pharmacia Lettre*, 4(6), 1883-1887.

[9] Zareba, S., Pomykalski, A. and Marzec, Z., 2004. Spectrophotometric determination of Fe(II) and Zn(II) in the pharmaceutical multivitamin preparation with microelements. *Acta Poloniae Pharmaceutica*, 61(3), 175-179.

[10] Stanislaw, Z., 1995. Spectrophotometric determination of zinc in pharmaceutical multimineral preparations by azo-dye derivatives of Benz imidazole and 1,2,4-triazole. *Pharmaceutica Acta Helvetiae*, 70(2), 195-198.

[11] Bhalotra, A. and Puri, B.K., 1999. Trace determination of zinc in standard alloys, environmental and pharmaceutical samples by fourth derivative spectrophotometry using 1-2-(thiazolylazo)-2-naphthol as reagent and ammonium tetraphenylborate supported on naphthalene as adsorbent. *Talanta*, 49(3), 485-493.

[12] Saeed, A. and Shabir, G., 2018. Synthesis and characterization of high wash fastness novel azo reactive dyes incorporating aromatic bridged diamines. *Arabian Journal of Chemistry*, 11(1), 111-119.

[13] Rush, R.M., and Yoe, J.H., 1954. Colorimetric determination of zinc and copper with 2-carboxy-2-hydroxy-5-sulfoformazylbenzene. *Analytical Chemistry*, 26(8), 1345-1347.
[14] Karpińska, J. and Kulikowska, M., 2002. Simultaneous determination of zinc (II), manganese(II) and iron(II) in pharmaceutical preparations. *Journal of Pharmaceutical and Biomedical Analysis*, 29(1-2), 153-158.
[15] Alabidi, H.M., Alabidi, A.M. and Makki, N.F., 2018. Synthesis and spectroscopic studying of new azo ligand from 2-naphthol derivative and it's complexes with some transition metal ions. *Al- Qadisiyah Journal of Pure Science*, 23(1), 186-195.
[16] Ali, A.A.M. and Alabidi, H.M., 2019. Synthesis and spectroscopic study of some transition metal complexes with 2-(4-iodo phenyl azo)-4, 5-diphenyl imidazole. *Journal of Physics: Conference Series*, 1294 (5), https://doi.org/10.1088/1742-6596/1294/5/052021
[17] Geary, W. J., 1971. The use of conductivity measurements in organic solvents for the characterization of coordination compounds. *Coordination Chemistry Reviews*, 7(1), 81-122.
[18] Stuart, B. 2000. Infrared spectroscopy. In *Kirk-Othmer Encyclopedia of Chemical Technology*. New Jersey: John Wiley&Son.
[19] Korn, M.D.G.A., Ferreira, A.C., Teixeira, L.S.G. and Costa, A.C.S., 1999. Spectrophotometric determination of zinc using 7-(4-nitrophenylazo)-8-hydroxyquinoline-5-sulfonic acid. *Journal of the Brazilian Chemical Society*, 10(1), 46-50.
[20] Khedr, A.M., and Gaber, M., 2005. Spectrophotometric studies of the reaction of zinc (II) with some azo-triazol compounds and its application to the spectrophotometric determination of microamounts of zinc(II). *Spectroscopy Letters*, 38(4-5), 431-445.
[21] Amin, A.S.,1994. Spectrophotometric determination of zinc in pharmaceutical samples with some salicylic azo compounds. *Analytical Letters*, 27(1), 95-102.
[22] Zaręba, S., 1995. Spectrophotometric determination of zinc in pharmaceutical multimineral preparations by azo-dye derivatives of benzimidazole and 1, 2, 4-triazole. *Pharmaceutica Acta Helvetiae*, 70(2), 195-198.
[23] Zaręba, S. and Pomykalski, A., 2003. Spectrophotometric determination of Zn in pharmaceutical preparations: Antioxidant and zincuprin forte by azo-dye derivatives of thriazolodiazophenols. *Sectio AA-Chemia*, 6, 94-100.

Review article

Digital Industrial Control Systems: Vulnerabilities and Security Technologies

Ibrahim Adepoju Adeyanju[1]*, Erhovwosere Donald Emake[1], Olatayo Moses Olaniyan[1], Elijah Olusayo Omidiora[2], Temitope Adefarati[3], Godwin Obruozie Uzedhe[4] and Nnamdi Stephen Okomba[1]

[1]Department of Computer Engineering, Federal University, Oye-Ekiti, Nigeria
[2]Department of Computer Science and Engineering, Ladoke Akintola University of Technology, Ogbomoso, Nigeria
[3]Department of Electrical and Electronics Engineering, Federal University, Oye-Ekiti, Nigeria
[4]Department of Electrical and Electronics Engineering, Federal University of Petroleum Resources, Effurun, Nigeria

Received: 6 February 2020, Revised: 17 August 2020, Accepted: 28 August 2020

Abstract

Digital Industrial Control Systems (ICS) are complex electromechanical systems composed of components such as sensors, actuators, programmable logic controllers and communication devices interconnected to perform monitoring and control tasks in different industries. ICS have many and varied applications in critical infrastructures across the globe. However, security is an important factor for any ICS operation. In recent times, there have been a myriad of security threats and attacks by malicious elements on ICS, which has become a concern to organizations and researchers. The development of internet and communication systems has also exacerbated such security concerns. Activities of these malicious elements on ICS can result in serious disasters in industrial environments, human casualties and financial loss. Every ICS network element should be protected to avoid threats, attacks and maintain safe reliable infrastructure. Research efforts have been dedicated to improve ICS security for several decades and are still ongoing. This paper reviews ICS threats, vulnerabilities, cyber-physical attacks and security technologies over the last two decades (2000-2019).

Keywords: Industrial Control Systems; security; ICS; vulnerabilities; threats; cyber-attack; security technologies
DOI 10.14456/cast.2021.18

*Corresponding author: Tel.: +234 813 287 6689
E-mail: ibrahim.adeyanju@fuoye.edu.ng

1. Introduction

Digital Industrial Control Systems (ICS) are composed of various Information and Communication Technology (ICT) network components and associated devices that interact within a process loop to control physical entities [1]. These electro-mechanical complex systems respond to real-time data acquisition, system monitoring and automatic control and management of industrial processes [2]. Today, many nations and organizations' critical infrastructures rely on and are driven by ICS controllers to render control functions [3]. Currently, modern society controlled ICS processes include petroleum and gas refining [4], pipelines and distribution [5], electrical energy generation, transmission and distribution [6], water treatment and distribution [7, 8], chemical processing, pharmaceutical, food and beverage production, railway transportation and air traffic control [9]. ICS integrate computing and communication capabilities with monitoring and control of entities in the physical world [10].

There is a growing concern with respect to the abuse of technology devices associated with ICT and ICS environments including system networks and internet connectivity [11-13]. Implementation practices of ICS systems have introduced a wide range of security vulnerabilities [14]. Presently there is a very high rate of vulnerability and cyber-attacks globally on ICS; some of these threats and attacking agents includes terrorist network groups, dissatisfied employees, hostile governments and other malicious intruders [15]. Cyber- attack consequences are very devastating with effects ranging from disruption or damage of critical infrastructural operations [16, 3] to significant effect on public health, safety and destruction of lives and properties [15-18]. An in-depth understanding of the vulnerabilities, threats and attacks is crucial to the defense mechanisms and security methodologies of any ICS environment.

Security threats to ICS are becoming the biggest challenge for industrial system operations. Hence, it's vital to understand the current trend in the design of ICS, their threats, associated vulnerabilities and state-of-the-art security technologies that can serve as protection mechanisms. For the remainder of this paper, Section 2 gives an overview of Digital ICS, types and architectures while Sections 3 and 4 discusses the threats and vulnerabilities, respectively. The trend of Cyber-physical attacks on ICS is provided in Section 5 followed by a review of available security technologies and their limitations in Section 6. Section 7 maps digital ICS vulnerabilities and threats to appropriate security technologies. Section 8 concludes this review paper with a summary and projection towards improved and better secured digital ICS.

2. Overview of Digital Industrial Control Systems

Control Systems have been used in industries for real time control and monitoring of infrastructures. Critical infrastructures monitored and controlled by ICS are based on several types of field devices with information transmitted from remote station to master station. Supervisory and automated commands such as instruction to collect data from sensor connected with remote station can be initiated through the ICS communication field devices. Alarm status, breakers opening and closing status information and time synchronization check are enabled to effectively transmit data from control station or master station to field devices. ICS has a broad-based application in industrial environments ranging from production, supervision and corporate network.

Sensors, actuators, PLCs process units and communication devices are key components that are usually networked together in an ICS. A typical ICS environment is segmented into field device network or production network, supervisory and corporate network. An ICS could be exposed to vulnerabilities and cyber-physical attacks. This is especially true when the field device at the production network is driven by PLC devices connected to sensors and actuators. Usually, the

control system is equipped with wireless and wired communication capability designed with communication protocol for effective interaction among other ICS components.

2.1 Basic digital industrial control systems (ICS)

In an ICS operating environment, PLCs with different capabilities collaborate to attain various expected goals. The following are the basic digital ICS commonly used in manufacturing, oil and gas industry and other industrial environments [19]. They include:

Supervisory Control and Data Acquisition (SCADA): SCADA is usually deployed to control and manage long distanced assets accustomed with centralized knowledge acquisition and supervisory management. This means that operations are often monitored and controlled from another location at a long distance, typically with wireless facilities connected to facilitate operations [20-22]. SCADA reduces stress on staff from travelling to numerous operational sites when effectively deployed [23].

Distribution Control System (DCS): DCS is a control and monitoring mechanism used mostly in industries such as manufacturing, power generation, chemical producing, oil refineries, waste water treatment, etc. It encompasses a centralized design structure for supervision of the whole control loop. DCS is largely utilized in factories or on production sites; process parameters of the production plants are monitored and controlled with supervisory and regulatory control frame works within the working environment [24]. With several PLCs linked together as a distributed system, numerous tasks are effectively managed and performed. DCS is often utilized. However, actual implementation of ICS in industrial surroundings might typically be a hybrid of DCS and SCADA. Figure 1 clearly shows the basic forms of ICS and their functions.

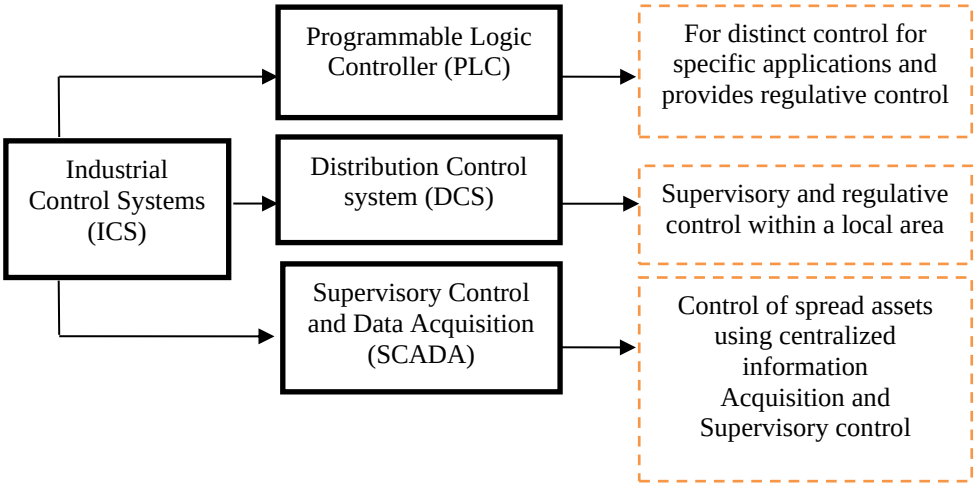

Figure 1. Basic forms of Digital Industrial Control Systems

Programmable Logic Controller (PLC): This is a skid mounted mechanism used for distinct control operations or specified applications, providing restrictive control [25, 26]. PLC is a hardware component domiciled in each DCS and SCADA system. The mounted device is equipped with capability of managing activities inside and delivers feedback signals that control devices like sensors and actuators.

2.2 Digital industrial control systems architecture

Each Digital Industrial Control System has a process loop system of both electronic and mechanical components [9] to control the physical operations of machines. Figure 2 shows the basic operation of an industrial control system. An operator issues set-points commands from the Human-Machine Interface (HMI) to machines, either domestically in-plant or via terminal control devices, typically named as field devices. The system then transmits detector information back to the controller making certain observance and control of the technical facilities to run mechanically and hitch-free. The functions of various ICS components are briefly highlighted.

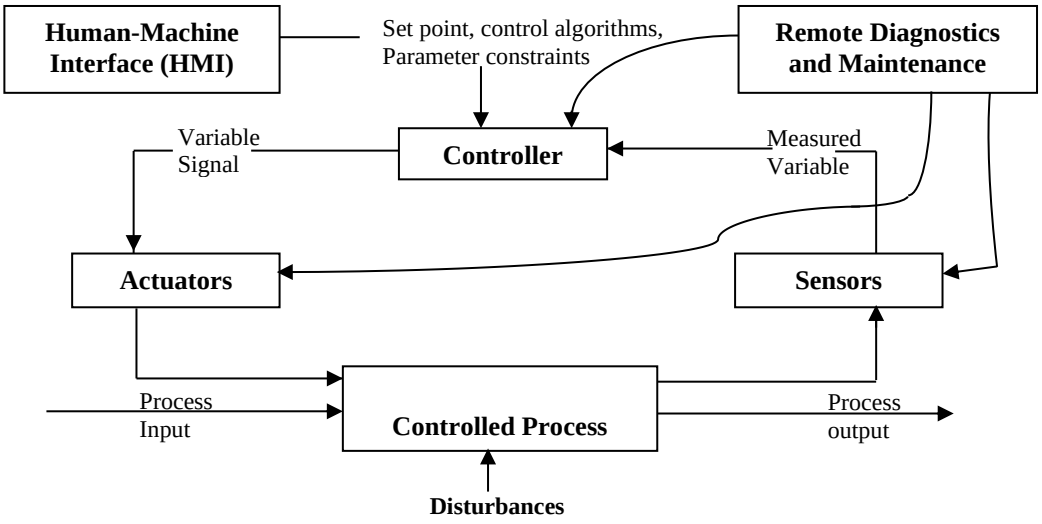

Figure 2. ICS Operation [9]

Control Loop: Various electronic/mechanical parts like sensors for measurement, controller hardware like PLCs, actuators like control valves, breakers, switches, motors, and communication of variables form the group as the ICS control loop, as showed in Figure 2. Interpreted signals from these interconnected parts are variables that are measured by sensors with the help of the controller.

Controller: The role of the controller housed by the PLC is to interpret the signals and generate the right processed variable output. The controller component accesses the issued set point commands from the HMI, then transmits signal to the actuators, but the complete method changes with any slight disturbances which might lead to new detector signals that have been known to vary the state of the method in restraint.

Remote Diagnostics and Maintenance Utilities: These maintenance utilities are extremely important in ICS operation, and are designed to stop system failure when enabled. They additionally have the potential to spot and help systems to recover from varied failure modes. Varied technologies and applications are incorporated in them for smooth functionality.

Human Machine Interface (HMI): HMI is the graphic interface unit that is capable of dealing with all human-machine interactions. The graphic interface is formed of hardware and software systems that enable operators' inputs to be translated as signals for machines that in turn give the specified result to the user. The HMI is employed for proper observation, configuration of

desired set-points and adjusting control formulas that likewise establish parameters within the controllers of an ICS.

2.3 Digital industrial control systems characterization

For better understanding of ICS operation and security approach, three basic characteristics associated with ICS were proposed: cyber, cyber-physical and physical [1, 27, 28].

Cyber characteristics: The feature of ICS which considers computational data, communications, and interactions that don't have any link with the physical world, i.e. physical infrastructure. However, due to communication and interaction between corporation's networks both within and outside ICS environment, these computational devices (controller) and other communication devices are now prone to cyber threats, vulnerabilities and threat attacks.

Physical characteristics: ICS with physical characteristics include any physical components present in the ICS architecture, e.g., sensors, actuators, etc. that their properties may be exposed to security concerns.

Cyber-physical characteristics: ICS with interactive devices and control data are open to the physical world. Therefore, there is the existence of digital interference in the entire ICS environment. Here, the cyber aspect and physical world has a communication link. Today this category of ICS is common as most organizations and their operations are connected to/through the internet. Modern ICS integrate both information technology (IT) and industrial components working together to achieve industrial set goals. These components are varied into layers of functionalities and operations [27, 29].

3. Threats to Digital Industrial Control Systems

Threats confronting ICS are numerous with several sources including malicious intruders, terrorist teams, hostile governments, dissatisfied staff, industrial spies and natural sources such as system complexities, instrumentation failures and natural disasters [30, 10]. This paper outlines four possible classifications of threats facing industrial control systems and briefly describes their activities in the ICS environment.

Adversarial threats: This threat poses malicious intentions from individuals such as script kiddie, hackers, industrial spies, cyber warriors, terrorist groups, or from organizations including competitors, suppliers, partner firms and hostile governments of nations/states [10]. The activities of this adversarial threat targets cyber resources, exploiting available ICT capabilities. The available data and resources become their motivational drive. They initiate and sustain distributed attacks on digital ICS whose networked components are exposed to the internet. The role of malicious internal/insider threat actors, e.g. disgruntled employees or dissatisfied staff, are clear examples of this threat category.

Structural threats: This embodies information technology (IT) related devices such as storage device, processing and communication equipment, sensors, controllers and power supply software [10]. Most examples of structural threats occur as a result of ageing or outdated software packages, breakdown or conditions that exceed expected operational parameters. Their effects are very disruptive and devastating to personnel and ICS operation.

Accidental threats: Equipment handlings by employees are the major cause of this class of threat. It also embodies inaccurate steps taken by instrumentation handler, operators or individual within the course of executing daily tasks.

Environmental threats: This includes natural or artificial disaster (e.g. fire, flood/tsunami, windstorm/tornado, hurricane, earthquake, bombing, overrun), uncommon natural incidence (e.g.,

sunspots), infrastructure failure, telecommunications or electrical power outage [31, 10]. This threat also has a large-scale effect on industrial control systems.

4. Existing Vulnerabilities in Digital Industrial Control Systems

Classification of Digital ICS vulnerabilities can assist in taking proactive steps in implementing applicable security approaches. It has been discovered recently that almost all types of attacks on ICS can be orchestrated and that a substantial range of those attacks are because of the vulnerabilities of industrial applications [32, 33]. The exposure of a system to any potential attack is understood as system vulnerability [34]. One major event that played out on ICS vulnerabilities and security was the Stuxnet Microsoft Windows PC worm discovered in July 2010 that specifically targeted the industrial software system of an Iranian nuclear facility. Stuxnet exploited several vulnerabilities within the execution space and also within the ICS protocol implementation [35]. Hidden in the industrial facilities, the virus was made to spread through U-disk and other system equipment in the local area network, [36, 37] controlling the operation of the centrifuge system using the vulnerabilities of the operating system. ICS vulnerabilities are, therefore, categorized into six groups: Policy and Procedure, Architecture and Design, Configuration and Maintenance, Physical, Software Development, and Communication and Network Configuration Vulnerabilities [10].

Policy and Procedure Vulnerabilities: This vulnerability is a result of poor ICS security audit policies, lack of ICS specific configuration change management, inadequate formal training and awareness program on ICS security measures and lack of administrative mechanisms for security enforcement. Other reasons for this vulnerability include inadequate security on architecture and design, lack of specific continuity of operations or disaster recovery plans, and inadequate programs plans and procedures for detection and response to security breach. Solutions to this type of vulnerability include routine training of control engineers on security of ICS, design of specific security procedures, and guidelines on equipment implementation with regular updates. Prioritized incident detection and response to minimize loss and destruction should be the main features of the designed ICS security procedures.

Architecture and Design Vulnerabilities: This vulnerability is due to factors such as inadequate data collection of event history, insufficient integrated security features in ICS architecture, and undefined security perimeters. Solutions include retention of accurate, proper and sufficient data to determine future security breaches, routine security monitoring to identify security controls issues, and clearly defined security perimeters that are vital to ensure proper security control configuration to avoid unauthorized access to systems and data.

Configuration and Maintenance Vulnerabilities: These are a function of improper configuration management, update patches in operating system without exhaustive testing, inadequate testing of security changes, unsecured passwords generation, Denial of Service (DoS), and insufficient authentication/access control for the configuration and other software. Other factors include improper identification of security breaches, ineffective real-time monitoring of logs and endpoint sensors, and insufficient testing of installed anti-virus software in the ICS environment. Counter measures to this vulnerability include effective use of software to prevent DoS attacks, crucial software testing before deployment and proper keeping of accurate logs to detect security breaches.

Physical Vulnerabilities: These include lack of backup power, voltage spikes due to radio frequency, electromagnetic pulse (EMP) or static discharge, loss of environmental control, unsecured physical ports and unauthorized personnel having physical access to ICS equipment. Possible solutions are proper shielding, grounding and surge suppression of electrical equipment, disabling all universal serial bus (USB) and PS/2 ports, and restrictions on personnel who have

physical access to the ICS environment. Safety requirements, such as emergency shutdowns or restarts to avoid disaster should also be put in place.

Software Development Vulnerabilities: Causes of this type of vulnerability include inadequate authentication, privileges, and access control in software, installed security capabilities not enabled by default and improper data validation. Solutions are prevention of unauthorized access with proper configuration and the enabling of installed ICS security capabilities.

Communication and Network Configuration Vulnerabilities: These are caused by non-existent or improperly configured firewalls, insecure industry-wide ICS protocols, authentication issues traceable to both wireless clients and access points, inadequate data protection between wireless clients and access points. The proper configuration of firewalls between networks, such as corporate networks control, is required to prevent unnecessary data flow and attacks from malware. A solution to this vulnerability is to place priority on data flow controls and restriction of information among systems based on data characteristic. Other solutions include the keeping of accurate and proper logs, enforcement of standard ICS protocol authentication at all levels.

5. Cyber-Physical Attacks and Digital Industrial Control Systems

Digital ICS operations are safety-critical, since they are employed in wide application domains. Their disruption/failure, whether accidental or intentional, will have harmful results on our society at large, damaging infrastructures, property and even persons. The cyber-attacks on the Ukrainian electrical grid [38] and the Mirai attack [39] are a handful of legendary events that followed the Aurora experiment, where an engine was attacked and destroyed solely by cyber means [40]. The Aurora experiment was the first documented cyber-attack on ICS that caused serious damage to the Iranian nuclear program.

5.1 Impact of cyber-attacks on industrial control system operations

The impact of cyber-attacks on ICS environment depends on the target's nature of operation or the motivation of cyber criminals following the attack. Impact can be internal or external. Common techniques of ICS cyber-attacks and related potential impact include the following [41]

- *Changes observed by altering system operations application configurations*: Once systems set-point data or vital parameters are altered, unwanted or unpredictable outcomes result. Such change could be done to mask malware behavior or any malicious activity. These could also conjointly have an effect on the output of a threat actor's target.
- *Change in PLC, RTUs and other controllers:* Observed changes in controllers and other associated devices can equally lead to damage of equipment or facilities. These can further cause control process malfunction and disable control over a process.
- *Misinformation in line with operations*: False or misleading operational commands could lead to implementation of unwanted or reserve actions owing to wrong knowledge. Such an occurrence might modify the programmable logics. This can jointly facilitate concealment of malicious activity, which is the incident itself or the injected code.
- *Alteration of safety controls procedures*: Forestalling the proper operation of safety measures can endanger the lives of workers, and external clients might be put a risk.

5.2 Possible consequences of ICS cyber-attacks

The securing of systems is vital and compelling as business reliance on interconnectivity increases on a daily basis. However, Denial of Service (DoS) attacks and malware (e.g., worms, viruses) are becoming extremely common and have a direct impact on ICS. Cyber-attacks usually have physical and eventful effect. Consequential impacts of ICS attacks can be classified as follows [10]:

Physical Impacts: This type of impact underscores a set of direct consequences of ICS failure. Effects of this impact include personal injury and loss of life damage/loss of property associated with ICS environment. Physical impact is categorized as first order impact in terms of degree of assessment.

Economic Impacts: ICS incidents occur with a strong resultant physical impact. Physical impacts may result in repercussions to system operations that in turn lead to a bigger economic sabotage on the production facilities, organization, or other equipment that are dependent on the ICS. Unavailability of necessary infrastructure (e.g., electric power generation and distribution, transportation) can have a high economic impact. These effects may negatively impact the native, regional, national or presumptively international economy. Economic impact is categorized as second order impact in terms of degree of assessment.

Social Impacts: The consequences of this impact result from the loss of public confidence in a company, with failed ICS due to cyber-attacks. Social impact consequences can be very unpleasant and dreadful. Social impact is categorized as second order impact in terms of degree of assessment.

5.3 ICS cyber-physical attacks

The control loop of a typical ICS constitutes an industrial process application view which can be implemented following a hierarchy of industrial computing systems that makes it vulnerable to threat attacking agents. The controller, which is usually known as the PLC, is a system that implements two logical processes: (a) it controls autonomously the connected device(s) at the lower level of the hierarchy, and takes in input device information and controlling actuators, and (b) it executes a part of a distributed application that controls the complete plant underneath the direction of the SCADA system, and acts with the SCADA system and presumably with different PLCs [42, 28].

ICS can therefore be said to be exposed to computational attacks and data attacks in a cloud-based environment. Although clouds are much more vulnerable to associated threats just as is the internets, both are important factors in ICS operation. Therefore, to successfully secure digital ICS, sophisticated techniques are needed to equally secure clouds. Usually, a cloud is built with the help of the internet with both having security concerns on ICS operations. Although access to data in a cloud-based environment is made possible using virtual machines via the internet, both client and provider reside at their separate geographical areas [43, 44]. Cloud computing environments ensure easy access to ICS operational data at any time and at any location.

Digital ICS cloud-based environment requires standard protocols to effectively provide efficient security for operational parameters/other process control data during transmission. Two basic types of attacks on ICS cloud-based environments are internal/insider and external attacks [45].

Insider/Internal Attacks: This attack type leverages on the open platform in clouds. They are very high-risk and harmful compared to external attacks. These attacks are caused by valid or legitimate users of clouds, who gain access to networks in the following manners: Packet Dropping, Device Isolation, Route Disruption, Modification Based Attacks, and Attacks Based on Fabrication [45]. Attackers can easily bypass the security mechanisms because of the various access links they

have to the system. They can as well gain access to the services of Cloud in a normal manner, therefore, proactive measures on internal attacks generated by the malicious insider devices call for huge attention [45-47].

External Attacks: External attack causes congestion by introducing and propagating fake routing information thereby preventing connecting devices from providing active services. External attacks within the cloud are almost like external attacks in a traditional computing environment. Attacks of this type can be effectively handled by preventive measures and employing techniques like firewall or authentication to detect attacks in ICS environment.

5.4 Cyber-attack classification

A detailed classification of cyber-attacks on digital industrial control systems (ICS) is diagrammatically presented for a better understanding of threat attacks associated with ICS. Figure 3, shows ICS attacks (internal/insider or external) further grouped into four attack classification; (i) reconnaissance (ii) response and measurement injection (iii) command injection, (iv) denial of service. Seventeen types of attacks under the above mentioned four classifications were further identified as current cyber-attack on ICS-MODBUS communication protocol [48, 49].

Reconnaissance: Intelligent attackers gather system network information, map the network architecture and determine the device characteristics like manufacturer model number, supported network protocols, system address and system memory map. Four intelligence operation attacks against MODBUS servers include; the address scan, the perform code scan, the device identification attack and also the points scan. The address scan consistently scans to find ICS servers configured to a network. The perform code scan identifies supported network operations which can be performed for an associate noted server. The device identification attack permits an associated attacker to be told a discovered device's trafficker name, product code, major and minor revision, et cetera. The points scan permits the offender to create a device memory map [49].

Response and Measurement Injection Attacks: This kind of attack occurs in ICS without adequate authentication tools to check that the real source of received data packets during polling is real. Polling is a method used for remote operations, where each transmitted query returns a response packet, containing sensor readings, between clients and the server. Such responses are saved as measurements to influence the feedback control loop. Intruders can inject the response packets and modify to give wrong sensor values. Without effective authentication to identify the packet source, the ICS can be injected with wrong sensor values which can adversely affect the ICS. Response injection attacks are classified into two categories; Naive Malicious Response Injection (NMRI) attacks and Complex Malicious Response Injection (CMRI) attacks.

Command injection: In the type of attack, incorrect commands (control/ configuration) are sent into a control system to cause sabotage. Because supervisory control actions are taken by human operators, intruders can try to mimic the operators to inject supervisory actions to exploit the control system. The activities of this category of attacks by hackers focus on remote terminals coded typically with C programming language using ladder logic and registers to implement their goals. Possible effects of command injections include unauthorized alteration of device configurations, interruption of ICS device communications, unauthorized adjustment of process set points and interruption process control. The malicious command injection attacks by hackers are grouped into three categories as shown in Figure 3; Malicious State Command Injection attacks, Malicious Parameter Command Injection attacks, and Malicious Function Code Injection attacks.

Denial of Service Attacks: Denial of Service (DOS) attacks against ICS attempt to stop some portion of the cyber physical system completely from functioning in other to effectively disable the entire system. DOS attacks would possibly target the cyber system or the physical system. DOS cyber system attacks target communication links, disabling programs running

on system endpoints that control the system, log data, and govern communications. DoS attacks on physical system vary from the manual opening or closing of valves and switches to destruction of components of the physical process that forestall operation [47-51]. The aim is to crash the PLC by sending a very large number of packets within a very small-time frame [52].

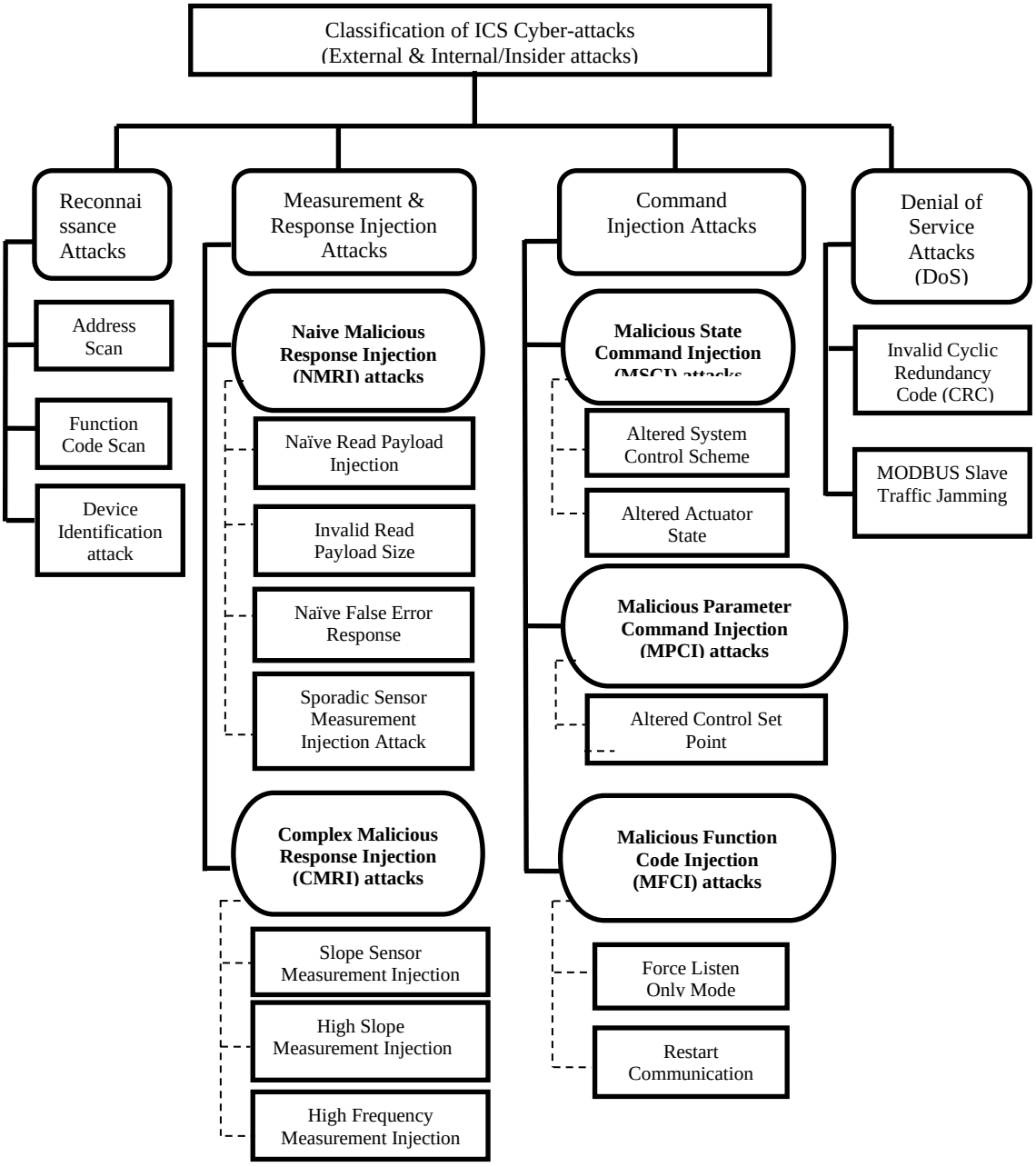

Figure 3. Types of attacks on ICS-MODBUS Communication protocol [49]

6. Security Technologies for Digital Industrial Control Systems

Digital ICS have wide application in critical infrastructure across the globe. Malicious attacks on ICS by threat agents can lead to serious consequences [47]. Therefore, a proactive security measure is an important factor to protect these critical infrastructures. In this section, current security technologies employed in Digital ICS environments to secure them from threat attacks are discussed. Generally, current ICS security technologies can be classified into two broad technologies [6] as shown in Figure 4.

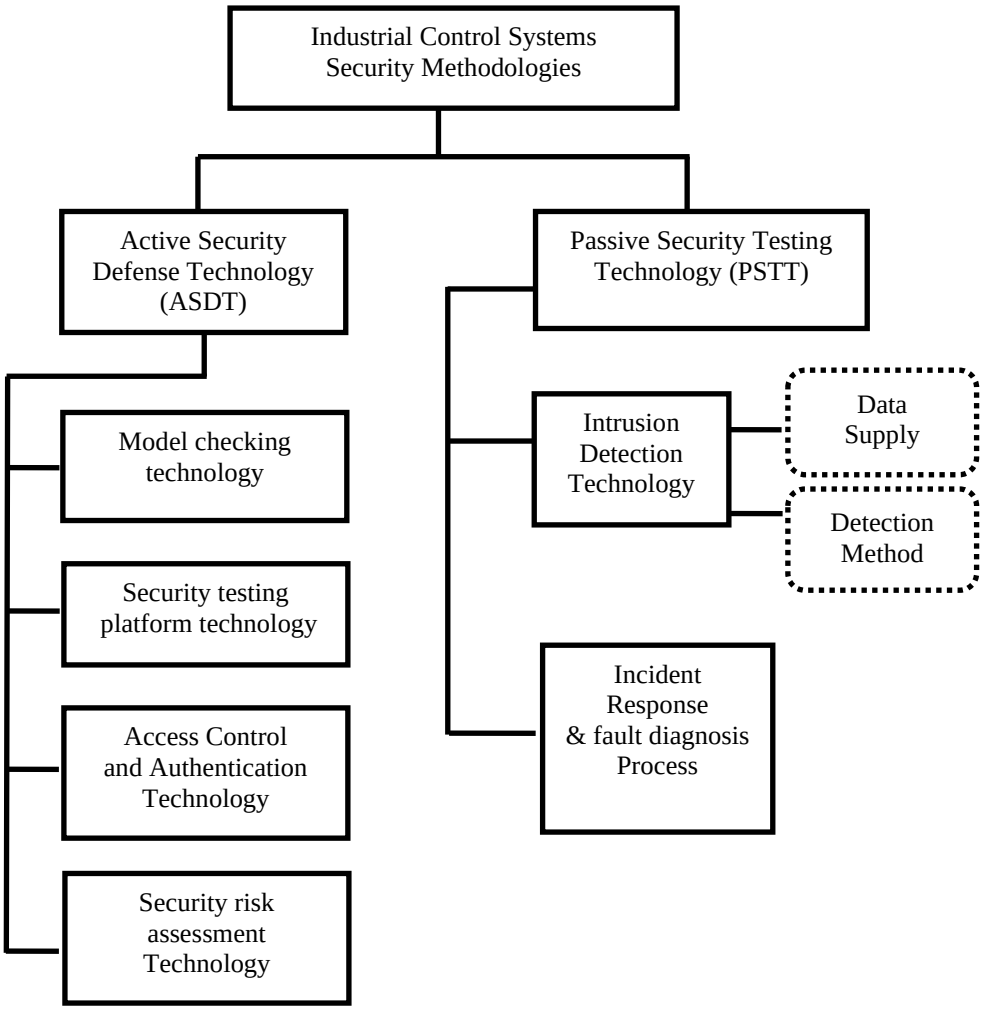

Figure 4. ICS security methodologies [6]

6.1 Active security defense technology

Four techniques are defined under this class of security technologies: They include:

Model checking: This focuses on applying information technology (IT) to ICS security [53]. Considering a recent incident of ICS attack, Stuxnet, a sophisticated cyber software worm that targets SCADA in critical infrastructure companies was found to have been uploaded on the PLC that control industrial automation processes [54]. Additionally, the internet worm allowed attackers to gain total control of critical operations of a process plant from remote locations [55]. In order to effectively handle ICS security flaws, a security mechanism, known as simple non-programmable hardware chips or STCB, to secure ICS/SCADA systems was developed [56].

The low complexity of STCB chips permits verification and facilitates the building block of complicated trusted functionalities of system controllers [57]. However, this security approach assumes that all functional processed data from sensors and actuators are seen to be impersonated by malicious attacks [6]. To enhance this, an associated approach was developed to facilitate a semi-automated security system verification of control systems by a completely unique application of model checking. This was made possible by a research group who enjoyed considerable success recorded with a technique that used historically automated software package verification. The designed model was completely different from model-checking applications, and it had the flexibility to uncover missing safety and security properties that ought to forestall catastrophes caused by malicious activities [56, 58].

Another security approach using checking model technology was demonstrated for High Integrity Communications (HIC). A subversion-resistant guard was built with the help of GEMSOS (GemSeal guards) based on the network ahead of every existing component like the controllers and edge clients. This security approach used seal packets that are sent between controllers and edge clients with a label for their source. The guards forward every labelled packet across the un-trusted network to a guard at the destination with solely crypto seal that binds a label to an identical destination label allowed but unlabeled or altered packets cannot enter the destination [57, 59].

Security testing platform: Recent discovery on proliferation of cyber-attacks on ICS shows that large numbers of security vulnerabilities exist in ICS [33]. However, the ever-increasing rate of attacks on ICS resulted in the development of security test-beds that became very crucial for the evaluation of the protection of ICS tools and products. One among such test-bed designed security models was for evaluating the security of industrial applications by providing completely different metrics for static testing, dynamic testing and network testing in industrial settings. Comparing the model with alternative detection platforms, this platform covered all components of ICS and provided metrics for evaluation [60]. Also proposed was another security solution that used cryptography applications to protect communication (SCADA/DNP3 protocol communication) from abnormal attacking scenarios. This was based on existing and current SCADA/DNP3 associated security issues within each test-bed that was implemented [61]. The demonstrated scheme effectively compensated for the shortage of performance of the firewall, and IPsec SSL/TLS in a digital ICS environment.

Authentication and Access Control: This technology establishes access management for ICS by checking to ascertain if user's credentials are on identical page to the credentials readily available on database of licensed users or in a data authentication server. Any process by which a system carries out verification and identification of a user who wishes to access the system is known as authentication. However, access control is typically based on the identity of the user who requests access to a resource. Authentication is essential to effectively secure control systems, and to execute this security strategy, user authentication is therefore implemented through credentials which at a minimum consist of a user ID and password. Distributed firewalls are deployed and been added as protective layer among internal subnet compared with traditional boundary firewall [62]. Firewalls

sit between a router and application server to provide access control. Router configurations add to the collective firewall capability by screening the data presented to the firewall.

Security risk assessment: Understanding security risk assessment process can be useful for security engineers, inspectors, insurance underwriters and general quality assurance/audit staff. Security risk assessment can be helpful for ICS operations and maintenance personnel who can offer some new perspective on the facilities' risk posture. The key aspect of this technology is that it simply identifies problems and their associated risks as a starting point in order to avoid waste of time and resources. This technology is very important for the mitigation of identified risks.

6.2 Passive security testing technology

Two main techniques are identified under this class of security technology: Intrusion Detection Technology and Incident Response and Fault Diagnosis Process [6].

Intrusion Detection Technology: Intrusion detection is a passive security defense strategy that observes and analyses the events taking place in an information system with the aim of discovering signs of security issues [63]. It consists of a device or software application that monitors systems network behavior, and IDT gathers and analyses system information for malicious activity or policy violations [64]. Any discovered malicious activity or violation is typically reported or collected centrally using a security information and event management system. IDT detects whether there is intending disruption in form of attack against digital ICS systems by continuously comparing with known intrusion model or making decision and analysis for the unknown intrusion model [6]. In IDT, new detection rules are created specifically for ICS systems, and communication protocol in networks are equally designed with the needed specification. These new rules in the designed model are mainly based on attack signatures, anomaly detections, probabilistic models, system specifications as well as the behavior of ICS components [65]. Iterative estimation of Hurst parameter for rapid detection, advanced samplings for classification of anomaly detection, and network intrusion detection with semantics-aware capability have been previously proposed [66-68]. Information theory has been described based on the concept of symbolic dynamics known as a data-driven technique [69]. Statistical technique for detection of network anomalies was proposed and became known as the signal processing approach [70]. Later, intrusion technique for ICS effective operation was proposed and immediately deployed [71, 72]. The intrusion detection system (IDS) uses different data sources available from the monitored ICS. This detection technology detects the presence of an intrusion and immediately sounds an alarm, prompting response to the threat agent wanting to disrupt ICS operation. IDS is classified and determined by the type of information source and the detection techniques used [73]. The effectiveness of IDS techniques and their application in Cyber physical systems is founded on a two design and classification approach namely the detection approach and the audit material approach [74].

Incident Response and fault diagnosis Process: A comprehensive incident response is a significant tool in ICS cyber security, taking cognizance of the various threat attacks facing enterprises. ICS threats are counted to be among the foremost critical aspect of a nation's infrastructure. Mis-configuration, human error, failure, and attackers target ICS and cause them to lose availability and integrity [6]. Emergency response and fault diagnosis ability helps further protection and safety for ICS. In this approach a defense strategy called "Defense in Depth", which describes the configuration of each defense layer, is shown in Figure 5. Before an exploitation of zero-day attack can affect the system, a multilayered defense with safety functions initiates and perform certain emergency actions. Moreover, even with minimal software installation and network connections, the system acts robustly against unknown cyber-attacks. To improve security concerns, ICS network security incident response and troubleshooting process was proposed [75]. The goal of the incident response set up is to permit the organization to manage the cost and injury related to

incidents and to enable a faster recovery of the cost systems [76]. Security incidents in ICS can be very harmful to systems and networks.

6.3 Depth defense strategy

Overall, complete digital ICS security cannot be achieved solely on a single security technology solution. Therefore, it becomes imperative to integrate a range of security technologies hierarchically to boost the defense capability of industrial systems.

The United States Department of Home Security [32] proposed a "defense in depth" strategy, as shown in Figure 5 [6]. The model is segmented into five layers. The first layer is the use of commercial firewalls. The deployment and use of firewall, intrusion detection, vulnerability scanning and other proactive security measures can be helpful in mitigating possible ICS attacks acting as an integral protection [32, 77].

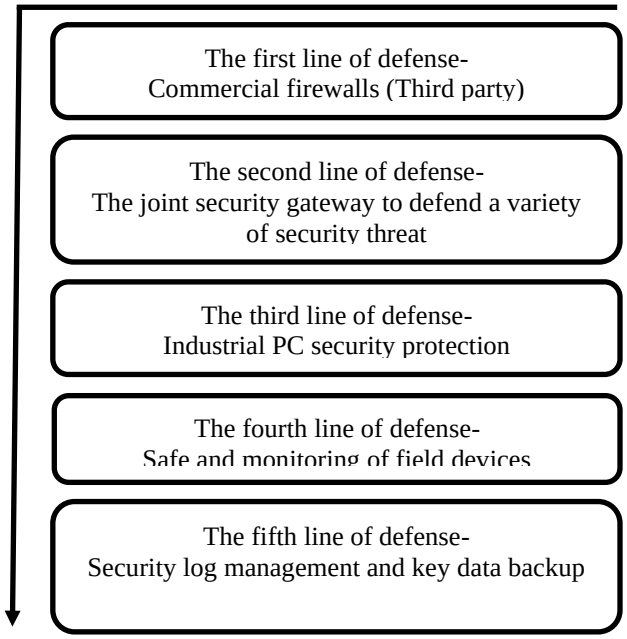

Figure 5. ICS security defense in depth model [32, 6]

Man-in-the-Middle attacks can be averted by securing field device communications networks by deploying and safe guarding the environment using field level firewalls designed for PLCs, IEDs, and SCADA RTUs [78]. The second layer is the joint security approach to defending from a variety of security threats. This is done by insulating the office network from external network using commercial firewalls, while attention is placed on security gateway which mainly insulates work area to control area. The third layer is the protection and security of industrial PCs from prevailing threat attacks and vulnerabilities. The fourth layer is the monitoring of field devices, while security log management and data backup is taken care of by the fifth layer.

7. Mapping Digital ICS Vulnerabilities to Security Technologies

This paper has presented a detailed and comprehensive analysis of current digital ICS threats attack, vulnerabilities, and available ICS security technologies designed to effectively handle prevailing ICS attacks. In this section, different categories of vulnerabilities are mapped to appropriate security technologies for a better analysis. Table 1 summarizes these mappings.

Categories of digital industrial control systems' vulnerabilities have distinct attacking methods which can be handled with different security technologies. Detailed control strategies are highlighted as part of the security technologies for each specific vulnerability; these control approaches are a vital aspect of ICS security. It is advisable that organizations should always prepare employees working in ICS environment with all necessary training for safe and secured operations.

Table 1. Vulnerabilities, attack method and corresponding security techniques in a digital ICS environment adapted from Stouffler *et al*. [10] and Fielder *et al*. [79]

S/N	Vulnerabilities category	Attack Method (Type)	Security Technology	Control description
1	Policy & Procedural Vulnerabilities	-Social Engineering (External)	Security Risk Assessment Technology	- Specific security procedures - Documented formal security training and awareness program for employees
2.	Physical Vulnerabilities	-Removable device driver malware (External)	Security Testing platform Technology	- Consistent and effective defensive posture, removable media check before use
3	Architecture and Design Vulnerabilities	-Malicious Remote Access (External)	Access control Authentication Technology	- Unauthorized access control
4	Architecture and Design Vulnerabilities	-Cross site scripting (External) -SQL command injection, removable device driver Malware, Buffer overflow, Man- in -Middle (Internal)	Model Checking Technology	- Network data validation & integrity check - Retention of accurate, proper & sufficient data to determine future security breach
5	Software Development Vulnerabilities	- Internet Malware, Removable device driver Malware (External) - LAN based Injection (Internal)	Model Checking Technology	- Anti-virus software
6	Communication and Network Configuration Vulnerabilities	- Internet Malware, Malicious Remote Access (External) - Authentication Bypass, Removable device driver malware, Buffer overflow, Man- in -Middle (Internal)	Intrusion Detection Technology	- Demilitarization and Firewalls
7	Configuration and Maintenance Vulnerabilities	- Malicious Remote Access (External) - Authentication Bypass & Misuse of Access Authority (Internal)	Incident Response & Diagnosis Technology	- Consistent and effective defense posture. - Standard & adequate anti-virus

8. Conclusions

An in-depth review on digital industrial control system architectures, threat attacks and vulnerabilities is presented in this paper. One major concern across the globe is the security of critical infrastructures that are basically driven by Digital Industrial Control Systems (ICS). Many such critical infrastructures are facing huge cyber-attacks with consequential impact on the economies of the affected nations. Cyber-attacks on ICS poses serious threats to lives and properties. Today, ICS are also exposed to new threat agents, due to internet-connectivity in most industrial environment and this situation calls for more proactive security solutions, especially with the cyber-physical aspects of ICS. Although significant progress has been recorded in the development of varied techniques for securing digital ICS, more security solutions are needed to combat the new wave of cyber-physical attacks on critical infrastructures across the globe. This paper reviewed modern security technologies that when carefully studied will be very useful for ICS security researchers, assets owners and organizations who seek to build more proactive security solutions that will help in tackling threat attacks and vulnerabilities associated with ICS.

References

[1] Coletta, A. and Armando, A., 2015. Security monitoring for industrial control systems. *Proceedings of the 1st Conference on Cybersecurity of Industrial Control Systems, CyberICS 2015, and the First Workshop on the Security of Cyber Physical Systems, WOS-CPS 2015*, Vienna, Austria, September 2015, LNCS 9588, 48-62.

[2] Hu, Y., Yang, A. Li, H., Sun, Y. and Sun, L, 2018. A survey of intrusion detection on industrial control systems. *International Journal of Distributed Sensor Networks*, 14(8), https://doi.org/10.1177/1550147718794615

[3] Obodoeze, F., Obiokafor, F.N. and Asogwa, T., 2018. SCADA for national critical infrastructures: Review of the security threats, vulnerabilities and countermeasures. *International Journal of Trend in Scientific Research and Development*, 2(2), 974-982.

[4] Weiss, J., 2010. *Protecting Industrial Control Systems from Electronic Threats*. New York: Momentum Press.

[5] Hentea, M., 2008. Improving security for SCADA control systems. *Interdisciplinary Journal of Information, Knowledge, and Management*, 3, 73-86.

[6] Fan, X., Fan, K., Wang, Y. and Zhou, R., 2015. *Overview of Cyber-security of Industrial Control System*. [online] Available at: http://toc.proceedings.com/27630webtoc.pdf

[7] Cardenas, A.A., Amin, S. and Shankar, S., 2008. *Research Challenges for the Security of Control Systems*. [online] Available at: https://people.eecs.berkeley.edu/~sastry/pubs/Pdfs%20of%202008/CardenasResearch2008.pdf

[8] Uchenna, P., Ani, D., Hongmei, M.H. and Tiwari, A., 2016. Review of cybersecurity issues in industrial critical infrastructure; manufacturing inperspective. *Journal of Cyber Security Technology*,1(1), 32-74.

[9] Stouffer, K., Falco, J. and Scarfone, K., 2013. Guide to industrial control systems (ICS) security, *NIST Special Publication 800-82 Revision 1*, http://dx.doi.org/10.6028/NIST.SP.800-82r1

[10] Stouffer, K., Pillitteri, V., Lightman, S., Abrams, M. and Hahn, A., 2015. Guide to industrial control systems (ICS) security. *NIST Special Publication 800-82 Revision 2*, http://dx.doi.org/10.6028/NIST.SP.800-82r2

[11] Alcaraz, C. and Zeadally, S. 2013. Critical control system protection in the 21st century. *Computer* 46(10), 74-83.

[12] Miller, B. and Rowe, D., 2012. A survey of SCADA and critical infrastructure incidents. *Proceedings of the 1st Annual conference on Research in information technology*, October 2012, 51-56.
[13] Shaw, W.T., 2006. *Cybersecurity for SCADA Systems.* Tulsa: PennWell Corp.
[14] Sajid, A., Abbas, H. and Saleem, K., 2016. Cloud-assisted IoT-Based SCADA systems security. A review of the state of the art and future challenges. *IEEE Access*, 4, 1375-1384.
[15] Radvanovsky, A. and McDougall, R., 2009. *Critical Infrastructure: Homeland Security and Emergency Preparedness*. 2nd ed. Boca Raton: CRC Press.
[16] Hathaway, O.A., Crootof, R., Levitz, P. Nix, H., Nowlan, A., Perdue, W. and Spiegel, J. 2012. The law of cyber-attack. *California Law Review*, 100(4), 817-885.
[17] Bernard, T., Hsu, T., Perlroth, N. and Lieber, R., 2017. *Equifax Says Cyberattack May Have Affected 143 Million in the U.S.* [online] Available at: https://www.nytimes.com/2017/09/07/business/equifax-cyberattack.html.
[18] Bisson, D., 2017. *10 of the Most Significant Ransomware Attacks of 2017.* [online] Available at: https://www.tripwire.com/state-of-security/security-data-protection/cyber-security/10-significant-ransomware-attacks-2017/
[19] Lu, T., Guo, X., Li, Y., Peng, Y., Zhang, X., Xie, F. and Gao, Y., 2014. Cyberphysical security for industrial control systems based on wireless sensor networks. *International Journal of Distributed Sensor Networks*, 10(6), 1-17.
[20] Kim, T.H., 2010. Integration of wireless SCADA through the internet. *International Journal of Computers and Communications*, 4(4), 75-82.
[21] Kovaliuk, D.O., Huza, K.M. and Kovaliuk, O.O., 2018. Development of SCADA system based on web technologies. *International Journal of Information Engineering and Electronic Business*, 10(2), 25-32.
[22] ENISA, 2007. *A Strategic Approach to Protecting SCADA and Process Control.* [online] available at*:* http://documents.iss.net/whitepapers/SCADA.pdf, 2007
[23] Butts, J. and Shenoi, S., 2014. Critical infrastructure protection VIII. *Proceeding of the 8th IFIP WG 11.10 International Conference, ICCIP 2014*, Arlington, VA, USA, March 17-19, 2014, 65-78.
[24] Anand, S., Sarkar, S. and Rajendra, S., 2012. Application of distributed control system in automation of process industries. *International Journal of Emerging Technology and Advanced Engineering*,, 2(4), 377-383.
[25] Kiran, A.R., Sundeep, B., Vardhan, S.C. and Mathews, N., 2013. The principle of programmable logic controller and its role in automation. *International Journal of Engineering Trends and Technology*, 4(3), 500-502.
[26] Wang, C., Liu, M.X.A. and Zhang, J., 2017. The application of PLC control system in oil and gas pipeline transportation. *Proceeding of the 2nd International Conference on Mechanical Control and Automation (ICMCA)*, doi:10.12783/dtetr/icmca2017/12334
[27] Peng, Y., Wang, Y., Xiang, C., Liu, X., Wen, Z., Chen, D. and Zhang, C., 2015. Cyber-physical attack-oriented industrial control systems (ICS) modeling, analysis and experiment environment. *2015 International Conference on Intelligent Information Hiding and Multimedia Signal Processing (IIH-MSP)*, 322-326, doi: 10.1109/IIH-MSP.2015.110
[28] National Institute of Standards and Technology, 2016. *Framework for Cyber-Physical Systems. Volume 1, Overview*. National Institute of Standards and Technology (NIST) Special Publication 1500-201, US Departemnt of Commerce, USA.
[29] Didier, P., Macias, F., Harstad, J., Antholine, R. and Johnston, S.A. 2011. *Converged Plantwide Ethernet (CPwE) Design Implementation Guide*. [online] Available at: https://belorg.by/wp-content/uploads/rockwell/td/enet-td001_-en-p.pdf

[30] Rao B.S., Chakravarthi, C.V. and Jawahar, A., 2017. Industrial Control Systems Security and Supervisory Control and Data Acquisition (SCADA). *International Journal for Modern Trends in Science and Technology*, 3(10), 109-118.

[31] Kang, D., Lee, J., Kim, S. and Park, P., 2009. Analysis on cyber threats to scada systems.. *2009 Transmission & Distribution Conference & Exposition: Asia and Pacific*, doi: 10.1109/TD-ASIA.2009.5357008.

[32] DHS, 2009. *Recommended Practice: Improving Industrial Control Systems Cybersecurity with Defense-In-Depth Strategies, Control Systems Security Program*. [online] Available at: https://inldigitallibrary.inl.gov/sites/sti/sti/3375141.pdf

[33] NCSD, 2009. *Common Cyber Security Vulnerabilities in Industrial Control Systems.* [online] Available at: https://www.us-cert.gov/sites/default/files/recommended_practices/DHS_ Common_Cybersecurity_Vulnerabilities_ICS_2010.pdf

[34] Piscitello, D., 2015. *Threats, Vulnerabilities and Exploits-Oh My*! [online] available at: https://www.icann.org/news/blog/threats-vulnerabilities-and-exploits-oh-my

[35] Zhu, B. and Shankar, S., 2010. *SCADA-specific Intrusion Detection/Prevention Systems: A Survey and Taxonomy*. [online] Available at: https://pdfs.semanticscholar.org/1027/2f29fff 747d7efccab3b58d64ffd1112c811.pdf?_ga=2.23427642.1638346716.1598251145-10156915 36.1558354618

[36] ENISA, 2011. *Protecting Industrial Control System. Recommendations for Europe and Member States.* Heraklion: The European Network and Information Security Agency.

[37] Byres, E., Kay, J. and Carter, J., 2003. *The Myths and Facts Behind Cyber Security and Industrial Control*. [online] Available at: https://www.controlglobal.com/assets/Media/ Media Manager/ The_Myths_and_Facts_behind_Cyber_Security_Risks.pdf

[38] Sullivan, J.E. and Kamensky, D., 2017. How cyber-attacks in Ukraine show the vulnerability of the U.S. power grid. *The Electricity Journal*, 30(3), 30-35.

[39] Newman, L.H., 2016. *What We Know About Friday's Massive East Coast Internet Outage*. [online] Available at: https://www.wired.com/2016/10/internet-outage-ddos-dns-dyn/

[40] Langner, R., 2011. Stuxnet: Dissecting a cyber warfare weapon. *IEEE Security Privacy*, 9(3), 49-51.

[41] Knapp, E.D. and Langill J.T., 2014. *Industrial Network Security: Securing Critical Infrastructure Networks for Smart Grid, SCADA, and Other Industrial Control Systems*. 2nd ed. Amsterdam: Elsevier.

[42] Katina, P.F., Despotou, G., Calida, B.Y., Kholodkov, T. and Keating, C.B., 2014. Sustainability of systems of systems. *International Journal of System of Systems Engineering*, 5(2), 93-113.

[43] Dewangan, B.K., Agarwal, A. and Venkatadri, M., 2019. Energy-aware autonomic resource scheduling framework for cloud. *International Journal of Mathematical, Engineering and Management Sciences*, 4(1), 41-55.

[44] Oberoi, P., Mittal, S., Gujral, K.R., 2019. ADRCN: A framework to detect and mitigate malicious Insider Attacks in Cloud-Based environment on IaaS. *International Journal of Mathematical, Engineering and Management Sciences*, 4(3), 654-670.

[45] Boppana, R.V. and Su, X., 2007. *Secure Routing Techniques to Mitigate Insider Attacks in Wireless Ad Hoc Networks*. [online] Available at: https://pdfs.semanticscholar.org/ 2885/ 0ddfbf73c09118fd8e14d1c6c1dc34141c74.pdf

[46] Omar, M., Mohammed, D. and Nguyen, V., 2017. Defending against malicious insiders: a conceptual framework for predicting, detecting, and deterring malicious insiders. *International Journal of Business Process Integration and Management*, 8(2), 114-119.

[47] Gao, J., Chai, S., Zhang, B. and Xia, Y., 2019. Research about DoS attack against ICPS. *Sensors*, 19(7), 1542, https://doi.org/10.3390/s19071542

[48] Morris, T., Srivastava, A., Reaves, B., Gao, W., Pavurapu, K. and Reddi, R., 2011. A control system testbed to validate critical infrastructure protection concepts. *International Journal of Critical Infrastructure Protection,* 4(2), 88-103.

[49] Morris, T.H. and Geo, W., 2013. Industrial Control System Cyber Attacks. *1st International Symposium for ICS & SCADA Cyber Security Research (ICSCSR)*, September 16-17, 22-29.

[50] Silberschatz, A., Galvin, P.B. and Gagne, G., 2013. *Operating System Concepts*. 9th ed. New Jersey: John Wiley & Sons.

[51] Varalakshmi, P. and Selvi, S.T., 2013. Thwarting DDoS attacks in grid using information divergence. *Future Generation Computer Systems,* 29(1), 429-441.

[52] Naoum, S., Chehab, A., Elhajj, I. H. and Kayss, I., 2013. Internal security attacks on SCADA systems. *Proceeding of the 3rd International Conference on Communications and Information Technology (ICCIT-2013): Digital Information Management & Security*, Beirut, 22-27.

[53] Naedele, M., 2007. Addressing IT Security for Critical Control Systems. *Proceedings of the 40th Hawaii International Conference on Systems Science (HICSS-40 2007): IEEE Computer Society*, Waikoloa, USA, 3-6 January, 2007, 40.

[54] Niland, M., 2003. *Computer Virus Brings Down Train Signals*. [online] Available at: http://www.informationweek.com/news/13100807.

[55] Roberts, P.F.Z., 2005. *PnP Worms Slam 13 DaimlerChrysler Plants*. [online] Available at: http://www.eweek.com/c/a/Security/Zotob-PnP-WormsSlam-13-DaimlerChrysler-Plants/

[56] Velagapalli, A. and Ramkumar, M., 2011. Minimizing the TCB for securing SCADA systems. *Proceedings of the 7th Annual Workshop on Cyber Security and Information Intelligent Research (CSIIRW'11)*, October 12-14, 2011. Article No.19, https://doi.org/10.1145/2179298.2179319

[57] Heckman, M., Schell, R. and Reed, E., 2011. Using a high assurance TCB for infrastructure security. *Proceedings of the 7th Annual Workshop on Cyber Security and Information Intelligence Research-CSIIRW*, October 12-14, 2011, Article No. 55, https://doi.org/10.1145/2179298.2179359

[58] Hewett, R. and Kijsanayothin, P., 2013. Securing system controllers in critical infrastructures. *Proceedings of the 8th Annual Cyber Security and Information Intelligence Research Workshop-CSIIRW*, January 2013, 1-4.

[59] Aesec, 2007. *GemSeal Guard*. [online]. Available at: http://aesec.com/guards/Aesec-GemSeal-SCADAConcept-070220.pdf .

[60] Azimi, M., Sami, A. and Khalili, A., 2014. A security test-bed for industrial control system. *Proceedings of the 1st International Workshop on Modern Software Engineering Methods for Industrial Automation- MoSEMInA*, New York, 2014, 26-31.

[61] Shahzad, A. and Musa, S.A., 2014. A review: Industrial control system (ICS) and their secuity issues. *American Journal of Applied Sciences,* 11(8), 1398-1404,

[62] Jie, P. and Li, L., 2012. Analysis of information security for industrial control system. *Process Automation Instrumentation,* 33(12), 36-39.

[63] Yasakethu, S. and Jiang, J., 2013. Intrusion detection via machine learning for SCADA system protection. *Proceedings of the 1st International Symposium for ICS & SCADA Cyber Security Research*. Leicester, UK , September 16, 2013, 101-105.

[64] Valdes, A. and Cheung, S., 2009. Intrusion monitoring in process control systems. *Proceedings of the 42nd Hawaii International Conference on System Sciences*. Washington, DC., USA, January, 2009, 1-7.

[65] Drias, Z., Serhrouchni, A. and Vogel, O., 2015 . Analysis of cyber security for industrial control systems. 2015 *International Conference on Cyber Security of Smart Cities, Industrial Control System and Communications (SSIC),* Shanghai, China, August, 2015, 1-8.

[66] Wang, X., Pang, L., Pei, Q. and Li, X., 2010. A scheme for fast network traffic anomaly detection. *2010 International Conference on Computer Application and System Modeling (ICCASM 2010)*, Taiyuan, China, 2010, V1-592-V1-596.
[67] Androulidakis, G., Chatzigiannakis, V. and Papavassiliou, S., 2009. Network anomaly detection and classification via opportunistic sampling. *IEEE/ACM Transaction on Networking*, 23(1), 6-12.
[68] Scheirer, W. and Chuah, M. C., 2008. Syntax vs. semantics: competing approaches to dynamic network intrusion detection. *International Journal of Security and Networks*, 3(1), 24-35.
[69] Chakraborty, S., Sarkar, S. and Ray, A., 2008. Symbolic identification and anomaly detection in complex dynamical systems. *Proceedings for the American Control Conference(ACC)*, Seattle, USA, 11-13 June, 2008, 2792-2797.
[70] Thottan, M. and Ji, C., 2003. Anomaly detection in IP networks. *IEEE Transactions on Signal Processing*, 51(8), 2191-2204.
[71] Tan, K. and Maxion, R., 2003. Determining the operational limits of an anomaly-based intrusion detector. *IEEE Journal on Selected Areas in Communications*, 21(1), 96-110.
[72] Liu, C.-C., Ten, C.-W. and Hong, J., 2011. Anomaly detection for cybersecurity of the substations. *IEEE Transactions on Smart Grid*, 2(4), 865-873.
[73] Debar, H., Marc, D. and Wespi, A., 2000. A revised taxonomy for intrusiondetection systems. *Annales Des Telecommunications*, 55(7-8), 361-378.
[74] Mitchell, R., & Chen, I.-R. (2014). *A survey of intrusion detection techniques for cyber-physical systems. ACM Computing Surveys*, 46(4), 1-29.
[75] Takano, M., 2014. ICS Cybersecurity incident response and the troubleshooting process. *Proceedings of the SICE Annual Conference*, Hokkaido University, Sapporo, Japan, 827-832.
[76] Conrad, E., Misenar, S. and Feldman, J., 2013. *Eleventh Hour CISSP*. 2nd ed. Amsterdam: Elsevier.
[77] Ning, P., Cui, Y. and Reeves, D. S., 2002. Constructing Attack Scenarios through Correlation of Intrusion Alerts. *Proceedings of the 9th ACM Conference on Computer and Communications Security*, Washington, D.C., 2002, 245-254.
[78] Bartman, T. and Carson, K., 2016. Securing communications for SCADA and critical industrial systems. *69th Annual Conference for Protective Relay Engineers (CPRE)*, College Station, TX, USA, April 4-6, 2016, 1-10.
[79] Fielder, A., Li, T. and Hankin, C., 2016. Defense-in-depth vs. critical component defense for industrial control systems. *4th International Symposium for ICS & SCADA Cyber Security Research (ICS-CSR)*, Queen's Belfast University, UK, August 23-25, 2016, 1-10.

Instructions for Authors

Current Applied Science and Technology journal contains research reports, articles concerning development work, reviews of the literature and research activities. The objectives are to publish and promote research contributions and innovative work in fields associated with applied science and technology. An electronic journal is provided on the website (https://www.tci-thaijo.org/index.php/cast/index). The editors reserve the right to require revision of the submitted manuscript as a condition for final acceptance.

The institute and the editorial board claim no responsibility for the contents or views expressed by the authors of individual articles. Copying is allowed provided that acknowledgement is made. All articles submitted for publication will be assessed by a group of distinguished.

Ethics:

The journal is committed to maintaining the high level of integrity in the content published and has a Conflict of Interest policy in place. The journal uses plagiarism detection software to screen the submissions. If plagiarism is found, the COPE guidelines on plagiarism will be followed. For more details, please see https://www.tci-thaijo.org/index.php/cast/navigationMenu/view/Publication_Ethics.

Page Charge: Free

Submission of Manuscripts:

Manuscripts must be written in English and submitted online. Manuscripts are to be reviewed (double blinded) by at least 3 referees specializing in relevant fields. Revised manuscripts have to be sent online.

All manuscripts should be submitted to: https://www.tci-thaijo.org/index.php/cast/index

Contact:

Editor of Current Applied Science and Technology
King Mongkut's Institute of Technology Ladkrabang
1 Soi Chalongkrung 1, Ladkrabang District,
Bangkok 10520, Thailand
Tel: 662-329-8136
Fax: 662-329-8221
Email: cast@kmitl.ac.th

Manuscript Preparation Guide:

General: Manuscripts must be typewritten using *Microsoft Word for Windows*, single-spaced with margin set-up (in page set up menu) as follows (see also the document template):

Top Margin	1.5"	Bottom Margin	1.5"
Left Margin	1.5"	Right Margin	1.5"

Good quality printouts using A4 paper size are required. Format should be a single column. Times New Roman font type is required. Font sizes for various text functions are as follows:

Text functions	Size *	Typeface
Title	14 (CT)	Bold
Author and co-authors	11 (CT)	Normal
Address for correspondence	11 (CT)	Normal
Abstract and main text	10 (LJ)	Normal
Section heading and number including "Abstract", "Acknowledgement", "References"	12 (CT)	Bold
Subsection heading and number	11 (LJ)	Bold

* CT = Center Text, LJ = Left Justified.

The corresponding author should be noted (included a Fax number and E-mail address) and indicated with an asterisk. Full postal addresses must be given for all co-authors, keyed to names (if required) by superscripted Arabic numbers.

Paper Length: Should not normally exceed 10 pages including figures and tables
Spelling: American English
Abstract: Should not exceed 250 words
Keywords: Should not exceed 8 keywords
Text: Authors are requested to use the following order when typing:-

All research reports (Full Length or Short Reports): Title, Authors, Affiliations, Abstract, Keywords, Introduction (in reserch papers this must be confined to relevant matters, and must not be a general review of cognate literature), Materials and Methods, Results and Discussion, Conclusions, Acknowledgements, References.

Reviews and Discussion Papers will be considered in any format appropriate to the purposes of the authors, although adherence to the general guidelines described above is encouraged.

Line Art Figures: Figures can be drawn using several packages such as Win Draw®, Auto CAD®, Corel Draw®, VISIO® etc.

Photographs: Actual size photographs are acceptable. However, they can also be put into a text stream using a good-resolution scanner. All photographs must be clear when printed in monochrome.

Graphs: Several packages available today can produce attractive and professional graph presentation. Some also provide curve-fitting function, which can be useful. However, two-dimensional bar charts are preferred. All graphs must be clear in monochrome printing.
Equations and complex expressions: Math CAD®, Math Writer® and Equation Editor® (included in Microsoft Word®) are acceptable for presentation of this type of material.

Citations: Citations in the text should be denoted by numbers between square brackets (i.e. [1, 2], [1-3], [1, 3-8]…) *in the order of first appearance in the text.*

References: References should be numbered to correspond with the text citations. References must be arranged as follows:

Books

Authors, Initials., Year. *Title of Book.* Edition (only include this if not the first edition). Place: Publisher.

Example:

[1] Barker, R., Kirk, J. and Munday, R.J., 1988. *Narrative Analysis*. 3rd ed. Bloomington: Indiana University Press.

Chapters of edited books

Chapter authors' surname(s), initials., Year of book. Title of chapter. In**:** Book editor(s) initials. surnames, ed. or eds. *Title of Book*. Place of publication: Publisher. Chapter number or first and last page numbers.

Example:

[2] Samson, C., 1970. Problems of information studies in history. In: S. Stone, ed. *Humanities Information Research*. Sheffield: CRUS, pp. 44-68.

E-books

Author, Year, *Title of Book*. [e-book] Place of publication: Publisher. Available through: include e-book source/database, web address or URL.

Example:

[3] Carlsen, J. and Charters, S., eds. 2007. *Global Wine Tourism*.[e-book] Wallingford: CABI Pub. Available through: Anglia Ruskin University Library website <www.libweb.anglia.ac.uk>.

Journal articles

Author, Initials., Year. Title of article. *Full Title of Journal*, Volume number (Issue number), Page numbers.

Example:

[4] Ross, A.B., Junyapoon, S., Jones, J.M., Williams, A. and Bartle, K.D., 2005. A study of different soots using pyrolysis–GC–MS and comparison with solvent extractable material. *Journal of Analytical and Applied Pyrolysis*, 74(1-2), 494-501.

In case of online journal articles without page number:

Author, Initials., Year. Title of article. *Full Title of Journal*, Volume number (Issue number), DOI-based link.

Example:

[5] Mondal, N.K. and Basu, S., 2019. Potentiality of waste human hair towards removal of chromium (VI) from solution: kinetic and equilibrium studies. *Applied Water Science*, 9(49), https://doi.org/10.1007/s13201-019-0929-5

Proceedings

Author, Initials., Year. Title of article. *Full Title of Proceedings*, Place of Conference, Date, page.

Example:

[6] Thanaboripat, D., Ruangrattanametee, V. and Srikitkademwat, K., 2010. Control of growth and aflatoxin production of aflatoxin producing fungi in corn by salts. *Proceeding of the 8th International Symposium on Biocontrol and Biotechnology*, Pattaya, Thailand, October 4-6, 2010, 283-289.

Patent
Inventor name, Initial(s)., Assignee., Year. *Title*. Place. Patent number (status, if an application).
Example:
[7] Leonard, Y., Super Sports Limited., 2008. *Tin Can Manufacture and Method of Sealing*. Canada. Pat. 12,789, 675.

Dissertation
Author, Year of publication. *Title of Dissertation*. Level. Official name of University.
Example:
[8] Richmond, J., 2005. *Customer Expectations in the World of Electronic Banking: a Case Study of the Bank of Britain.* Ph.D. Anglia Ruskin University.

Websites
Authorship or Source, Year. *Title of Document*. [online] Available at: include web site address/URL (Uniform Resource Locator).
Example:
[9] NHS Evidence, 2003. *National Library of Guidelines*. [online] Available at: http://www.library.nhs.uk/guidelines

Acknowledgements: These should be as brief as possible.

Proofs:
Proofs will be sent to the corresponding author and *must* be returned as soon as possible. Corrections should be restricted to typesetting errors.

Copyright:

Page Numbering:
All pages must be sequentially numbered, preferably by using the automatic page numbering function on your computer.

Copyright Material:
It is the authors' responsibility to obtain written permission from the copyright holder (usually the book or journal publisher) to use copyright material, and to send a copy of this consent with the manuscript. This consent is not normally denied but it is an international legal requirement that it be obtained.

Note:

Please note that authors are urged to check their proofs carefully before returning, since the inclusion of late corrections cannot be guaranteed.

Author(s) are responsible for ensuring that the submitted manuscript fully meets the requirements specified in the above Instructions. Manuscripts which fail to do so will be returned unedited to the Author(s) for correction in accordance with the above requirements, before they can be submitted to the processes of Referee evaluation.

1.5 ”

TEMPLATE

Enter title here (14 PT type size, Title Case, Bold, Centered)

Author Information entered here:
Name (in full)

Affiliation
City
Country
(11 pt type size, upper and lower case, centered under the title)

How to Use This Document Template

Insert the information in your document in place of the text here. For the body of your document, use Times New Roman 10 pt. Font, upper and lower case, double-spaced. Allow an extra half space above a line containing superscripts and/or below a line containing subscripts. The whole text should be left-justified. The headings should be 12 pt size, uppercase, bold and centered.

1.5” 1.5”

Abstract (12pt)

Maximum 250 words here. (10 pt)
.....
.....
.....
.....
.....

Keywords: (10 pt)

Maximum of 8 words

1. Introduction (12 pt)

Clearly explain the nature of the problem, previous work, purpose, and contribution of the paper (10 pt).
.....
.....
.....
.....
.....

*Corresponding author: Tel.: ……..... Fax: …….
E-mail: ……

2. Materials and Methods (12 pt)

.....
.....
.....
.....

3. Results and Discussion (12 pt)

.....
.....…

4. Conclusions (12 pt)

Clearly indicate advantages, limitations and possible applications (10 pt).
.....
.....

5. Acknowledgements (12 pt)

A brief acknowledgement section may be included here (10 pt).
.....
.....

References (12 pt)

References must be numbered in the order cited in the manuscript and indicated in the text by a number in square brackets (e.g. [1, 2]) (10 pt).

Example of References must be arranged as follows:

[1] Barker, R. Kirk, J. and Munday, R.J., 1988. *Narrative Analysis*. 3rd ed. Bloomington: Indiana University Press.
[2] Samson, C., 1970. Problems of information studies in history. In: S. Stone, ed. *Humanities Information Research*. Sheffield: CRUS, pp. 44-68.
[3] Carlsen, J. and Charters, S., 2007. *Global Wine Tourism*. [e-book] Wallingford: CABI Pub. Available through: Anglia Ruskin University Library website <www.libweb.anglia.ac.uk>.
[4] Ross, A.B., Junyapoon, S., Jones, J.M., Williams, A. and Bartle, K.D., 2005. A study of different soots using pyrolysis-GC-MS and comparison with solvent extractable material. *Journal of Analytical and Applied Pyrolysis*, 74(1-2), 494-501.
[5] Thanaboripat, D., Ruangrattanametee, V. and Srikitkademwat, K., 2010. Control of growth and aflatoxin production of aflatoxin producing fungi in corn by salts. *Proceeding of the 8th International Symposium on Biocontrol and Biotechnology*, Pattaya, Thailand, October 4-6, 2010, 283-289.

[6] Leonard, Y., Super Sports Limited., 2008. *Tin Can Manufacture and Method of Sealing*. Canada. Pat. 12,789, 675.
[7] Richmond, J., 2005. *Customer Expectations in the World of Electronic Banking: a Case Study of the Bank of Britain.* Ph.D. Anglia Ruskin University.
[8] NHS Evidence, 2003. *National Library of Guidelines*. [online] Available at: http://www.library.nhs.uk/guidelines

Note:

Tables and Graphs: Minimum of 10 pt type size, all captions should be upper and lower case, centered. Each table and figure must be on a separate page (or pages if required), ***and must be embedded in the text.***

Illustrations and Photographs: Halftones, minimum of 10 pt type size, bold, captions should be in upper and lower case, centered. Images must be computer-designed with clearly visibility.

Contact

Editor of Current Applied Science and Technology
King Mongkut's Institute of Technology Ladkrabang
1 Soi Chalongkrung 1, Ladkrabang District
Bangkok 10520, Thailand
Tel: 662-329-8136 Fax: 662-329-8221
E-mail: cast@kmitl.ac.th
Website: https://www.tci-thaijo.org/index.php/cast/index

KING MONGKUT'S INSTITUTE OF TECHNOLOGY LADKRABANG
1 Soi Chalongkrung 1, Ladkrabang District Bangkok 10520, Thailand
Tel: 662-329-8136 Fax: 662-329-8221
E-mail: cast@kmitl.ac.th
Website: https://www.tci-thaijo.org/index.php/cast/index